B-6421-B

NAS-4436
CR-57210

STUDY OF "RATIO" AUTOMATICALLY ASSEMBLED STRUCTURES

FINAL REPORT

15 JUNE 1963 to 15 JUNE 1964

GDA-DDG64-017

CONTRACT NUMBER NAS7-228

P. Slysh
G. H. Nowak
J. R. Lloyd
E. J. Kaminski

Prepared by

GENERAL DYNAMICS/ASTRONAUTICS
A DIVISION OF GENERAL DYNAMICS CORPORATION

San Diego, California

1 July 1964

ABSTRACT

This study was sponsored by the Office of Advanced Research and Technology, NASA Headquarters, Washington, D.C., and was under the management of Norman J. Mayer, Chief, Advanced Structures and Materials Application Space Vehicle Structures Research.

RATIO automatically assembled spaceborne structures consist of sectionalized, prefabricated panel members which are nested with respect to each other in a stack having an efficient packaging density. These structures and an equipment for automatically assembling them are described.

Preliminary parametric data is developed for the design of RATIO antenna structures.

Detailed computer programs are developed for determining the steady state loads and deflections in the antenna structures. Programs for computing the effects of these deflections on the far field radiation of the antenna are about half completed.

TABLE OF CONTENTS

		PAGE
I.	SUMMARY	I-1
	1.0 GENERAL	I-1
	2.0 "RATIO" STRUCTURES	I-1
	2.1 AUTOMATIC ASSEMBLY MACHINERY	I-2
	2.2 ANTENNA CONFIGURATION	I-2
	3.0 ANALYTICAL MODELS	I-4
	3.1 PLANAR MODEL	I-4
	3.2 DETAILED MODEL	I-5
	4.0 RELATED PROBLEM AREAS	I-8
	5.0 OTHER APPLICATIONS FOR "RATIO" STRUCTURES	I-8
	6.0 RECOMMENDATIONS FOR FUTURE INVESTIGATIONS	I-9
	6.1 COMPUTER PROGRAMS FOR STRUCTURAL ANALYSIS	I-9
	6.2 PARAMETRIC DATA	I-9
	6.3 ELASTIC STABILITY	I-9
	6.4 THERMAL STABILITY	I-10
	6.5 PACKAGING AND AUTOMATIC ASSEMBLY	I-10
	6.6 OTHER APPLICATIONS FOR "RATIO" STRUCTURES	I-11
	6.7 STRUCTURAL ANALYSIS TECHNIQUES	I-11
II.	"RATIO" AUTOMATICALLY ASSEMBLED STRUCTURES	II-1
	1.0 GENERAL	II-1
	2.0 STRUCTURAL CONFIGURATION	II-1
	2.1 ACTUATOR AND FEED, STOWAGE AND DEPLOYMENT	II-4
	2.2 STOWED ANTENNA	II-5
	3.0 REFLECTOR ASSEMBLY PROCEDURE	II-8
	3.1 BASIC MOTIONS	II-8

		PAGE
	3.2 REFLECTOR CONTOUR	II-11
	3.3 PANEL FASTENING OF DEPLOYED ANTENNA	II-11
	3.4 PANEL FASTENING OF STOWED ANTENNA	II-15
4.0	"RATIO" AUTOMATIC ASSEMBLY MACHINERY	II-15
	4.1 GRIPPER-FASTENER FRAME	II-15
	4.2 ANTENNA PACKAGE CLAMP SHAFT	II-18
	4.3 GRIPPER FRAME TRANSPORT ACTUATORS	II-18
5.0	OVERALL CYCLIC PERFORMANCE	II-19
	5.1 MOTION CONTROL PROGRAMMER	II-22
	5.2 AT COMPLETION OF DEPLOYMENT	II-22
6.0	ASSEMBLY EQUIPMENT POWER AND WEIGHT	II-23
7.0	ALTERNATE PANEL ASSEMBLIES	II-23
8.0	SUMMARY OF FEATURES OF "RATIO" AUTOMATICALLY ASSEMBLED ANTENNA STRUCTURES	II-25
III.	PRELIMINARY ANALYSIS OF A SIMPLIFIED PLANAR MODEL	III-1
1.0	GENERAL	III-1
2.0	DEFINITION OF MODEL	III-1
	2.1 SYMMETRY	III-1
	2.2 FIXED NUMBER OF PANELS	III-2
	2.3 ROTATION AXES	III-2
	2.4 ON-BOARD MASSES AND THEIR DISTRIBUTION	III-6
	2.5 LUMPED PARAMETERS	III-7
	2.6 SHEAR, FLEXURAL AND TORSIONAL STIFFNESS	III-7
	2.7 PARASITIC AND LOAD-CARRYING STRUCTURAL MASSES	III-7
	2.8 DEFLECTION LIMITED STRUCTURE	III-7

		PAGE
2.9	VARIABLE STRUCTURAL PROPERTIES	III-8
2.10	INERTIAS OF STRUCTURAL AND ON-BOARD MASSES	III-8
2.11	STRUCTURAL BEAM LENGTHS	III-8
3.0	METHOD OF ANALYSIS	III-8
3.1	DEFINITION OF TERMS	III-8
3.2	NON-TAPERED CONFIGURATION	III-11
3.2.1	STRUCTURAL PROPERTIES	III-11
3.2.2	MASS AND INERTIAL PROPERTIES	III-14
3.2.3	LOADING CONDITIONS	III-16
3.3	TAPERED CONFIGURATION	III-17
3.3.1	STRUCTURAL PROPERTIES	III-17
3.3.2	MASS AND INERTIAL PROPERTIES	III-24
3.3.3	LOADING CONDITIONS	III-30
3.4	SLEWING AND TURNING RATE LIMITATIONS	III-31
3.4.1	OPTIMUM MASSES OF NON-PROPULSIVE POWER AND FLYWHEEL SYSTEMS	III-34
3.4.2	FLYWHEEL SATURATION	III-37
3.5	REFLECTOR DISTORTIONS	III-38
3.5.1	FACTORS AFFECTING ANTENNA PERFORMANCE	III-38
3.5.2	REFLECTOR WEIGHTED RMS DEFLECTIONS	III-40
3.6	SCALING FACTORS	III-41
3.6.1	ALTERNATE SCALING PROPORTIONS	III-45
4.0	SPECIFIC STRUCTURAL DEFLECTION ANALYSES	III-48
4.1	SELECTION OF STRUCTURAL CONFIGURATIONS AND LOADING CONDITIONS	III-48
4.2	DEFLECTION PATTERNS	III-51

		PAGE
4.2.1	MONOTONIC DEFLECTION PATTERNS	III-63
4.2.2	PATTERN INFLECTIONS	III-63
4.3	WEIGHTED RMS DEFLECTIONS	III-64
4.3.1	AFFECTS OF STRUCTURAL TAPERING AND ACTUATOR DISTRIBUTIONS	III-71
4.3.2	AFFECTS OF STRUCTURAL MASS FRACTIONS	III-72
4.3.3	AFFECTS OF ILLUMINATION FUNCTIONS	III-72
4.3.4	O-A AXIS VS. O-B ROTATION	III-79
4.3.5	SCALING OF d VS. L	III-82
4.4	TURNING AND SLEWING RATES	III-82
4.4.1	TRADE-OFFS OF REFLECTOR DISTORTIONS TURNING RATES AND SLEWING RATES	III-89
4.5	LIMITATIONS ON DEFLECTIONS	III-89
4.6	SUMMARY OF RESULTS	III-90
IV.	DETAILED "RATIO" MODEL ANALYSIS	IV-1
IV-A.	STRUCTURAL LOADS	IV-1
1.0	GENERAL	IV-1
2.0	GEOMETRY OF STRUCTURE	IV-1
3.0	REACTION LOADS	IV-3
4.0	FLYWHEEL AND ANTENNA TURNING RATES	IV-4
5.0	MODEL FUNCTIONS FOR ANTENNA TURNING RATES	IV-7
6.0	APPLIED TORQUES	IV-8
7.0	INERTIA OF DISH	IV-10
8.0	REACTION FORCES OF FEED	IV-11
9.0	SUMMARY	IV-12

		PAGE
10.0	STATUS	IV-13
11.0	CONCLUSION	IV-13
IV-B.	RADIATION PATTERNS	IV-15
1.0	INTRODUCTION	IV-15
2.0	ASSUMPTIONS	IV-16
3.0	FAR FIELD REPRESENTATION	IV-17
4.0	PHASE FUNCTION	IV-22
5.0	THE UNIT VECTORS $\bar{n}$ AND $\bar{s}$	IV-24
6.0	NORMALIZED RADIATION INTENSITY	IV-27
7.0	NUMERICAL INTEGRATION	IV-28
8.0	COMPUTATIONAL PROCEDURE	IV-35
APPENDIX A -	STRUCTURAL ANALYSIS	A-1
1.0	GENERAL	A-1
1.1	GENERAL APPROACH	A-1
1.1.1	NOMENCLATURE	A-2
2.0	STIFFNESS DETERMINATION	A-5
2.1	STIFFNESS MATRIX OF A SINGLE ELEMENT	A-5
2.2	STIFFNESS MATRIX OF A BAY	A-10
3.0	METHOD OF ANALYSIS	A-12
3.1	MATHEMATICAL FORMULATION OF THE ANALYSIS	A-12
4.0	THERMAL LOADING	A-15
5.0	LOADS NOT APPLIED AT THE JOINTS	A-18
6.0	MEMBERS WITH NON-UNIFORM PROPERTIES	A-19

	PAGE
APPENDIX B - THERMAL DISTORTIONS	B-1
1.0 GENERAL	B-1
2.0 THERMAL GRADIENT	B-3
3.0 INDUCED DISTORTIONS	B-6
3.1 EFFECTS OF (V_{sT}/V_{cT}) ON ELASTIC RIGIDITY	B-10
4.0 DEPENDENCE OF V_{cT}/V_{sT} ON THE SUBDIVISION OF A STRUCTURAL VOLUME	B-11
5.0 INTERPRETATION OF RESULTS	B-13
APPENDIX C - SIMPLE BEAM APPROACH	C-1
1.0 STRUCTURAL, MASS AND INERTIAL PROPERTIES	C-2
2.0 BEAM DEFLECTIONS	C-5
3.0 WEIGHTED RMS DEFLECTIONS	C-9
4.0 CONCLUSIONS	C-13
APPENDIX D - SIMPLE STRUCTURAL-BEAM APERTURE	D-1
APPENDIX E - MEASUREMENT OF "RATIO" APERTURE DISTORTIONS	E-1
APPENDIX F - CONTROL SYSTEM CONSIDERATIONS	F-1
1.0 INTRODUCTION	F-1
2.0 CONTROL AXES	F-1
3.0 CONTROL SYSTEM DESCRIPTION	F-5
4.0 METHOD OF ANALYSIS	F-7

TABLE OF FIGURES

FIGURE		PAGE
I-1	RATIO automatically assembled antenna.	I-3
I-2	Outline of computer programs.	I-6
II-1	Schematic of a RATIO antenna.	II-2
II-2	Structural panel, including an inertial actuator and feed action.	II-3
II-3	Outline of antenna package.	II-6
II-4	Four basic assembly motions, stack A stationary.	II-9
II-5	Four basic assembly motions, assembled panel B stationary.	II-10
II-6	Assembly program for emplacing panels.	II-12
II-7	Locations and orientations of male or female fastener sections on a panel.	II-13
II-8	RATIO automatic assembly machinery.	II-16
II-9	Gripper-fastener assembly.	II-17
II-10	Operations cycle diagram.	II-20
III-1	RATIO antenna, panel construction.	III-3
III-2	One quadrant of a planar model showing grid coordinates for rotation about the O-A axis.	III-4
III-2a	One quadrant of model showing grid coordinates for rotation about the O-B axis.	III-5
III-3	Beam crossection.	III-13
III-4	Normalized force F_{OA}/a_A LM at structural junctions in Fig. III-2.	III-18
III-4a	Normalized forces F_{OB}/a_A LM(0.707) at structural junctions in Fig. III-2a.	III-19
III-5	Reaction forces due to individual on-board masses and torques due to individual attitude actuators for cases 1 to 4.	III-20

FIGURE		PAGE
III-6	Values of the quantity $k_2\left\{ \right\}_1^{\frac{1}{2}}$ in Eq. (15).	III-23
III-7	Average normalized beam crossection areas $49\ A\ p_S/(1.26)\ 10^{-5}\ K\ L\ k'_{S2}$.	III-25
III-8	Average normalized crossection moment of inertia I/I.	III-26
III-9	Values of the quantity $(n-1)^2\ k_2\left\{ \right\}_1^{\frac{1}{2}}$ in Eq. (18).	III-28
III-10	Values of the quantity $(n_1-1)^2\ k_2\left\{\left[1 - (I_1/I_o)\right]\left[(m_1-1)^2 + (n_.-1)^2\right]^{\frac{1}{2}}/8\right\}_2^{\frac{1}{2}}$ in Eq. (20)	III-29
III-11	Normalized forces $F_{OA}/(6.3)\ 10^{-6}\ a_A\ K\ L^3$ at the structural junctions.	III-32
III-12	Normalized forces $F_{OB}/(4.5)\ 10^{-6}\ a_A\ K\ L^3$ at the structural junctions.	III-33
III-13	Solar and nuclear (unshielded) power sources 1961.	III-35
III-14	Cosine illumination weighting factors.	III-42
III-15	Configurational and loading condition factors for tapered and non-tapered structures, L = 300, k_F = 0.05, K = 0.1.	III-49
III-16	Parameter values for configurations I, II, III, non-tapered and tapered, K = 0.1.	III-50
III-17 to III-26	Normalized reflection patterns.	III-53 to III-62
III-27 to III-32	Normalized reflector distortions vs. reflector size.	III-65 to III-70
III-33 to III-38	Normalized reflector distortions vs. k_S.	III-73 to III-78
III-39	Ratio of d for uniform illumination to d for cosine illumination, O-A axis rotation.	III-80

FIGURE		PAGE
III-40	Ratio of d for O-B to d for O-A axis rotation, non-tapered structure, L = 300.	III-81
III-41	Ratio of scaled to computed values of d at L = 300 for O-A axis rotation.	III-83
III-42	Normalized maximum turning rate, non-tapered structures.	III-84
III-43	Normalized maximum turning rate, tapered structures.	III-85
III-44	Normalized slewing rate, non-tapered structures.	III-87
III-45	Normalized slewing rate, tapered structures.	III-88
III-46	Limitations on frequency, reflector size, and rms distortions.	III-91
III-47	Influence of changes in independent parameters.	III-92
IV-1	Paraboloidal geometry.	IV-18
A-1	Designations for displacements at two ends of an element.	A-6
A-2	Stiffness matrix of a generic element.	A-8
A-3	An elementary bay.	A-11
A-4	Forces of thermal loading.	A-17
B-1	Assumed structural model.	B-4
B-2	Deflection parameter vs. V_{sT}/V_{cT}.	B-9
D-1	Structural beam-aperture model.	D-2
D-2	Normalized power pattern.	D-5
E-1	Instrumentation of nodal deflections along a straight line.	E-3
E-2	Structural grid.	E-4
F-1	Control axes.	F-3
F-2	Diagram of attitude control system.	F-6

I. SUMMARY.

1.0 GENERAL.

The purpose of this study is to investigate the application of RATIO automatically assembled structures to spaceborne paraboloidal, antennas. The study investigates the available trade-offs in the antenna structural properties to achieve given r-f and maneuverability characteristics in the antenna. Emphasis is placed on developing and simulating the relationships between the antenna structural, maneuverability, and r-f parameters. Specific attention is given to the influences of material properties, structural configuration, antenna r-f geometry, slewing rates and on-board masses on the structural properties of the RATIO antennas.

Because of necessary minimum investments in weight of automatic assembly equipments, it is estimated that the RATIO antennas are attractive, from a weight point of view, for reflector sizes in excess of 20 to 30 feet. Antenna sizes as large as 10,000 feet are considered.

2.0 "RATIO" STRUCTURES.

RATIO automatically assembled structures, described in Section II, are subdivided into panel sections which are nested with respect to each other in a stack having a highly efficient packaging density. The nested panels, which mount such subsystems as the antenna r-f feed and the attitude controllers, re-enforce one another to minimize the structural rigidity needed to handle the boost-phase shock and vibration loads. Because of this, primary attention is given to the loads imposed on the orbited and deployed structure and to the investigation

of the effects of these loads on structural distortions. These distortions are evaluated in terms of the r-f performance of the RATIO antennas.

In orbit RATIO structures are basically deflection limited. It is estimated that the greatest structural deflections will result from the steering torques generated by the attitude controllers. Accordingly, the greatest attention is given to these deflections. Structural errors due to manufacturing tolerances, assembly tolerances and thermal distortions which also influence the antenna performance are given only secondary consideration at this time.

2.1 AUTOMATIC ASSEMBLY MACHINERY.

Automatic assembly machinery described in Section II, is attached to the stack of panels. When the stack has been orbited, the machinery, operating at low speeds and with negligible driving accelerations, assembles the antenna. A typical configuration of the machinery, may or may not be man supervised, is shown in Fig. I-1.

2.2 ANTENNA CONFIGURATION.

An easily analyzed antenna configuration is chosen in which the assembled reflector consists of a grid of structural members as shown in Fig. I-1. A tetrapod structure supports the r-f feed and electronics. The attitude control actuators, in the form of sets of three orthogonal flywheels or equivalent, are located on the backside of the structure where they do not interfere with the r-f performance of the antenna.

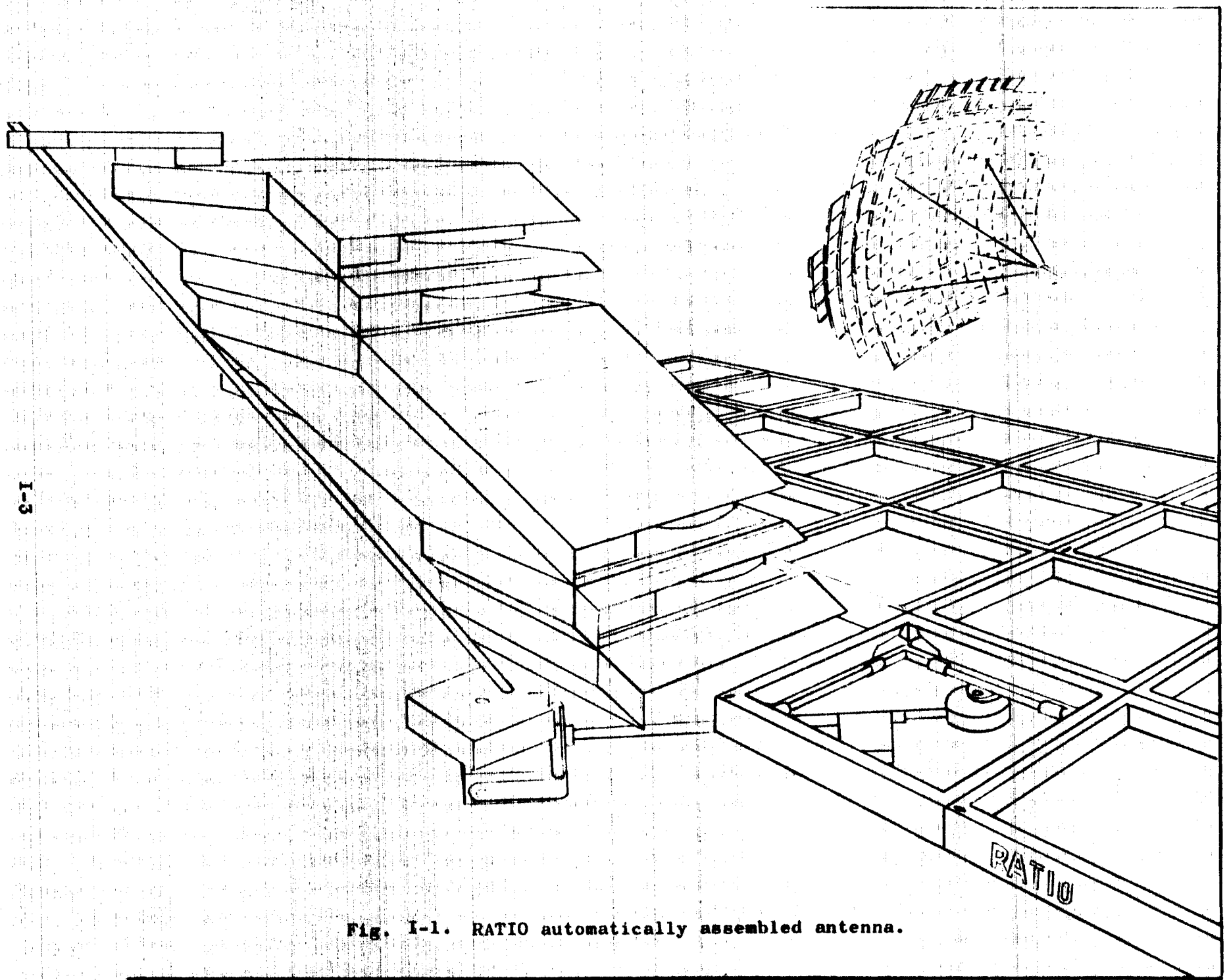


Fig. I-1. RATIO automatically assembled antenna.

3.0 ANALYTICAL MODELS.

In Section III analyses are made of simplified, planar parametric models of RATIO antennas. More detailed models are analyzed in Section IV.

3.1 PLANAR MODEL.

To perform preliminary analyses discrete-parameter structural and r-f models are assumed for the RATIO antennas. These models are planar with the reflector mass, the masses of the attitude actuators (plus the associated non-propulsive power supply), and the masses of the r-f feed system (plus its electronics and power supply) concentrated at the reflector structural junctions.

The planar model is accelerated about a control axis and the reaction forces are computed at each of the structural junctions. In putting these forces into the GD/A structural analysis program, the deflections are computed at each of the structural junctions. Typical deflection patterns for the deflection components perpendicular to the planar surface and parallel to the r-f axis are shown in Figs. III-17 to III-26. The other five deflection components at each of the junctions (i.e. two orthogonal linear and three orthogonal rotary deflections) are neglected in this case.

The rms of the computed normal deflections vs. reflector size are displayed in Figs. III-27 to III-32, and the dependence of these deflections on the structural mass fraction (k_S) is shown in Figs. III-33 to III-38.

The choice of parameters to minimize the normalized rms deflections do not generally correspond with the choice of parameters to maximize the allowable turning and slewing rates. Figs. III-42 to III-45 indicate turing and slewing rates vs. structural mass fractions. Fig. III-47 indicates the influence of changes in independent parameters on the deflections and turning and slewing rates.

3.2 DETAILED MODEL.

As in the case of the planar model a lumped-constant spring-mass system is assumed for the detailed structural model. Also, in the detailed r-f model the phase distortions across the aperture (due to structural distortions) are considered at discrete areas on the aperture. These phase errors are summed together with other geometric factors to establish the far field radiation of the antenna.

As a result of this study, 7090 computer programs have been developed for the detailed analyses of the reaction loads and torques at the structural junctions (due to prescribed attitude maneuvers) and the resultant structural deflections. Programs for computing the far field radiation patterns and finally for automatically plotting these patterns on a SC 4020 microfilm recorder are in approximately a 50 percent completion stage. Fig. I-2 outlines these programs.

The program inputs in Fig. I-2 include:

Structural geometry: the grid spacing of the structural beams, type of feed support structure, number of panels, location of feed, etc.

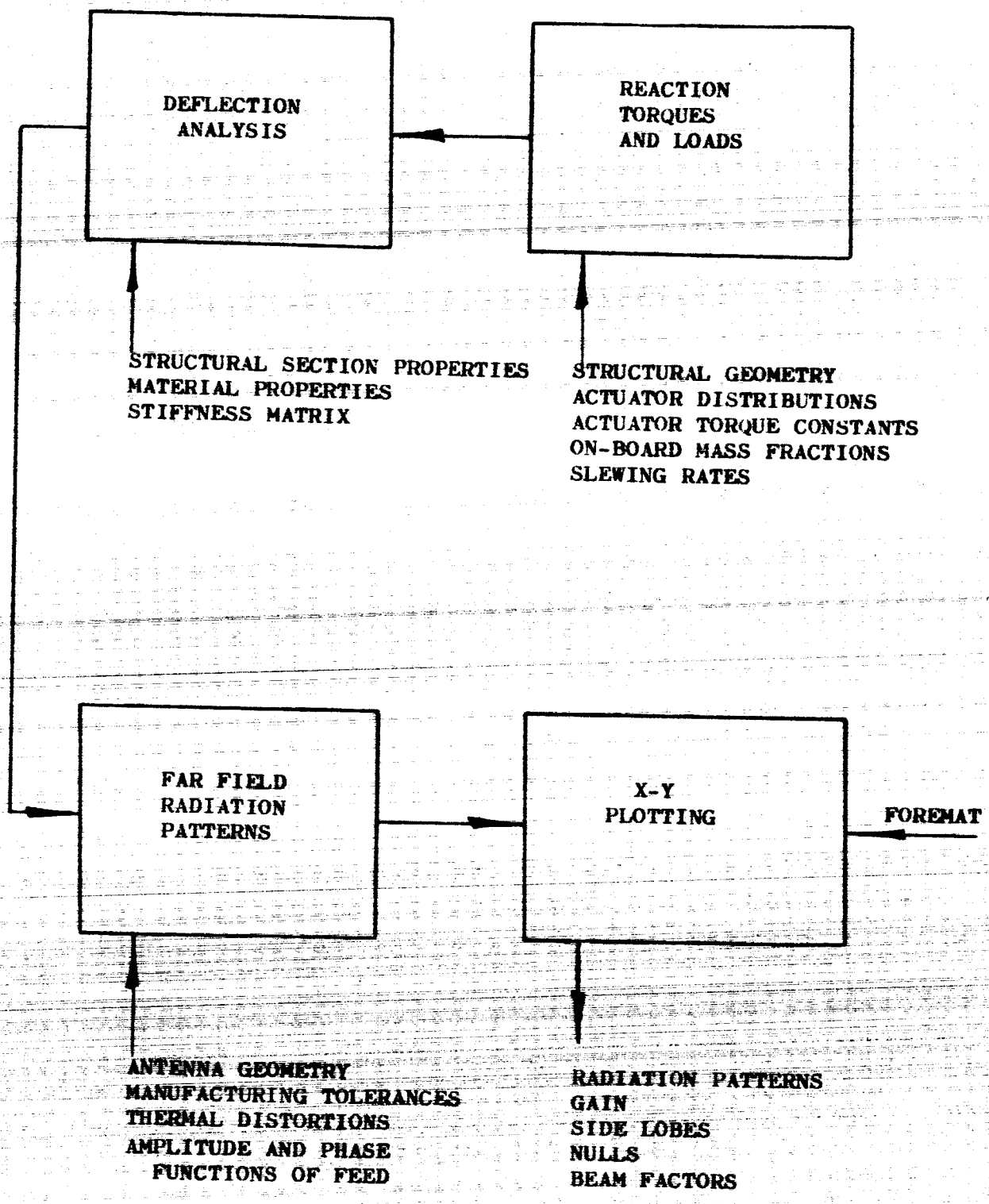


Fig. I-2. Outline of computer programs.

Actuator distributions: the number of actuator and the locations of the actuators.

Actuator torque constants: the torque-to-mass ratios of the actuators.

On-board mass fractions: the ratios of the masses of the feed, actuators, non-propulsive power system, etc. to the over-all antenna mass.

Slewing rates: steady state angular accelerations about one or more control axes.

Antenna geometry: the focal-length-to-diameter ratio, location of feed with respect to focal point, aperture blockage, reflector contour, etc.

Manufacturing tolerance and thermal distortions: these affect the far field radiation and must be added to the deflections caused by the reaction torques and loads.

The major program outputs are the radiation patterns from which the gain, side lobes, nulls and beam factors can be determined.

The accuracy of the structural and r-f models, and methods of analysis depend on the fineness and accuracy ot the structural sub-divisions. It is possible by refining subdivisions to improve the accuracy and to eventually approach an error-free analysis of the structural deflections. Likewise, by increasing the detail in the subdivision of the aperture, the far field radiation can be established with increased accuracy. Matrix partitioning methods make it possible to substantially extend the capabilities of the 7090 for these computations.

4.0 RELATED PROBLEM AREAS.

The appendix of this report summarizes the work done in various areas that are related with RATIO structures.

5.0 OTHER APPLICATIONS FOR "RATIO" STRUCTURES.

Because the investigated RATIO antennas have paraboloid of revolution reflectors the results of this study are applicable, in part, to solar collectors. The major differences between the structural requirements of spaceborne antennas and concentrators arise from (1) the generally greater parasitic weights of the continuous concentrator reflector surfaces compared to screen mesh antenna reflector surfaces, (2) the need to primarily control reflector surface angular deviation tolerances on the concentrator reflector surface rather than the linear tolerances which are more significant in the case of the antenna.

RATIO automatically assembled structures may also be used to deploy large solar panels, as well as cylindrical, spherical, lenticular or toroidal structural configurations which may serve as space stations, re-entry bodies, or lunar shelters. This study does not consider these RATIO applications.

6.0 RECOMMENDATIONS FOR FUTURE INVESTIGATIONS

6.1 COMPUTER PROGRAMS FOR STRUCTURAL ANALYSIS

The computer programs for loads and deflections on the detailed RATIO antenna structure are complete and the programs for the far field radiation and pattern plotting are about half complete. It is recommended that the incomplete programs be completed so that benefit can be derived from the work done in formulating them.

In combination these programs provide a powerful tool for the analysis and evaluation of various antenna structures under the influence of mechanical loads.

6.2 PARAMETRIC DATA

When the detailed computer programs are completed it is possible to generate data on the tradeoffs between the antenna structural and r-f performance parameters. It is recommended that this data be developed and that it include the parameters considered in Section III as well as the many omitted parameters, as spelled out in Section III. The development of this data serves to (1) test the validity of the results in Section III, (2) provide data on the structural parameters that need to be further researched or optimized.

6.3 ELASTIC STABILITY

Because of the minimal loads imposed on the RATIO antenna structures due to boost-phase shock and vibration, and because the deployed structures are deflection limited, it follows that extremely light weight, efficient structures can be used. These structures are fundamentally limited by the allowable

minimum cross sectional wall thickness that can be used in the structural members. It is recommended that sample sections as applied to RATIO antennas be tested to study the structural material and configurational factors that influence the elastic stability of these sections.

6.4 THERMAL STABILITY

For the same reasons that RATIO structures may be limited by elastic instability they may also be limited by thermal instability. It is recommended that the existing computer program for analyzing structural deflections due to mechanical loads, be extended to include thermal loads. It is also recommended that influence of spectral surface qualities and configuration factors on structural thermal gradients be investigated. With knowledge about the thermal gradients, and programs to evaluate the structural distortions they induce, it will be possible to effectively investigate RATIO thermal stability problems.

6.5 PACKAGING AND AUTOMATIC ASSEMBLY

Further study of alternate means for subdividing the antenna structure into panels that can be nested and then automatically assembled would contribute to a better understanding of the pros and cons of RATIO antenna structures. It is recommended that alternate automatic assembly methods as well as competitive unfurling and inflating methods be investigated on a comparative basis to determine the range of antenna sizes, reflector surface tolerances, packaging densities, specific structural weights, etc. for which the different methods are most applicable.

The square grid structure considered in the study is inherently less stable than a triangular grid structure. It is recommended that automatically assemblable structures using triangular panels be investigated.

6.6 OTHER APPLICATIONS FOR "RATIO" STRUCTURES

As a result of the work on RATIO antenna structures it has been found that the RATIO structures and automatic assembly methods can be applied to solar concentrators, and large solar panels, as well as to cylindrical, spherical, lenticular, and toroidal structures for space station, re-entry body, or lunar shelter applications. It is proposed that these applications be investigated.

As in the case of the antennas, means for sectionalizing, packaging, and automatically assembling the structures should be studied. Investigations should also be made of pressure sealing of the enveloped structures (for space station and lunar shelter applications) by extensions of the automatic assembly process. The assembly process could be used for roll sealing, or triggering the explosive sealing of mating panel edges. Manual methods for sealing the joints, after the structure has been assembled, should also be looked into.

6.7 STRUCTURAL ANALYSIS TECHNIQUES

Inevitably structural analysis of future large RATIO structures will require solving systems of simultaneous equations numbering many times those which may be solved in the current state of the art (this is about 1500 or 2000).

Computer technology seems unlikely to afford a solution to this problem. Core size, which now is the limiting factor, appears to be staying in the 30-40 K region.

It is therefore recommended that effort be expended to face this problem along these lines:

(a) Full exploitation of the Structural Principles of Symmetry and Anti-Symmetry.

(b) Further development of the method of substructures.

(c) Exploitation of the inherent symmetry of structural analysis matrices in devising methods of solution - i.e., improving inversion and solving subroutines.

II "RATIO" AUTOMATICALLY ASSEMBLED STRUCTURES
(By P. Slysh)

1.0 GENERAL

This section describes an idealized RATIO antenna system including its structures, attitude actuators, feed deployment, and in-orbit automatic assembly machinery. The described antenna has been chosen because of its relatively, symmetrical and easy-to-analyze structure. This description serves as the first step in defining the RATIO structures that are analyzed in Section III and IV.

A specific 100-foot-reflector-diameter antenna is assumed for the description. RATIO automatically assembled structures are however applicable to many other antenna configurations ranging from approximately 30 to 1000 feet in diameter and greater.

2.0 STRUCTURAL CONFIGURATION

The selected antenna configuration shown schematically in Fig. 1 consists of a sectionalized reflector, feed, tetrapod feed support, and a four-flywheel inertial (attitude) actuator system. The four actuators are located on the back of the reflector at the junction between the feed support and the reflector.

The reflector is sectionalized into the semi-hat panel configuration as outlined in Fig. 2. The four panels that mount the feed and actuator sections, shown in Fig. 2, are relatively massive and rigid structures. The remaining 198 panels that form the reflector are fitted with a screen mesh suitable for reflecting r-f energy and are (relatively) significantly less massive and rigid. With the use of thin-wire-fine-mesh screens (weighing

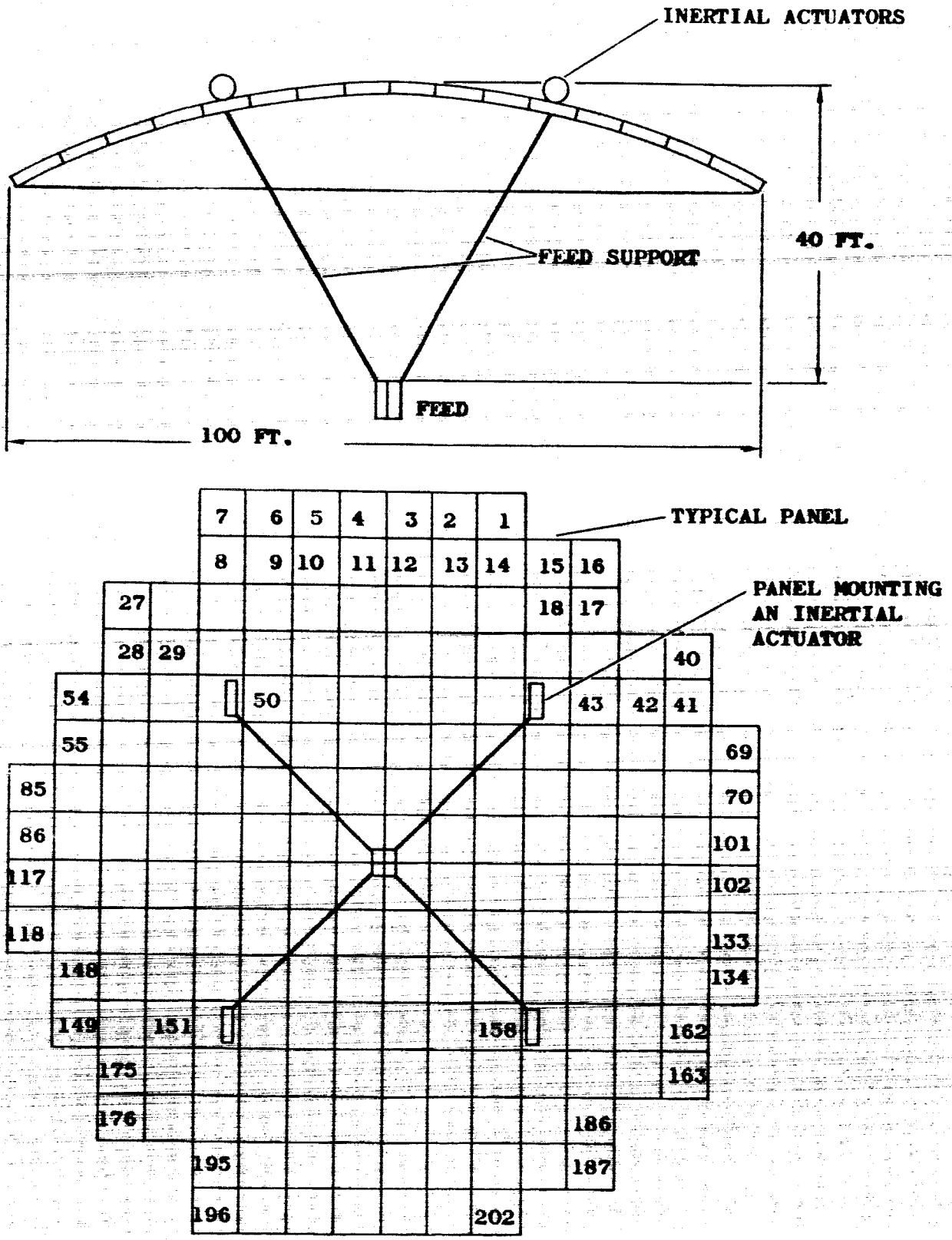


Fig. II-1. Schematic of a RATIO antenna.

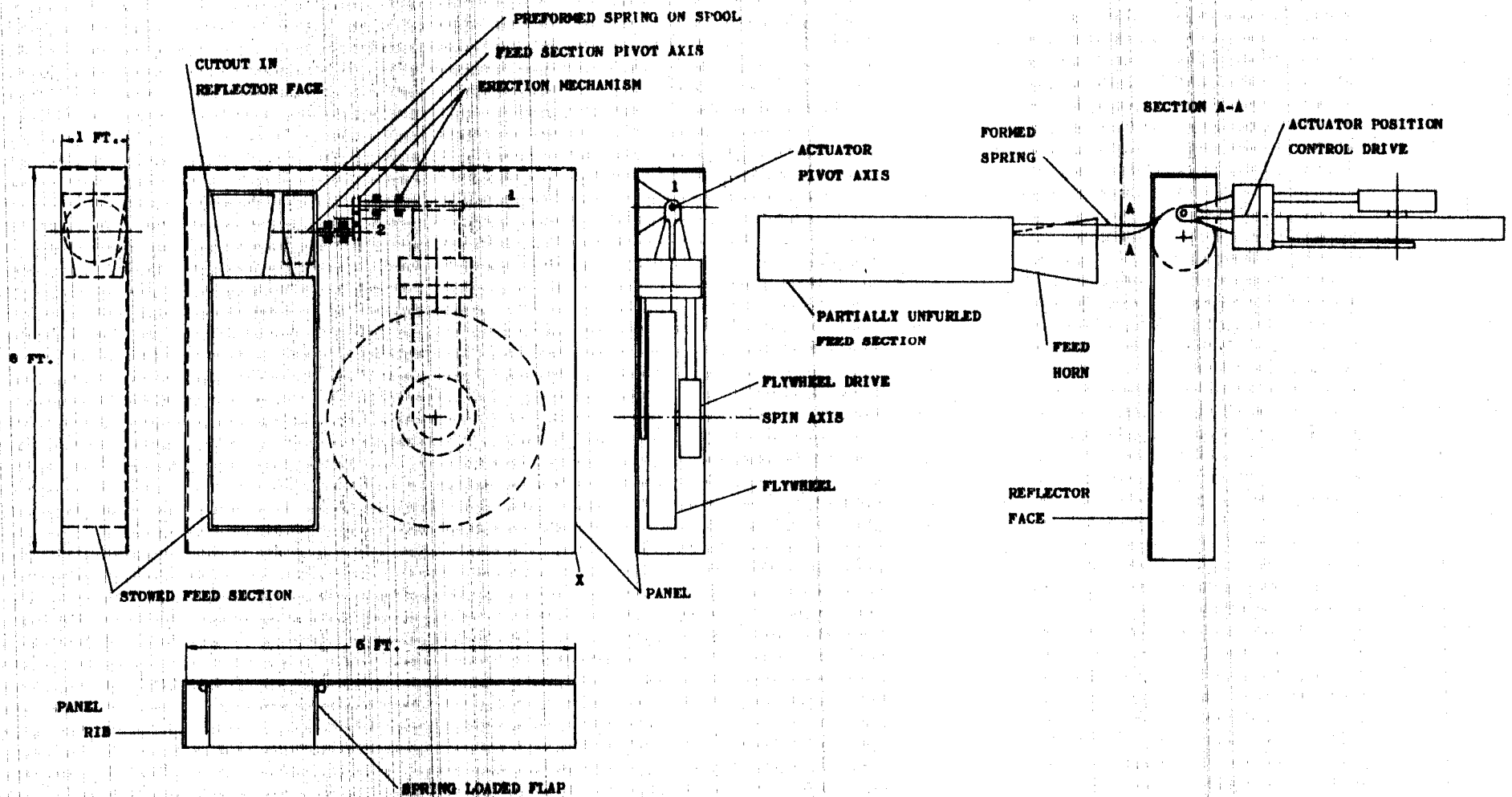


Fig. II-2. Structural panel, including an inertial actuator and feed action.

0.003 to 0.007 pounds per square foot) it is possible to obtain reflector surface adequate for operation at frequencies up to 10 Gc and corresponding structures plus reflector surface that have on the order of 80 to 90 percent open area. Because of this open area the thermal gradients from the front to back or edge to edge on the reflector structure tend to be minimized.

The structure in Fig. 1 has a uniform depth back structure. It is possible however to vary this depth as a function of distance from the center or any part of the reflector.

2.1 ACTUATOR AND FEED, STOWAGE AND DEPLOYMENT

As indicated in Fig. 2, the actuators consist of a flywheel, flywheel drive and an actuator position control drive. For stowage, the actuator is pivoted about pivot axis 1 parallel to the reflector face.

Each of the feed sections, consist typically of a feed horn, and sections of the receiver, transmitter or non-propulsive power systems. The feed section is pivoted about axis 2 which is parallel to the reflector face.

A motor or spring driven erection mechanism is provided for pivoting the actuator assembly about axis 1, toward the back side of the reflector and for simultaneously pivoting the feed section about axis 2, toward the front side.

The feed section and the preformed spring on which it is supported must pass through a cutout in the reflector face. The cutout is flanked by two flaps which spring close to form a continuous reflector surface when the feed section has been erected.

The feed section is driven by a preformed spring into assembly at the focus. As shown in Fig. 2, the spring, would in the flat on a spool, assumes a circular cross-section when unrolled. Guidance for the spring is provided

at the transition from the flat to circular form to direct the motion of the unfurling feed section toward the focus. When the four feed sections have reached the focus, a magnetic or mechanical latching may be used to guide and fasten the sections together.

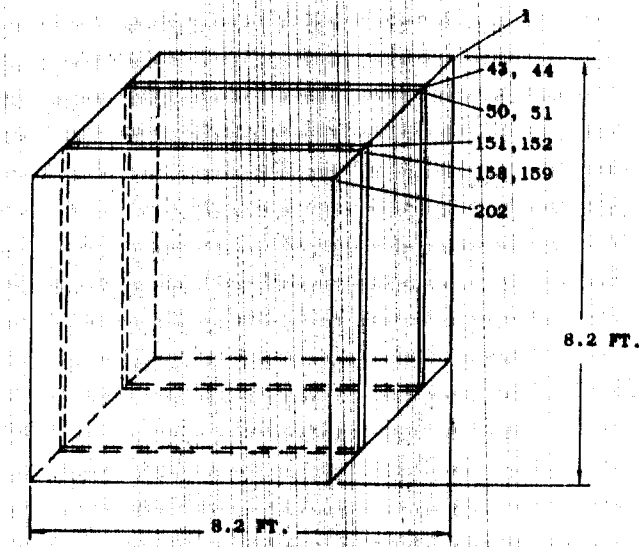
The stored energy in the rolled spring is used to actuate the unrolling action and the rate of unrolling may be controlled by a motor or rotary damper. If motors are used they may be employed when the antenna is assembled to adjust or continuously control the position of the feed relative to the reflector.

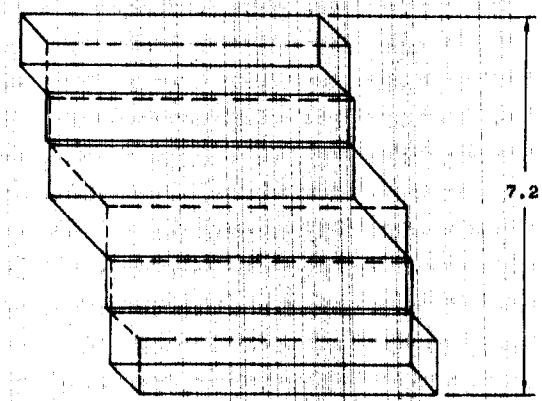
2.2 STOWED ANTENNA

The chosen panel shapes, and the manner in which the actuators and feed sections are mounted on four of these panels allow the entire antenna to be stowed as shown in Fig. 3. The numbers in Fig. 3 refer to sequence in which the panels are assembled, per Fig. 1, and label the ribless corner (point X in Fig. 2) of the panels.

The stack height in Fig. 3 is based on a 1/8 inch panel thickness in a direction perpendicular to the reflector surface and a stacking height of 12 inches for the four panels on which the feed and attitude actuator sections are mounted.

The means for fastening the antenna panels to each other may require that local fasteners be attached to edges and corners of the panels. These fasteners may have a minimum cross section dimension that is greater than the panel thickness. To prevent the fasteners from increasing the over-all stacking height, they are located at staggered positions along the panel edges and corners, and cutouts are appropriately provided along the edges and





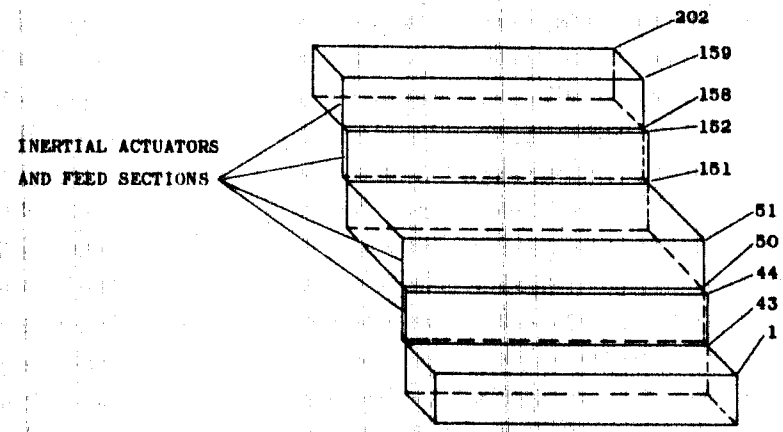


Fig. II-3. Outline of antenna package.

corners such that the fasteners and cutouts dovetail when the panels are stacked. The loss in structural rigidity due to these cutouts can be kept small by building up the panel structure around cutouts.

Since the 6 x 6 foot panels are relatively small sections of the 100 foot paraboloid, their curvature has a negligible effect on the height of the stack. Stand off bosses on the back side of the panel faces may be used to compensate for the reflector curvature in the stacked condition.

Excluding the four panels that mount the actuators and feed sections, approximately 85% of the material in the face and ribs of each panel is cut-out to reduce weight. The cutout face sections are replaced with very light weight screen mesh. The cutout rib sections are rigidized, where possible, by edge flanges. Flanges on rib edges parallel the reflector face and are turned out, away from the rib and face.

Using the above cutouts and aluminum as the construction material, the total estimated weight of the reflector panels is under 2000 lbs. (i.e. about 0.2 lbs. per square foot). This reflector can be built with a surface accuracy of at least 0.08 feet which make it applicable for frequencies up to 1.2 kmc. The heavier it is made or the tighter the surface tolerances, the higher the operating frequency.

Assume that the antennas must turn at a maximum rate of 10^{-2} rad. per sec. and that the flywheels having a radius of gyration of 1.7 feet are made of steel with a 100,000 psi yield strength. Then the weight of the actuator system will be under 400 lbs.

The volume allocated in the four feed sections allows for at least 2400 pounds of such equipment as a four horn monopulse feed, a communication and tracking receiver, command control transmitters, ground link communication equipment, a solar cell non-propulsive power system, a thermal control system, and data processing equipment.

3.0 REFLECTOR ASSEMBLY PROCEDURE

The kinematics of the RATIO assembly procedure is explained in this section. The mechanism for carrying out the procedure is described in Section 4.0.

3.1 BASIC MOTIONS

Four basic assembly motions of the panels are used to assemble the reflector. These are shown in Figs. 4 or 5. Fig. 4 outlines the basic motions with B as the moved panel, and A as the stationary stack. In effect A is the position of B before the motion has taken place. The motions to achieve the indicated relative panel positions are defined as I, IR, II and IIR. Motions I and II consist of linear translations of B with respect to A, while motions IR and IIR consist of linear and rotary translations. The same motions are shown in Fig. 5 with the B stationary and A experiencing the relative motion.

In Figs. 4 and 5, point a_1 on stack A corresponds with the point b_1 on panel B before B was removed from A. The point c is fixed with respect to A, and, in Fig. 5, c' is the initial position of c before the assembly motion has taken place.

A rotary actuator at point c, and attached to the stack A, carries an extendable boom which moves a second rotary actuator from point a_1 to point b_1. The second rotary actuator rotates the panel about a_1, as a_1 moves toward b_1.

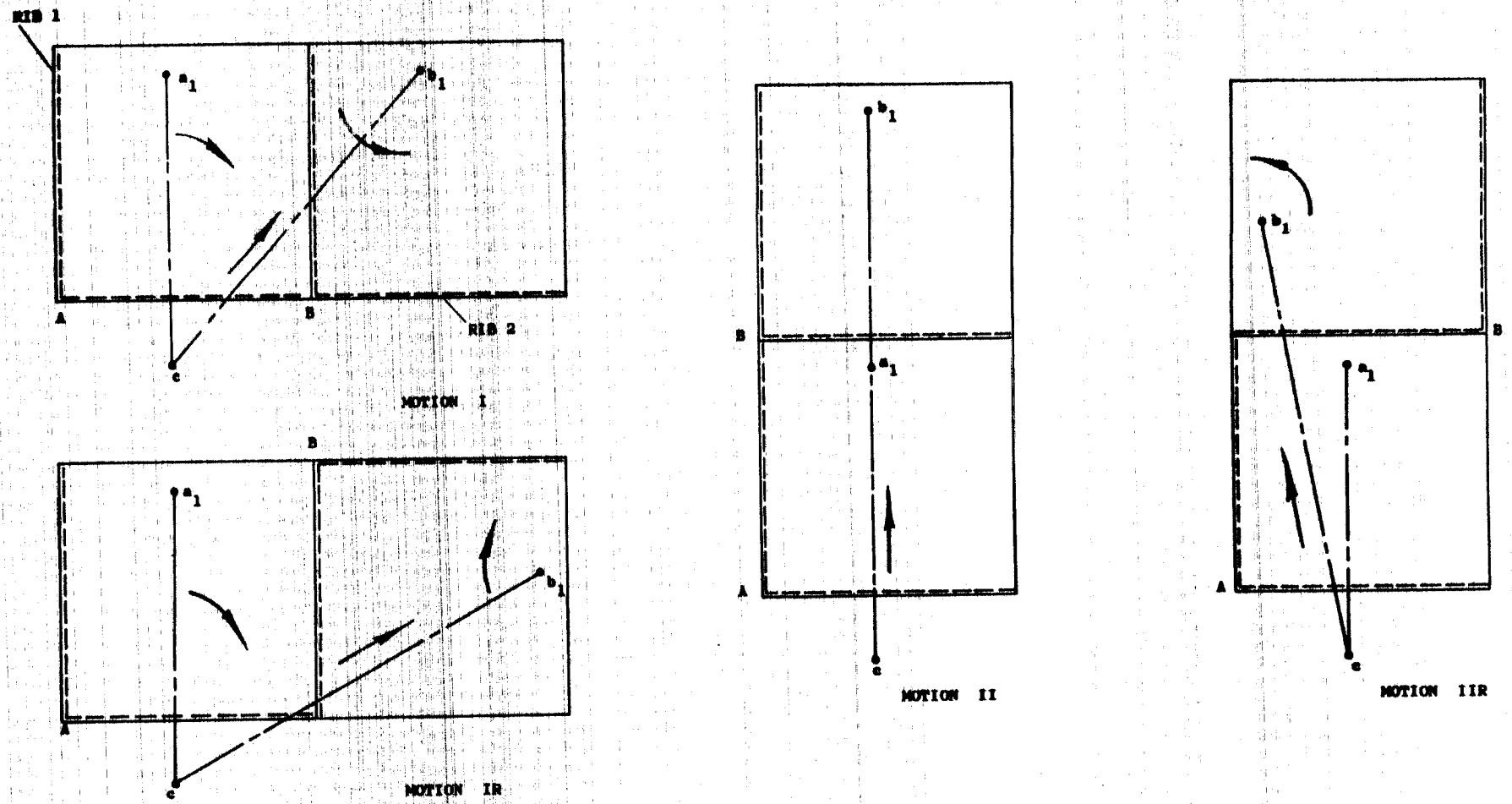


Fig. II-4. Four basic assembly motions, stack A stationary.

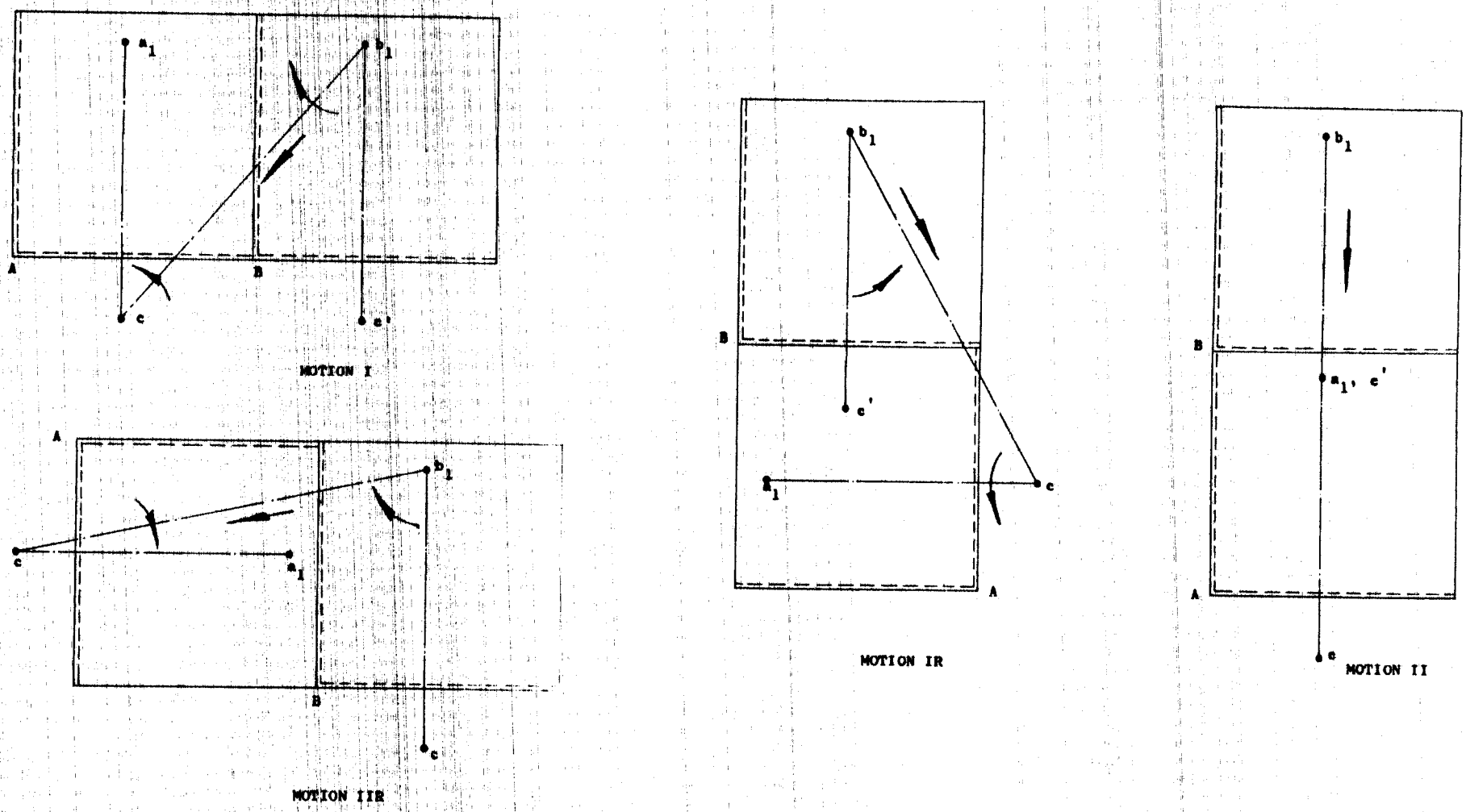


Fig. II-5. Four basic assembly motions, assembled panel B stationary.

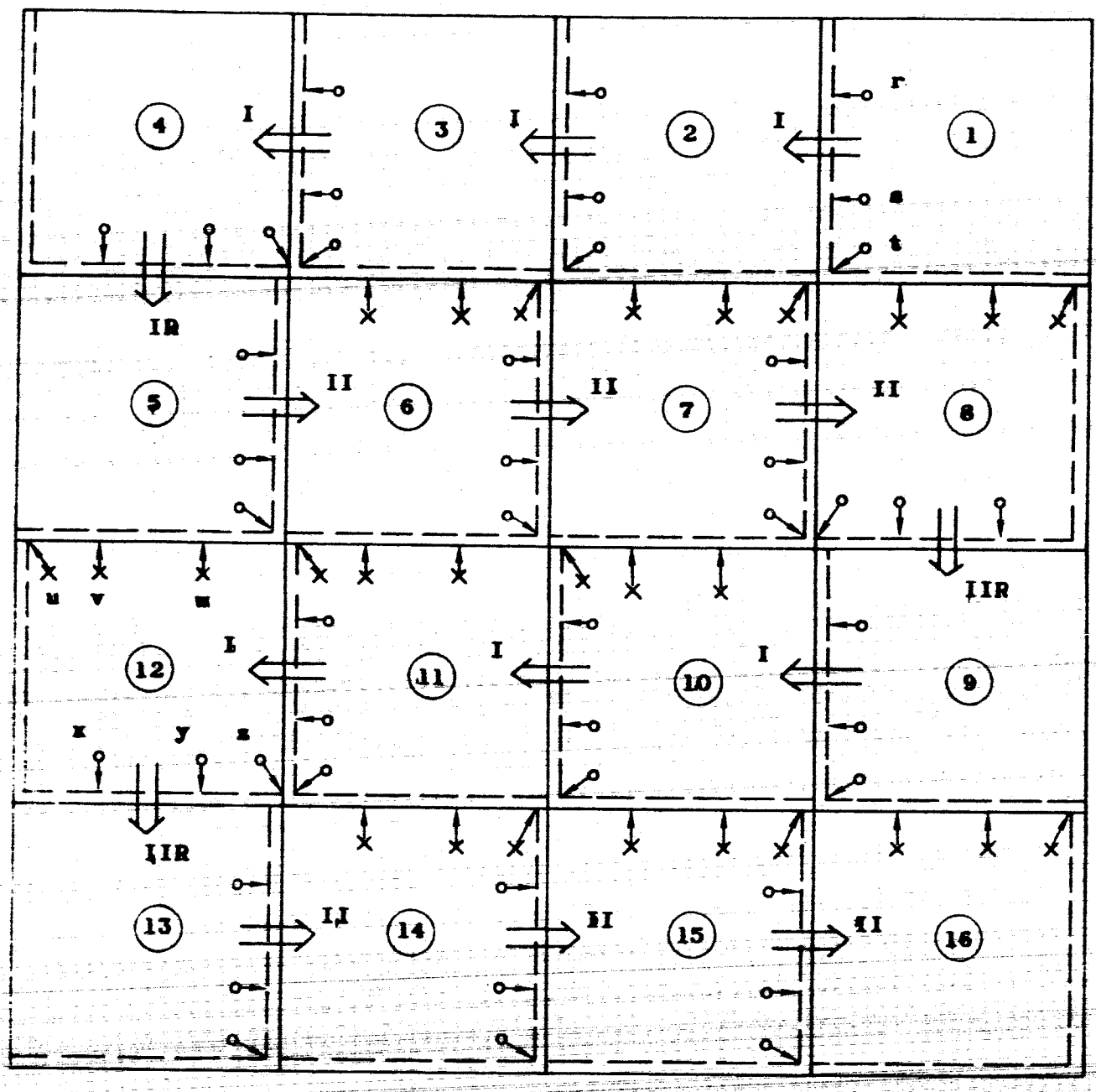
An example of the use of the basic motions to assemble a simple square panel is shown in Fig. 6. The panels are numbered in the order they are assembled. The manner in which the assembly grows can be visualized by fixing the panels B as in Fig. 5. It is seen that motion I is used for the right-to-left emplacements, and motion II for the left-to-right emplacements. IR is used for the transition from I to II, and IIR for the transition from II to I.

3.2 REFLECTOR CONTOUR

It is evident, because of motions IR and IIR, that the panel rows must sequentially terminate in pairs. This serves to explain the shape of the reflector contour shown in Fig. 1. The limitations that this imposes on the smoothness of the reflector contour can be reduced by contouring the edge panels. Thus, if such panels as 1, 7, 16, 27, 40, 69, 85, 118, 134, 163, 176, 196 and 202 in Fig. 1, are contoured, the edge irregularity can be, if desired, greatly reduced. The contouring is facilitated by the minimum requirements for rib re-enforcement of the edge panels.

3.3 PANEL FASTENING OF DEPLOYED ANTENNA

Looking at the face of a panel, see Fig. 7, identify the two ribs as rib 1 and rib 2, where rib 2 is clockwise with respect to rib 1. A-1, A-2; will refer to the face edges that border on ribs 1 and 2; and a-1, a-2 to the face edges on the opposite sides of and parallel to ribs 1 and 2. A-A, and B-B will denote the corners along which the two ribs intersect, and 1-1, 2-2 the other two rib edges parallel to A-A or B-B. The letters A and a are used to designate the moving panel (per Fig. 5) and B and b the stationary panel.



CODE: (1), (2), -- DESIGNATES THE SEQUENCE OF PANEL EMPLACEMENTS.

⟹ I, II, IR, IIR, INDICATES THE MOTION TYPES.

o—— INDICATES FASTENING ACTION AFTER MOTION I, IR, II OR IIR HAS TAKEN PLACE.

×—— INDICATES INITIAL FASTENING ACTION BEFORE MOTION HAS TAKEN PLACE.

Fig. II-6. Assembly program for emplacing panels.

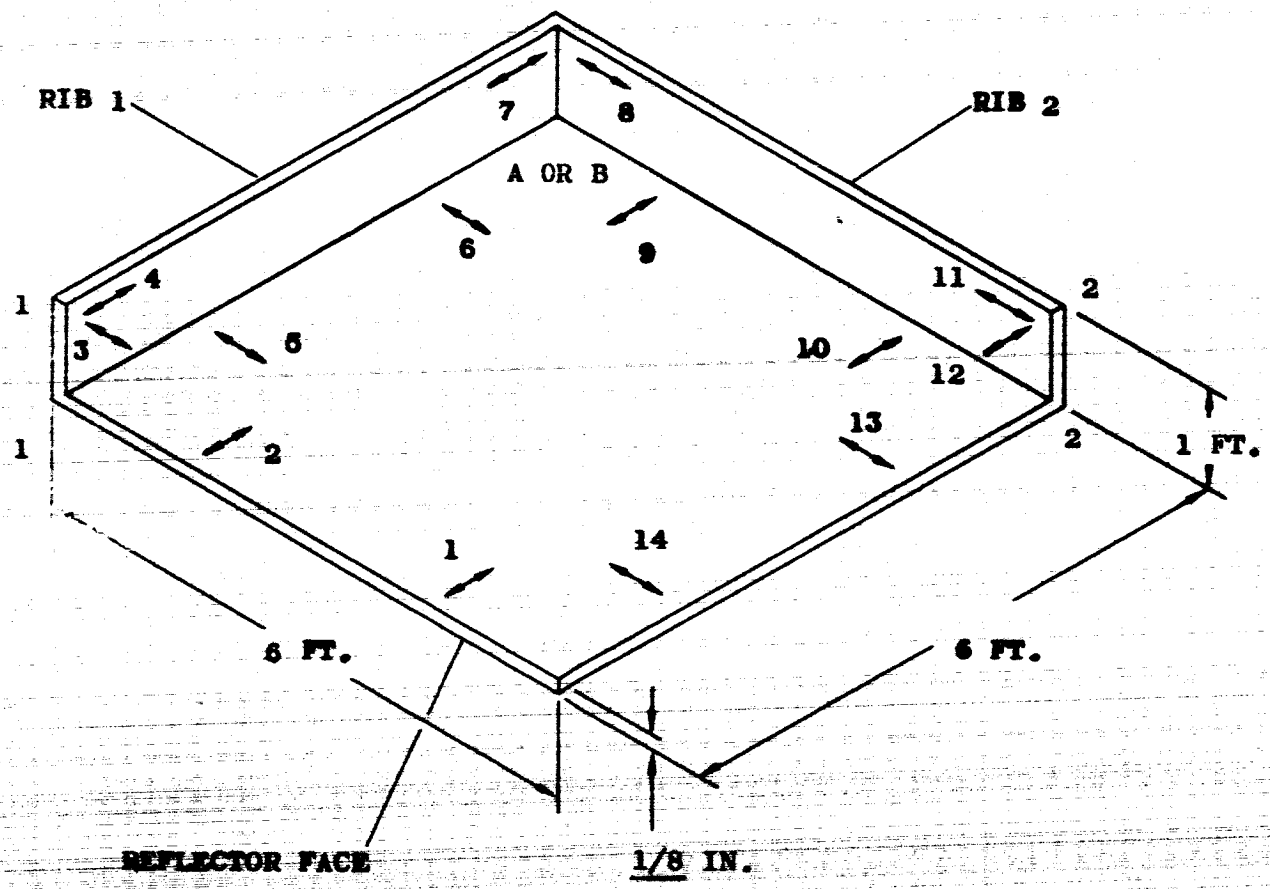


Fig. II-7. Locations and orientations of male or female fastener sections on a panel.

The panels may be fastened together between the face edges (i.e., between A-1 or A-2 and b-1 or b-2, also between B-1 or B-2 and a-1 or a-2), and between the rib edges (i.e., between A-A, 1-1, or 2-2, and 1-1 or 2-2, also between 1-1, or 2-2, and B-B, 1-1, or 2-2).

The fastenings that take place before and after emplacement of the panels, are indicated in Fig. 6. For example, in the case panel 1, fastening occurs at r and s between face edges A-1 and b-2, and at t between the rib edges A-A and 2-2. This action takes place after panel 1 has been removed from the stack located by the position of panel 2.

In the case of panel 12, the fastening action, v, w along a-1 and u along 1-1 takes place when panel 12 is initially emplaced and panel 13 has not moved. The fastenings at x, y, z on panel 12 occur after panel 13 has been emplaced.

The fastening actions may be accomplished by locally actuated fasteners, such as latches, captive nuts, bolts, rivets, explosive edges, etc. or by non-locally actuated fasteners, such as bayonet fittings, clips, keying sections, etc. as explained in Section 4.0. A panel frame that mounts the panel grippers are used to fixture each panel as it is transported according to basic motions I, IR, II or IIR. The panel grippers may also be employed to locally actuate fasteners. In the case of the non-locally actuated fasteners the fastening forces are applied through the equipment that transport the gripper frame.

It is evident from Fig. 6 that to achieve the various fastening actions, matching male and female sections of the fasteners must be appropriately positioned on the panels. Fig. 7 indicates the 14 possible locations and orientations for the male or female fastener sections. Fig. 7 also shows

that at any one time, either six or three fastening actions can be used on the peripheral panels, and that six fastening actions can always be used on each internal panel.

3.4 PANEL FASTENING OF STOWED ANTENNA

Some of the panel fasteners, used for assembling the deployed antenna may also be adapted for fastening the panels to each other in the stowed condition. These fasteners would logically be of the locally actuated type such that they may be disengaged to release the panels before panels are transported to their emplacement positions.

The fastenings between panels in the stowed condition can significantly contribute to re-enforcing the structure for handling boost-phase shock and vibration loads.

4.0 "RATIO" AUTOMATIC ASSEMBLY MACHINERY

One form of RATIO automatic assembly machinery is outlined in Figs. 8 and 9. This machinery has the following components:

4.1 GRIPPER-FASTENER FRAME

This mounts four actuated panel grippers which engage the panel at the bottom of the antenna package. When the engaged panel has been transported to its assembly position, via the gripper frame, the panel is secured in its emplaced position and the grippers disengage allowing the frame to return for another panel.

If locally actuated fasteners are used the grippers first serve to disengage the fasteners that hold the lowest panel to the stack. Then

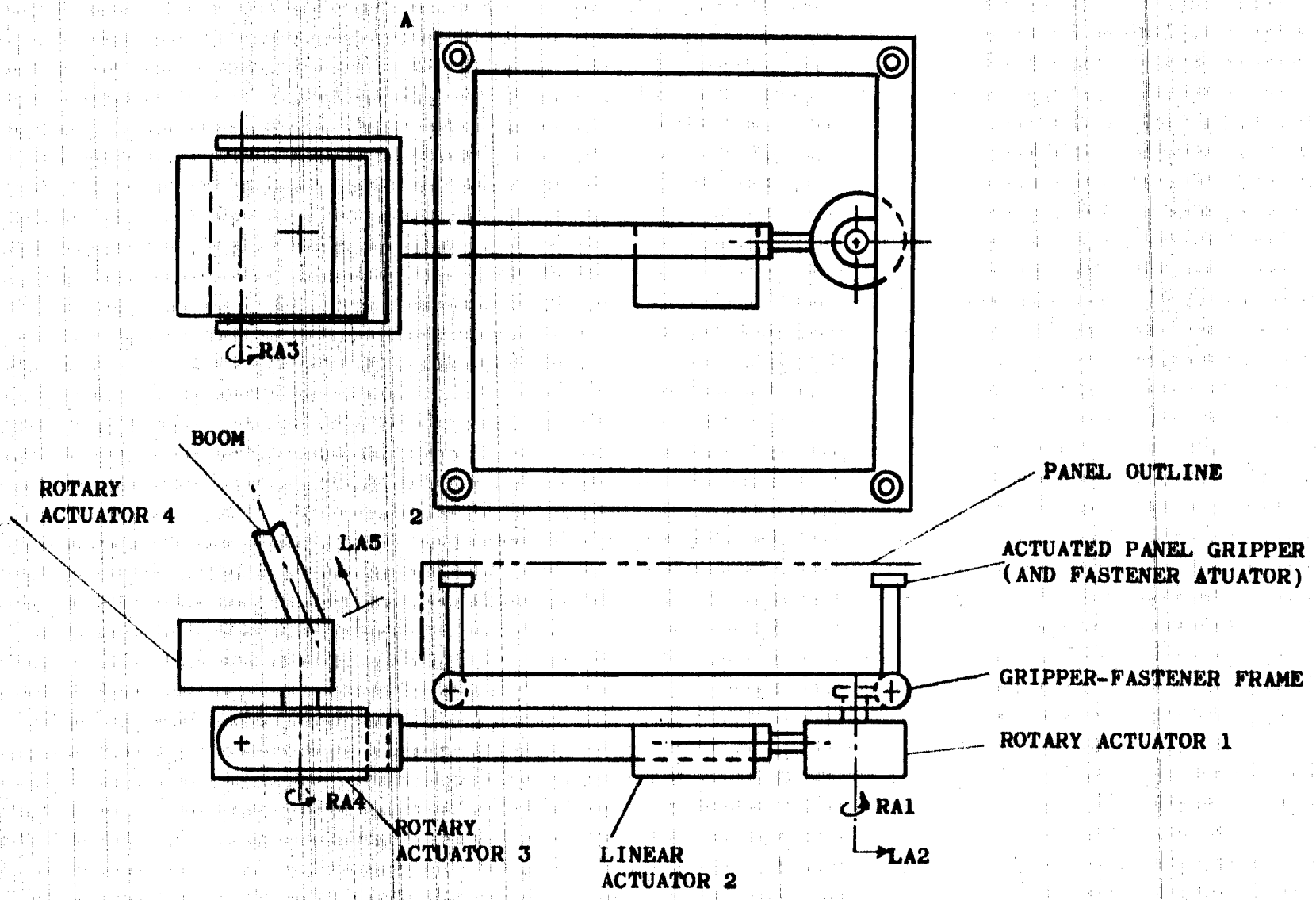


Fig. II-9. Gripper-fastener assembly.

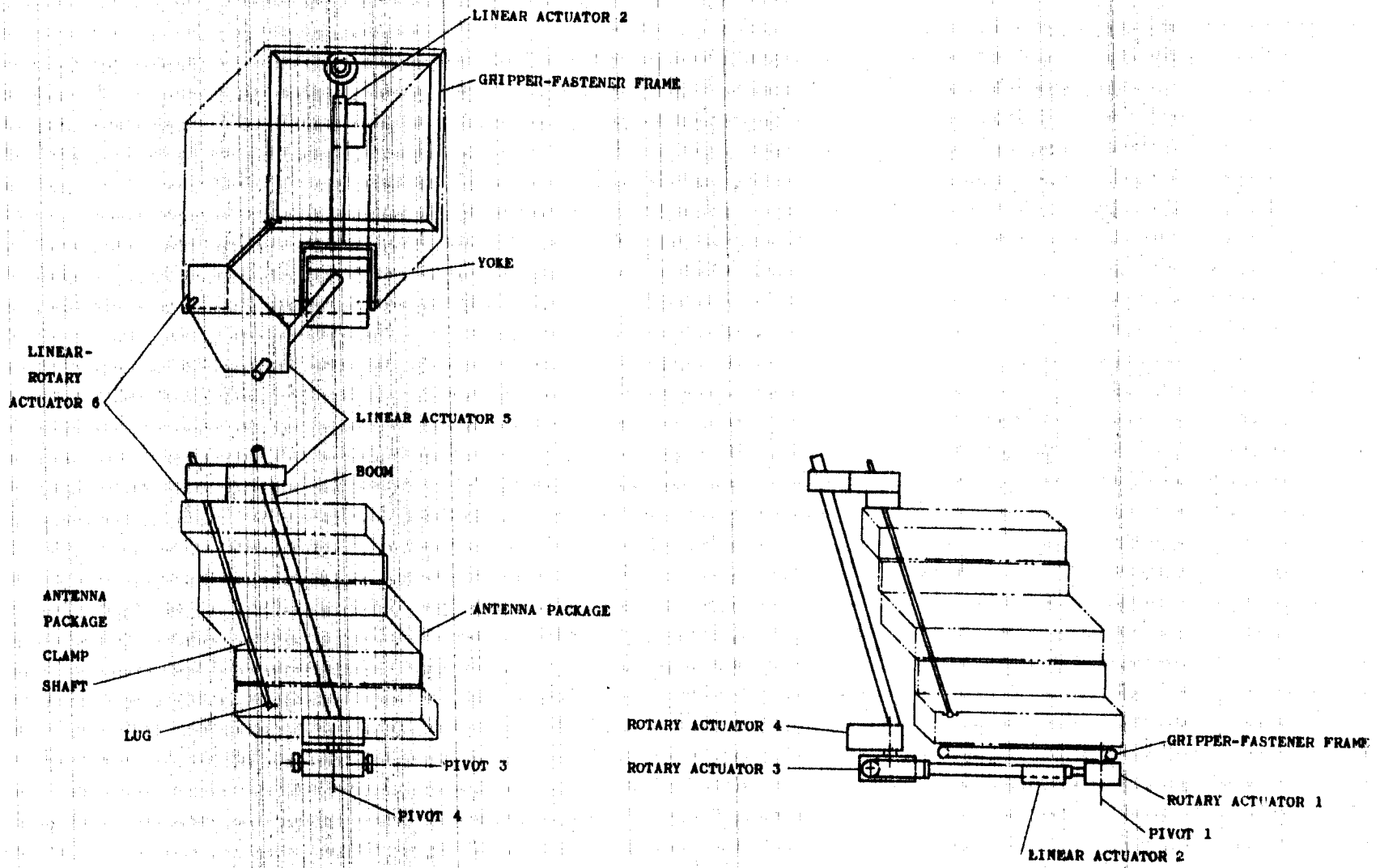


Fig. II-8. RATIO automatic assembly machinery.

when the panel has been transported to its assembly position the grippers act to secure it there.

4.2 ANTENNA PACKAGE CLAMP SHAFT

Whether, or not locally actuated fasteners are used to hold the antenna package together it may be desirable to maintain additional integrity in the package by clamping it together. The clamp shaft with a lug at its lower end and passing through the antenna package serves this purpose. The clamp shaft passes through clearance holes in each panel and the lug at its end engages the lowest panel in the antenna package. Rectangular or key shaped cutouts, through which the lug can pass are provided in each panel. The orientations of the cutouts are alternated between adjacent panels such that when the lug has passed through one panel it cannot pass through the succeeding one without being turned about the clamp shaft axis.

In operation the clamp shaft releases one panel at a time to the gripper fastener assembly.

4.3 GRIPPER FRAME TRANSPORT ACTUATORS

The linear and rotary actuators 1 through 5, in Figs. 8 and 9, cooperate to transport the gripper frame such that basic motions I, IR, II and IIR can be generated.

The gripper frame is mounted on actuator 1 and pivot 1 corresponds to point a, or b, in Figs. 4 and 5. Likewise pivot 4 of actuator 4 corresponds to point c in these figures. The linear motion between a, or b, and c is generated by actuator 2.

The actuator 3 pivots the gripper frame to initially separate the lowest panel from the antenna package. When the panel has been transported to its assembly position the pivot motion is reversed to align the edges of the mating panels. After the panel has been assembled actuator 3 further pivots the gripper frame so that the grippers, on their return motion, can pass over the rib of the assembled panel.

As the panels are removed from the antenna package the gripper-fasten assembly must be moved up to remain at the correct level with respect to the lowest panel in the stack. The support boom driven by actuator 5 serves this function. At the completion of each basic motion actuator 5 advances the boom by one panel thickness. In the case of the panels that mount the feed and attitude control actuators the boom is advanced a distance equal to the length of the feed or actuator package.

As the panels are removed from the antenna package, the initial lateral position of the gripper frame with respect to the boom may change to properly position the gripper frame with respect to lowest panel in the package. It is possible to achieve this initial position by limit switch controlling actuator 2 on its return motion. Sensors that contact the lowest panel may be used to activate these limit switches.

5.0 OVERALL CYCLIC PERFORMANCE

The (basic) motions I, IR, II, IIR and associated gripper fastener events are described as a function of time in Fig. 10.

The angular rotations of actuators 1, 3, 4 and 6 are denoted by RA1, RA3, RA4, and RA6, and linear motions of actuators 2, 5 and 6 by LA2, LA5, and LA6, as shown in Fig. 9.

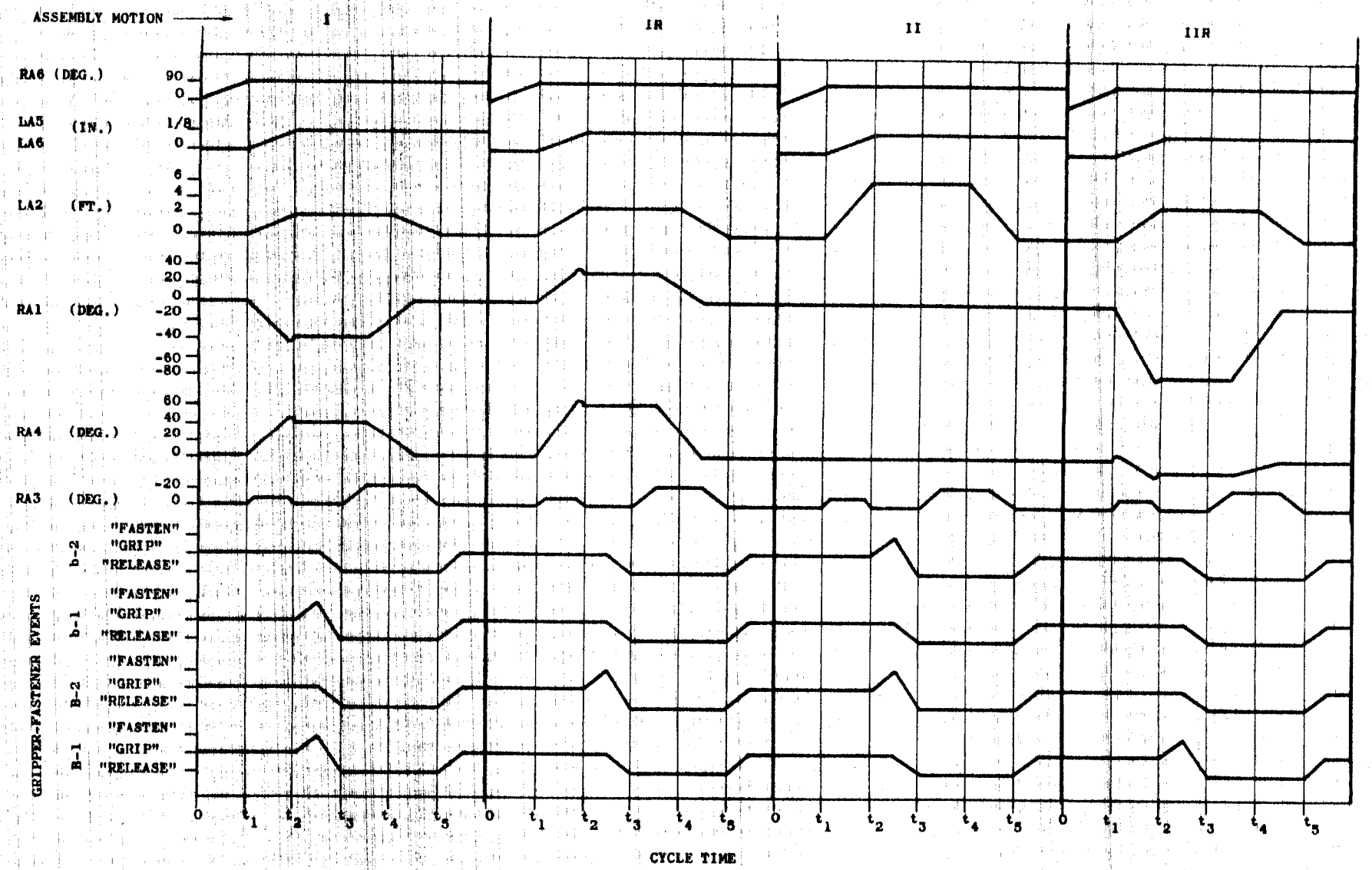


Fig. II-10. Operations cycle diagram.

The states of the gripper-fastener assembly are denoted as "release", "grip", "fasten", and are referenced with respect to the sides of the panel on which they occur. Thus B-1, B-2, b-1 and b-2, as explained in Section 2.3 (and Fig. 7), designate the sides of the panel on which the fastening takes place. Here when the fastening action is indicated along a panel face edge it is understood to be accompanied by fastening action on one of the closest rib edges.

The following sequence of actuator motions and gripper-fastener events occur for basic motion I (see Fig. 10).

(o to t_1) The actuators are initially at their starting positions, and the gripper fastener mechanism is in a state "grip". The first motion is RA6 of the clamp shaft to release a panel at t_1.

(t_1 to t_2) Between t_1 and t_2 the boom and clamp shaft are advanced a panel thickness by LA5 and LA6, and the actuator motions RA1, LA2, RA3, and RA4 cycle to carry a panel from the antenna stack to its assembly position. The small RA3 motions are used to depress and then raise the level of the panel during the time it is being translated and rotated by LA2, RA1 and RA4. The over-shoots in RA1 and RA4 produce a butting final approach between mating panels.

(t_2 to t_3) At t_2 the panel has been emplaced. At t_3 the gripper-fastener releases the assembled panel and commences to return to its starting position. Since it must now pass by a panel rib the rotations RA3 are relatively large. Both the forward and reverse motions of actuators 1 to 4 are

synchronized to avoid interference with the antenna package. At t_6, at the completion of the return motion, the "grip" state exists and the cycle can now be repeated.

5.1 MOTION CONTROL PROGRAMMER

It is possible to control the actuator and gripper-fastener cycles by a programmer. The programmer may select the cycle (i.e., motions I, II, IR, or IIR) and initiates the first phase of the cycle. Sensors may monitor the termination of each phase. In the event that a motion or event is not completed due to a malfunction, the programmer may initiate an override or a recycling of that motion or event. The override is permissible when the malfunction does not affect panel handling or when the failure, as in a fastener, does not undermine the integrity of the assembled structure. Redundancy in the grippers, fasteners and drive motors may be provided to enhance reliability.

The programmer may also be used to recycle one or more complete basic motions that precede one in which a failure has occurred. Thus if the "fasten" state does not occur, possible due to improper panel seating, the complete recycling of the previous basic motion may result in proper seating and allow for successful deployment.

5.2 AT COMPLETION OF DEPLOYMENT

When the reflector assembly has been completed the assembly equipment may be driven away from the last panel by chemical or mechanical means or if it does not interfere with the antenna performance it may remain attacned to the last assembled panel.

6.0 ASSEMBLY EQUIPMENT POWER AND WEIGHT

The peak power requirement for an individual actuator occurs when the inertia of the assembled antenna, as it appears at the actuator axis, is equal to the inertia of the unassembled antenna package. Assuming non-conservative drives it is desirable to minimize this power by using the lowest possible assembly speed that avoids coulomb friction (or stiction) in the drives and is consistent with the antenna operational requirements.

Assuming a one minute cycle time to install a panel, or an over-all assembly time of about four hours, approximately 800 watt-hours are required to handle the assembly inertial loads and 200 watt-hours are estimated for the fastening actions.

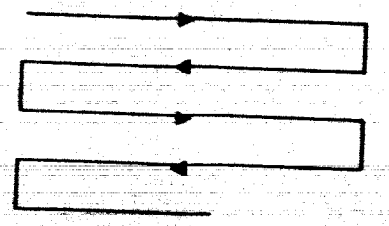
A 30-pound silver zinc battery pack should be adequate for these energy requirements.

It is estimated that the over-all weight of the RATIO automatic assembly equipment, including the battery pack, is under 150 pounds. This is approximately 7.5 percent of the reflector structure.

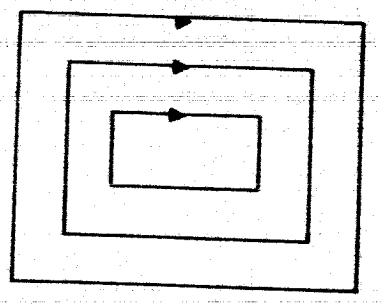
7.0 ALTERNATE PANEL ASSEMBLIES

The described panel assembly procedure results in the sequence of panel emplacements that follow a serpentine. This and alternate assembly sequences are shown in Fig. 11.

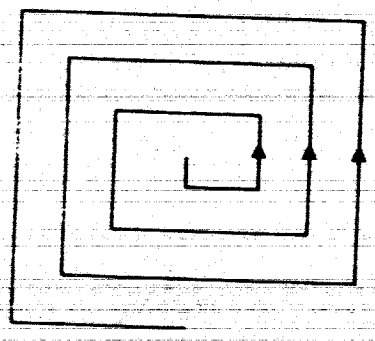
An examination of square and square spiral assembly sequences, shown in Figs. 11b, and 11c, indicate that only two rows or two columns of panels may be emplaced with a continuous back rib structure if only four basic motions are used. In the case of the square spiral, the number of basic motions, must be increased to six to produce continuous rib-to-rib butting.



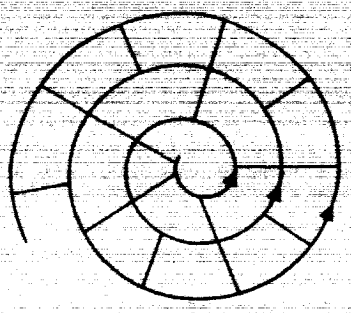
(a) SERPENTINE



(b) SQUARE



(c) SQUARE SPIRAL



(d) CIRCULAR SPIRAL

Fig. II-11. Alternate panel assembly sequence.

The circular spiral sequence in Fig. 11d suffers from: (a) irregular sections which do not readily stack, (b) continuously different (although closely related) assembly motions, and (c) a discontinuous back rib structure.

The serpentine sequence in Fig. 11 has none of the disadvantages of the other panel assemblies.

8.0 SUMMARY OF FEATURES OF "RATIO" AUTOMATICALLY ASSEMBLED ANTENNA STRUCTURES

(a) The packaging density can be very high. Theoretically, if no cut-outs are used on the panels (in which case the panels could be made much thinner), the packaging density is equivalent to the density of the structural material.

(b) In the stowed or packaged state the panels are nested, and can be fastened together, to greatly minimize the structural rigidity needed to handle shock and vibration loads during boost.

(c) In deploying the antenna no flexing in the structural members is required. The structural panels which are prefabricated to fit together in a stress free condition against a ground mold are assembled in a stress free condition in orbit.

(d) The assembly machinery operates at very low speed and very low driving accelerations. The dynamics of the machinery in terms of the machinery development or the loads it imposes on the antenna structure (during assembly) are negligible.

(e) The assembled antenna has a systematic, easy-to-analyze back rib structure. The panel ribs may be varied to taper the over-all structure or to smooth the contour.

(f) The sizes of the antenna structures are considerably in excess of sizes achievable for comparable antennas for unfurling and inflating methods.

(g) The estimated weight of the assembly equipment (including its power supplies and controls) for a single-package, 100-foot, 2800-pound antenna is under 150 pounds.

(h) Unlike the unfurlable and inflatable approaches the same deployment concept applies to a wide range of structural sizes.

(i) The structure and the assembly equipment uses available materials, and components.

(j) There are only four basic assembly motions with which the antenna is assembled. These systematic motions may be open-loop controlled by limit switch and relay logic.

(k) The reliability of the assembly equipment may be enhanced by redundant drives and simple mechanical components.

(l) The dimensional integrity is generally not effected by micrometeorite bombardment.

(m) The large mechanically open structural area minimizes thermal gradients due to solar radiation.

(n) On board equipment, such as inertial actuators, may be permanently mounted, the panels to be in a proper operating position when the antenna is deployed.

(o) The assembly equipment could be controlled or supervised by a man in orbit to significantly enhance its reliability. (Note: The structure is likely to be so fragile that the man would best handle

it by means of the assembly equipment in the event of a partial equipment failure.)

(p) The antenna assembly is a repeatable and reversible process. The full-scale antenna can be assembled and dimensionally checked out on a (ground based) paraboloidal frame or mold. The fits between the panels can be adjusted so that the antenna lies on the mold in an unstrained condition.

III. PRELIMINARY ANALYSIS OF A SIMPLIFIED PLANAR MODEL

(By P. Slysh, deflection computations by E. J. Kaminski)

1.0 GENERAL.

Before proceeding with the detailed analysis of RATIO antenna structures it is desirable to perform a preliminary investigation of these structures to determine: (a) where possible, the qualitative or quantative characteristics of the structures in terms of their effects on the antenna r-f performance and maneuverability, (b) the significant and negligible parameters, and (c) the types and ranges of structural and r-f parameters that should be investigated.

In the following sections simplified models are defined, the methods of analysis are outlined and justified, and preliminary parametric data on the trade-offs beyween the structural and r-f performance features are displayed.

2.0 DEFINITION OF MODEL.

One quadrant of a simplified, planar model of the RATIO antenna, to be used in the analysis of the next section, is shown in Figs. III-2 and III-2a. This model has the following features:

2.1 SYMMETRY.

The periphery of the reflector has been chosen to give the structure eight-way diametral symmetry. This symmetry significantly minimizes the complexity of the structural deflection analysis. The actual reflector configuration (Fig. III-1) has only two-way symmetry because of geometrical factors in the procedure for automatically assembling the reflector panels.

2.2 FIXED NUMBER OF PANELS.

The antenna in Fig. III-1 has 202 panels (i.e. squares) in the reflector structure and in Fig. III-2 there are 208 panels. Approximately these numbers of panels are necessary, based on preliminary considerations in Ref. (1), to cause the stowed stack of reflector panels to roughly form an equal-sided parallelopiped. In practice, it is possible that panel thickness variations or specific packaging requirements, say for a non-equal-sided parallelopipeds (i.e. possible due to specific envelope limitations of booster nose cone), may effect the number of panels that should be used. To reduce the total number of in-orbit assembly operations, it may also be desirable to reduce the number of panels to the smallest possible number (if this does not unreasonably complicate the automatic assembly equipment).

While the above and other factors influence the number of panels into which the reflector should be subdivided (and entail tradeoff studies of their own) it has been decided, at this time, to hold the number of reflector panels in Fig. III-2 at 208.

2.3 ROTATION AXES.

For purposes of this study the antenna is actuated about either the O-A or O-B axis by a reaction flywheel system in which the spin axes of the flywheels are parallel to either the O-A or O-B axis. There will be no gyroscopic torques acting on the structure. The actuation about the O-A and O-B axes will generate representative structural deflection patterns.

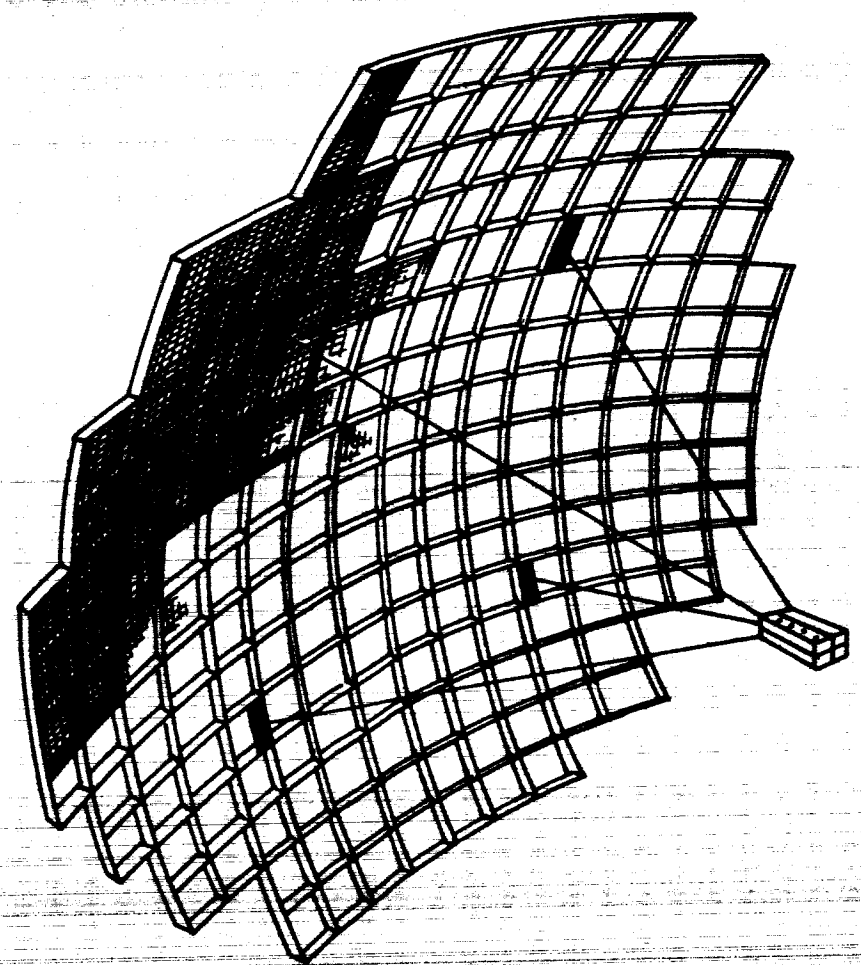


Fig. III-1. RATIO antenna, panel construction.

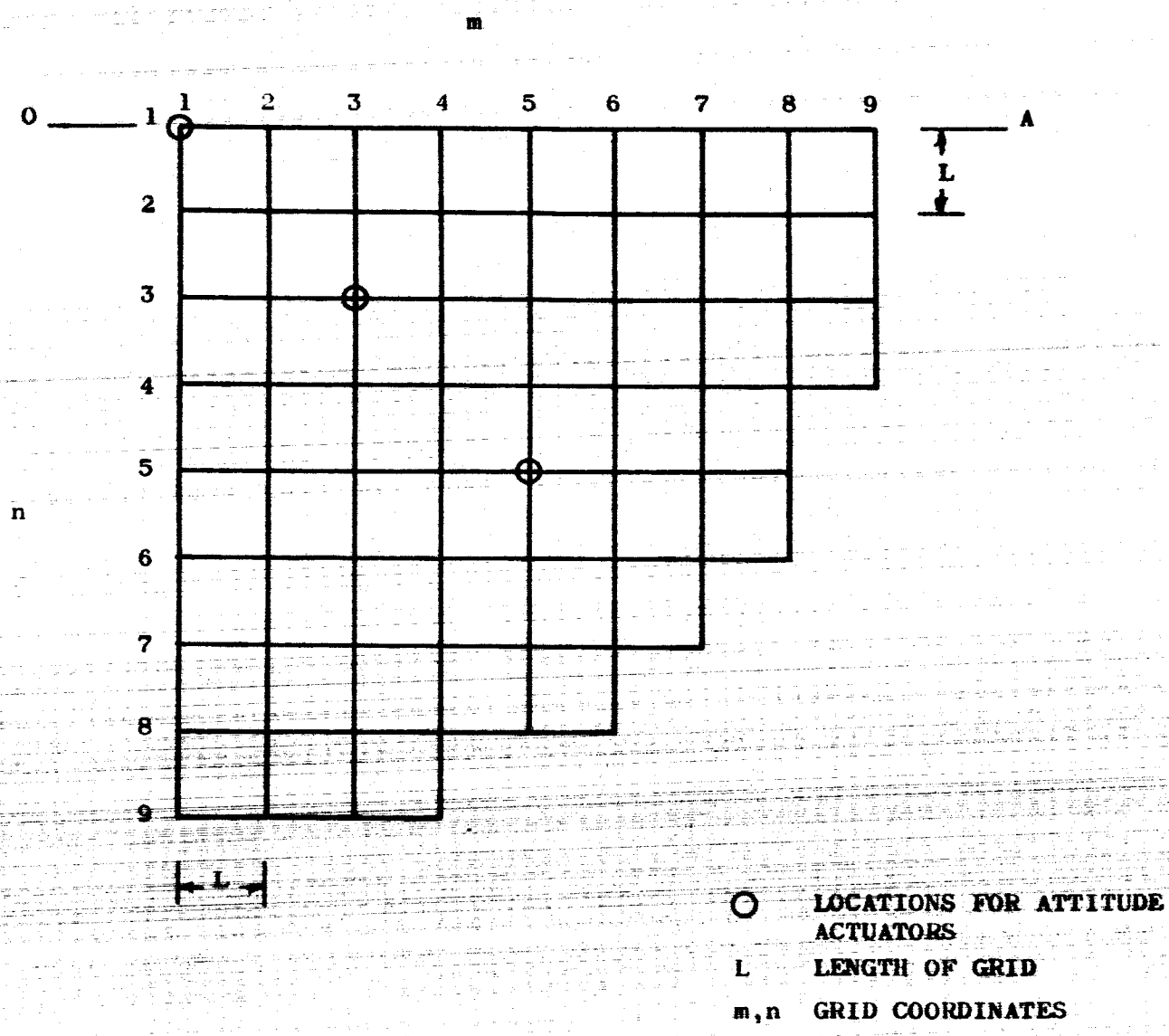
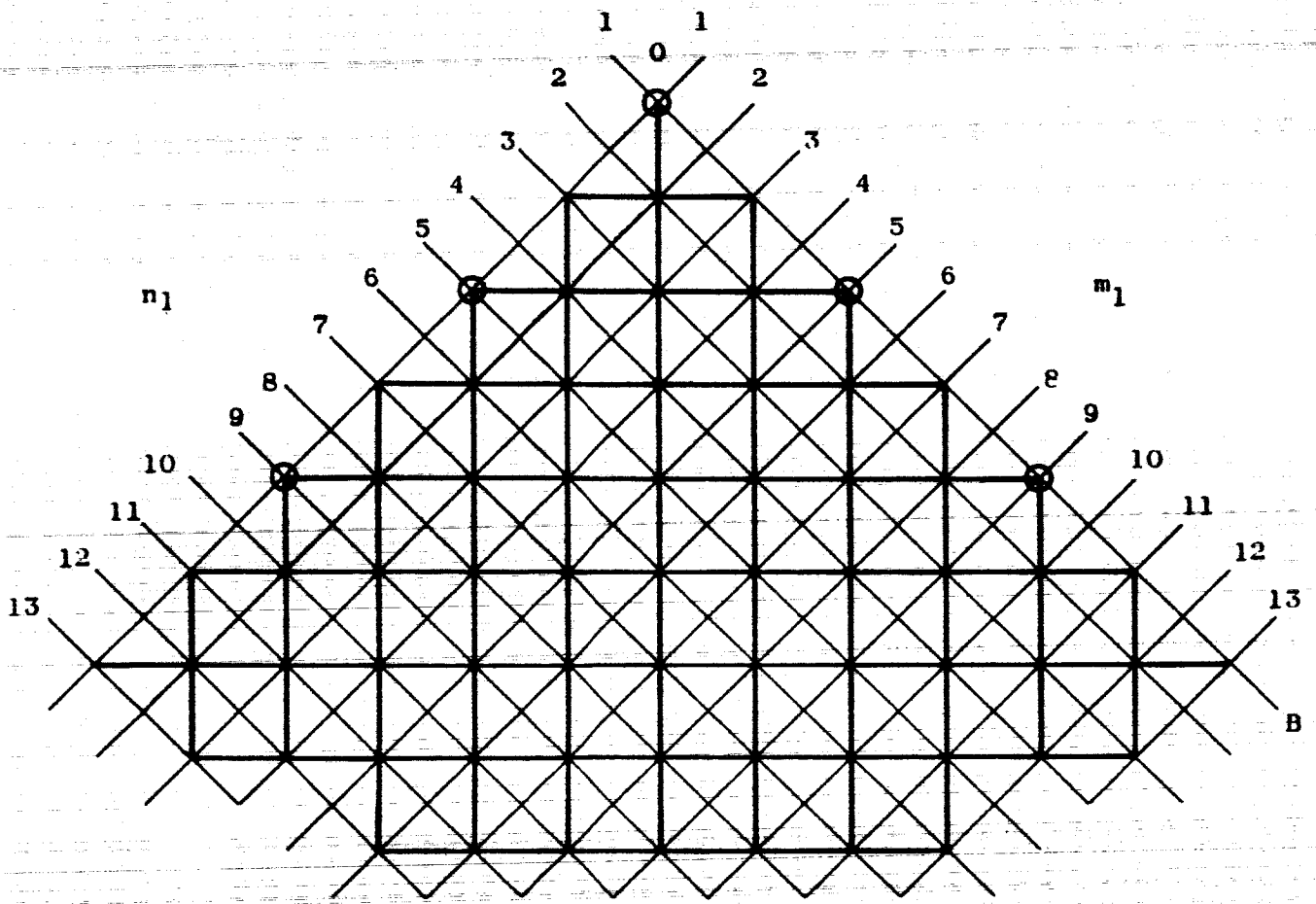


Fig. III-2. One quadrant of a planar model showing grid coordinates for rotation about the O-A axis.



○ LOCATIONS FOR ATTITUDE ACTUATORS

L LENGTH OF GRID

m_1, n_1 GRID COORDINATES

Fig. III-2a. One quadrant of model showing grid coordinates for rotation about the O-B axis.

2.4 ON-BOARD MASSES AND THEIR DISTRIBUTION.

The mass of the r-f feed, its support structure, and its electronics, as well as the attitude actuators plus their controls and non-propulsive power supply are included in the locations for the attitude actuators shown in Fig. III-2. Four typical distributions for these masses will be considered:

Case 1, All of the masses located at the (1,1) grid coordinate point (in Fig. III-2).

Case 2, The masses equally distributed at the (3,3), (-3,3), (3,-3), and (-3,-3) points.

Case 3, The masses equally distributed at the (5,5), (-5,5), (5,-5), and (-5,-5) points.

Case 4, The masses equally distributed at the (3,3), (-3,3), (3,-3), (-3,-3), (5,5), (-5,5), (5,-5), and (-5,-5) points.

The inclusion of the feed mass with the actuator mass is, in part, justified by the fact that the feed support structure is likely to be mounted on the reflector at the same structural junctions on which the actuators are mounted. (In Case 1, a pylon feed support is implied; in Cases 2 and 3, tetrapod supports are implied; and in Case 4, an octapod support is implied.) This first order accounting for the mass of feed is assumed, at this time, to be dissociated from such factors as the focal-length-to-diameter ratio, the possible use of actuators located on the feed or feed support structure, etc.

The chosen locations for the actuators are such that approximately equal mass moments of inertias result about the turning axes in the plane of the aperture.

2.5 LUMPED PARAMETERS.

A lumped constant spring-mass system is assumed for the structure in Fig. III-2. The structural masses, as well as the mass of the attitude actuators, feed, etc., are lumped at the structural junctions. Massless, uniform-crossection beams are assumed between the structural junctions.

2.6 SHEAR, FLEXURAL AND TORSIONAL STIFFNESS.

The chosen beam properties are such that the beam stiffness due to deflections in shear is negligible compared to the flexural stiffness about the beam principal axes. The torsional stiffness of the beam and the flexural stiffness at right angles to the beam prinicipal axis are also negligible.

2.7 PARASITIC AND LOAD-CARRYING STRUCTURAL MASSES.

Parts of the structure are taken to be parasitic, or non-load carrying. These include: the screen on the reflector surface, the web sections of the beams, bolting sections, and fasteners. The flange sections forming I-beams through the structure are assumed to be the load carrying sections.

2.8 DEFLECTION LIMITED STRUCTURE.

Reflector distortions may be caused by structural deflections due to actuator reactions, manufacturing and assembly tolerances, thermal stress, and creep in the structural material. Only

structural deflections due to actuator reactions are considered here. The structure is deflection limited. The operation stress levels are assumed to be so low that possible web crippling in the beams can be ignored.

2.9 VARIABLE STRUCTURAL PROPERTIES.

The beams in Fig. III-2 can have the same or varying cross-sectional properties over the entire structure. However, between any two structural junctions the properties are assumed constant.

2.10 INERTIAS OF STRUCTURAL AND ON-BOARD MASSES.

The angular inertias of the lumped masses (including the actuators and feed) about their centers of mass are neglected.

2.11 STRUCTURAL BEAM LENGTHS.

All beams have the same length. This is consistent with the procedure for automatically assembling the antenna in Ref. (1). The equivalent of structural beam length variations can be obtained by varying the beam crossections.

3.0 METHOD OF ANALYSIS.

In the following sections the approximate model is defined in greater detail and relationships are established for trade-off studies of the more significant structural and r-f parameters.

3.1 DEFINITION OF TERMS.

a_A, a_{FW}, rad/sec^2, angular accelerations (slewing rates) of the antenna and flywheel about the O-A or O-B axis

A, in.^{2}, load carrying crossection of structural beam

B, in., total depth of structural beam

D, in., average diameter of the reflector

d, in., weighted rms deflections at the structural junctions in the direction of a normal to the plane of the aperture

E, psi, modulus of elasticity of structural material

F, lbs, force acting at structural junction

g, in./sec^2, gravity acceleration = 387

G, psi, shear modulus

I, in.^{4}, principal section moment of inertia of beam

I_o, I_1, in.^{4}, I at respectively the center and edges of a reflector

I_A, I_{OA}, I_{OB}, in-lb-sec^2, moment of inertia of the antenna about the O-A and O-B axes

K, lbs/ft^2, average weight per unit of reflector surface area for the load-carrying and parasitic parts of the antenna structure

$k_A = M_A/M_T$, $k_F = M_F/M_T$, $k_S = M_S/M_T$, the fractions of the total antenna mass, M_T, in the masses of the actuators, M_A, feed, M_F, and structure, M_S , $(k_A + k_F + k_S = 1)$

$k'_{AF} = (M_A + M_F) / M_S = (1 - k_S) / k_S$

$k_{S1} = M_{S1} / M_T$, $k_{S2} = M_{S2} / M_T$, the fractions of the parasitic mass of the structure to the load carrying mass of the structure

$k'_{S1} = M_{S1} / M_S = M_1 / M$, $k_{S2} = M_{S2} / M_S = M_2 / M$, the fractions of structural mass in the masses M_{S1} and M_{S2}

k_2, the number of structural members that meet at a structural junction

$k_o = r_o / B$, principal normalized radius of gyration of beam crossection

L, in., length of a grid member

m, n, coordinate designations for the structural junctions when the antenna is driven about the O-A axis, see Fig. 2; m_1 , n_1, see Fig. 2a

$M = M_1 + M_2$, lb-sec^2/in., mass of half of a beam including the associated parasitic mass, M_1, and load carrying mass, M_2

$M_A = M_{FW} + M_P$, lb-sec^2/in., the mass of the attitude actuator system which is equal to the mass of the flywheel, M_{FW}, and the mass of the non-propulsive power supply plus drives and control system electronics, M_P

M_F, lb-sec^2/in., mass of the r-f feed system, which includes its associated electronics, non-propulsive power supply, telemetry, command and control, data processing, etc.

$M_S = M_{S1} + M_{S2}$, lb-sec^2/in., total structural mass which is equal to the parasitic mass, M_{S1}, and load carrying mass, M_{S2}

$M_T = M_S + M_A + M_F$, lb-sec^2/in., total antenna mass

P, horsepower, power developed in the shaft connecting the flywheel to the actuator drive

ρ_S, ρ_{FW}, lb-sec^2/in.^{4}, mass density of structural and flywheel material

r_{FW}, in., radius of gyration of flywheel

r_o, in., radius of gyration of beam crossection

s, lbs/in.^{2}, maximum hoop stress that can be developed in the flywheel material

T, in-lb, torque developed by attitude actuator

t, in., flange thickness of beam crossection

W, in., flange width of beam crossection

w_A, w_{FW}, rad/sec, angular speed of the antenna and flywheel about the O-A or O-B axis

3.2 NON-TAPERED CONFIGURATION.

Non-tapered and tapered depths for the structural beams are to be considered. In the non-tapered configuration all beams have the same depth. In the tapered configuration the beam depths are a function of their radial distance from the center of the aperture.

3.2.1 STRUCTURAL PROPERTIES.

A beam crossection that results from the assembly of the stackable panels (per Ref. 1) is shown in Fig. III-3.

In the upper flange the butted (and fastened together) sections are considered to form one continuous crossection.

The flange dimension, W, is parallel to the reflector surface.

The area of the crossection assumed responsible for carrying flexural loads is, based on the proportions in Fig. III-3,

$$A = 3\ B^2\ (W/B)^2\ (t/W), \tag{1}$$

the depth of the beam is,

$$B = 2\ M_2/3\ L\ p_S\ (W/B)^2\ (t/W)^{\frac{1}{2}}, \tag{2}$$

and the principal section moment of inertia is,

$$I = (0.75)\ k_o^2\ B^4\ (W/B)^2\ (t/W). \tag{3}$$

The proportions in the crossection W/B and t/W are to be chosen, together with values for k'_{S2} or k'_{S1}, such that (for the anticipated operating stress levels) the web buckling distortions are negligible.

The k_o in Eq. (3) depends on the W/B and t/W. However, in this study, $k_o = 0.9$ is used and its dependence on W/B and t/W is neglected.

The parasitic mass M_1 or M_{S1} includes the mass of the beam web section. The web is assumed to carry no load. The stiffnesses due to deflections in shear and torsion are neglected.

The beam crossections that can be chosen are not limited to the flanged-beam crossection chosen here. The beam may take the form of a truss, and the flat flanges may be substantially reduced. The chosen crossection is, however, compatible with

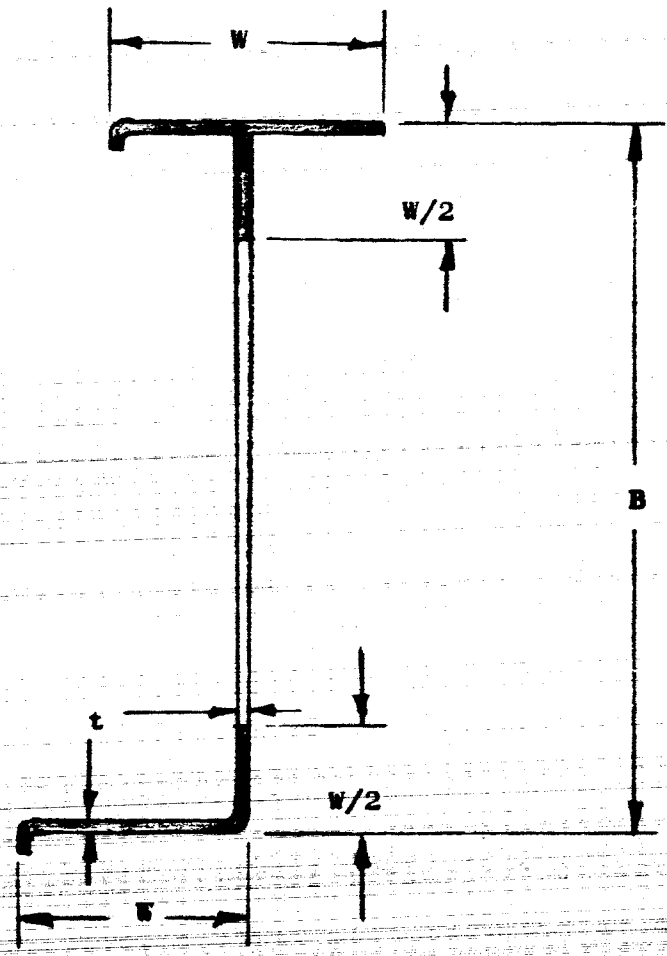


Fig. III-3. Beam crossection.

the proposed RATIO approach to stacking and automatically assembling the structural panels.

3.2.2 MASS AND INERTIAL PROPERTIES.

Summing up the area of the reflector surface from Fig. III-2 and multiplying by the structural weight per unit of reflector surface, K, the total structural mass is,

$$M_S = 0.00362\ L^2\ K, \tag{4}$$

and, since there are 896 half-length beams,

$$M = M_S/896. \tag{5}$$

The mass moments of inertia of the model about the OA and OB axes are obtained by adding the products of the masses at each structural junction and the squares of the corresponding normals from the junctions to, respectively, the OA and OB axes. The mass at a structural junction depends on the number of beams that meet at the junction and, if an actuator is mounted there, on the combined mass of the actuator feed, electronics, etc. Accounting for all of the antenna masses in this way, the mass moments of inertias for the cases defined in Section 2.4, are,

$$I_{OA} = M\ L^2\ (15{,}040 + V\ k'_{AF}), \tag{6}$$

$$I_{OB} = M L^2 (15{,}810 + V k'_{AF}), \qquad (7)$$

where, V has the following valves,

Case	V
1	0
2	3,584
3	14,300
4	8,960

Using M from Eq. (5), Eqs. (6) and (7) can also be written,

$$I_{OA} = L^4 K (0.0615 + V_o k'_{AF}), \qquad (6a)$$

$$I_{OB} = L^4 K (0.0645 + V_o k'_{AF}), \qquad (7a)$$

where,

Case	V
1	0
2	0.00146
3	0.05830
4	0.03620

3.2.3 LOADING CONDITIONS.

The inertial reaction forces at the structural junctions act normal to the plane of the aperture. The reaction force at a junction, located at a distance (n-1) L from the O-A neutral axis, and having k_2 beams per junction is,

$$F_{OA} = (n-1)\, k_2\, a_A\, L\, M, \tag{8}$$

and for rotation about the O-B axis,

$$F_{OB} = (n_1-1)\,(0.707)\, k_2\, a_A\, L\, M \tag{9}$$

Since the angular acceleration, a_A, the beam length, L, and the mass per half beam length, M, are the same at each junction, it is evident that the force, F, changes only with

the number of beams per junction, k_2, and its coordinate location n or n_1. Figs. III-4 and III-4a indicate the forces at the junctions normalized with respect to a_A M L.

For each of the cases described in Section 2.4 the individual actuators are assumed to generate the same torque when operating about axes parallel to either O-A or O-B. The on-board mass associated with the individual actuators is the same for each case. Using these assumptions, the forces and torques are described in Fig. III-5. The forces in Fig. III-5 are in addition to the forces described in Figs. III-4 and III-4a.

Note that the inertias I_{OA} and I_{OB} in Fig. III-5 are also a function of the cases defined in Section 2.4 and Eqs. (6) and (7).

3.3 TAPERED CONFIGURATION.

A structural configuration is assumed in which the principal section moments of inertia of the beams are reduced as a linear function of their distance from the center of the aperture. A first order assessment is to be made of the effects on structural efficiency of this form of tapering as compared with no tapering.

3.3.1 STRUCTURAL PROPERTIES.

Defining I_o as the principal section moment of inertia at m=1, n=1, in Fig. 2, and I_1 as the section inertia at m=9, n=1, (and at n=9, m=1) then the section inertia at the other junction is,

$$I = I_o - (I_o - I_1)\left[(m-1)^2 + (n-1)^2\right]/8 \qquad (10)$$

n \ m	1	2	3	4	5	6	7	8	9
1	0	0	0	0	0	0	0	0	0
2	4	4	4	4	4	4	4	4	3
3	8	8	8	8	8	8	8	8	6
4	12	12	12	12	12	12	12	12	6
5	16	16	16	16	16	16	16	12	
6	20	20	20	20	20	20	20	10	
7	24	24	24	24	24	24	12		
8	28	28	28	28	21	14			
9	24	24	24	16					

Fig. III-4. Normalized force $F_{OA}/a_A LM$ at structural junctions in Fig. III-2.

n_1 \ m_1	1	2	3	4	5	6	7	8	9	10	11	12	13
1	0		0		0		0		0		0		0
2		4		4		4		4		4		4	
3	8		8		8		8		8		8		8
4		12		12		12		12		12		9	
5	16		16		16		16		16		16		
6		20		20		20		20		20		10	
7	24		24		24		24		24		18		
8		28		28		28		28		21			
9	32		32		32		32		24				
10		36		36		36		27					
11	40		40		40		30						
12		44		33		22							
13	24		24										

Fig. III-4a. Normalized forces $F_{OB}/a_A LM(0.707)$ at structural junctions in Fig. III-2a.

O-A AXIS ROTATION

n \ m	1	3	5
1	T_1, F_1		
3		T_2, F_2	
5			T_3, F_3

O-B AXIS ROTATION

n_1 \ m_1	1
1	T_{11}, F_{11}
5	T_{21}, F_{21}
9	T_{31}, F_{31}

$$F_{1\,2\,3} = Y_{1\,2\,3}\, M_S\, a_A\, L\, k'_{AF}$$

$$F_{11\,21\,31} = Y_{1\,2\,3}\, (1.41)\, M_S\, a_A\, L\, k'_{AF}$$

$$T_{1\,2\,3} = Z_{1\,2\,3}\, I_{OA}\, a_A$$

$$T_{11\,21\,31} = Z_{1\,2\,3}\, I_{OB}\, a_A$$

CASE	Y_1	Y_2	Y_3	Z_1	Z_2	Z_3
1	0			1		
2		1/2			1/4	
3			1			1/4
4		1/4	1/2		1/8	1/8

Fig. III-5. Reaction forces due to individual on-board masses and torques due to individual attitude actuators for cases 1 to 4.

The beam crossection proportions (t/W), (W/B), indicated in Fig. III-3, as used for the non-tapered structure, are to be applied to the tapered structure. Eliminating B and I from Eqs. (1), (3) and (10), and solving for A,

$$A = 3.46\ (W/B)(t/W)^{\frac{1}{2}} \left\{ I_o - (I_o - I_1)\left[(m-1)^2 + (n-1)^2\right]^{\frac{1}{2}}/8 \right\}^{\frac{1}{2}} / k_o, \qquad (11)$$

and from Eqs. (3) and (10),

$$B = \left[I_o - (I_o - I_1)(m^2 + n^2)^{\frac{1}{2}}/8 \right]^{1/4} / \left[0.75\ k_o^2\ (W/B)^2\ (t/W) \right]^{1/4}. \qquad (12)$$

It is evident from Eq. (11) that the crossection area, A, at a junction varies as the square root of the junction distance from the center of the aperture. And from Eq. (12) it is seen that the beam depth at a junction, B, varies as the fourth root the distance.

The values of I_o, A_o and B_o at the center of the aperture are obtained from Eqs. (10) to (12) by setting m=n=1.

The average weight per unit of reflector surface area, K, is to be the same for the tapered and non-tapered structures. Therefore from Eq. (4),

$$M_{S2} = 0.00362\ L^2\ K\ k'_{S2}. \qquad (13)$$

Assuming that the beam properties at each junction remain constant for one half of a beam length from the junction, then M_{S2} can be determined by summing the masses at each junction,

$$M_{S2} = p_S\,(L/2) \sum_{m=n=1} k_2\,A, \tag{14}$$

where the summation is over the junctions in all four quadrants.

Substituting A from Eq. (11) into Eq. (14), then equating Eqs. (14) and (13), and solving for I_o,

$$I_o = (0.0021\ L\ K\ k_o\ k'_{S2})^2/(t/W)(W/B)^2$$

$$\left[p_S \sum_{m=n=1} k_2 \left\{1- \left[1- (I_1/I_o)\right]\left[(m-1)^2+(n-1)^2\right]^{1/2}/8\right\}^{1/2}\right]^2. \tag{15}$$

I_o from Eq. (15) can now be substituted into Eqs. (11) and (12) for the evaluation of A and B or A_o and B_o.

It is noted that the special case in which $(I_1/I_o) = 1$ corresponds to the non-tapered structure.

In this case $(I_1/I_o) = 0.2$ is to be assumed. With this assumption, Fig. III-6 shows the values of the quantity $k_2\{\ \}_1^{1/2}$ in Eq. (15) at the junctions in one quadrant. Summing these values for the four quadrants,

$$I_o = (1.32)\ 10^{-11}\ (K\ k_o\ L\ k'_{S2})^2/p_S^{\,2}\ (W/B)^2\ (t/W). \tag{16}$$

n \ m	1	2	3	4	5	6	7	8	9
1	4.00	3.80	3.55	3.35	3.10	2.83	2.55	2.20	1.35
2	3.80	3.70	3.52	3.32	3.08	2.80	2.50	2.17	1.33
3	3.55	3.52	3.38	3.20	2.98	2.72	2.45	2.10	1.26
4	3.35	3.32	3.20	3.05	2.83	2.59	2.30	1.96	0.77
5	3.10	3.08	2.98	2.83	2.64	2.40	2.11	1.33	
6	2.83	2.80	2.72	2.59	2.40	2.16	1.87	0.75	
7	2.55	2.50	2.45	2.30	2.11	1.87	0.78		
8	2.20	2.17	2.10	1.96	1.33	0.75			
9	1.35	1.33	1.26	0.77					

Fig. III-6. Values of the quantity $k_2 \left\{ \right\}_1^{\frac{1}{2}}$ in Eq. (15).

Substituting Eq. (16) into Eq. (11), the values of the load carrying crossection area, A, are determined for each structural junction. The A's between adjoining junctions are then obtained by taking averages of the A's at the adjoining junctions. These average A's in normalized form are presented in Fig. III-7.

By a similar procedure the average normalized crossection moments of inertia of the beams between junctions are computed and presented in Fig. III-8.

3.3.2 MASS AND INERTIAL PROPERTIES.

The mass properties for the non-tapered structure, as per Eqs. (4) and (5), also hold for the tapered structure.

The mass moment of inertia in the case of the tapered structure, as in the case of the non-tapered structure, is equal to the inertia of the structure, plus the inertia of of the actuator and feed. Designating the latter inertia by I_{Al}, the inertia about the O-A axis is,

$$I_{OA} = (L/2)\, p_S \sum_{n=m=1} (n-1)^2\, L^2\, k_2\, A + I_{Al}, \qquad (17)$$

substituting A from Eq. (11) and I_o from Eq. (16) into Eq. (17),

$$I_{OA} = (6.4)\, 10^{-7}\, L^4\, K \sum_{n=m=1} (n-1)^2\, k_2 \left\{ \right\}_1^{\frac{1}{2}} + I_{Al}, \qquad (18)$$

n or m \ (m-1)-m or (n-1)-n

	1-2	2-3	3-4	4-5	5-6	6-7	7-8	8-9
1	0.975	0.920	0.865	0.807	0.740	0.669	0.592	0.500
2	0.937	0.953	0.855	0.800	0.735	0.663	0.584	0.493
3	0.885	0.863	0.823	0.773	0.712	0.645	0.567	0.473
4	0.835	0.815	0.780	0.734	0.676	0.610	0.532	0.438
5	0.773	0.757	0.726	0.683	0.630	0.565	0.486	
6	0.703	0.690	0.663	0.625	0.570	0.504	0.421	
7	0.679	0.617	0.592	0.552	0.499	0.425		
8	0.547	0.534	0.507	0.466	0.408			
9	0.446	0.432	0.403					

Fig. III-7. Average normalized beam cross-section areas 49 A $p_S/(1.26)\ 10^{-5}$ K L k'_{S2}.

n or m \ (m-1)-m or (n-1)-n	1-2	2-3	3-4	4-5	5-6	6-7	7-8	8-9
1	0.950	0.850	0.750	0.650	0.550	0.450	0.350	0.250
2	0.870	0.815	0.730	0.638	0.540	0.440	0.342	0.245
3	0.787	0.745	0.628	0.597	0.507	0.415	0.322	0.226
4	0.696	0.663	0.609	0.539	0.459	0.374	0.285	0.194
5	0.595	0.572	0.527	0.468	0.398	0.320	0.237	
6	0.495	0.475	0.440	0.389	0.320	0.255	0.180	
7	0.395	0.380	0.350	0.305	0.250	0.186		
8	0.297	0.285	0.257	0.217	0.167			
9	0.197	0.186	0.163					

Fig. III-8. Average normalized cross-section moment of inertia I/I_o.

where $\{\ \}_1^{1/2}$ is defined in Eq. (15).

As before using $(I_1/I_o) = 0.2$, values for the quantity $n^2 k_2 \{\ \}_1^{1/2}$ are given in Fig. III-9 for the junctions in one quadrant. Summing these values for the four quadrants,

$$I_{OA} = (0.0460)\ L^4\ K + I_{A1}. \tag{19}$$

In a similar manner, using the values in Fig. III-10,

$$I_{OB} = (L/2)\ p_S \sum_{m_1=m_1=1} (1/2)(n_1-1)^2\ L^2\ k_2\ A + I_{B1}$$

$$= (6.4)\ 10^{-7}\ L^4\ K \sum_{n_1=m_1=1} (n_1-1)^2\ k_2 \Big\{ \Big[1 - (1-(I_1/I_o)) \Big]$$

$$\Big[(m_1-1)^2 + (m_1-1)^2 \Big]^{1/2} /8 \Big\}_2^{1/2} + I_{B1}$$

$$= (0.0540)\ L^4\ K + I_{B1}. \tag{20}$$

An examination of Figs. III-9 and III-10 indicates the contributions of the structural mass at the different junctions to the inertias I_{OA} and I_{OB}.

n \ m	1	2	3	4	5	6	7	8	9
1	0	0	0	0	0	0	0	0	0
2	3.80	3.70	3.52	3.32	3.08	2.80	2.50	2.17	1.33
3	14.20	14.10	13.50	12.80	11.90	10.90	9.80	8.40	5.10
4	30.20	29.90	28.80	27.30	25.40	23.30	20.70	17.65	6.95
5	49.50	49.30	47.70	45.30	42.20	38.40	33.90	21.30	
6	70.60	70.00	68.00	64.60	60.00	54.00	46.90	18.70	
7	91.20	90.00	87.90	82.60	76.40	67.50	28.10		
8	107.90	106.70	103.00	96.00	86.66	36.70			
9	86.40	85.00	80.80	49.40					

Fig. III-9. Values of the quantity $(n-1)^2 k_2 \left\{ \right\}_1^{1/2}$ in Eq. (18).

n_1/m_1	1	2	3	4	5	6	7	8	9	10	11	12	13
1	0		0		0		0		0		0		0
2		3.80		3.52		3.20		2.83		2.40		1.88	
3	14.80		14.25		13.30		11.92		10.34		8.48		2.99
4		31.70		30.20		27.70		24.50		20.70		11.95	
5	54.00		53.70		49.50		44.70		39.00		31.30		
6		80.00		77.00		70.60		62.50		52.50		19.30	
7	109.50		107.30		100.90		91.20		78.40		45.50		
8		138.70		133.30		122.50		107.90		62.00			
9	169.00		165.80		156.20		139.40		86.40				
10		194.50		186.00		170.30		107.40					
11	216.00		212.00		196.00		126.40						
12		227.00		153.00		94.00							
13	112.50		108.00										

Fig. III-10. Values of the quantity $(n_1-1)^2 k_2 \left\{1 - \left[1 - (I_1/I_o)\right] \left[(m_1-1)^2 + (n_1-1)^2\right]^{1/2}/8\right\}_2^{1/2}$ in Eq. (20).

The values I_{A1} and I_{B1}, in Eqs. (19) and (20), depend on the actuator-distribution case definitions given in Section 2.4. Using these definitions the mass moments of inertia are finally given by,

$$I_{OA} = L^4 K (0.0460 + V_o k'_{AF}), \tag{21}$$

$$I_{OB} = L^4 K (0.0540 + V_o k'_{AF}), \tag{22}$$

where V_o has the values given in Section 3.2.2.

A comparison of Eqs. (21) and (22) with Eqs. (6a) and (7a) indicates that, for the same L and K, the tapering has reduced the contribution of the structural mass to the inertia by a factor of 1.2 to 1.3. Since the over-all structural mass is the same for the tapered and non-tapered structures the contribution of the masses of the actuators and feeds to the inertia is not changed.

3.3.3 LOADING CONDITIONS.

The reaction force at a junction, located at a distance (n-1) L from the neutral axis, and having k_2 beams per junction is,

$$F_{OA} = (n-1) k_2 a_A L p_S (L/2) A, \tag{23}$$

and for rotation about the O-B axis,

$$F_{OB} = (0.707)(n_1-1)\, k_2\, a_A\, L\, p_S\, (L/2)\, A. \qquad (24)$$

Placing I_o from Eq. (15) into Eq. (11), performing the indicated summation and then substituting A from Eq. (11) into Eqs. (23) and (24),

$$F_{OA} = (6.3)\ 10^{-6}\ a_A\ K\ L^3\ (n-1)\ k_2 \left\{ \right\}_1^{1/2} \qquad (25)$$

$$F_{OB} = (4.5)\ 10^{-6}\ a_A\ K\ L^3\ (n_1-1)\ k_2 \left\{ \right\}_2^{1/2} \qquad (26)$$

where $\left\{ \right\}_1^{1/2}$ is given in Eq. (15), and $\left\{ \right\}_2^{1/2}$ is given in Eq. (20).

Using Eqs. (25) and (26), the normalized forces at the junctions for rotation about the O-A and O-B axes are computed and shown in Figs. III-11 and III-12.

A comparison of Figs. III-11 and III-4, and III-12 and III-4a, indicates that the reaction forces at the junctions are substantially reduced by tapering the structure.

The reaction forces due to on-board masses and the torques generated by the attitude actuators as presented in Fig. III-5 (for the non-tapered structures) also apply to the tapered structure.

3.4 SLEWING AND TURNING RATE LIMITATIONS.

All on-board, non-structural masses are contained in M_A and M_F. The M_F (mass of the feed) is taken as an independent variable.

n \ m	1	2	3	4	5	6	7	8	9
1	0	0	0	0	0	0	0	0	0
2	3.80	3.70	3.52	3.32	3.09	2.80	2.50	2.18	1.32
3	7.10	7.05	6.75	6.40	5.95	5.45	4.90	4.20	2.55
4	10.62	9.99	9.60	9.10	8.46	7.76	6.90	5.85	2.31
5	12.32	12.32	11.92	11.32	10.55	9.60	8.50	5.32	
6	14.12	14.00	13.60	12.93	12.00	10.80	9.40	3.74	
7	15.20	15.00	14.65	13.77	12.73	11.25	4.70		
8	15.41	15.25	14.70	13.74	12.40	5.23			
9	10.81	10.61	10.12	6.18					

Fig. III-11. Normalized forces $F_{OA}/(6.3)\ 10^{-6}\ a_A KL^3$ at the structural junctions.

$n_1 \backslash m_1$	1	2	3	4	5	6	7	8	9	10	11	12	13
1	0		0		0		0		0		0		0
2		3.80		3.53		3.20		2.83		2.40		1.88	
3	7.40		7.15		6.60		6.95		5.15		4.25		1.5
4		10.60		10.00		9.20		8.20		6.90		3.96	
5	13.50		13.20		12.40		11.20		9.80		7.85		
6		16.00		15.40		14.14		12.50		10.50		3.86	
7	18.20		17.90		16.80		15.20		12.80		7.60		
8		19.70		19.00		17.50		15.30		9.30			
9	21.10		20.60		19.50		17.40		10.70				
10		21.60		20.60		18.90		12.00					
11	21.60		21.20		19.60		12.60						
12		20.60		14.60		8.50							
13	9.40		9.00										

Fig. III-12. Normalized forces $F_{OB}/(4.5)\ 10^{-6}\ a_A\ KL^3$ at the structural junctions.

However, the M_A (mass of the actuators), is equal to the mass of the flywheels, M_{FW}, plus the mass of the non-propulsive power supply, M_P. And M_{FW} and M_P are dependent on the required antenna slewing and turning rates. Expressions will now be developed for M_P, and M_{FW}.

3.4.1 OPTIMUM MASSES OF NON-PROPULSIVE POWER AND FLYWHEEL SYSTEMS.

Fig. III-13 summarizes the weight-power characteristics of the commonly considered non-propulsive power systems for space applications. Based on the data in Fig. III-13, and adding a weight penalty of approximately 30% for the mass of the drives and control system electronics, the shaft power developed by the actuator is conservatively estimated to be,

$$P = 3.25\ M_P^{1.43} \tag{27}$$

The power P is used to accelerate the inertias of the drive-motor armature, the drive gearing, the flywheel, and the antenna. Assuming that half of the power goes into accelerating the armature and gear train inertias (which would result in maximum shaft power delivered to the antenna) then the torque delivered to the antenna is,

$$I_A\ a_A = (P/2)\ 6600/(w_{FW} + w_A). \tag{28}$$

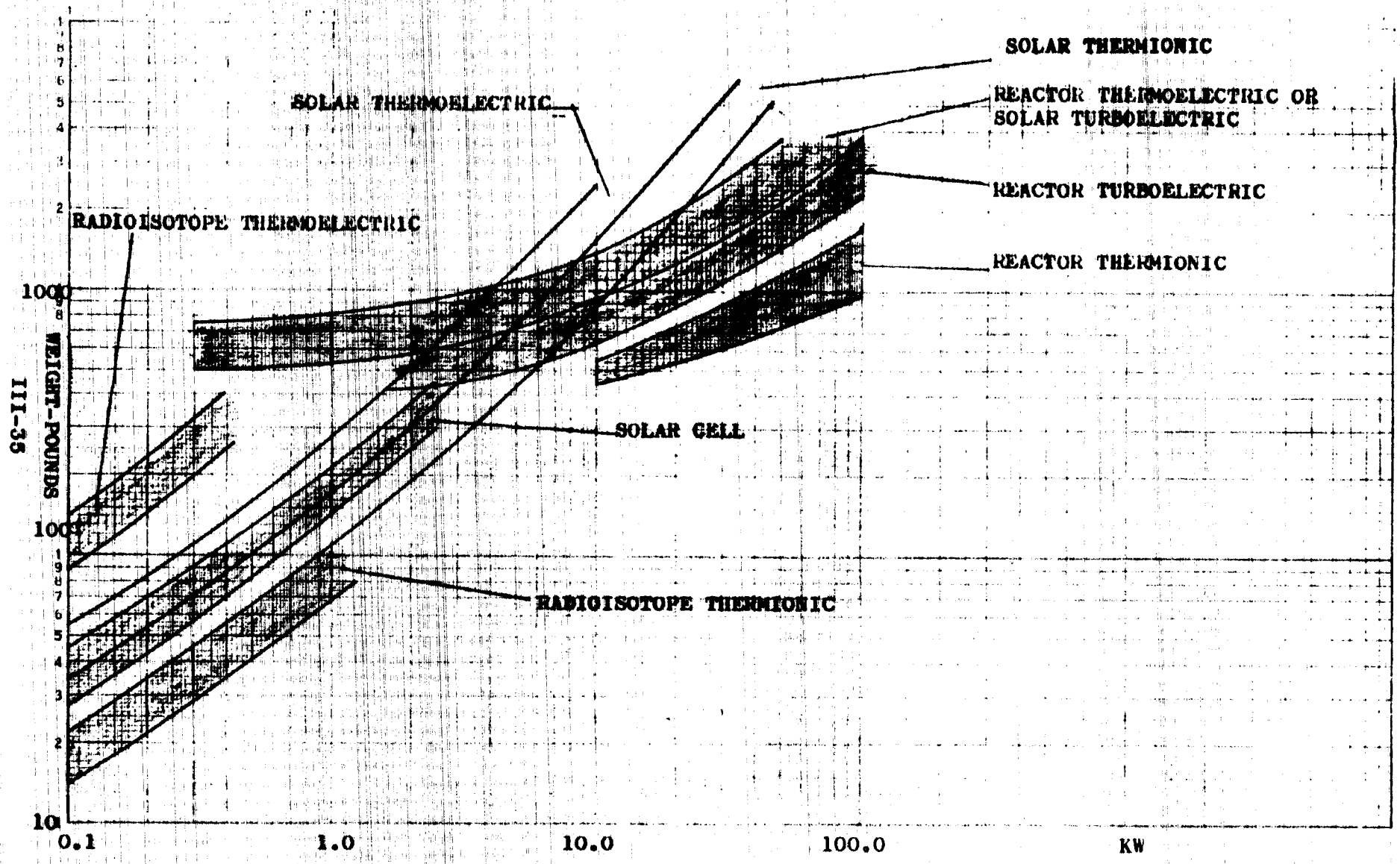


Fig. III-13. Solar and nuclear (unshielded) power sources 1961.

Assuming that the beam properties at each junction remain constant for one half of a beam length from the junction, then M_{S2} can be determined by summing the masses at each junction,

$$M_{S2} = p_S\,(L/2) \sum_{m=n=1} k_2\,A, \tag{14}$$

where the summation is over the junctions in all four quadrants.

Substituting A from Eq. (11) into Eq. (14), then equating Eqs. (14) and (13), and solving for I_o,

$$I_o = (0.0021\ L\ K\ k_o\ k'_{S2})^2/(t/W)(W/B)^2$$

$$\left[p_S \sum_{m=n=1} k_2 \left\{1- \left[1- (I_1/I_o)\right]\left[(m-1)^2+(n-1)^2\right]^{1/2}/8\right\}^{1/2}\right]^2. \tag{15}$$

I_o from Eq. (15) can now be substituted into Eqs. (11) and (12) for the evaluation of A and B or A_o and B_o.

It is noted that the special case in which $(I_1/I_o) = 1$ corresponds to the non-tapered structure.

In this case $(I_1/I_o) = 0.2$ is to be assumed. With this assumption, Fig. III-6 shows the values of the quantity $k_2\{\ \}_1^{1/2}$ in Eq. (15) at the junctions in one quadrant. Summing these values for the four quadrants,

$$I_o = (1.32)\ 10^{-11}\ (K\ k_o\ L\ k'_{S2})^2/p_S^2\ (W/B)^2\ (t/W). \tag{16}$$

Therefore, if 59% of the actuator mass is used for the non-propulsive power system (or 41% for the flywheels) the product of the antenna angular acceleration and turning rate in maximized. These percentages, which essentially result from the assumptions in Eq. (27), have an estimated tolerance of $\pm$ 10% depending on the specific non-propulsive power system and antenna configuration.

From Eqs. (31) and (33),

$$a_A \, w_A = 2100 \, M_A^{2.43} \, r_{FW}^2 / I_A^2. \qquad (34)$$

The a_A in Eq. (34) is limited by the maximum allowable distortions which may be induced in the structure. These are outlined in Section 4.5.

3.4.2 FLYWHEEL SATURATION.

The maximum turning rate of the antenna in Eq. (34) depends on the maximum flywheel turning rate which can be used in Eq. (29). This maximum turning rate in turn depends on the flywheel radius of gyration, r_{FW}, material specific weight, p_{FW}, and maximum operating stress level, s_{FW}.

$$w_{FW\,max} = (s_{FW}/p_{FW})^{\frac{1}{2}} / r_{FW}. \qquad (35)$$

Using Eqs. (35) and (30) in Eq. (29),

$$w_{A\,max} = (s_{FW}/p_{FW})^{1/2}\, M_{FW}\, r_{FW}/I_A. \qquad (36)$$

It is evident from Eqs. (34) and (36) that w_A and a_A are increased by increasing the r_{FW}. In this study, $r_{FW} = L/3$ is to be used so that the flywheel can be mounted on and stowed with a structural panel. If necessary, flywheels with $r_{FW} > L$ may be deployed. However, the weight penalty for this deployment would have to be evaluated and justified.

3.5 RELECTOR DISTORTIONS.

3.5.1 FACTORS AFFECTING ANTENNA PERFORMANCE.

The far field radiation pattern of a RATIO antenna is, in part, a function of the number of wavelengths in the aperture, the aperture amplitude illumination function, the illumination intensity at the edge of the aperture, the aperture blockage due to the feed and feed support structure, and the phase distortions due to reflector (and feed) irregularities. These parameters are generally specified to achieve certain far field radiation performance objectives. Thus, to maximize the gain or minimize the beamwidth of the main lobe, the number of wavelengths in the aperture are increased. To reduce the side lobe level, the edge illumination intensity aperture blockage, and phase distortions are reduced, while the illumination is tapered from a maximum at the center of the aperture to a minimum at the edge of the aperture.

The requirements for maximum gain, in some cases, conflict with the requirements for minimum side lobes. For example, reducing the edge illumination and increasing the illumination taper reduces the gain as well as the side lobes. Further, increasing the illumination taper implies an increase in the aperture blockage brought about by enlarging of the feed. But aperture blockage reduces the gain and increases the side lobes. Therefore illumination tapering has an undesirable secondary affect on the gain as well as the side lobes.

However, by reducing the reflector caused phase distortions both the gain and side lobe performance are improved. The improvement depends upon the number of wavelengths in the aperture, the aperture blockage, the illumination taper, etc. As a rule of thumb, for greater than 20 wavelengths in the aperture and uniform or tapered illumination, phase distortions one-twentieth of a wavelength or less are negligible. Distortions at this level can be readily controlled on reflectors say 20 to 30 feet in diameter that operate at about one-foot wavelengths. However, in the typical case of one-hundred foot and greater reflectors that operate at wavelengths of a few inches such negligible distortions are not readily obtained. It is assumed in this study that the distortions are generally large enough to affect the antenna performance.

3.5.2 REFLECTOR WEIGHTED RMS DEFLECTIONS.

Different RATIO structural configurations and loading conditions are assumed in this study for which the elastic deflections are computed at each of the structural junctions. It is desirable to compare the influence of the deflections, and therefore the influence of these configurations and loading conditions, on the antenna performance.

The far field radiation pattern is predominantly a function of the radiation from each part of the reflector surface. Secondarily it depends on the radiation from the reflector back structure, feed support, feed housing, and the surrounding environment. Ignoring these secondary influences, the affects of the reflector deflections on r-f radiation can be assessed, on a first order basis, by determining d, the rms of the deflections weighted by the function describing the distributions of the r-f illumination intensity over the aperture. For purposes of this approximation only the deflections normal to the surface (i.e. nominally parallel to the r-f axis of the main lobe of the radiation pattern) are considered. Obviously, the greater this rms deflection the greater the deterioration of radiation performance. The radiation performance of different structural configurations and loading conditions can therefore be compared on the basis of their rms deflections.

It is interesting to note that, if the deflections tend to be larger at the edges than at the center of the reflector, as

they would be especially for tapered structures, then tapering the illumination produces a lower rms deflection than no tapering.

The rms deflection can serve as a guide to the minimum wavelength at which the antenna may be expected to operate satisfactorily.

Two types of weighting functions are to be considered. One based on uniform illumination across the aperture, and one based on cosine illumination. The weighting factors at the structural junctions for the cosine illumination to be used is given in Fig. III-14.

3.6 SCALING FACTORS.

In the definition of the structural model the following independent parameters are used:

K, reflector unit weight

L, length of grid

a_A, antenna angular acceleration

p_S, p_{FW}, density of structural and flywheel materials

E, modulus of elasticity

k'_{S1}, k'_{S2}, k_S, structural mass fractions

k_A, actuator mass fraction

W/B, t/W, beam crossection proprtions

s_{FW}, flywheel stress

O-A or O-B rotation axis

Actuator distribution case per section 2.4

n \ m	1	2	3	4	5	6	7	8	9
1	1.000	0.9848	0.9397	0.8660	0.7660	0.6428	0.5000	0.3420	0.1737
2	0.9848	0.9687	0.9245	0.8536	0.7547	0.6293	0.4848	0.3338	0.1668
3	0.9397	0.9245	0.8805	0.8090	0.7120	0.5890	0.4540	0.3007	0.1340
4	0.8660	0.8536	0.8090	0.7408	0.6428	0.5284	0.3907	0.2419	0.0854
5	0.7660	0.7547	0.7120	0.6428	0.5548	0.4384	0.3090	0.1651	
6	0.6428	0.6293	0.5890	0.5284	0.4384	0.3272	0.2079	0.0698	
7	0.5000	0.4848	0.4540	0.3907	0.3090	0.2079	0.0906		
8	0.3420	0.3338	0.3007	0.2419	0.1651	0.0698			
9	0.1737	0.1668	0.1340	0.0854					

Fig. III-14. Cosine illumination weighting factors.

Of these, K, L, a_A, p_S, E, k_S, p_{FW}, s_{FW}, the rotation axis, and actuator distribution are to be the most significant and generally varied parameters in this study. For a given k_S, rotation axis, and actuator distribution, as well as given values for the other independent parameters, the following scaling factors are determined for the more important dependent variables in terms of K, L, a_A, p_S, p_{FW}, s_{FW}. These factors follow from the derivations in the preceding sections.

$$M,\ M_S,\ M_A,\ M_P,\ M_{FW},\ M_T,\ M_F \sim L^2\ K \tag{37a}$$

$$B \sim (LK/p_S)^{1/2} \tag{37b}$$

$$I \sim (LK/p_S)^2 \tag{37c}$$

$$I_A \sim K\ L^4 \tag{37d}$$

$$r_{FW} \sim L \tag{37e}$$

$$w_A \sim K^{0.43}/a_A\ L^{1.14} \tag{37f}$$

$$w_{A\ max} \sim (s_{FW}/p_{FW})^{0.5}/L \tag{37g}$$

$$F,\ F_1,\ F_2,\ F_3 \sim L^3\ K\ a_A \tag{37h}$$

$$A \sim L\,K/p_S \tag{37i}$$

$$T \sim K\,L^4\,a_A \tag{37j}$$

In view of the definitions in Section 2.6 the major deflection-limiting-structural stiffness is due to flexure about principal axes of the beams. For this condition the local structural deflections, and therefore the weighted rms deflections, d, scale approximately as,

$$d \sim L^4\,a_A\,p_S^2/EK\,. \tag{37k}$$

The scaling of d with L^4 in Eq. (37k) has a probable accuracy of $\pm$ 50%. This is due to the presence of L and L^2 terms (in addition to the predominant L^3 terms) in the stiffness matrix of a generic structural element. The greater the L the better the accuracy. The data in Section 4.3.5 indicates the actual dependence of d on L.

The other scaling factors in Eq. (37k) are completely valid within the constraints set by Section 2.6.

It is evident from Eq. (37k) that d is minimized by minimizing p_S^2/E. The following are typical values of p_S^2/E for some common structural materials,

	$(g^2 p_S^2/E)\ 10^{-9}$
Steel	2.60
Aluminum	1.00
Magnesium	0.64
Ceramics	0.60
Phenolics	1.00

Ceramics and magnesium have an apparent advantage over the other materials in this case. It is however pertinent that dimensional stability of the material under other influences, such as thermal gradients and creep, must be considered before a final material selection is made. It is also pertinent that the parasitic weight penalties (i.e. as for fasteners) are not expected to be the same for the different materials, and need to be evaluated in making the material selection.

3.6.1 ALTERNATE SCALING PROPORTIONS.

Due to chosen proportions in the beam crossection the beam depth, B, scales with $(KL)^{\frac{1}{2}}$. As a result the deflections, d, scale with $L^4 K^{-1}$.

If it is assumed that B scales linearly with L and is independent of K, then

$$A \sim L K/p_S,$$

$$I \sim L^3 K/p_S,$$

$$M \sim L^2 K,$$

$$F \sim L^3 K a_A,$$

and

$$d \sim L^3 a_A p_S/E.$$

In this case d does not depend on K. Apparently, while increasing the K increases the I the F is also increased by a like amount. Hence there is no advantage gained by increasing the mass of the load-carrying structure.

Likewise, if it is assumed that B does not scale with L or K, but is held constant,

$$A \sim L K/p_S,$$

$$I \sim B^2 L K/p_S,$$

$$M \sim L^2 K,$$

$$F \sim L^3 K a_A,$$

and

$$d \sim L^5 a_A p_S/B^2 E.$$

4.0 SPECIFIC STRUCTURAL DEFLECTION ANALYSES.

4.1 SELECTION OF STRUCTURAL CONFIGURATIONS AND LOADING CONDITIONS.

Three tapered and three non-tapered structural configurations, having the following basic parameters, have been selected and are described in Figs. 15 and 16.

For purposes of this analyses the following parameters have been chosen. These parameters are common to all the configurations.

$L = 300, 200, 100$

$k_S = 0.80, 0.65, 0.50$

Actuator Cases 1, 2, 3, 4 (per Section 2.4)

$K = 0.1$

$a_A = 0.01$

$(W/B) = 0.14$

$(t/W) = 0.01$

$p_{FW} = 7.3 \times 10^{-4}$ (Steel), $p_S = 2.59 \times 10^{-4}$ (alum.)

$s_{FW} = 5 \times 10^4$ (Steel)

$k'_{S2} = 0.75$

$k_o = 0.9$

$k_F = 0.05$

$(I_1/I_o) = 1.0$, for non-tapered structures

$(I_1/I_o) = 0.2$, for tapered structures

$E = 10^7$, for aluminum

Figs. 15, 16, and the above describe six different configurations for each of which, because of the chosen values for k_S and corresponding actuator distribution cases, there are

Again d is independent of K. The added stiffness added by increasing K is again negated by the increased loads.

Continuing along the same lines, the thickness of the web and flange sections of the beam crossection can be assumed to be held constant. In this case the depth of the beam would scale linearly with KL and,

$$d \sim L^3 a_A p_S / E K^2.$$

Here a pronounced advantage is gained by increasing K.

It is believed that beam proportions chosen in Section 3.2.1 produce the most realistic scaling factors. While possible alternate structural proportions may result in more desirable scaling factors as indicated above, they do not directly take into account the proportions that effect the compliances due to local flange or web buckling. As such they are not realistic.

LOADING CONDITION	ACTUATOR DIST. CASE	AXIS	k_S	M_A	M_T	k'_{AF}	Eqs. (6),(7) (21), (22) I_A (10^7)		Eq. (33) M_p	Eq. (34) $w_A\ a_A\ (10^{-7})$		Eq. (36) $w_{A\ MAX}\ (10^{-2})$	
							(N-T)	(T)		(N-T)	(T)	(N-T)	(T)
1	1	O-A	0.80	6.1	40.6	0.25	4.9	3.7	3.6	7.2	12.8	4.20	5.60
2	2	O-A	0.80	6.1	40.6	0.25	5.4	4.0	3.6	6.0	10.9	3.80	5.10
3	2	O-A	0.65	12.2	50.0	0.54	5.7	4.4	7.2	28.6	48.2	7.10	10.00
4	2	O-A	0.50	18.3	65.0	1.00	6.3	4.9	10.8	63.0	105.0	9.80	12.50
5	3	O-A	0.80	6.1	40.6	0.25	6.3	4.9	3.6	4.3	6.7	3.25	4.20
6	3	O-A	0.65	12.2	50.0	0.54	7.6	6.3	7.2	16.0	24.1	5.35	6.50
7	3	O-A	0.50	18.3	65.0	1.00	9.8	8.4	10.8	24.0	33.3	6.3	7.30
8	4	O-A	0.80	6.1	40.6	0.25	5.9	4.5	3.6	4.9	8.4	3.45	4.40
9	4	O-A	0.65	12.2	50.0	0.54	6.7	5.3	7.2	20.5	33.0	6.10	7.75
10	4	O-A	0.50	18.3	65.0	1.00	8.0	6.7	10.8	39.0	59.0	7.70	9.25
11	1	O-B	0.80	6.1	40.6	0.25	5.1	4.4	3.6	6.6	8.6	4.00	4.60
12	2	O-B	0.80	6.1	40.6	0.25	5.2	4.7	3.6	6.4	7.9	3.94	4.35
13	2	O-B	0.65	12.2	50.0	0.54	5.5	5.0	7.2	30.6	37.0	7.40	8.20
14	2	O-B	0.50	18.3	65.0	1.00	6.0	5.6	10.8	68.0	98.0	10.20	11.00
15	3	O-B	0.80	6.1	40.6	0.25	6.0	5.6	3.6	4.8	6.9	3.41	3.67
16	3	O-B	0.65	12.2	50.0	0.54	7.4	6.9	7.2	16.8	19.2	5.50	5.90
17	3	O-B	0.50	18.3	65.0	1.00	9.5	9.1	10.8	28.0	30.9	6.50	6.80
18	4	O-B	0.80	6.1	40.6	0.25	5.6	5.2	3.6	5.4	6.3	3.66	3.94
19	4	O-B	0.65	12.2	50.0	0.54	6.4	6.0	7.2	22.4	25.9	6.40	6.80
20	4	O-B	0.50	18.3	65.0	1.00	7.8	7.3	10.8	41.0	46.5	8.10	8.70

(N-T) NON-TAPERED
(T) TAPERED

Fig. III-15. Configurational and loading condition factors for tapered and non-tapered structures, L = 300, k_F = 0.05, k = 0.1.

	NON-TAPERED CONFIGURATIONS			TAPERED CONFIGURATIONS			
PARAMETER	I	II	III	PARAMETER	I T	II T	III T
L	300	200	100	L	300	200	100
D	5400	2933	1467	D	5400	2930	1467
r_{FW}	100	67	33		100	67	33
M_S, Eq.(4)	32.5	14.5	3.6	M_S, Eq.(4)	32.5	14.5	3.6
M, Eq.(5)	0.036	0.016	0.004	M, Eq.(5)	0.036	0.016	0.004
M_2	0.027	0.012	0.003	M_2	0.027	0.012	0.003
A, Eq.(1)	0.68	0.45	0.23	A_o Eq.(11)	1.1	0.73	0.37
B, Eq.(2)	34.0	27.5	19.6	B_o Eq.(12)	61.0	49.4	35.1
I, Eq.(3)	160	71	18	I_o Eq.(16)	420	186	67
				A	Fig. 7	Fig. 7	Fig. 7
				I	Fig. 8	Fig. 8	Fig. 8
M_A, M_T, M_p	(1)	(0.4450)	(0.1110)	M_A, M_T, M_p	(1)	(0.4450)	(0.1110)
I_A	(1)	(0.1970)	(0.0123)	I_A	(1)	(0.1970)	(0.123)
$w_A a_A$	(1)	(1.59)	(3.46)	$w_A a_A$	(1)	(1.59)	(3.46)
$w_{A\ MAX}$	(1)	(1.5)	(3.0)	$w_{A\ MAX}$	(1)	(1.5)	(3.0)
F, Fig.4, 4a	(1)	(0.2960)	0.0370	F, Fig.11,12	(1)	(0.2960)	(0.0370)
T, Fig.5	(1)	(0.1970)	0.0124	T, Fig. 5	(1)	(0.1970)	(0.0124)

QUANTITIES IN ( ) ARE SCALING FACTORS FOR QUANTITIES IN FIG. 15 AND LOADING CONDITIONS AS INDICATED

Fig. III-16. Parameter values for configurations I, II and III, non-tapered and tapered, K = 0.1.

twenty different loading conditions.

The loading conditions (i.e. reaction forces, F, and torques, T, at the structural junctions) are obtained with the aid of Figs III-4, III-4a, and III-5 for the non-tapered structures, and Figs. III-11, III-12, and III-5 for the tapered structures.

The scaling factors for the configuration and loading conditions, in Fig. III-16, are computed with Eqs. (37a) to (37j).

While the weighted rms deflection, d, is expected to scale accurately with respect to a_A, p_S, E, and K, as discussed in connection with Eq. (37k), specific values for a_A, p_S, E, and K have been selected in the above for computational purposes.

4.2 DEFLECTION PATTERNS.

The loading conditions plus crossectional and mass properties computed in Section 4.1 are used as input data for the GD/A (IBM7090) deflection analysis program.

Input data for the following specific structural configurations and loading conditions used:

Configuration	Loading Conditions
I	1 to 20
II	1 to 10
III	1 to 10
I T	1 to 10
III T	1 to 10

The results presented in this and the following sections are based on these data.

In addition to the above data a minor-axis moment of inertia of 10 in.^{4} has been used to satisfy the program input requirements. This inertia has not been scaled as I_o or I for the other configurations. Therefore for the smaller (L = 100) configurations, it is comparable with the principal-axis inertia. However, because of the nature of the loading conditions the influence of the minor-axis inertia on flexural rigidity is not significant.

The program computes the three orthogonal linear and angular deflections at the junctions, as well as the coordinate forces and torques acting on each of the structural members.

Here we are only concerned with the linear deflections normal to the reflector surface (i.e. nominally in the direction of the axis of the main lobe in the radiation pattern). In the more complete r-f radiation (IBM7090) program, described in the second quarterly report, Ref. (4), all linear and angular deflections are taken into account.

Normalized deflection patterns are presented in Figs. III-7 to III-26 for the tapered and non-tapered structures under the different loading conditions. The dark vertical lines in these figures represent the normal components of the deflections at the junctions in one quadrant of the structure.

The computed normalized deflection patterns in Figs. III-17 to III-27 are not affected by load level changes.

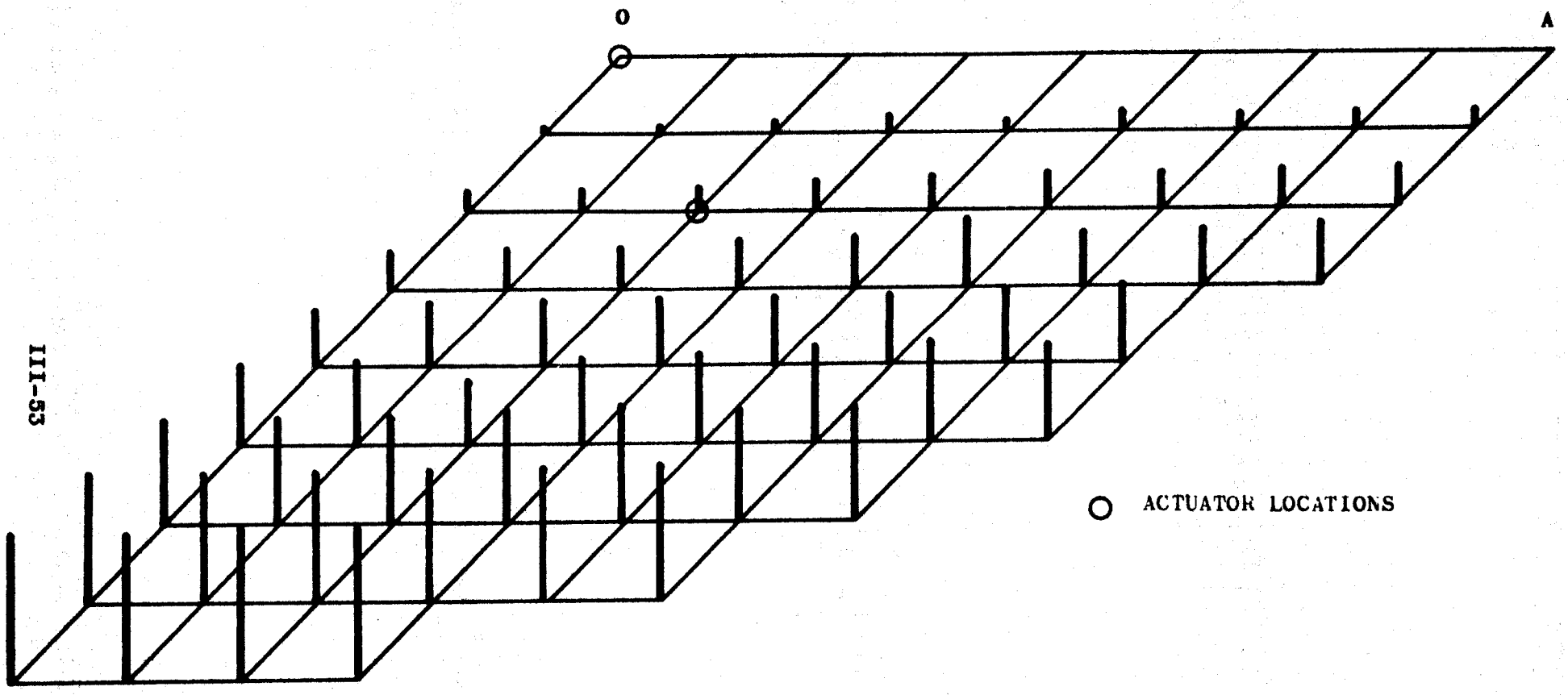


Fig. III-17. Normalized deflection patterns, non-tapered structures, loading conditions 1, 2, 3, 4.

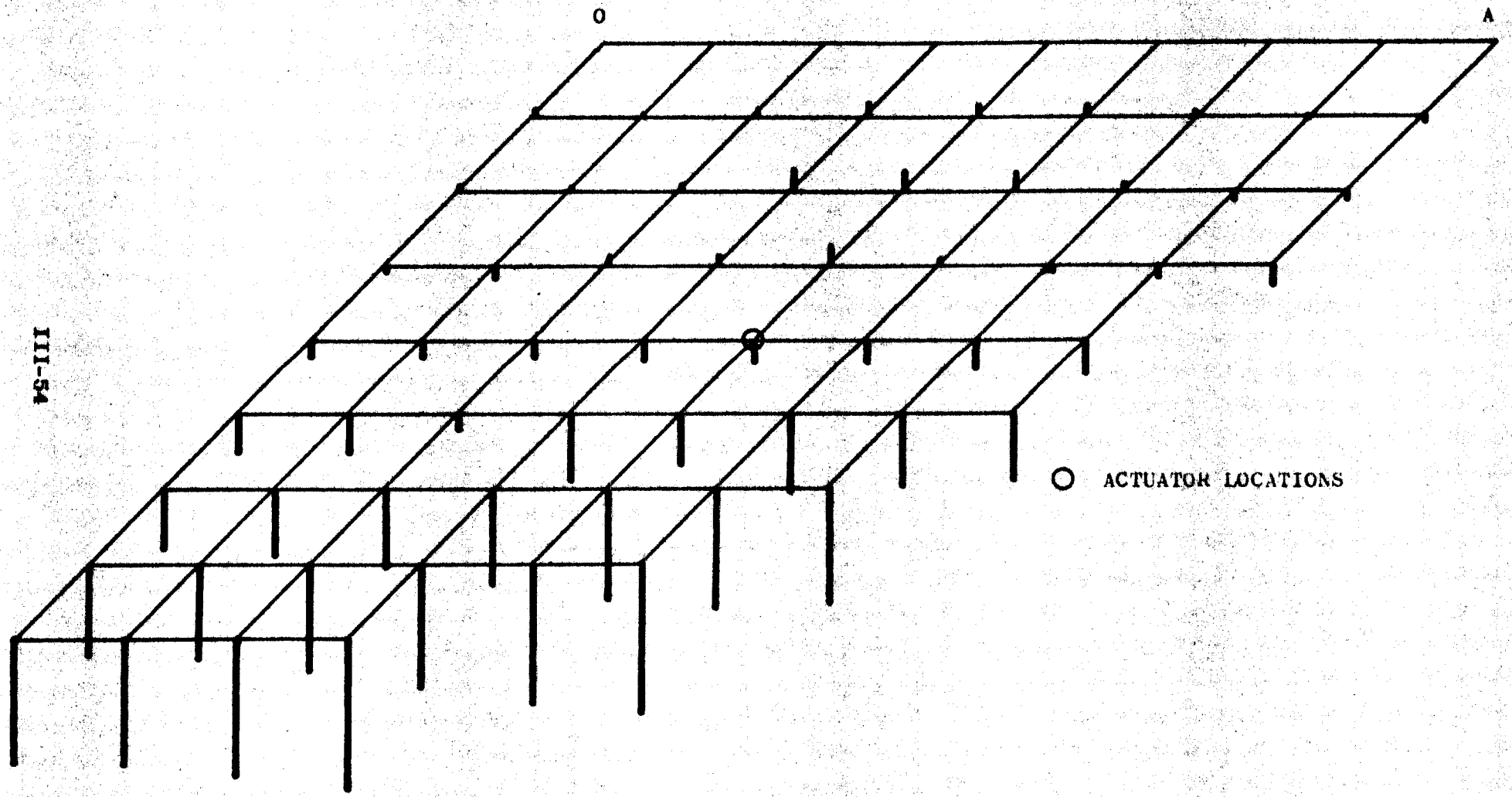


Fig. III-18. Normalized deflection patterns, non-tapered structures, loading conditions 5, 6, 7.

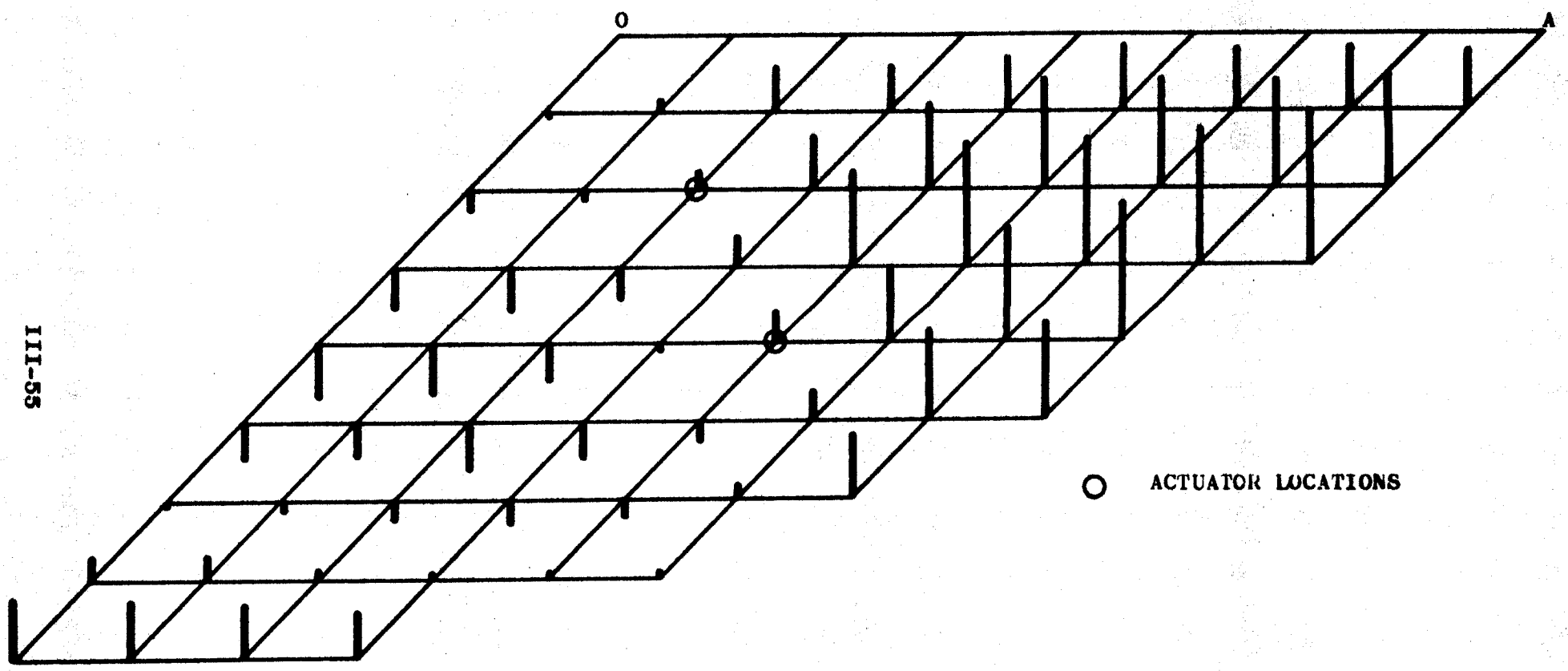


Fig. III-19. Normalized deflection patterns, non-tapered structures, loading conditions 8, 9, 10.

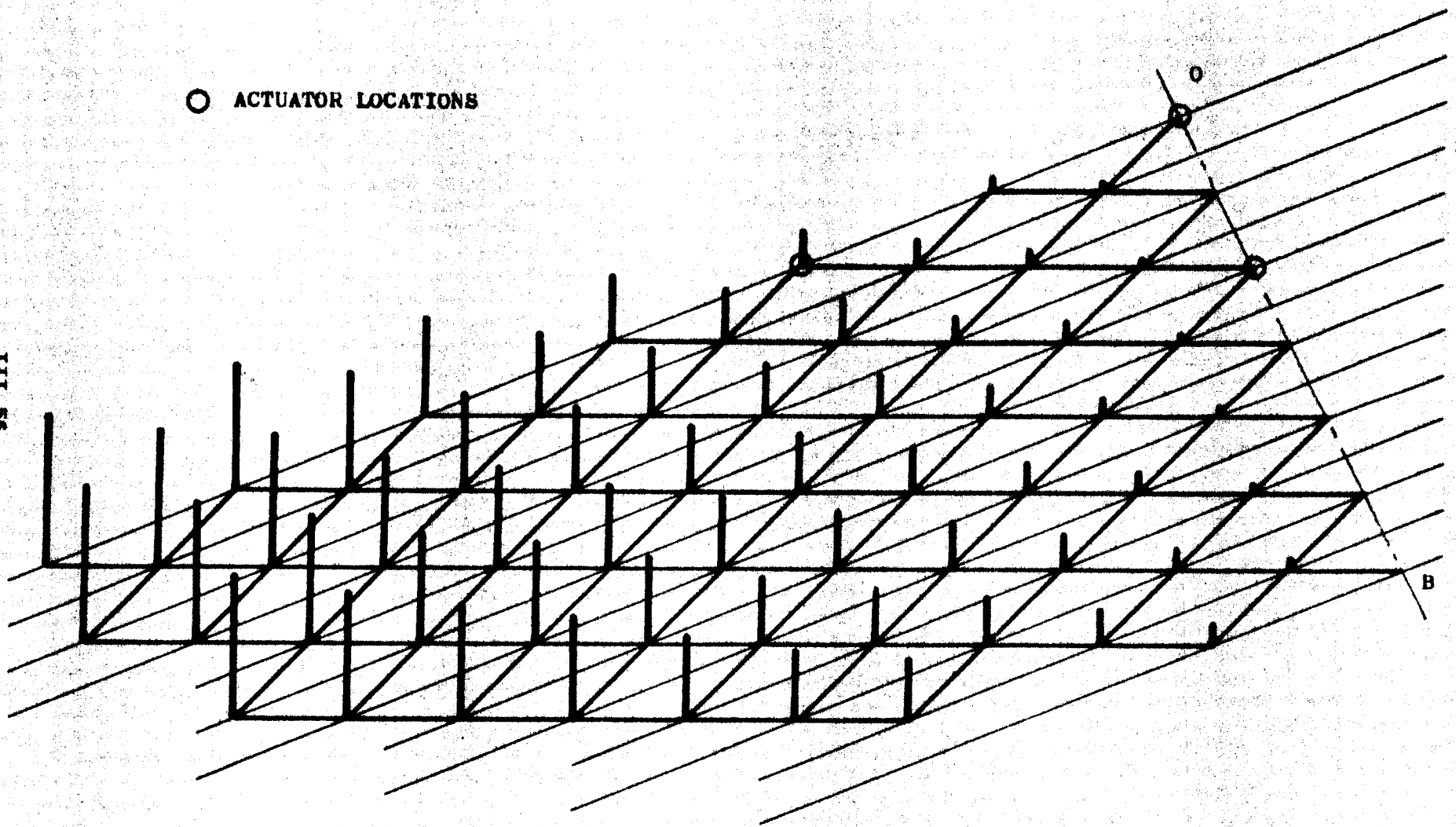


Fig. III-20. Normalized deflection patterns, non-tapered structures, loading condition, 11, 12, 13, 14.

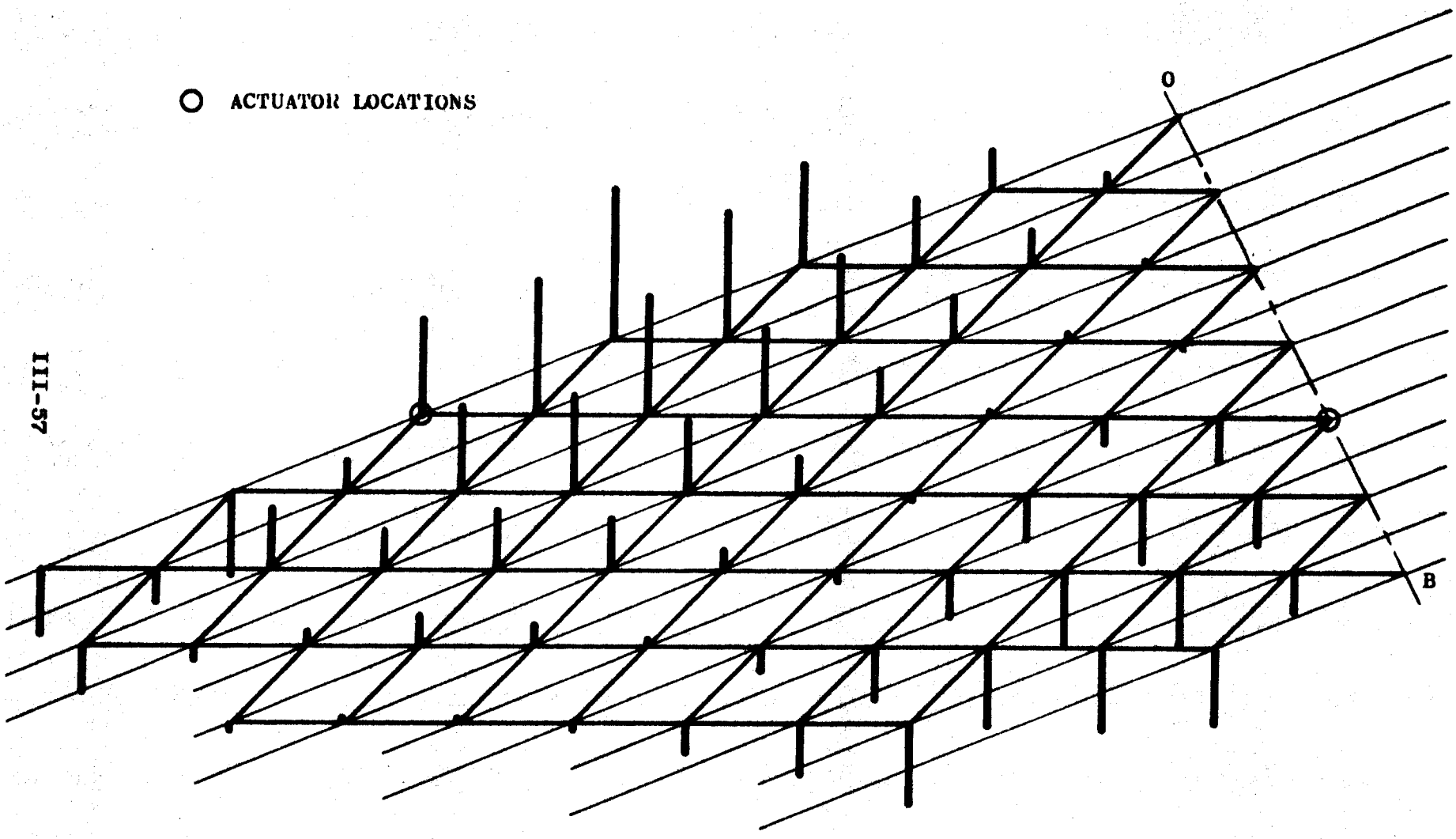


Fig. III-21. Normalized deflection patterns, non-tapered structures, loading conditions 15, 16, 17

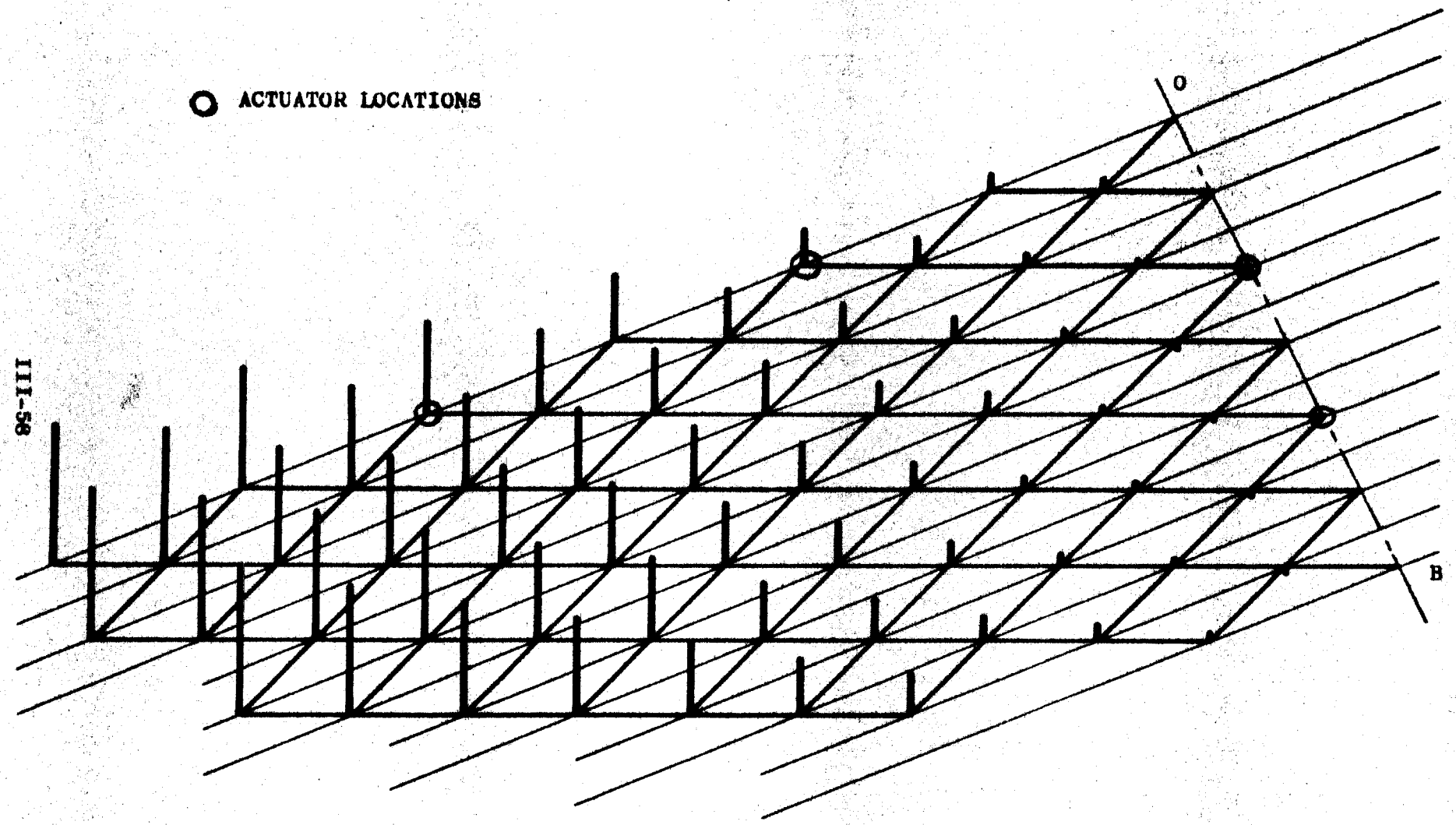


Fig. III-22. Normalized deflection patterns, non-tapered structures, loading conditions 18, 19, 20.

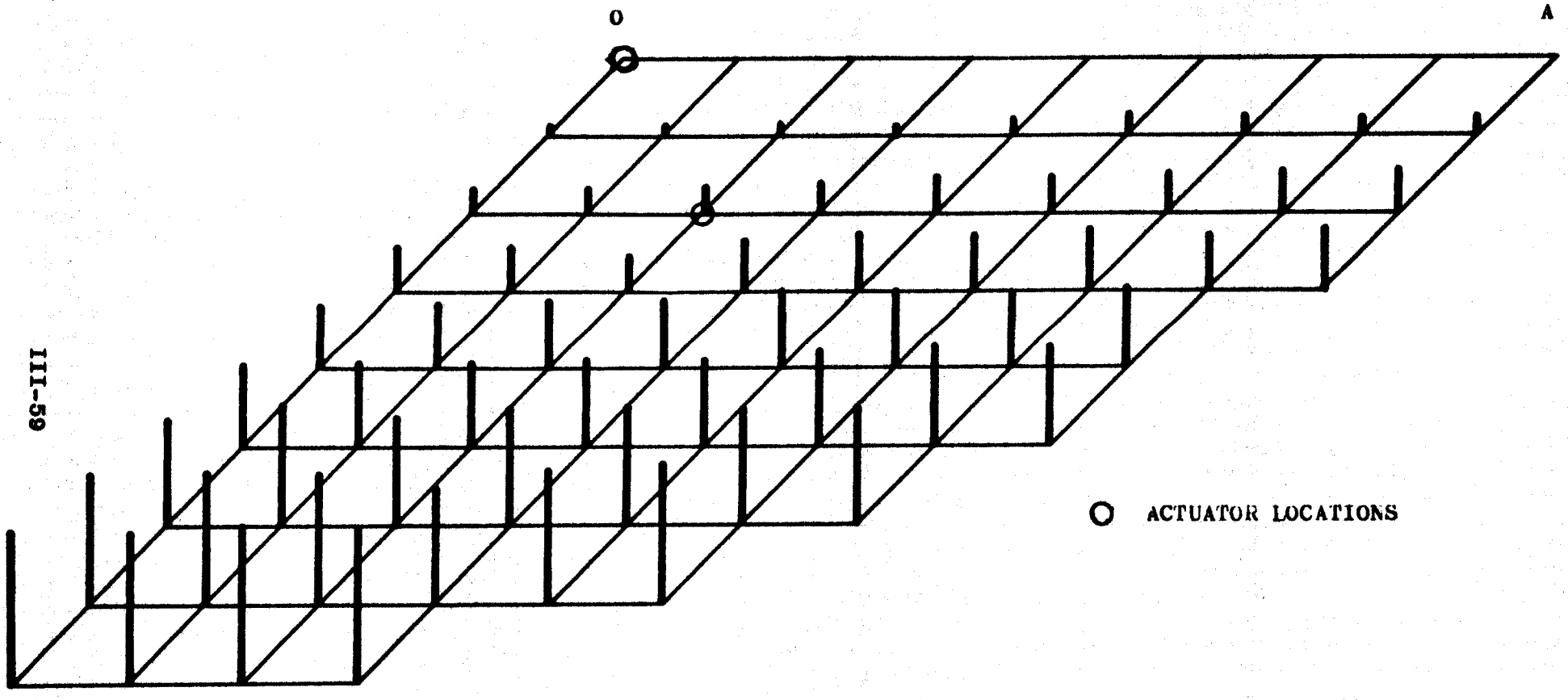


Fig. III-23. Normalized deflection patterns, tapered structures, loading conditions, 1, 2, 3, 4.

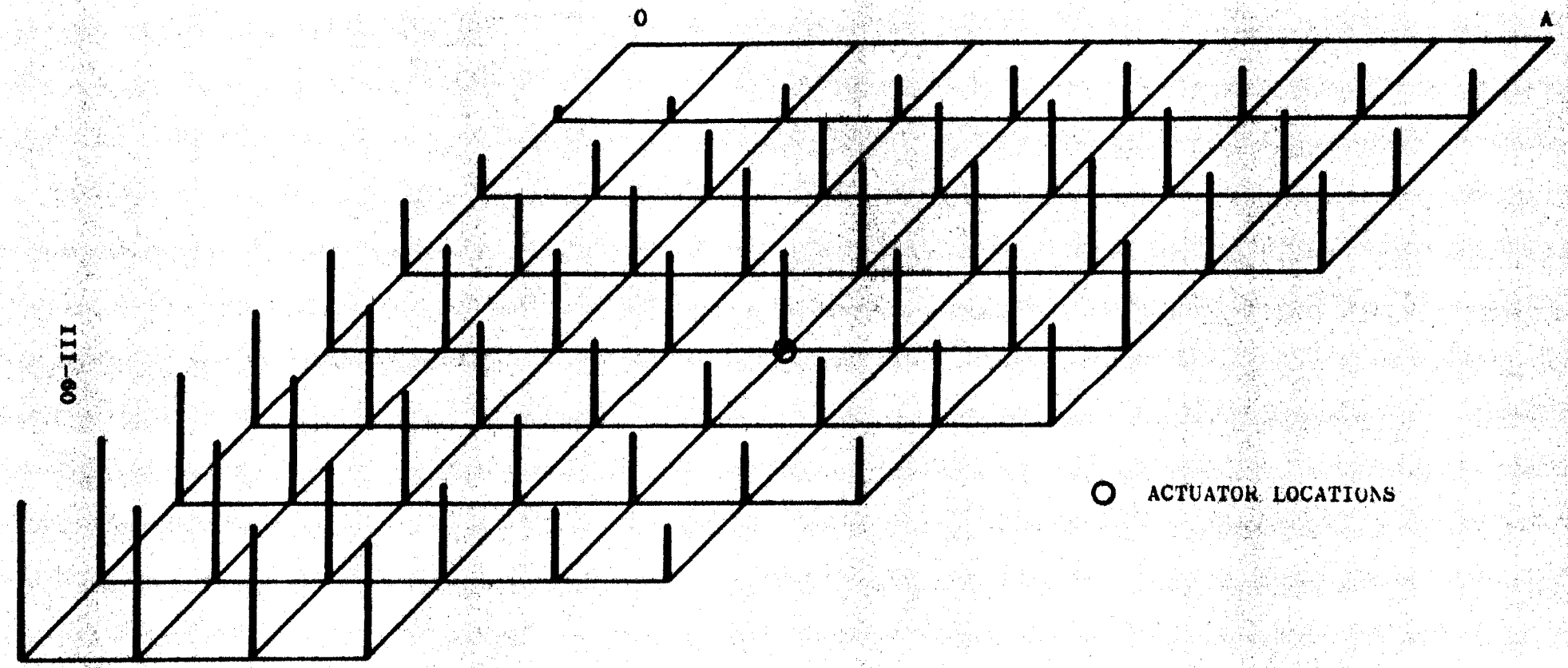


Fig. III-24. Normalized deflection patterns, tapered structures, loading conditions 5.

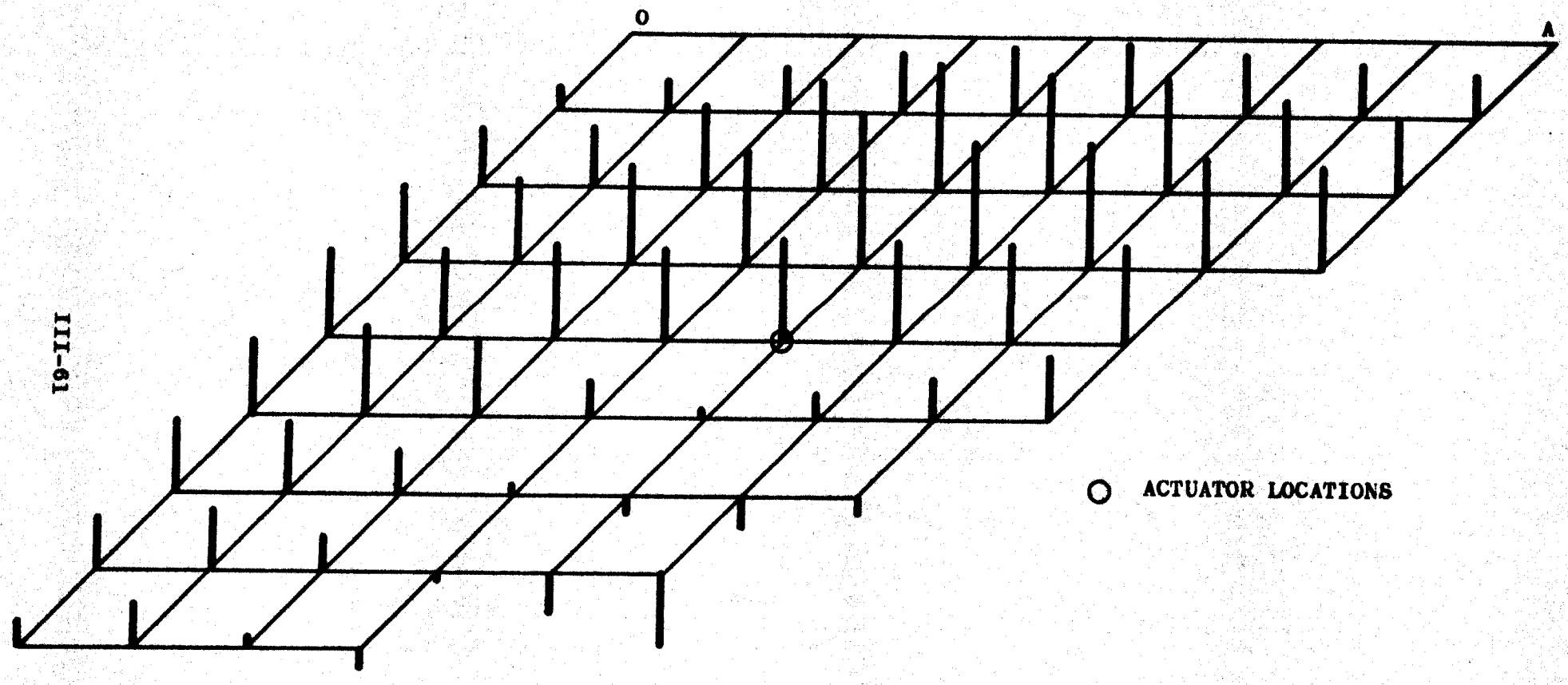


Fig. III-25. Normalized deflection patterns, tapered structures, loading conditions 6, 7.

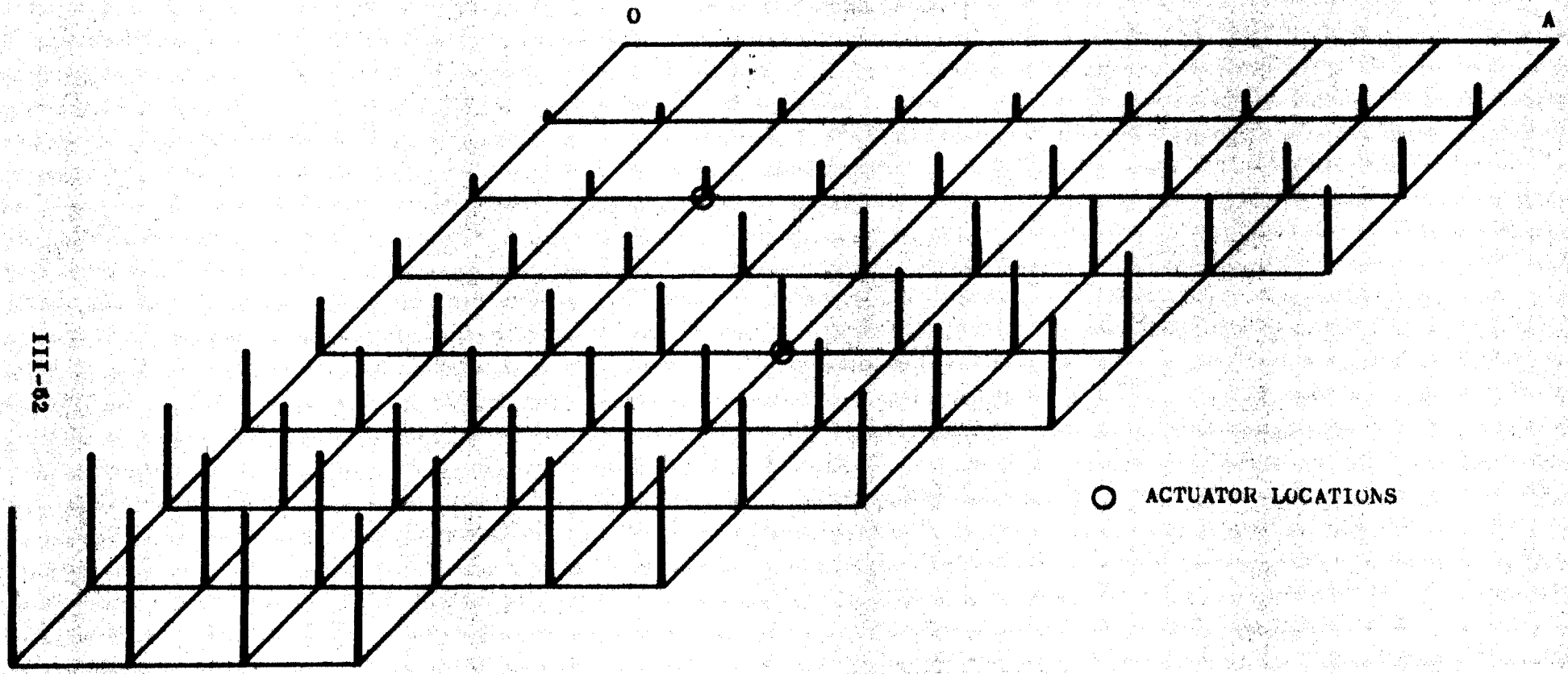


Fig. III-26. Normalized deflection patterns, tapered structures, loading conditions 8, 9, 10.

4.2.1 MONOTONIC DEFLECTION PATTERNS.

It is noted in Figs. III-17, III-20, III-22, III-23, and III-26 that the deflection patterns are very similar for the non-tapered structures under loading conditions 1, 2, 3, 4, 11, 12, 13, 14, 18, 19, 20, as well as for the tapered structures under loading conditions 1, 2, 3, 4, 8, 9, 10. These are the conditions in which the actuators are located at or near the center of the reflector (i.e. actuator distribution cases 1 and 2), or in which the masses and output torques of the individual actuators are reduced and have a maximum distribution over the structure (i.e. actuation distribution case 4). For these conditions the reaction forces and applied torques corporate to produce deflections that continuously increase with distance from the neutral axis.

4.2.2 PATTERN INFLECTIONS.

When the actuators are deployed at a substantial distance from the neutral axis, as in the actuator distribution case 3, there is a tendency for the actuator torques to deflect the structure between the actuators and neutral axis in a direction opposite to that normally caused by the reaction forces at the junctions. As a result, there generally are inflections in the patterns for loading conditions 5, 6, 7, 15, 16, 17. An exception to this for the tapered structures under loading condition 5 is noted in Fig. III-24. However, when the loads are increased in this case, Fig. III-25 indicates that an inflection does take place in the deflection pattern.

It is possible that inflections may be avoided or induced by adding or subtracting local stiffness in the vacinity of the actuator moments. The desirability of changing the stiffness would have to be evaluated in terms of the affects on the weighted rms deflections considered in Section 4.3.

It is interesting that the rms deflections, rather than individual peaks in the deflection pattern, have a major influence on the r-f radiation performance of a reflector.

The deflection patterns in Figs. III-17 to III-26 approximate the mode shapes at the fundamental resonant frequencies of the structure.

There is a tendency for inflections to develop in cases 2 and 4, however, because of the loading conditions or configuration properties they do not. A comparison of the patterns in Figs. III-19 and III-22 for case 4 actuators indicates the influence of O-A vs. O-B loading conditions on inflections.

4.3 WEIGHTED RMS DEFLECTIONS.

A computer program was set up to determine the weighted rms deflections, d, for each of the sixty loading conditions and five configurations described in Section 4.2. Figs. III-27 to III-29 show the nromalized rms deflections vs. reflector size for cosine illumination, the four actuator distribution cases, O-A axis rotation, three values of k_s, and non-tapered and tapered structures. Figs. III-30 to III-32 show the deflections for uniform illumination, the other parameters being the same.

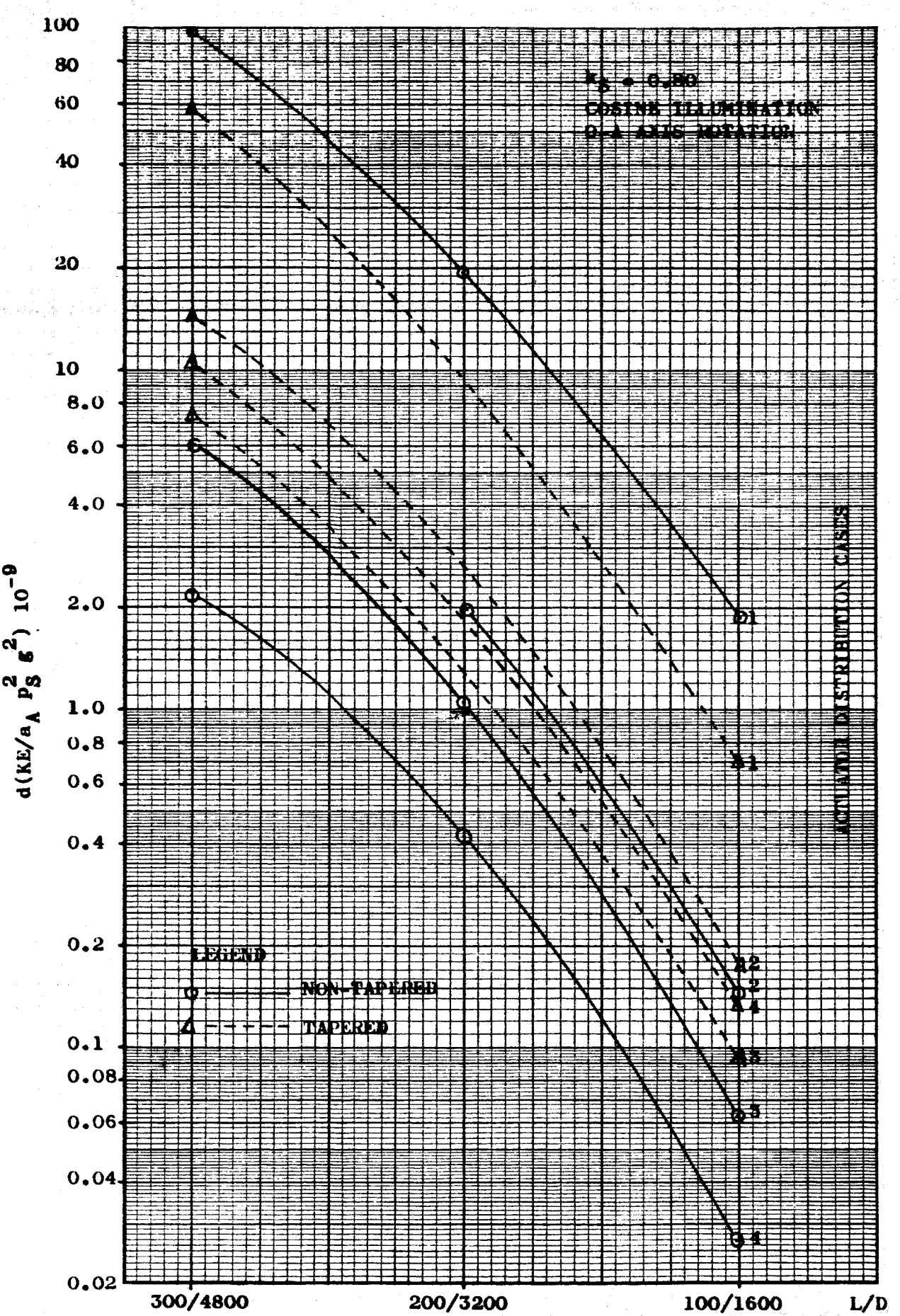


Fig. III-27. Normalized reflector distortions vs. reflector size.

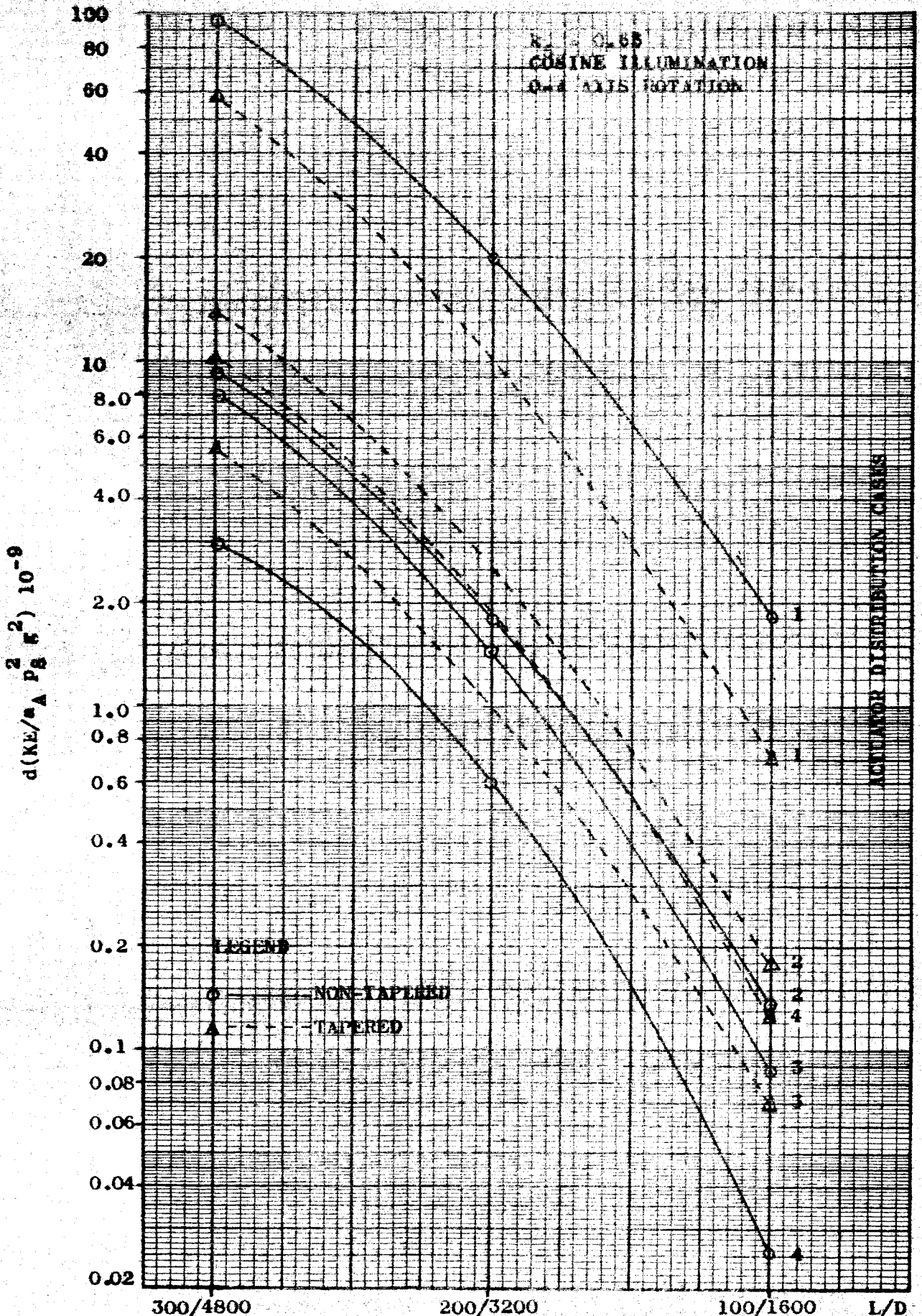


Fig. III-28. Normalized reflector distortions vs. reflector size.

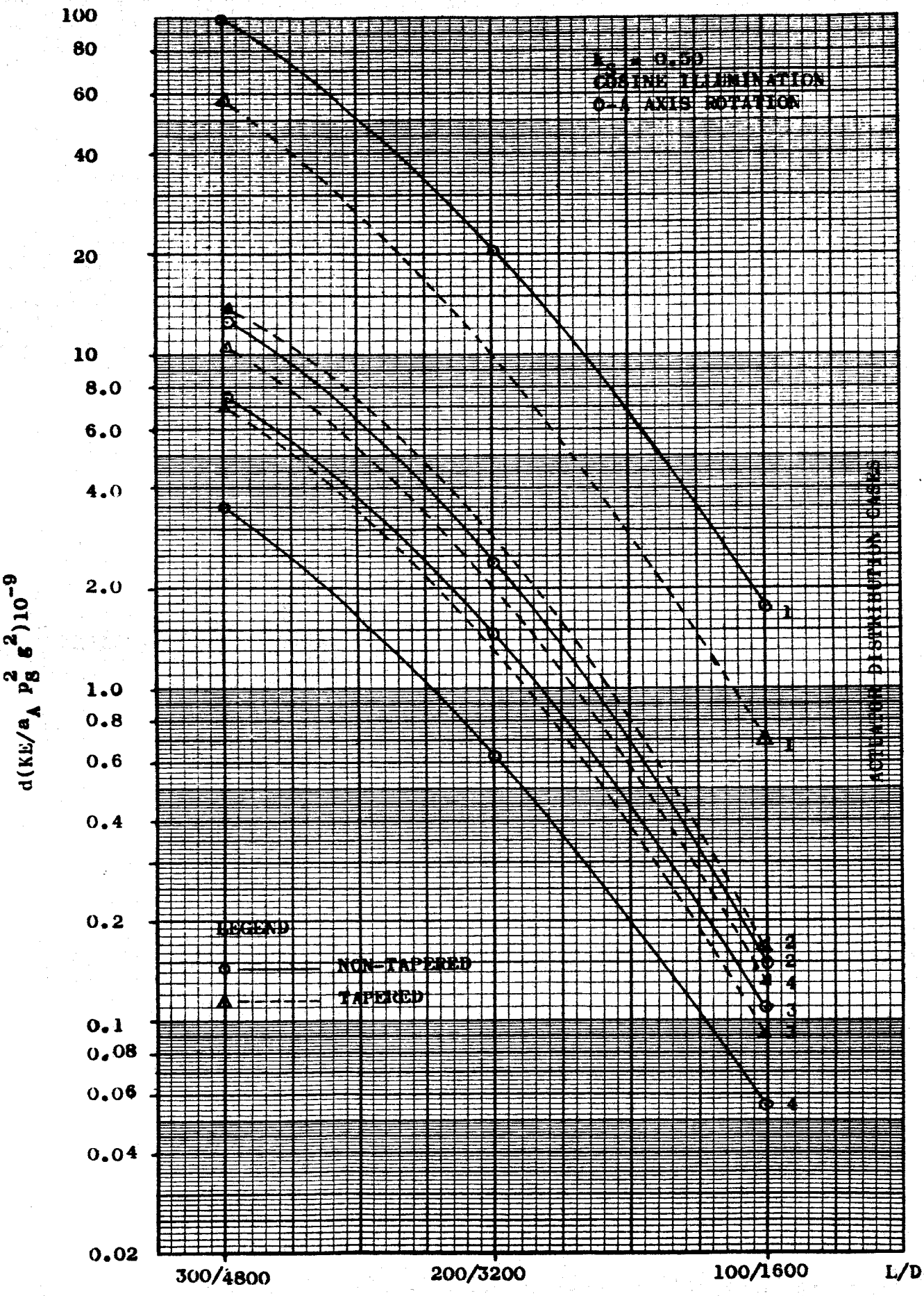


Fig. III-29. Normalized reflector distortion vs. reflector size.

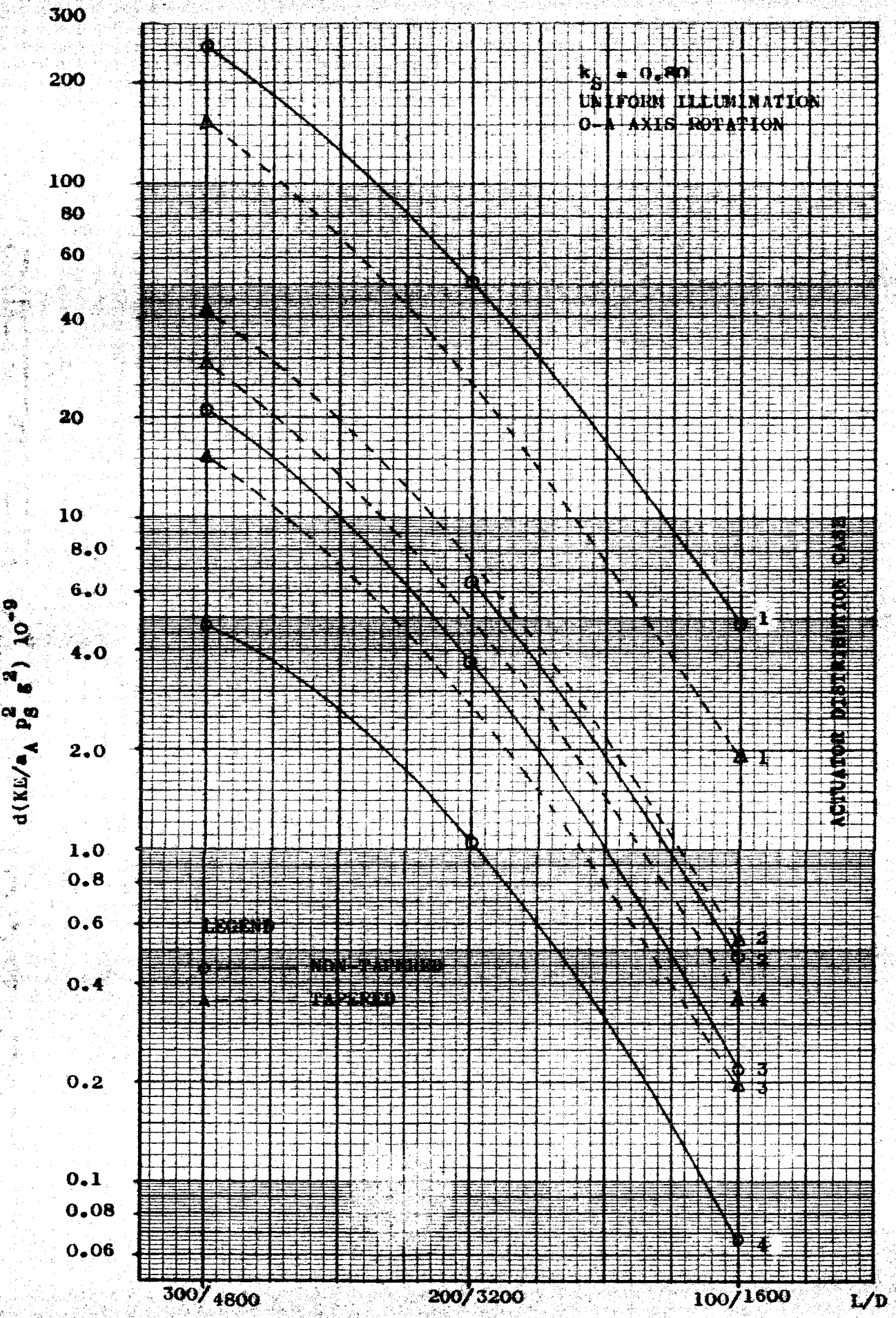


Fig. III-30. Normalized reflector distortion vs. reflector sizes.

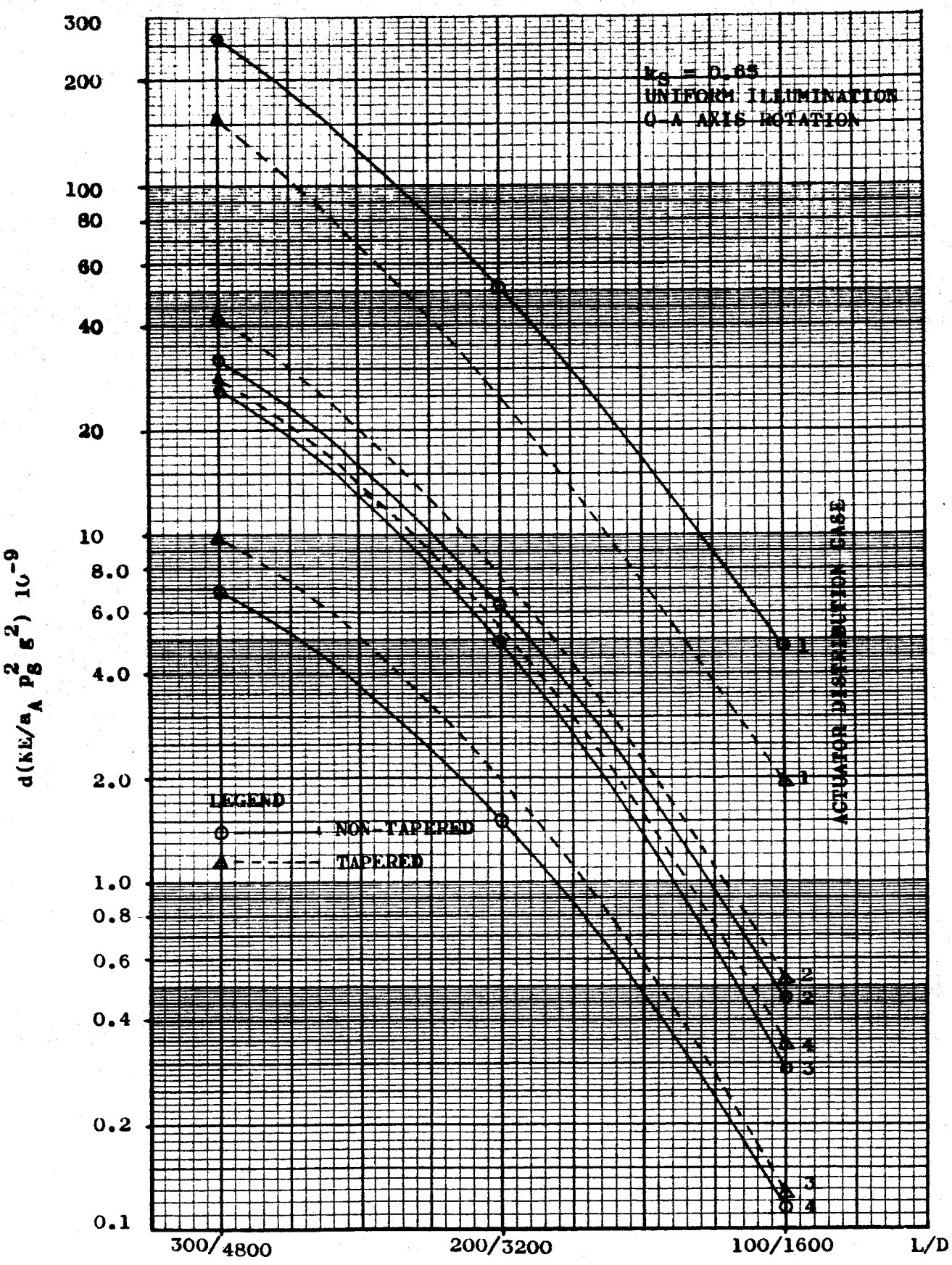


Fig. III-31. Normalized reflector distortions vs. reflector size.

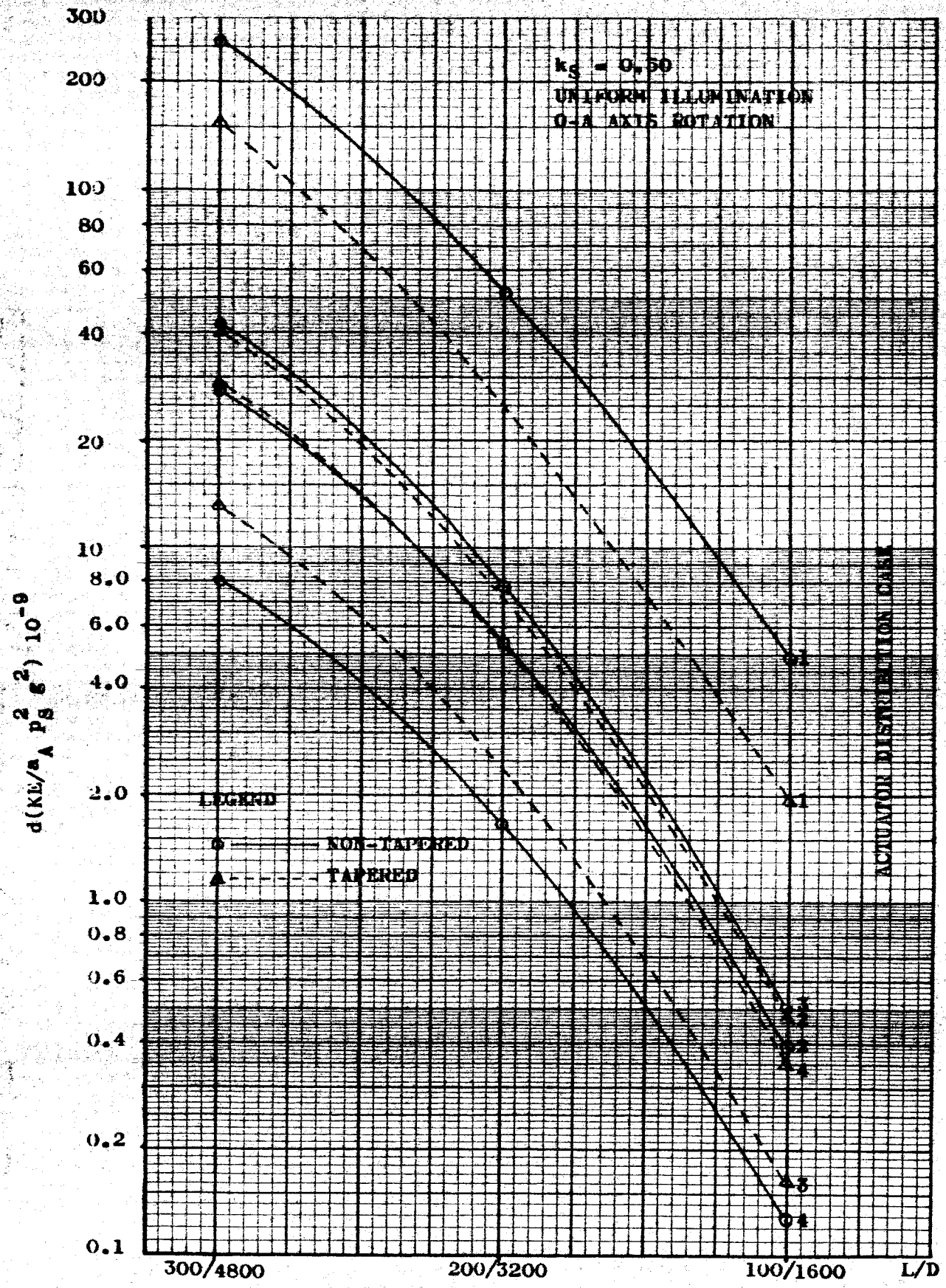


Fig. III-32. Normalized reflector distortions vs. reflector size.

The rms deflections, d, may be used with the information in Section 4.5 to nominally select the allowable operating r-f frequency. An approximate evaluation of the influence of d on antenna directivity, and side lobe level, may then be typically obtained with References (2) and (3).

It is relevant that the radiation analysis program, developed in part under this study, makes use of the individual deflections at the structural junctions, rather than d, to compute the far field radiation pattern. Once the pattern has been computed and plotted (automatically with the SC4020) the directivity and side lobe information is available. This approach, it is believed, yields much more useful and accurate results than available in the literature based on the d values.

4.3.1 AFFECTS OF STRUCTURAL TAPERING AND ACTUATOR DISTRIBUTIONS.

It is noted in Figs. III-27 to III-32 that the chosen actuator distribution cases have a pronounced affect on d. For the non-tapered structures the rms deflections progressively decrease from case 1 to 4. For the tapered structures the rms deflections decrease in the case order 1, 2, 4, 3. The lowest deflections are obtained with the chosen non-tapered structure and case 4 actuator distribution.

Structural tapering increases d in cases 1 and 4 and generally decreases d in cases 1 and 3. In case 4, where the actuators have their maximum distribution, the tapering is most detrimental. In case 1, where only one actuator is used at the

apex of the reflector, tapering is most beneficial. This indicates that the tapering and actuator distributions must be considered collectively to maximize their individual contributions to reducing d.

4.3.2 AFFECTS OF STRUCTURAL MASS FRACTIONS.

Because the actuator masses are lumped, and are assumed to have no angular moment of inertias about their centers of mass, changes in k_S (the structural mass fraction) in case 1, have no effect on d. For the other cases the k_S values have an effect on d as displayed in Figs. III-33 to III-38, for L = 300, 200, 100, and cosine and uniform illuminations.

It is evident from Figs. III-33 to III-38 that in most cases, the normally expected, the reduction of structural compliances, (i.e. the reduction of k_S) results in reduced r-f performance (i.e. increased d valves). In some of the cases, however, the opposite is true. It is expected that this latter occurrence is explained in part by the tendency in these cases for an inflection or an incipient inflection in the deflection pattern.

While uniform illumination generally increases the values of d, it does not significantly change the character of the d vs. k_S curves.

4.3.3 AFFECTS OF ILLUMINATION FUNCTIONS.

The chosen cosine illumination reduces the d values on the order of one-third of the d values for the uniform illumination. This follows from the nature of the loading conditions which

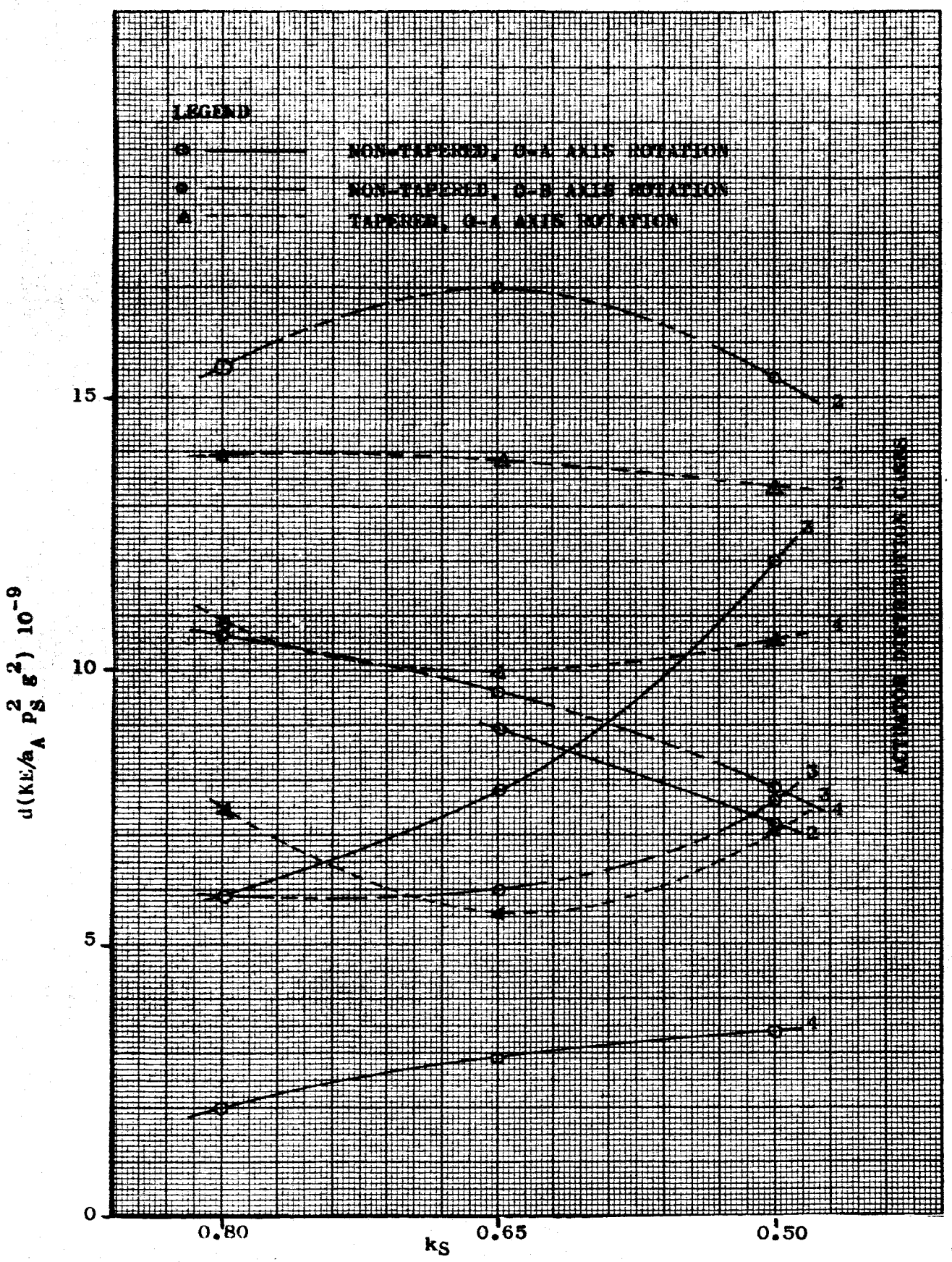


Fig. III-33. Normalized reflector distortions vs. k_S, L = 300, cosine illumination.

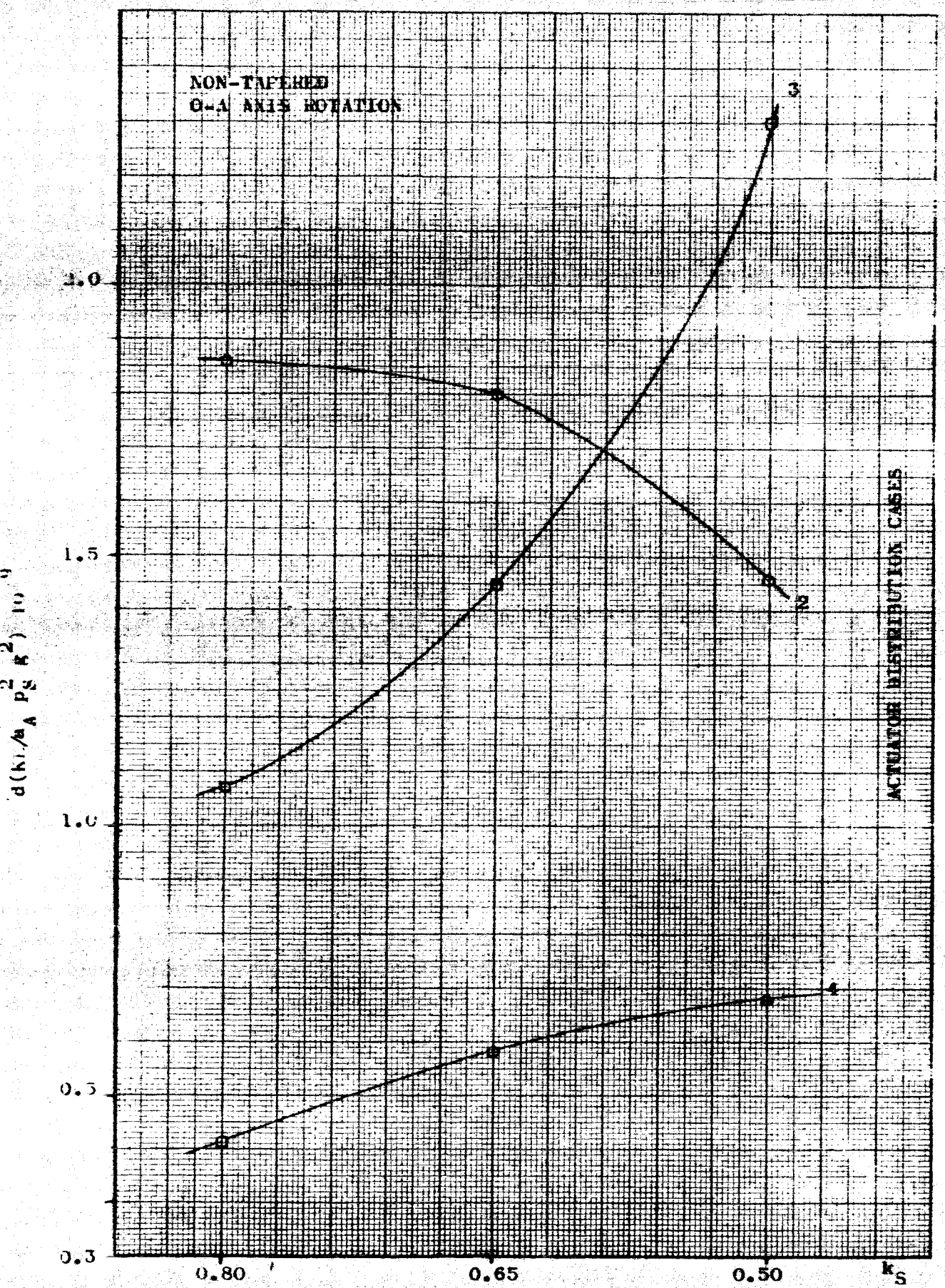


Fig. III-34. Normalized reflector distortions vs. k_S, L = 200, cosine illumination.

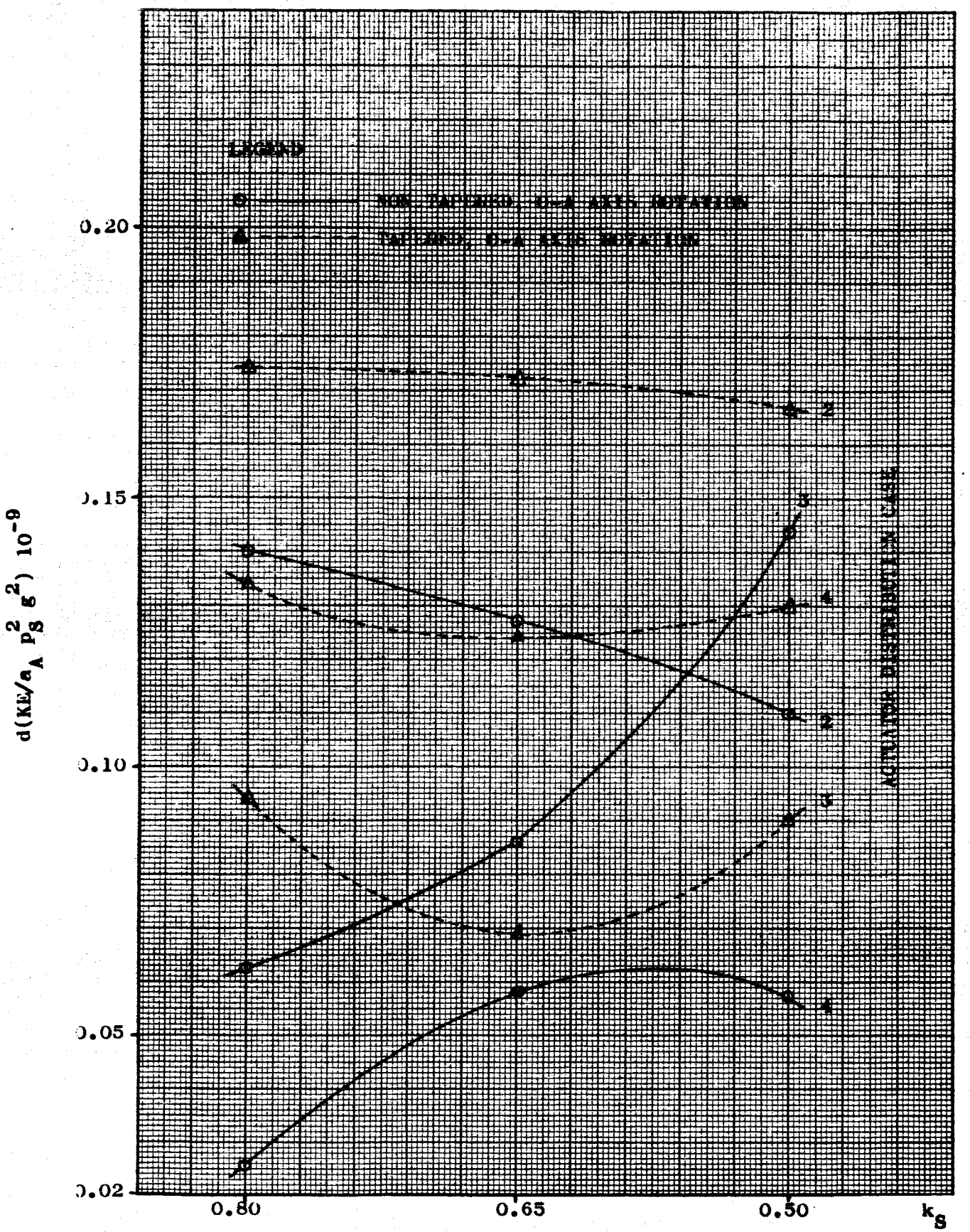


Fig. III-35. Normalized reflector distortions vs. k_S, L = 100, cosine illumination.

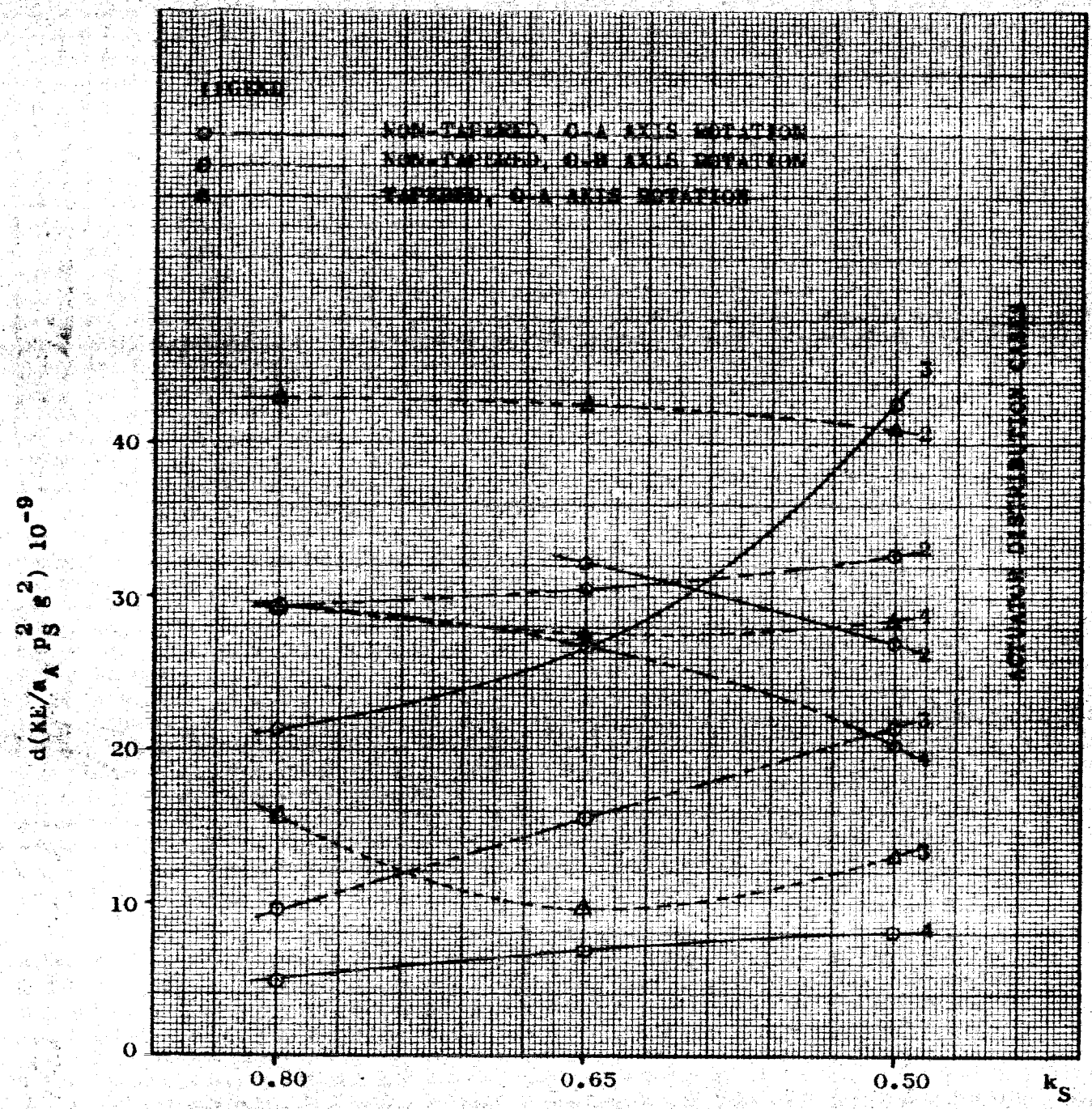


Fig. III-36. Normalized reflector distortions vs. k_S, L = 300 uniform illumination.

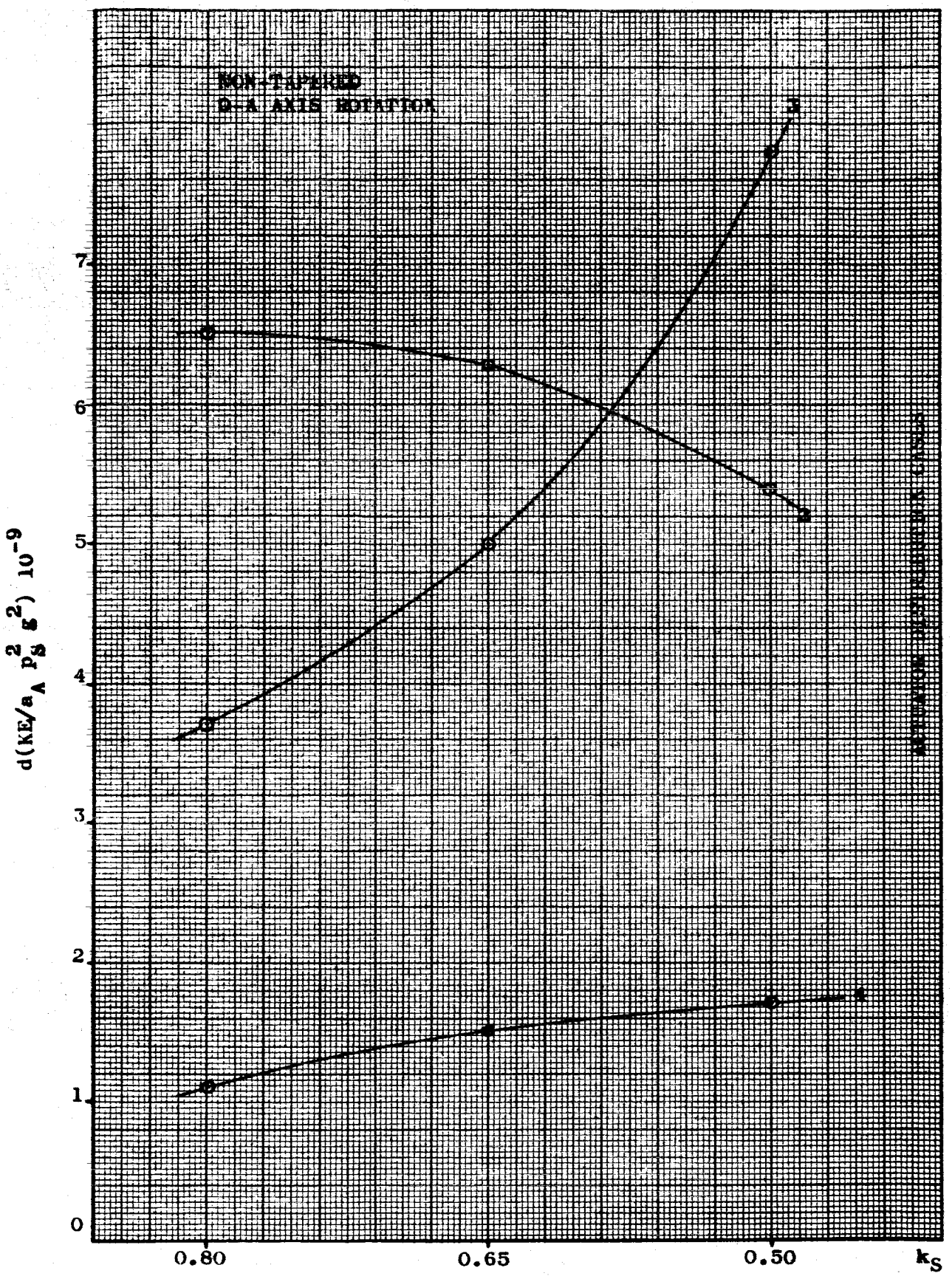


Fig. III-37. Normalized reflector distortions vs. k_S, L = 200 uniform illumination.

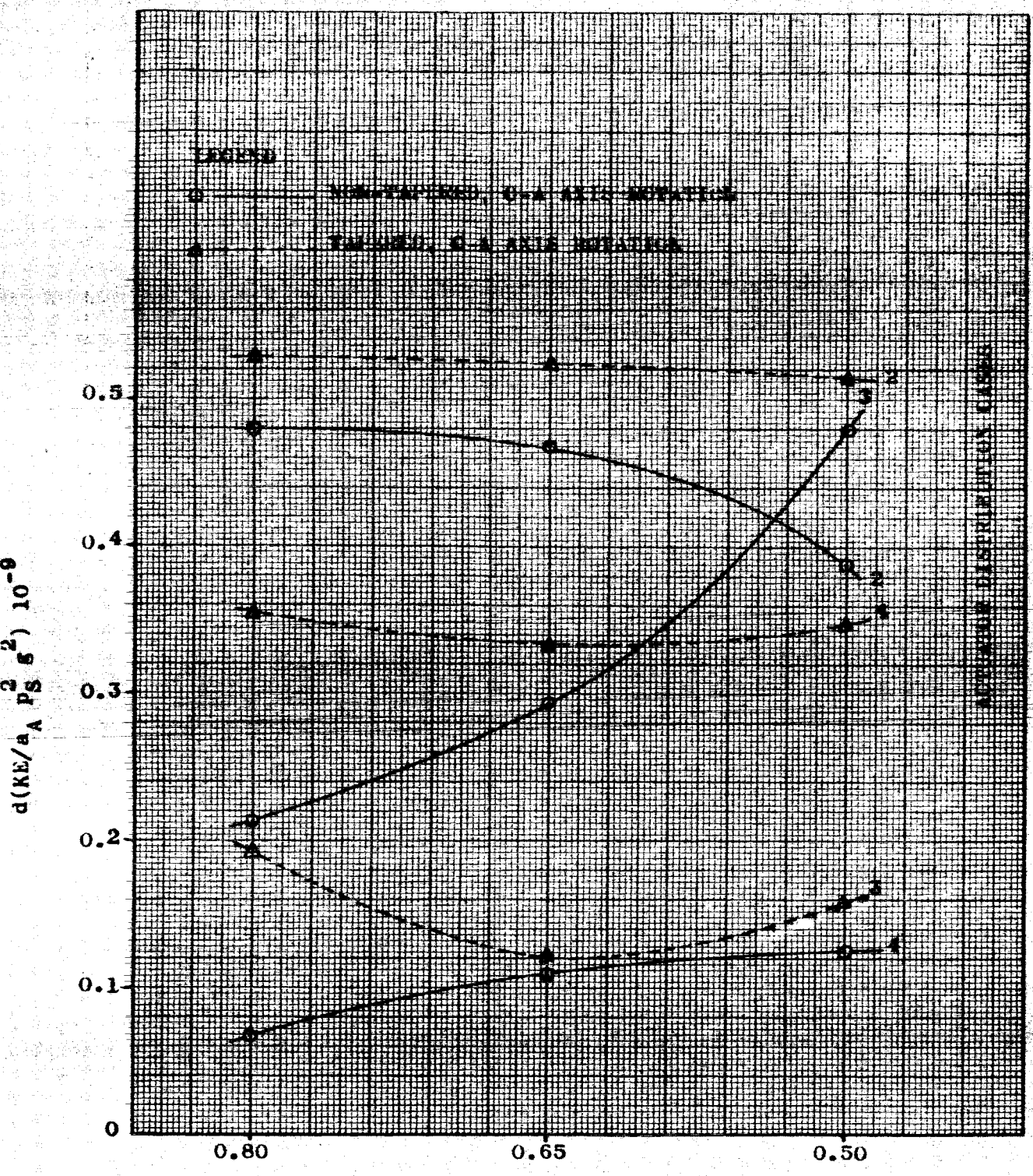


Fig. III-38. Normalized reflector distortions vs. k_S, L = 100 uniform illumination.

generally cause the junction deflections to increase with distance from the neutral axis, particularly when there are no inflections in the deflection pattern.

Fig. III-39 shows the ratio of d values for uniform illumination to the d values for cosine illumination. The ratios in Fig. III-39 indicate that the greatest improvement due to the cosine illumination generally takes place for the non-tapered structures.

4.3.4 O-A AXIS VS. O-B AXIS ROTATION.

Fig. III-40 shows the ratios of d for O-B to d for O-A axis rotation with cosine and uniform illumination. These ratios are based on the deflection data for the non-tapered structure with L = 300.

The small ratios, in Fig. III-40, for case 3 (compared to case 4) may be explained by the deflection pattern inflections which take place for both the O-A and O-B axis-rotations (see Figs. III-18 and III-21). In case 4, there are inflections in the O-A rotation axis patterns (see Fig. III-19) and none in the O-B rotation-axis patterns (see Fig. III-22). Since d tends to be larger when there are no inflections than when there are inflections it follows that the ratios in Fig. III-40 should be larger for case 4 than for case 3.

Also there are no inflections in the patterns for cases 1 and 2, and O-A and O-B axis rotation (see Figs. III-17 and III-20). By the above reasoning the d-ratios for case 4 are greater than corresponding the d-ratios for cases 1 and 2.

LOADING CONDITION	ACTUATOR DISTRIBUTION CASE	NON-TAPERED			TAPERED	
		L = 300	L = 200	L = 100	L = 300	L = 100
1	1	2.73	2.70	2.60	2.68	2.68
2	2		3.50	3.42	3.06	3.06
3	2	3.60	3.25	3.40	3.06	3.02
4	2	3.75	4.40	3.56	3.06	2.95
5	3	3.60	3.80	3.45	2.02	2.06
6	3	3.50	3.40	3.44	1.75	1.75
7	3	3.50	3.40	3.46	1.68	1.78
8	4	2.40	2.55	2.67	2.70	2.65
9	4	2.35	2.60	2.00	2.72	2.70
10	4	2.32	2.31	2.20	2.67	2.70
11	1	2.67				
12	2	3.26				
13	2	3.18				
14	2	3.23				
15	3	1.46				
16	3	2.60				
17	3	2.82				
18	4	2.94				
19	4	2.72				
20	4	2.60				

Fig. III-39. Ratio of d for uniform illumination to d for cosine illumination, O-A axis rotation.

LOADING CONDITIONS	ACTUATOR DISTRIBUTION CASES	COSINE ILLUMINATION	UNIFORM ILLUMINATION
1, 11	1	1.54	1.54
2, 12	2		
3, 13	2	1.90	1.68
4, 14	2	2.10	1.82
5, 15	3	1.00	0.45
6, 16	3	0.77	0.58
7, 17	3	0.63	0.52
8, 18	4	5.40	6.50
9, 19	4	3.24	5.40
10, 20	4	3.29	2.54

Fig. III-40. Ratio of d for O-B to d for O-A axis rotation, non-tapered structure, L = 300 .

The differences in the d-ratios for cases 1, 2, and 3 cannot be readily explained.

Except for part of case 4, the d-ratios in Fig. III-40 are smaller for the uniform illumination than for the cosine illumination. No simple explanation can be found for this occurrence.

Torsional rigidity in the structural members has been neglected in the d calculations. This rigidity, if included in the analysis, would have a greater influence in reducing the O-B deflections than in reducing the O-A deflections, and may therefore minimize the discrepancies shown in Fig. III-40.

4.3.5 SCALING OF d VS. L.

It is stated with respect to Eq. (37k) that there is a probable error in the scaling of d with L^4. The extent of this error is indicated in Fig. III-41. Here the values of d at L = 300 are obtained by L^4 scaling of the values at L = 100. The ratio is then taken of these values to the actually computed d values at L = 300. The available data allows for the computation of these ratios only for O-A axis rotation, as shown in Fig. III-41.

It can be seen in Fig. III-41 that the greatest scaling errors occur for the non-tapered structures. This is explained in part by the greater tendency for deflection-pattern inflection in the case of the non-tapered structures.

4.4 TURNING AND SLEWING RATES.

Figs. III-42 and III-43 show the normalized maximum turning rates $w_{A\ max}$ vs. k_g for the non-tapered and tapered structures, and

		COSINE ILLUMINATION		UNIFORM ILLUMINATION	
CASE	k_s	TAPERED	NON-TAPERED	TAPERED	NON-TAPERED
1	0.80	0.98	1.60	1.00	1.50
2	0.80	1.05		1.00	
2	0.65	1.00	1.23	0.99	1.47
2	0.50	1.00	1.22	0.97	1.16
3	0.80	1.01	0.85	1.01	0.82
3	0.65	0.99	0.88	1.00	0.89
3	0.50	1.00	0.96	1.00	0.95
4	0.80	0.99	1.03	0.98	1.14
4	0.65	1.00	1.57	1.00	1.37
4	0.50	0.99	1.33	1.00	1.37

Fig. III-41. Ratio of scaled to computed values of d at L = 300 for O-A axis rotation.

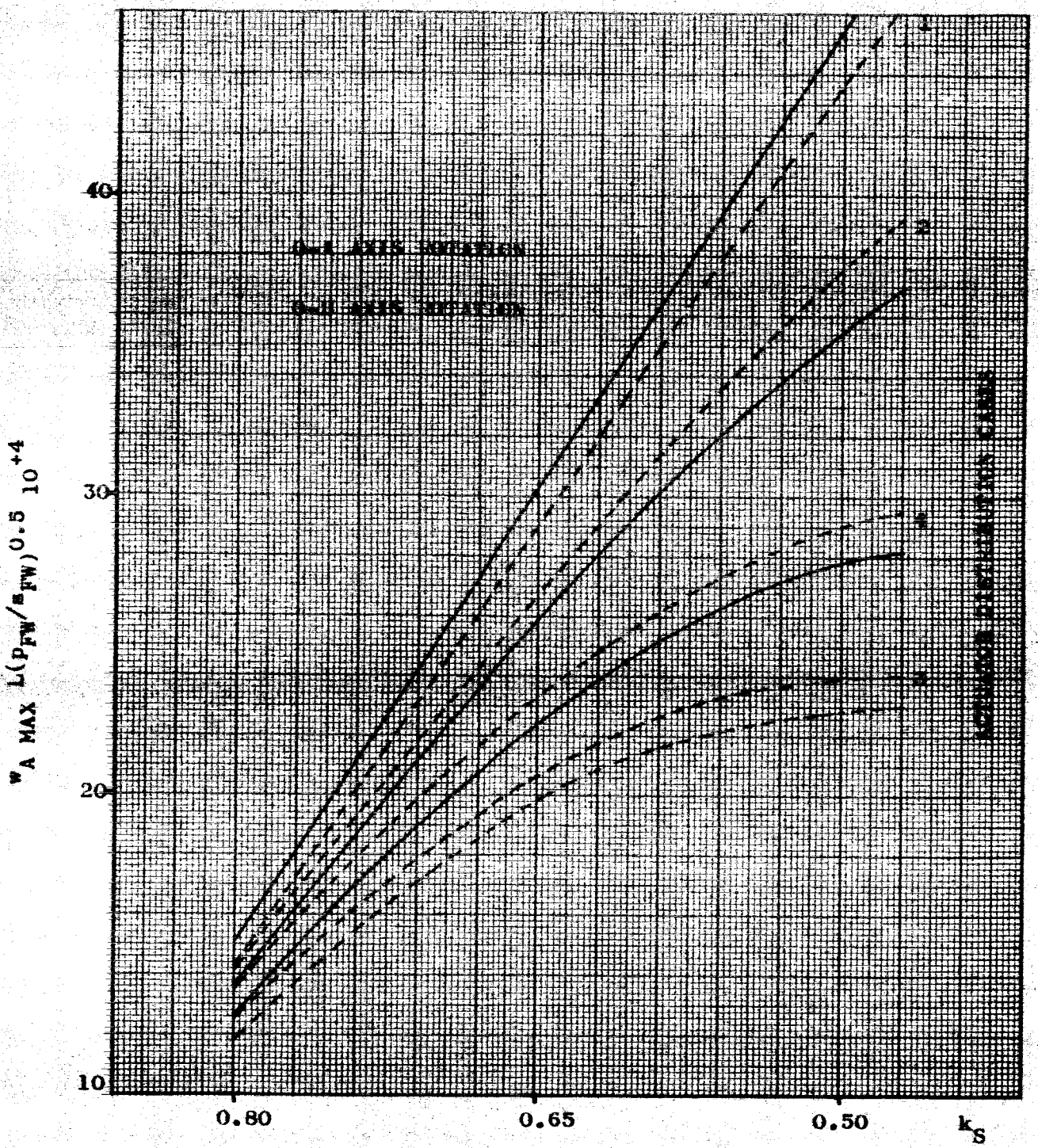


Fig. III-42. Normalized maximum turning rate, non-tapered structures.

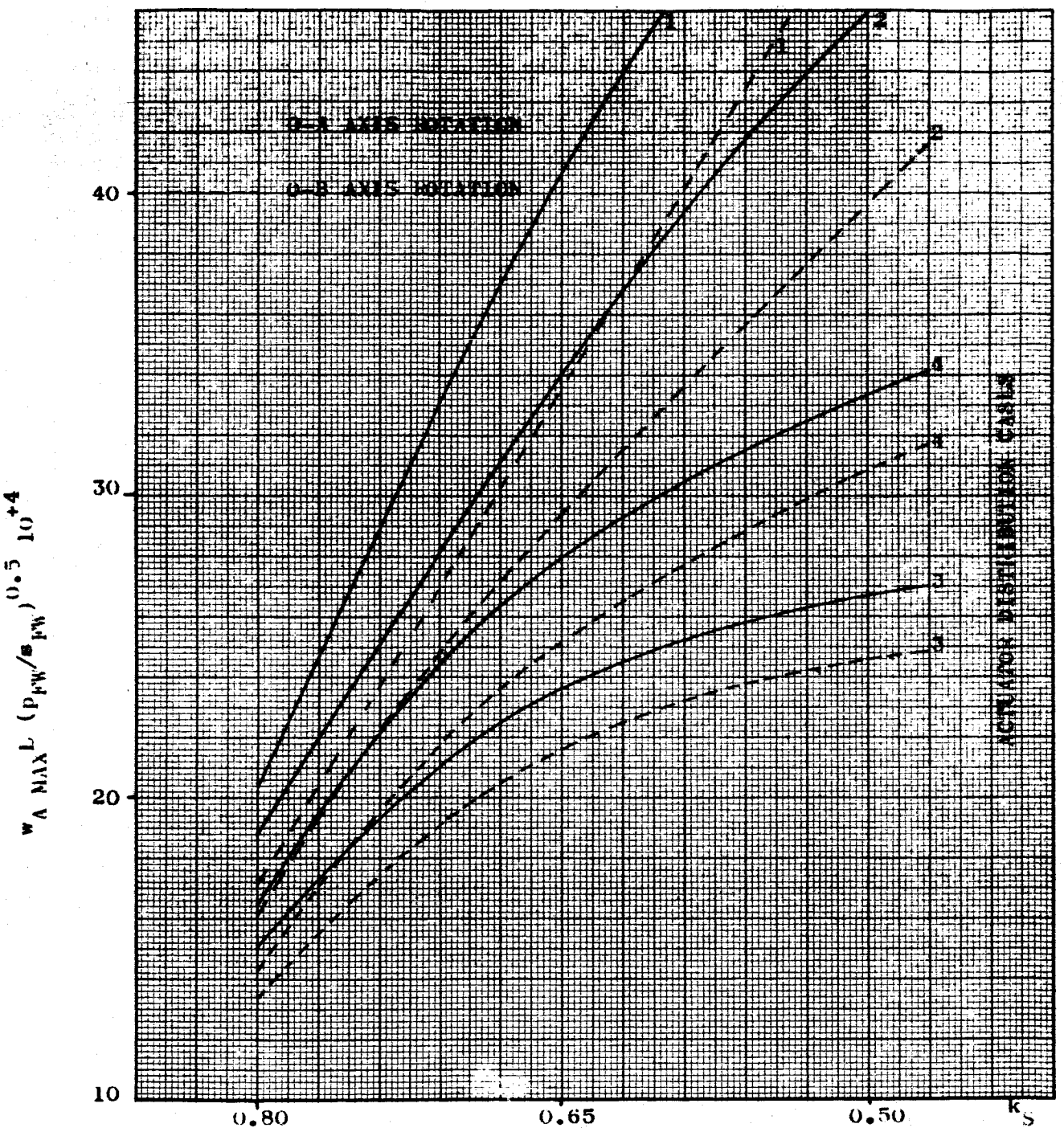


Fig. III-43. Normalized maximum turning rate, tapered structures.

the different actuator distribution cases. Figs. III-44 and III-45 show the normalized slewing rates a_A, vs. k_S for the same structures and cases. Figs. III-42 and III-45 are based on the data in Fig. III-15 and the scaling equations, Eqs. (37g) and (37f).

It follows from an examination of Figs. III-42 to III-45 that:

(1) The $w_{A\,max}$ and a_A in all cases increase with k_S, and for any given k_S, case, and rotation asis; and $w_{A\,max}$ and a_A are larger for the tapered than for the non-tapered structures. These characteristics follow firstly from the predominantly greater increase of M_{FW} (in Eq. (36)) with k_S than the I_A with k_S, and secondly because I_A is smaller for the tapered structures than for comparable non-tapered structures.

(2) The $w_{A\,max}$ and a_A for O-B axis rotation are smaller than these values for O-A axis rotation in the tapered structures and for case 1 of the non-tapered structures. At other times $w_{A\,max}$ and a_A for O-B axis rotation are greater than for O-A axis rotation. These occurrences are largely explained by the values of I_A in the different configurations and cases.

(3) The $w_{A\,max}$ and a_A performance is improved in the case order 3, 4, 2, 1.

(4) The greater the $s_{FW}/p_{FW}\,L$ ratio the greater the $w_{A\,max}$. Also the greater the $K^{0.43}/w_A\,L^{1.14}$ ratio the greater the a_A. It is noted that K does not influence $w_{A\,max}$ but

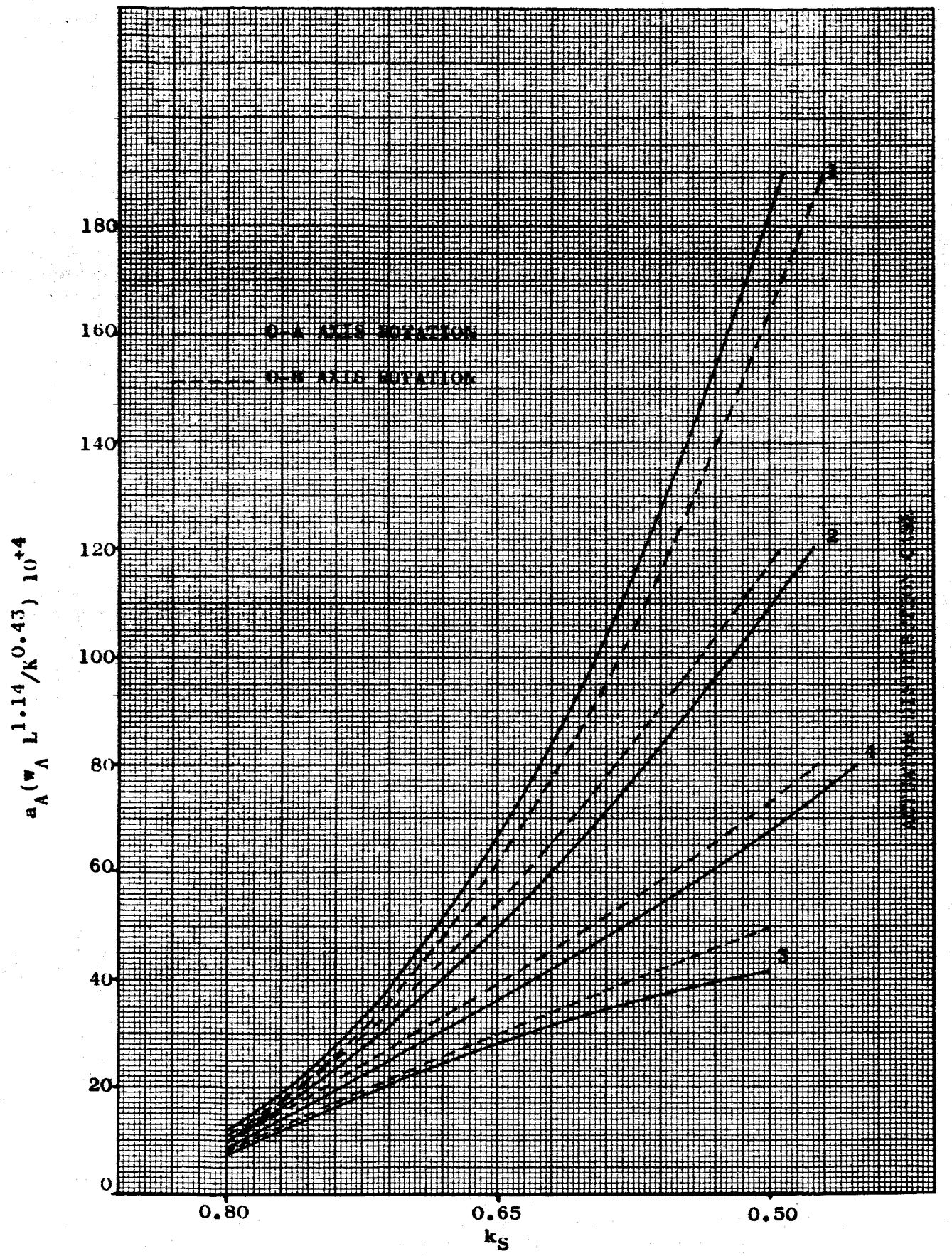


Fig. III-44. Normalized slewing rate, non-tapered structures.

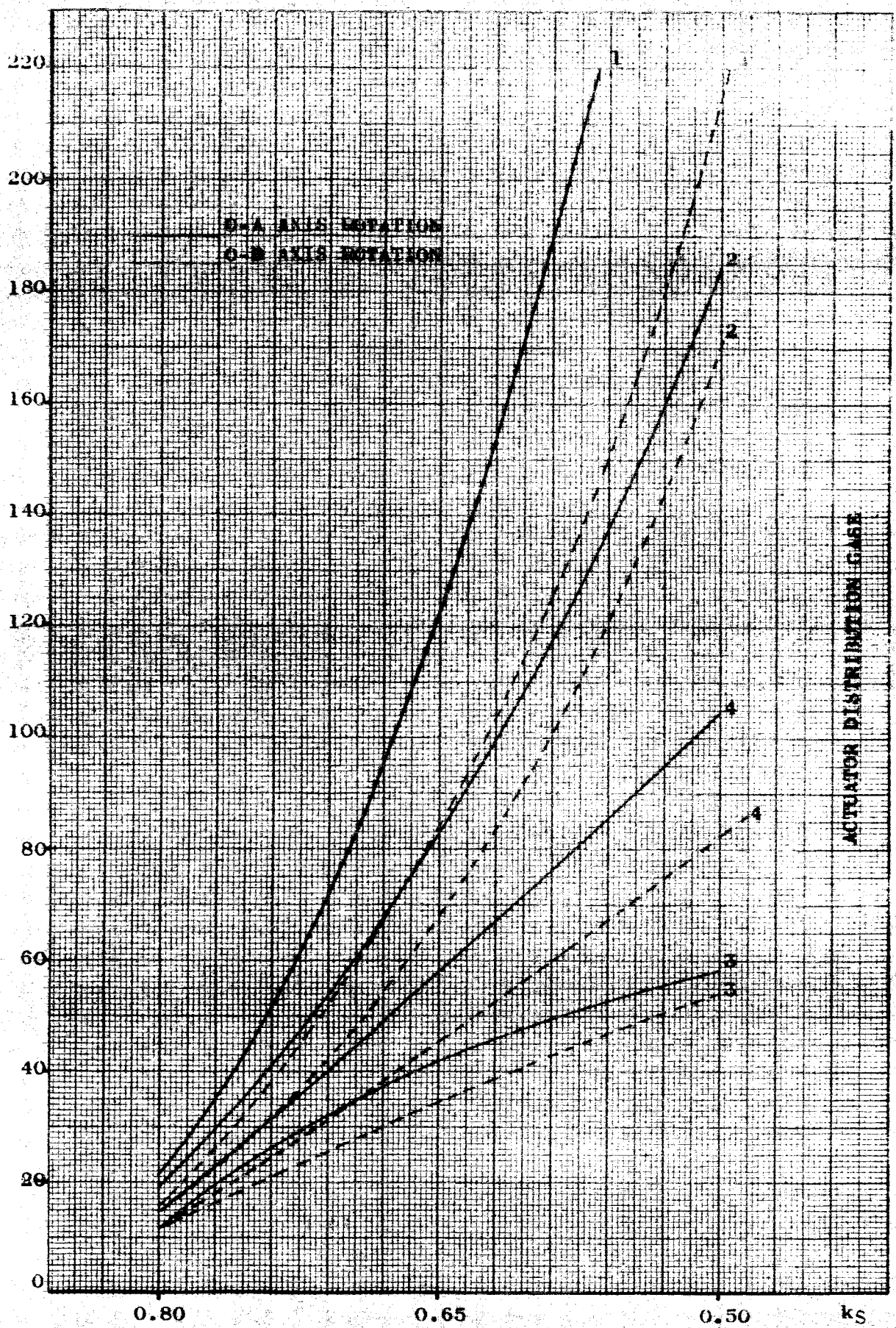


Fig. III-45. Normalized slewing rate, tapered structures.

does have an effect on a_A.

4.4.1 TRADE-OFFS OF REFLECTOR DISTORTIONS TURNING RATES AND SLEWING RATES.

A comparison of the d values in Figs. III-27 to III-38 and the $w_{A\ max}$ and a_A valves in Figs. III-42 to III-45 indicate the trade-offs available in the selection of k_S, case, L, etc. to achieve given performance objectives. The following observations are made on the basis of the information in the above figures:

(1) While low values of k_S, and cases 1 and 2 compared to cases 3 and 4 result in relatively high values of $w_{A\ max}$ and a_A they also result in high d values.

(2) Increasing the K and reducing L reduces d, and increases a_A and $w_{A\ max}$.

(3) If the downward or level trend of d vs. k_S is maintained for preferred rotation axes in cases 2 and 4 (as shown in Figs. III-33 to III-38) then lowering the valves of k_S, for these axes and cases, improves the d, $w_{A\ max}$, and a_A performance. Therefore cases 2 and 4 would be the most logic choices if the rotation axes are limited respectively to O-A and O-B. It is, however, not usually practical to use only one rotation axis.

(4) The tapered structures provide consistently better $w_{A\ max}$ and a_A performance but do not always provide better d performance.

4.5 LIMITATIONS ON DEFLECTIONS.

The computer program for determining deflections is based on small deflection theory. It is estimated that the theory is valid

for the distortions, and corresponding frequencies and reflector sizes, indicated in Fig. III-46.

The values in Fig. III-46 exceed the usual 1000 wavelengths-in-the-aperture upper limit and 1/10 to 1/30 of-a-wavelength-aperture-distortion lower limit. The upper limits on aperture distortions in Fig. III-46, which are critical to the accuracy of the deflection analysis program, are also excessively large.

4.6 SUMMARY OF RESULTS.

Fig. III-47 summarizes the positive and/or negative influences of designated changes in the independent structural and operational parameters on designated changes in d, a_A, and $w_{A\ max}$. The influences of an individual parameter is assumed to take place while the other parameters are held fixed. Therefore a $\pm$ sign in Fig. III-47 indicates that a positive or negative influence can take place depending on the values of associated parameters. When no signs appear in Fig. III-47 the independent parameters have no influence on the dependent parameters.

The + signs in Fig. III-47 generally indicate the desirability of the independent parameter change, and a - sign the undesirability of the change. It is evident that the influences on a_A and $w_{A\ max}$ are not always compatible with the influences on d.

Quantitative data on the above is contained in this report.

FREQUENCY Mc	REFLECTOR SIZE, D, IN.	WAVELENGTHS IN APERTURE	RMS DISTORTIONS d, IN.	FRACTION OF A WAVELENGTH DISTORTIONS
20,000	360 to 3,000	600 to 5,000	0.0144 to 12	0.024 to 20
10,000	360 to 6,000	300 to 5,000	0.0120 to 24	0.010 to 20
1,000	600 to 24,000	50 to 2,000	0.0360 to 180	0.003 to 15
100	1200 to 120,000	10 to 1,000	0.12 to 1200	0.001 to 10

Fig. III-46. Limitations on frequency, reflector size, and rms distortions.

REFERENCES

(1) "Antenna Engineering Handbook", H. Lasik McGraw Hill, 1961.

(2) "Physical Limitations on Antennas", J. Ruze Technical Report 248, Oct. 1952, Research Laboratory for Electronics, MIT.

INFLUENCE OF:	ON: DECREASING d	INCREASING a_A	INCREASING W_{AMAX}
CHANGING FROM O-A TO O-B ROTATION AXIS	±	±	±
CHANGING FROM NON-TAPERED TO TAPERED STRUCTURES	±	+	+
CHANGING FROM UNIFORM TO NONUNIFORM ILLUMINATION	+		
CHANGING FROM CASE 1 to 2	+	-	-
2 to 3	±	-	-
3 to 4	±	+	+
INCREASING K	+	+	
L	-	-	-
E	+		
a_A	-		-
s_{FW}/p_{FW}			+
k_S, k'_{S2}	±	-	-
p_S	-		
w_A		-	
r_{FW}		+	+
k_o	+		
k_F	-	-	-

Fig. III-47. Influence of changes in independent parameters.

IV. DETAILED "RATIO" MODEL ANALYSIS

IV-A. STRUCTURAL LOADS

(By G. H. Nowak, checked by P. Slysh)

1.0 GENERAL

Attitude maneuvering of the chosen RATIO antenna is achieved by inertial (including gyroscopic) reactions against the flywheels. The imposed torsional loads on the structure, due to the actuators, give rise to a set linear inertial loads and finally to a distribution of elastic deflections over the entire structure. In this study only the steady state loads are considered.

The study of the dynamic performance of RATIO structures as part of the over-all attitude control system must start with the steady state analysis. It is tentatively estimated that the results of the subject steady state analysis will be valid for RATIO systems in which the resonant frequency of the structure is approximately an octave higher than the highest characteristic frequency of the attitude controller.

2.0 GEOMETRY OF STRUCTURE

For purposes of initially simplifying the analysis of the component forces and torques it is assumed that the panel structure forms a grid of equal length and constant cross-section beams. The distributed mass of the reflector structure is lumped at the junctions of the grid. The weights of the inertial actuators (each of which include sets of three orthogonal flywheels) are also lumped at the junctions, where, likewise, the legs of the tetrapod feed structure are assumed to be mounted.

An x, y, z coordinate system is assumed with its origin at the apex of the paraboloid and its z-axis coincident with the focal axis. The chosen structure is such that a junction corresponds with the apex.

The coordinates, x, y, z, of the mass at the junction of the m^{th} column and n^{th} row of the grid are given as solutions to,

$$mL/f = \log_e \left[x/2f + \left[1 + (x/2f)^2\right]^{1/2}\right] + \left[x/2f\right]\left[1 + (x/2f)^2\right]^{1/2}, \quad (1)$$

$$nL/f = \log_e \left[y/2f + \left[1 + (y/2f)^2\right]^{1/2}\right] + \left[y/2f\right]\left[1 + (y/2f)^2\right]^{1/2}, \quad (2)$$

$$4fz = x^2 + y^2, \; r_n \leq x_m^2 + y_m^2 \quad (3)$$

where f is the focal length, and L is the length of the grid.

If it is assumed that the antenna rotates about the center of gravity of the antenna structure then the coordinates of the mass are described in a new coordinate system, r_1, r_2, r_3. With the origin of the new coordinate system at the chosen center of mass,

$$r_1 = x, \quad (4)$$

$$r_2 = y, \quad (5)$$

$$r_3 = (x^2 + y^2)/4f - \left\{ \left\{ \left[(1 + r_o^2/4f^2)^{3/2} - 1 \right](3/5)/\left[(1+r_o^2/4f^2)^{3/2} - 1 \right] \right. \right.$$
$$\left. - 1 \right\} \; f + (m_1/k\bar{A}) \sum_{i=1}^{N} \left\{ \left[(x_T)_i^2 + (y_T)_i^2 \right] / 4f \right.$$
$$\left. + M_F Z_F / k\bar{A} \right\} k\bar{A}/(N m_1 + M_F + k\bar{A}) \quad , \tag{6}$$

where

r_o, the mean radius of the aperture,

x_T, y_T, coordinates of a torque actuator set,

m_1, mass of a torque actuator set,

N, number of torque actuator sets,

k, mass density of the surface of the reflector,

M_F, mass of the feed system,

Z_F, distance of the feed from the apex of the paraboloid,

$\bar{A}$, the area of the paraboloidal reflector,

$$\bar{A} = (8\pi/3) f^2 \left\{ \left[1 + (r_o/2f)^2 \right]^{3/2} - 1 \right\} . \tag{7}$$

Since the Euler equations govern the motion, the angular rate components of the antenna in the mass-centered-coordinate system, w_1, w_2, w_3, are interdependent time functions.

3.0 REACTION LOADS

To develop typical loading conditions it is assumed that the given initial angular rates about the r_1, r_2, r_3 axes are $w_{10} = w_{20} = 0$ and $w \neq 0$;

and the required, final (steady state) angular rates are $w_{1\infty}$ and $w_{2\infty}$. The $w_{3\infty}$ is assumed to vanish. The final angular rates are approached asymptotically, and the same time constant, $1/a$, is used to describe the exponential angular rate increase or decrease about the three axes.

Under the above conditions, and as a consequence of the varying gyroscopic and inertial reactions, the maximum reaction forces at the structural junctions are developed at some time after the initial attitude control torques are applied and before the final angular rates are achieved. The components of these maximum reaction forces at each of the structural junctions are,

$$(P_{mn})_{\substack{2\\3}} = U_{mn} \{ w_1 (w_1 r_{\substack{1\\1}} + w_2 r_{\substack{2\\2}} + w_3 r_{\substack{3\\3}}) - r (w_{\substack{1\\1}}^2 + w_{\substack{2\\2}}^2 + w_{\substack{3\\3}}^2) + r \dot{w}_{\substack{3\\2}} - r \dot{w}_{\substack{2\\3}} \}, \qquad (8)$$

where U_{mn} is the mass concentrated at the (m,n) junction.

4.0 FLYWHEEL AND ANTENNA TURNING RATES

Three orthogonal flywheel sets at each of the actuator stations (of the chosen model) are replaced by a single set of orthogonal flywheels. These flywheels are taken to have angular rates n_1, n_2, n_3, about their spin axes respectively in the x, y, z directions. The three flywheels are assumed to have the same inertial properties. If the three flywheels turn with

angular rates n_1, n_2, n_3 then w_1, w_2, w_3 are functions of these flywheel rate functions according to the set of Euler equations,

$$\dot{n}_1 + n_3 w_2 - n_2 w_3 = -\dot{w}_1 [1 + (J_1 + 2J_B)/J_A] - w_2 w_3 (J_o - J_1)/J_A + (J_s/J_A)(n_s w_s - n_s w_s), \quad (9)$$

$$\dot{n}_2 + n_1 w_3 - n_3 w_1 = -\dot{w}_2 [1 + (J_1 + 2J_B)/J_A] - w_3 w_1 (J_o - J_1)/J_A + (J_s/J_A)(n_1 w_3 - n_3 w_1) \quad (10)$$

$$\dot{n}_3 + n_2 w_1 - n_1 w_2 = -\dot{w}_3 [1 + (J_1 + 2J_B)/J_A] + (J_s/J_A)(n_2 w_1 - n_1 w_2), \quad (11)$$

where,

J_A is the inertia of the composite flywheel about its spin axis,

J_B is the inertia about an axis perpendicular to the spin axis,

J_o is the inertia of the reflector about the focal axis,

J_1 is the inertia about an axis perpdendicular to the focal axis.

Under the steady state conditions,

$$\dot{n}_{1\infty} = \dot{n}_{2\infty} = \dot{n}_{3\infty} = \dot{w}_{1\infty} = \dot{w}_{2\infty} = \dot{w}_{3\infty} = 0. \quad (12)$$

Using the values in Eqs, 9, 10, 11, and 12,

$$-n_{2\infty} w_{3\infty} + n_{3\infty} w_{2\infty} = w_{2\infty} w_{3\infty} (J_o - J_1)/J_A , \quad (13)$$

$$n_{1\infty} w_{3\infty} - n_{3\infty} w_{1\infty} = w_{1\infty} w_{3\infty} (J_o - J_1)/J_A , \quad (14)$$

$$-n_{1\infty} w_{2\infty} + n_{2\infty} w_{1\infty} = 0. \quad (15)$$

The determinant of the system of Eqs. 13, 14, 15, is,

$$\begin{vmatrix} 0 & -w_{3\infty} & w_{2\infty} \\ w_{3\infty} & 0 & -w_{1\infty} \\ -w_{2\infty} & w_{1\infty} & 0 \end{vmatrix} = 0, \tag{16}$$

therefore, solutions for $n_{1\infty}$, $n_{2\infty}$ exist if the equations are homogeneous, or when,

$$w_{1\infty} = w_{2\infty} = 0, \qquad w_{3\infty} \neq 0, \tag{A}$$

or,

$$w_{3\infty} = 0, \qquad w_{1\infty} \neq 0, \; w_{2\infty} \neq 0. \tag{B}$$

The condition (A) characterizes the case in which the dish is turning about its focal axis. The condition (B) is for the case in which the dish is turning about an axis perpendicular to the focal axis.

Considering Case (B), it follows that,

$$n_{2\infty}/n_{1\infty} = w_{2\infty}/w_{1\infty}, \tag{17}$$

and,

$$n_{3\infty} = 0. \tag{18}$$

5.0 MODEL FUNCTIONS FOR ANTENNA TURNING RATES

From the energy consideration expressions can be found for $n_{1\infty}$ and $n_{2\infty}$ in terms of the steady state values $w_{1\infty}$, $w_{2\infty}$, and the initial values n_{10}, n_{20}, n_{30}, w_{10}, w_{20}, w_{30}:

$$n_{1\infty} = -\left[1 + (J_1 + 2J_B)/J_A\right] w_{1\infty} + R^{1/2} w_{1\infty}/(w_{1\infty}^2 + w_{2\infty}^2)^{1/2}, \tag{19}$$

$$n_{2\infty} = -\left[1 + (J_1 + 2J_B)J_A\right] w_{2\infty} + R^{1/2} w_{2\infty}/(w_{2\infty}^2 + w_{1\infty}^2)^{1/2}, \tag{20}$$

where,

$$\begin{aligned} R = {} & \left\{ n_{10} + \left[1 + (J_1 + 2J_B)/J_A\right] w_{10} \right\}^2 \\ & + \left\{ n_{20} + \left[1 + (J_1 + 2J_B)/J_A\right] w_{20} \right\}^2 \\ & + \left\{ n_{30} + \left[1 + (J_o + 2J_B)/J_A\right] w_{30} \right\}^2 . \end{aligned} \tag{21}$$

The angular rates w_1 and w_2 are constant only when w_3 is zero. This allows the choice of a simple set of model functions for w_1, w_2 and w_3: ie.

$$w_1 = w_{1\infty}(1 - e^{-at}), \tag{22}$$

$$w_2 = w_{2\infty}(1 - e^{-at}), \tag{23}$$

$$w_3 = w_{30} e^{-at}, \tag{24}$$

where $1/a$ is the time constant dependent mainly on the time constant of the motor-inertia-wheel combination. The chosen set of functions, Eqs. 22, 23, 24, is only one of a large family of possible sets.

With a given set of model functions, the Eqs. 9, 10, 11 have to be solved to find the corresponding time functions n_1, n_2, n_3 of the flywheels. Eqs. 9, 10, 11, with w_1, w_2, w_3 from Eqs. 22, 23, 24 represent the attitude control equations of the inertia-wheel-driven RATIO antenna.

6.0 APPLIED TORQUES

The torques, T_1, T_2, T_3, applied to the antenna are described by the Euler equations,

$$T_1 = \dot{w}_1 J_1 + w_2 w_3 (J_e - J_1), = \sum_{m,n} \left[(r_{mn})_2 (P_{mn})_3 - (r_{mn})_3 (P_{mn})_2 \right], \tag{25}$$

$$T_2 = \dot{w}_2 J_1 - w_1 w_3 (J_e - J_1), = \sum_{m,n} \left[(r_{mn})_3 (P_{mn})_1 - (r_{mn})_1 (P_{mn})_3 \right], \tag{26}$$

$$T_3 = \dot{w}_3 J_e, = \sum_{m,n} \left[(r_{mn})_1 (P_{mn})_2 - (r_{mn})_2 (P_{mn})_1 \right] \tag{27}$$

Since w_1, w_2 and w_3 (from Eqs. 22, 23, 24) are known functions of time, T_1, T_2, T_3 are functions of time and represent the torque loads on the structure.

For purposes of studying the structural deflection the maximum torque magnitude,

$$T_{max} = (T^2_{1max} + T^2_{2max} + T^2_{3max})^{1/2} , \tag{28}$$

is taken to exist at the time $t = t_o$, when,

$$T_{1max}(dT_1/dt) + T_{2max}(dT_2/dt) + T_{3max}(dT_3/dt) = 0. \tag{29}$$

Evaluating Eq. 29 using Eqs. 25, 26, 27, yields,

$$t_o = 1/a \log \{ (3/4) [1 + (1 - 8A/9)^{1/2}] \} , \tag{30}$$

where,

$$A = 1 + [a^2/(J_o^2 - J_1^2)] [J_1^2/w_{30}^2 + J_o^2/(w_{1o}^2 + w_{2o}^2)] . \tag{31}$$

For $t = t_o$ the components of the maximum torque are,

$$T_{1\,max} = w_{1o} a J_1 + (1/16) w_{2o} w_{30} (J_o - J_1) [1 - (9 - 8A)^{1/2}] [3 + (9 - 8A)^{1/2}], \tag{32}$$

$$T_{2\,max} = w_{2o} a J_1 + (1/16) w_{1o} w_{30} (J_o - J_1) [1 - (9 - 8A)^{1/2}] [3 + (9 - 8A)^{1/2}], \tag{33}$$

$$T_{3\,max} = -w_{30} \cdot J_o [3 + (9 - 8A)^{1/2}]/4. \quad (34)$$

Assuming there are N structural junctions occupied by a set of three flywheels, then the total number of flywheels are 3N, and the torques applied to the dish per flywheel are,

$$t_1 = T_{1max}/N, \quad (35)$$

$$t_2 = T_{2max}/N, \quad (36)$$

$$t_3 = T_{3max}/N, \quad (37)$$

7.0 INERTIA OF DISH

The locations for the N flywheels are abritrary. The i^{th} flywheel's coordinates are,

$$(x_T)_i, (y_T)_i, (z_T)_i = [(x_T)_i^2 + (y_T)_i^2]/4f, \quad (38)$$

where,

$i = 1, 2, \ldots\ldots N.$

Using these notations the moments of inertia of the dish about its principal axes are,

$$J_o = m_1 \sum_{i=1}^{N} \{ (x_T)_i^2 + (y_T)_i^2 \} + (64\pi kf^4/15) [1 - (1 + h/f)^{3/2} (1 - 3h/2f)], \quad (39)$$

$$J_1 = (m_1) \sum_{i=1}^{N} \{ [(x_T)_i^2 + (y_T)_i^2] /4f - Z_o \}^2 + 4\pi kf^4/105 \{ (1 + h/f)^{3/2} [35 (1 + Z_o/f)^2 - 42(1 + Z_o/f) (1 + h/f) + 15 (1 + h/f)^2] - 15 + 7 (1 - 5Z_o/f) (1 + Z_o/f) \} + J_o/2 + M_F(Z_F - Z_o)^2, \quad (40)$$

where h is the depth of the dish ($h = r_o^2/4f$), m_1 is the mass of one flywheel set, and Z_o is the distance of the antenna center of mass from the apex of the dish. That is,

$$Z_o = [k\bar{A}/ (Nm_1 + M_F + k\bar{A})] \{ f \{ 3/5[(1 + r_o^2/4f^2)^{5/2} - 1]/ [(1 + r_o^2/4f^2)^{3/2} - 1] - 1 \} + (m/k\bar{A}) \sum_{i=1}^{N} [(x_T)_i^2 + (y_T)_i^2] /4f + M_F Z_F/k\bar{A} \}. \quad (41)$$

8.0 REACTION FORCES OF FEED

In addition to the above force and torques a set of forces exist between

the junction of the structural bay (tetrapod) and the reflector. These forces can be determined from the forces F_1, F_2, F_3 (in the r_1, r_2, r_3 directions) acting on the feed as,

$$F_1 = M_F \left\{ w_{11} w_{31} (Z_F - Z_o) + \dot{w}_{21} (Z_F - Z_o) \right\}, \tag{42}$$

$$F_2 = M_F \left\{ w_{21} w_{31} (Z_F - Z_o) - \dot{w}_{11} (Z_F - Z_o) \right\}, \tag{43}$$

$$F_3 = M_F (w_{11}^2 + w_{21}^2) (Z_F - Z_o) . \tag{44}$$

where w_{11}, w_{12}, w_{13} and their derivatives are values for which Eqs. 32-34 are a maximum, that is,

$$\begin{matrix} w \\ 11 \\ 21 \end{matrix} = \begin{matrix} w \\ 1\infty \\ 2\infty \end{matrix} (1/4)[1 - (9-8A)^{1/2}], \tag{45}$$

$$w_{31} = w_{30} (1/4)[3 + (9-8A)^{1/2}], \tag{46}$$

$$\begin{matrix} \dot{w} \\ 11 \\ 21 \end{matrix} = \begin{matrix} w \\ 1\infty \\ 2\infty \end{matrix} (a/4)[1 - (9-8A)^{1/2}], \tag{47}$$

$$\dot{w}_{31} = w_{30} (a/4)[3 + (9-8A)^{1/2}] . \tag{48}$$

In Eqs. (45) to (48) when (9-8A) is negative, then

$$w_{11} = w_{21} = 0,\ w_{31} = w_{30},\ \dot{w}_{11} = w_{1\infty} a,\ \dot{w}_{21} = w_{2\infty} a, \text{ and } \dot{w}_{31} = -w_{30} a.$$

9.0 SUMMARY

The steady state forces (Eq. 8) and the steady state torques (Eqs. 32, 33, 34) have been established using a given set of model functions for antenna turning rates (Eqs. 22, 23, 24). The forces and torques are based on the defined system inertias (Eqs. 39, 40, etc.), on the masses of the feeds and

inertia wheels, as well as on the initial and final angular rates and accelerations of the flywheels and antenna.

10.0 STATUS

The equations describing the forces and torques acting on a reflector structure have been programed for a 7090 computer. This program has been applied to determining the structural-junction coordinates, as well as the component forces and torques at the structural junctions for cases up to 5 in Table 1. Also listed in Table 1 are the structural beam properties (corresponding to the indicated k values) which constitute one of the inputs to the structural deflection analysis. The beam properties are defined by,

I_{xx} = the maximum section moment of inertia,

I_{yy} = the minimum section moment of inertia,

A = the cross-section area.

11.0 CONCLUSION

From the work done to date we are satisfied that the computer program for determining structural loads performs satisfactorily.

TABLE I

INPUT PARAMETERS FOR STRUCTURAL ANALYSIS

Input Parameter	Parameter Dimensions	Case 1	Case 2	Case 3	Case 4	Case 5
r_o	in.	600	600	600	600	3000
L	in.	60	60	60	60	300
f	rad./sec.	960	960	960	960	4800
a	rad./sec.	1.0	1.0	0.1	0.1	0.1
w_{30}	rad./sec.	1.0	1.0	0.1	0.1	0.1
$w_{1\infty}$	rad./sec.	1.0	1.0	0.1	0.1	0.1
$w_{2\infty}$	rad./sec.	1.0	1.0	0.1	0.1	0.1
k	lb.-sec.^{2}/in.^{3}	(7)10^{-6}	(7)10^{-6}	(7)10^{-6}	(7)10^{-6}	(7)10^{-6}
N	-	4	4	4	4	8
M_1	lb.-sec.^{2}/in.	0	0	0	1	4
m_1	lb.-sec.^{2}/in.	1	1	1	1	2
Actuator Location m	-	±2	±5	±5	±5	±3±6
Actuator Location n	-	±2	±5	±5	±5	±3±6
Beam Properties						
I_{xx}	in.^{4}	31	31	31	31	3600
I_{yy}	in.^{4}	1	1	1	1	10
A	in.^{2}	0.8	0.8	0.8	0.8	4.0

IV-B. RADIATION PATTERNS

(By G. H. Nowak, checked by G. A. Burns and P. Slysh)

1. INTRODUCTION

The formation of antenna radiation patterns by reflectors from scattering and diffraction are of fundamental importance in antenna theory. There are several approximate methods of analyzing radiation patterns. Exact solutions of the scattering problem have been obtained for only a limited number of cases involving simple primary fields and reflectors of simple geometry, such as spheres and cylinders. These problems are treated in standard works on electromagnetic theory, to which the reader is referred for the results.[1] In treating reflectors of shapes other than spherical or cylindrical it is necessary to resort to approximate techniques. Several such methods, which yield very good results at high frequencies, are the (1) geometrical-optics method, (2) current density-distribution method, (3) aperture-field method, and (4) scalar diffraction method.

Both the current-distribution and aperture-field methods led to a calculation of the scattered field as arising from a distribution of sources over an open-surface, the boundary of which is defined by the system of reflected rays. In contrast to the geometrical-optics method, the field at any point may be found as the superposition of contributions from all elements of the source distribution. In general, therefore the latter two methods will lead to nonzero field intensities in the region of space not covered by the system of rays; also, in the region of rays, the fields will differ from those obtained on the basis of geometrical scattering. These deviations from

---

[1] See, for example, J. A. Stratton, Electromagnetic Theory, McGraw-Hill, New York, 1941, Chapter 9.

geometrical propagation of the scattered field lead one rather naturally to the scalar diffraction method.

Experiments have shown that whenever the dimensions of an aperture are large compared with the wavelength, the diffraction effects are minimized as the major portion of the field pattern is concentrated in the region covered by the rays from the aperture. On the basis of this fact a common high-frequency approximation technique is used for all problems of the type involving a parabolic reflector. The mathematical details have been developed, and we need only summarize here the general ideas in the application of the results to our problem.[2] In the case of a parabolic reflector the aperture area is associated with a surface Σ of infinite extent which divides all space into two separate regions. The problem is then equivalent to that of an aperture in an infinite screen on the surface Σ. It is assumed that the field over Σ is zero everywhere except over the aperture area; in effect, it is assumed that diffraction effects at wide angles with respect to the aperture-ray system are negligible. In the case of a parabolic reflector it is assumed that the aperture field is produced by geometrical reflection or refraction of the rays from the primary feed.

2. ASSUMPTIONS

In many antennas the field over the aperture is almost completely linearly polarized, only a small fraction of the energy being in the crossed-polarization component of the field. If the latter is neglected, the calculation of the diffraction field is simplified; by use of the high-frequency approximations, considered previously, the problem can be reduced to a scalar diffraction problem.

---

[2] See, for example, S. Silver, Microwave Antenna Theory and Design, Vol. 12 Radiation Laboratory Series, pp. 158-162, McGraw-Hill, New York, 1949.

The analysis presented herein is for a parabolic aperture of infinite conductivity; the aperture will be taken in the xy-plane as shown in Figure IV-1, and the electric field will be taken to be polarized in the x-direction. Further, in many antennas, where, although the distance to the primary feed is not large, the geometry of the body is such that the amplitude of the scattered wave at the primary feed is small. Hence, multiple scattering may be neglected in the analysis of the total field. This essentially says that one is neglecting the effect of the reflector on the general impedance characteristics of the antenna.

3. FAR FIELD REPRESENTATION

The diffraction field of an aperture area, A, is given by the scalar integral formula,

$$u_p = -(1/4\pi)\int_A (\psi\, \partial u/\partial n - u\, \partial\psi/\partial n)\, dS, \tag{1}$$

where u_p is the electromagnetic scalar potential at the field point, $P_1(x,y,z)$, defined by the locus vector $\bar{R}_1$, as shown in Figure IV-1; $\partial/\partial n$ represents the normal derivative with respect to the parabolic surface; the unit vector $\bar{n}$, normal to the surface, taken to be in the positive outward direction; $u(x,y,z)$ is the scalar potential of the electromagnetic field at the surface of the reflector due to the source field and is defined by,

$$u(x,y,z) = A(x,y,z) \exp[-jk_o L(x,y,z)] \tag{2}$$

where $A(x,y,z)$ and $L(x,y,z)$ are the amplitude and phase functions of the source field respectively; k_o is the wave number and equal to $2\pi/\lambda_o$ where λ_o

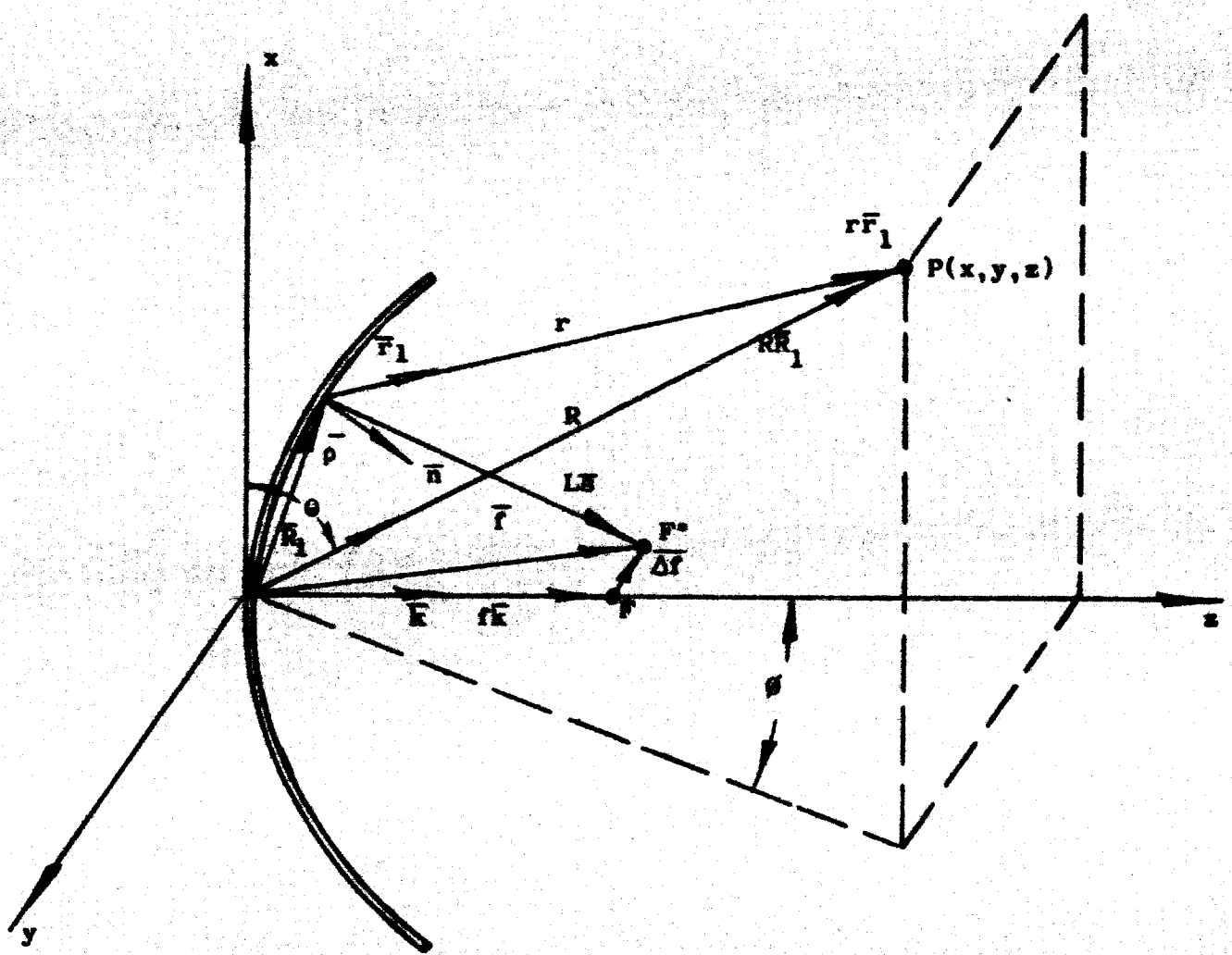


Fig. IV-1. Paraboloidal geometry.

is the free-space wavelength, and Ψ is the scalar potential of a field point on the reflector surface given by,

$$\Psi = \exp(-jkr)/r \tag{3}$$

where r is the distance from the field point to the reflector element on the surface.

It will be recognized that Equation (1) is the Kirchhoff scalar diffraction formula used in physical optics.[3] This equation can be regarded as the mathematical expression of Huygen's principle for a scalar wave; the resultant wave amplitude at the field point P (x,y,z) being expressed as a sum of contributions for the elements of surface dS. The first part of the integral is a summation of terms of the form $[\exp(-jkr)/r]\,(\partial u/\partial n)\,dS$ - a summation of the amplitudes of isotropic spherical wavelets arising from sources of strength proportional to $(\partial u/\partial n)\,dS$ on the surface elements dS. The second part of the integral can be interpreted similarly.

The derivative of u with respect to the surface normal, $\bar{n}$, is,

$$\partial u/\partial n = \bar{n} \cdot \nabla u = -jk_o u \bar{n} \cdot \nabla L + (u/A)\,\partial A/\partial n \,. \tag{4}$$

If the wavelength is short, k_o is large and the second term on the right-hand side of (4) is negligible in comparison with the first term. Therefore,

$$\partial u/\partial n \approx -jk_o u\, \bar{n} \cdot \nabla L. \tag{5}$$

---

[3] See, for example, M. Born, Optics, reprint by Edwards Bros., Ann Arbor, Mich., 1943.

Let $\bar{s}$ be a unit vector in the direction of the ray at the chosen point shown in Figure IV-1. If the wavefronts associated with the rays through the aperture are the surfaces L (x,y,z) equal to a constant, then the required phase distribution is k_o L (x,y,o). Thus,

$$k_o \nabla L = k \bar{s} \tag{6}$$

where k is the wave number and equal to $2\pi/\lambda$ where λ is the wavelength at the aperture. Applying this results to (5) yields,

$$\partial u/\partial n \approx - jku\bar{n} \cdot \bar{s}, \tag{7}$$

where the quantity $(\bar{n} \cdot \bar{s})$ is the cosine of the angle between the $\bar{n}$ and $\bar{s}$ unit vectors.

With regard to $\partial v/\partial n$, it is observed from (3) that,

$$\partial v/\partial n = \bar{n} \cdot \nabla v = (d/dr)\ (exp-jkr)\ (1/r)\ (\bar{n} \cdot \bar{r}_1)$$

or,

$$\partial v/\partial n = - (1/r^2)\ (exp-jkr)\ (jkr + 1)\ \ (\bar{n} \cdot \bar{r}_1).$$

In the Fraunhofer region or the far-zone, the distance r is large compared to a wavelength for all points on the surface so that the last term in the above equation is negligible in comparison to the first. We then have, as an approximation valid in the far-zone, that,

$$\partial\psi/\partial n \approx jk \left[\exp -jkr\right] (1/r)\ (\bar{n} \cdot \bar{r}_1) \qquad (8)$$

where the quantity $(\bar{n} \cdot \bar{r}_1)$ represents the cosine of the angle between the normal unit vector $\bar{n}$ and $\bar{r}_1$, the unit vector from the point on the aperture to the field point P (x,y,z).

With the aid of Equations (2), (3), (7), and (8), Equation (1) can be written as,

$$u_\rho\ (x,y,z) = (jk/4\pi)\int_A (A/r) \left[\exp -jk(r + L)\right] (\bar{s} + \bar{r}_1) \cdot \bar{n}\ dS. \qquad (9)$$

From Figure IV-1, it can be seen that,

$$\bar{r} = R\bar{R}_1 - \bar{\rho}, \qquad (10)$$

from which it follows,

$$r = (\bar{r} \cdot \bar{r})^{1/2} = (R^2 + \rho^2 - 2R\bar{R}_1 \cdot \bar{\rho})^{1/2},$$

or,

$$r = (R^2 + \rho^2)^{1/2} \left[(1 - 2R\bar{R}_1)/(R^2 + \rho^2)\right]^{1/2}. \qquad (11)$$

In the far-zone field the customary approximations are made with regard to distance. For R very large $r \approx R - \bar{R}_1 \cdot \bar{\rho}$ and $\bar{r}_1 \approx \bar{R}_1$. Equation (9),

therefore, becomes,

$$u_p = (jk/4\pi R)[\exp -jkR]\int_A A\,(x,y,z)[\exp -jk\,(L\,(x,y,z) - \bar{R}_1 \cdot \bar{\rho})] \quad \bar{n} \cdot [\bar{R}_1 + \bar{s}]\, dS\,. \tag{12}$$

4. PHASE FUNCTION

Attention will now be directed to the phase function L (x,y,z) appearing in Equation (12). Since the reflector surface is a distorted paraboloid then,

$$\bar{\rho} = \bar{\rho}_o + \Delta\bar{\rho}\,, \tag{13}$$

where,

$$\bar{\rho}_o = \bar{i}\,x + \bar{j}\,y + \bar{k}\,(x^2 + y^2)/\,4f \tag{14}$$

represents the undistorted surface and,

$$\Delta\bar{\rho} = \bar{i}\,\Delta x + \bar{j}\,\Delta y + \bar{k}\,\Delta z \tag{15}$$

is the distortion vector relative to the undistorted surface.

The unit vector, $\bar{R}_1$, is conveniently represented by the spherical cordinates θ and ϕ of Figure IV-1 as,

$$\bar{R}_1 = \bar{i}\,(\cos\theta)(\cos\phi) + \bar{j}\,(\cos\theta)(\sin\phi) \times \bar{k}\,(\sin\theta). \tag{16}$$

The location of the primary source field is given by,

$$\bar{f} = f\,\bar{k} + \Delta\bar{f} \tag{17}$$

where,

$$\Delta\bar{f} = \bar{i}\,\Delta x_f + \bar{j}\,\Delta y_f + \bar{k}\,\Delta z_f \tag{18}$$

represents the feed misalignment and f is the local length of the paraboloid measured in the z-direction.

Since,

$$L\bar{s} = \bar{f} - \bar{\rho}\ , \tag{19}$$

it follows that,

$$L = (f^2 + \rho^2 - 2\,\bar{f}\,.\,\bar{\rho})^{1/2}\ , \tag{20}$$

or with the aid of Equations (13), (14), (15), (17), and (18),

$$\begin{aligned} L = 1 = [&(x + \Delta x)^2 + (y + \Delta y)^2 + (x^2/4f + y^2/4f + \Delta z)^2 \\ &+ (\Delta x_f)^2 + (\Delta y_f)^2 + (f + \Delta z_f)^2 - 2(x + \Delta x)\Delta x_f \\ &- 2(y + \Delta y)\Delta y_f - 2(x^2/4f + y^2/4f + \Delta z)(f + \Delta z_f)]^{1/2}\ . \end{aligned} \tag{21}$$

From (13) through (16) it follows that,

$$\bar{R}_1 \cdot \bar{\rho} = (x + \Delta x)(\cos\theta)(\cos\phi) + (y + \Delta y)(\cos\theta)(\sin\phi) + (x^2/4f + y^2/4f + \Delta z)\sin\theta. \tag{22}$$

Let the phase function or the exponent of the exponential function $(L - \bar{R}_1 \cdot \bar{\rho})$ in the integral of Equation (12) be designated as $M(x,y)$. Then,

$$\begin{aligned} M(x,y) = \Big[& (x + \Delta x)^2 + (y + \Delta y)^2 + (x^2/4f + y^2/4f + \Delta z)^2 \\ & + (\Delta x_f)^2 + (\Delta y_f)^2 + (f + \Delta z_f)^2 - 2(x + \Delta x)\Delta x_f \\ & - 2(y + \Delta y)\Delta y_f - 2(x^2/4f + y^2/4f + \Delta z)(f + \Delta z_f) \Big]^{1/2} \\ & - (x + \Delta x)(\cos\theta)(\cos\phi) - (y + \Delta y)(\cos\theta)(\sin\phi) \\ & - (x^2/4f + y^2/4f + \Delta z)\sin\theta \quad . \end{aligned} \tag{23}$$

5. THE UNIT VECTORS $\bar{n}$ and $\bar{s}$

The unit vector $\bar{s}$ from (19), using (13), (14), (15), (17), and (18), is,

$$\bar{s} = (1/L)\left\{ \bar{i}(x + \Delta x - \Delta x_f) + \bar{j}(y + \Delta y - \Delta y_f) + \bar{k}\,(x^2/4f + y^2/4f - f + \Delta z - \Delta z_f) \right\} . \tag{24}$$

To determine the unit vector $\bar{n}$, normal to the distorted surface, we start by intersecting the paraboloid $z = x^2/4f + y^2/4f$ by the planes $x = x_m$, $y = y_n$ to obtain the parabolas of intersection $4fz - y^2 - x_m^2 = 0$, and $4fz - x^2 - y_n^2 = 0$. Lines tangent to these parabolas define a plane tangent to the paraboloid. Let us denote $\bar{p}$ and $\bar{q}$ as unit vectors tangent to the two intersected parabolas. The component representation of these vectors are,

$$\bar{p} = \left[\bar{i} + (x_m/2f)\,\bar{k}\right]\left[1 + (x_m/2f)^2\right]^{-1/2}, \tag{25}$$

$$\bar{q} = \left[\bar{j} + (y_n/2f)\,\bar{k}\right]\left[1 + (y_n/2f)^2\right]^{-1/2}. \tag{26}$$

From the structure analysis, the angular distortion $\Delta\phi_p$ in the $\bar{p}$ direction, and $\Delta\phi_q$ in the $\bar{q}$ direction are to be determined. As a result, the unit vector $\bar{p}$ and $\bar{q}$ are modified as,

$$\bar{p}^* = \bar{p} + \left[(\bar{p} \times \bar{q})/|\bar{p} \times \bar{q}|\right]\Delta\phi_q, \tag{27}$$

$$\bar{q}^* = \bar{q} + \left[(\bar{p} \times \bar{q})/|\bar{p} \times \bar{q}|\right]\Delta\phi_p. \tag{28}$$

The unit vector normal to the distorted surface is,

$$\bar{n} = (\bar{p}^* \times \bar{q}^*)/|\bar{p}^* \times \bar{q}^*|, \tag{29}$$

or in component form,

$$\vec{n} = \left[\bar{i}\,(p_2^* q_3^* - p_3^* q_2^*) + \bar{j}\,(p_3^* q_1^* - p_1^* q_3^*) + \bar{k}\,(p_1^* q_2^* - p_2^* q_1^*)\right]\left[(p_1^{*2} + p_2^{*2} + p_3^{*2})(q_1^{*2} + q_2^{*2} + q_3^{*2}) - (p_1^* q_1^* + p_2^* q_2^* + p_3^* q_3^*)^2\right]^{-1/2} . \tag{30}$$

The components in (30), of (27) and (28), using (25) and (26), are,

$$p_1^* = \left[1 + x_m^2/4f^2\right]^{-1/2} - (x_m/2f)\,\Delta\phi_q\left[1 + (x_m^2/4f^2) + (y_n^2/4f^2)\right]^{-1/2} , \tag{31}$$

$$p_2^* = (y_n/2f)\,\Delta\phi_q\left[1 + (x_m^2/4f^2) + (y_n^2/4f^2)\right]^{-1/2} , \tag{32}$$

$$p_3^* = (x_m/2f)\left[1 + (x_m^2/4f^2)\right]^{-1/2} + \Delta\phi_q\left[1 + (x_m^2/4f^2) + (y_n^2/4f^2)\right]^{-1/2} , \tag{33}$$

$$q_1^* = -(x_m/2f)\,\Delta\phi_p\left[1 + (x_m^2/4f^2) + (y_n^2/4f^2)\right]^{-1/2} , \tag{34}$$

$$q_2^* = \left[1 + y_n^2/4f^2\right]^{-1/2} - (y_n/2f)\,\Delta\phi_p\left[1 + (x_m^2/4f^2) + (y_n^2/4f^2)\right]^{-1/2} , \tag{35}$$

$$q_s^* = (y_n/2f)\left[1 + (y_n^2/4f^2)\right]^{-1/2} + \Delta\phi_p\left[1 + (x_m^2/4f^2) + (y_n^2/4f^2)\right]^{-1/2}. \quad (36)$$

6. NORMALIZED RADIATION INTENSITY

Since only the relative field potential is of interest the factor before the integral in (12) can be set equal to unity, and the integral can be written as,

$$\begin{aligned}\bar{u}_p &= \int_A A\,(x,y,z)\,[\exp -jkM\,(x,y,z)]\,\bar{n}.(\bar{R}_1 + \bar{s}) \\ &\quad \left[1 + (x_m^2/4f^2) + (y_n^2/4f^2)\right]^{1/2}\,dx\,dy \\ &= \int_A A\,(x,y,z)\,\cos kM\,(x,y,z)\,\bar{n}.(\bar{R}_1 + \bar{s}) \\ &\quad \left[1 + (x_m^2/4f^2) + (y_n^2/4f^2)\right]^{1/2}\,dx\,dy \\ &\quad - j\int_A A\,(x,y,z)\,[\sin kM\,(x,y,z)]\,\bar{n}.(\bar{R}_1 + \bar{s}) \\ &\quad \left[1 + (x_m^2/4f^2) + (y_n^2/4f^2)\right]^{1/2}\,dx\,dy = U - jV,\end{aligned} \quad (37)$$

where,

$$U = \int_A A\,(x,y,z)\,[\cos kM\,(x,y,z)]\,\bar{n}.(\bar{R}_1 + \bar{s}) \left[1 + (x_m^2/4f^2) + (y_n^2/4f^2)\right]^{1/2}\,dx\,dy\,, \quad (38)$$

and,

$$V = \int_A A(x,y,z)\,[\sin kM(x,y,z)]\,\hat{n}\cdot(\bar{R}_1 + \bar{s}) \left[1 + (x_m^2/4f^2) + (y_n^2/4f^2)\right]^{1/2} dx\,dy. \tag{39}$$

The magnitude of the normalized radiation intensity at the field point P (x,y,z) is therefore,

$$I = U^2 + V^2 . \tag{40}$$

7. NUMERICAL INTEGRATION

The coordinates of the structural junctions x_m; (m = 1,2,...N) and y_n; (n = 1,2,...N) are given as solutions of,

$$m\ell/f = \log_e\left[x_m/2f + (1 + x_m^2/4f^2)^{1/2}\right] + (x_m/2f)(1 + x_m^2/4f^2)^{1/2}, \tag{41}$$

$$n\ell/f = \log_e\left[y_n/2f + (1 + y_n^2/4f^2)^{1/2}\right] + (y_n/2f)(1 + y_n^2/4f^2)^{1/2}. \tag{42}$$

Equations (38) and (39) must be evaluated for each of the structural junctions.

a. Gaussian Method of Integration.

For the assumed integral,

$$I = \int_a^b F(x)\,dx , \tag{43}$$

one applies the transformation,

$$x = (b-a)/2\xi + (b+a)/2, \tag{44}$$

obtaining,

$$I = \left[(b-a)/2\right] \int_{-1}^{+1} F\left[\xi(b-a)/2 + (b+a)/2\right] d\xi \ . \tag{45}$$

Defining the quantity,

$$(b-a)/2 \ F\left[\xi(b-a)/2 + (b+a)/2\right] = G\ (\xi) \ , \tag{46}$$

then,

$$I = \int_{-1}^{+1} G\ (\xi)\ d\xi \ . \tag{47}$$

For the sequence (x_i) i = 1,2,....N, (y_i), exists such that,

$$y_i = F(x_i) \ , \ (i = 1,2,...N) \ . \tag{48}$$

From these sequences, two new sequences (ξ_i) i = 1,2,....N and (η_i) i = 1,2,....N can be defined as,

$$\xi_i = \left[2x_i - (a+b)\right]/(b-a) \ , \tag{49}$$

$$\eta_i = (b-a)y_i/2 = G(\xi_i) \ . \tag{50}$$

All values ξ_i obey the inequality,

$$-1 \leq \xi_1 \leq \xi_2 \leq \ldots \leq \xi_N \leq +1 \ . \tag{51}$$

In order to express $G(\xi)$ by an approximation, which assumes values η_i at ξ_i, one can apply the Lagrange polynomial,

$$G(\xi) \approx \sum_{i=1}^{N} \eta_i \ \phi(\xi)/(\xi-\xi_i) \ \phi'(\xi_i) \ . \tag{52}$$

where $\phi(\xi)$ is a polynomial of N^{th} order with zeros at $\xi = \xi_i$ for $i = 1,2,..N$, such as,

$$\phi(\xi) = \prod_{j=1}^{N} (\xi-\xi_j) \ . \tag{53}$$

Substituting Equation (52) into (47) yields,

$$I = \sum_{i=1}^{N} \eta_i P_i \ , \tag{54}$$

where

$$P_i = \left[1/\phi'(\xi_i)\right] \int_{-1}^{+1} \left[\phi(\xi)/(\xi-\xi_i)\right] d\xi \ , \tag{55}$$

are the weights and are independent of $G(\xi)$. These weights, P_i, can be computed for a specific set of (ξ_i) and used for different integrands.

The integrand of (55) can be written as,

$$\phi(\xi)/(\xi-\xi_i) = (\xi-\xi_1)(\xi-\xi_2)\ldots.(\xi-\xi_{i-1})(\xi-\xi_{i+1})\ldots(\xi-\xi_N) \ , \tag{56}$$

or after performing multiplication,

$$\phi(\xi)/(\xi-\xi_i) + \xi^{N-1} + a_1\xi^{N-2} + a_2\xi^{N-3} + \cdots + a_{N-2}\xi + a_{N-1} , \qquad (57)$$

where,

$$a_1 = -\sum_{\substack{j=1 \\ j\neq i}}^{N}{}' \xi_j = -\left[\xi_1 + \xi_2 + \cdots + \xi_{i-1} + \xi_{i+1} + \cdots \xi_N\right]$$

$$a_1 = -\sum_{i=1}^{N}{}' C_1\ (\xi_1, \cdots \xi_{i-1}, \xi_{i+1}, \cdots \xi_N) , \qquad (58)$$

$$\begin{aligned} a_2 = {} & \xi_1\xi_2 + \xi_1\xi_3 + \cdots + \xi_1\xi_{i-1} + \xi_1\xi_{i+1} + \cdots \xi_1\xi_N \\ & + \xi_2\xi_3 + \xi_2\xi_4 + \cdots + \xi_2\xi_{i-1} + \xi_2\xi_{i+1} + \cdots + \xi_2\xi_N \\ & + \xi_3\xi_4 + \xi_3\xi_5 + \cdots + \xi_3\xi_{i-1} + \xi_3\xi_{i+1} + \cdots \xi_3\xi_N \\ & + \cdots\cdots + \xi_{N-1}\ \xi_N = \sum{}' C_2(\xi_1, \xi_2, \cdots \xi_{i-1}, \xi_{i+1}, \cdots \xi_N), \end{aligned} \qquad (59)$$

$$\begin{aligned} a_3 = {} & \Big[\xi_1\xi_2\xi_3 + \xi_1\xi_2\xi_4 + \cdots + \xi_1\xi_2\xi_{i-1} + \xi_1\xi_2\xi_{i+1} + \cdots \\ & + \cdots \xi_1\xi_2\xi_N + \xi_2\xi_3\xi_4 + \xi_2\xi_3\xi_5 + \cdots + \xi_2\xi_3\xi_{i-1} \\ & + \xi_2\xi_3\xi_{i+1} + \cdots + \xi_2\xi_3\xi_N + \cdots + \xi_{N-2}\xi_{N-1}\xi_N\Big] \\ = {} & \sum{}' C_3\ (\xi_1, \xi_2 \cdots \xi_{i-1}, \xi_{i+1}, \cdots \xi_N) , \end{aligned} \qquad (60)$$

$$a_N = (-1)^N \xi_1 \xi_2 \xi_3 \ldots \xi_{i-1} \xi_{i+1} \ldots \xi_N \,. \tag{61}$$

The general coefficient is given as,

$$a_\nu = (-1)^\nu \sum{}' C_\nu (\xi_1, \xi_2 \ldots \xi_{i-1} \xi_{i+1}, \ldots \xi_N) \,, \tag{62}$$

where,

$$\sum{}' C_\nu (\xi_1, \xi_2, \ldots \xi_{i-1}, \xi_{i+1}, \ldots \xi_N) \,, \tag{63}$$

represents the sum of products of all elements ξ_K except $K = i$ belonging to the combination of the i^{th} class without repetition. The prime at the right of the summation symbol indicates that the value ξ_i must be excluded.

Integration of (57) between $\xi = -1$ and $\xi = +1$ results in,

$$\int_{-1}^{+1} [\phi(\xi)/(\xi-\xi_i)]\, d\xi = [1 - (-1)^N]/N + [a_1/(N-1)]\,[1 - (-1)^{N-1}]$$

$$+ [a_2/(N-2)]\,[1 - (-1)^{N-2}] + \ldots\ldots + 2a_{N-5}/5 \tag{64}$$

$$+ 2a_{N-3}/3 + 2a_{N-1} \,.$$

Because,

$$\phi'(\xi_i) = \xi_i^{N-1} + a_1 \xi_i^{N-2} + a_2 \xi_i^{N-2} + \ldots + a_{N-2}\xi_i + a_{N-1} \,, \tag{65}$$

it follows from (55) that,

$$p_i = \left\{[1 - (-1)^N]/N + [a_1/(N-1)]\,[1 - (-1)^{N-1}] + \ldots\ldots [2a_{N-3}]/3 + 2a_{N-1}\right\} / [\xi_i^{N-1} + a_1 \xi_i^{N-2} + \ldots\ldots a_{N-1}] \,. \tag{66}$$

If (66) is inserted in (54) and the summation is performed the integral I, in (43), is evaluated.

b. Numerical Evaluation.

In order to evaluate the integrals in (38) and (39) one variable (e.g., $x = x_n$) is held constant and the integration is performed over the other variable by means of (54) and (66).

Integrals U and V can be written in short form as,

$$\int_{x=-x_N,\ y=-\bar{y}(x)}^{x=x_N,\ y=+\bar{y}(x)} \Psi(x,y)\, dx\, dy \,, \tag{67}$$

where,

$$\Psi(x,y) = A\,(x,y,\ x^2/4f + y^2/4f) \begin{matrix}\cos\\ \sin\end{matrix} [k\,M\,(x,y,\ x^2/4f + y^2/4f)] \; \bar{n} \cdot (\bar{R}_1 + \bar{s})\,[1 + x^2/4f^2 + y^2/4f^2]^{1/2} \,, \tag{68}$$

and $\pm \bar{y}\,(x)$ are the boundary values of y for a given value of x.

For a specific value of $x = x_\ell$, assume a sequence (x_i) along the y = o axis defining the division points of the structural junctions in the

x-direction. Along $x = x_\ell$ the surface is divided along the y-direction. These points are defined by the sequence y_i $(i = 1,2,3,..K)$ as a function of x_ℓ.

Using (54), (67) can be written,

$$\int_{-x_N}^{+x_N} \int_{-\bar{y}(x)}^{+\bar{y}(x)} \Psi(x,y)\, dx\, dy = \int_{-x_N}^{+x_N} \sum_{i=1}^{K} \eta_i(x_\ell)\, p_i(x_\ell)\, dx , \tag{69}$$

where,

$$\eta_i(x_\ell) = \Psi(x_\ell, y_i) , \tag{70}$$

and $p_i(x_\ell)$ for $(i = 1,2,3,...K)$ are the weights. For each x_ℓ there are $K(\ell)$ weights.

To complete the integration,

$$\int_{-x_N}^{+x_N} \sum_{i=1}^{K} \eta_i(x_\ell)\, p_i(x_\ell)\, dx = \sum_{\ell=1}^{N} \sum_{i=1}^{K(\ell)} \eta_i(x_\ell)\, p_i(x_\ell)\, p_\ell$$

$$= \sum_{\ell=1}^{N} \sum_{i=1}^{K(\ell)} \Psi(x_\ell, y_i)\, p_i(x_\ell)\, p_\ell , \tag{71}$$

where p_ℓ are the weights for the division points along the x-axis.

The weight matrix,

$$p_i(x_\ell)\, p_\ell = W_{i\ell} \tag{72}$$

is an array of numbers obtained as the product of the ℓ^{th} weight of the integration interval along the Y-axis and the i^{th} weight of the integration interval along the axis $x = x_\ell$. The structural junction is designated by (ℓ, i). The value $\Psi(x_\ell, y_i)$ is the integrand at the point (ℓ, i). The approximation for the double integral (67) therefore is the sum of all products formed by the integrand at the structural junctions and the associated element of the weight matrix.

$W_{i\ell}$ remains constant for an antenna with a given focal length, diameter, and a given number of structural junctions at which the integrals (38) and (39) are to be evaluated. The integrand $\Psi(x_\ell, y_i)$ however changes as a function of the distortions in the aperture.

8. COMPUTATIONAL PROCEDURE

For the sets of numerical values given in the RATIO First Quarterly Report GD/A63-0856:

a. Coordinates and Deflections.

1. Compute and store values of x_m and y_n from (41) and (42).
2. Compute and store Δx, Δy, Δz for each (x_m, y_n). Δx, Δy, Δz are defined in (15). Assume $\Delta x_f = \Delta y_f = \Delta z_f = 0$ in (18).
3. Compute and store $\Delta\phi_p$, and $\Delta\phi_q$, as defined for (27) and (28), for each (x_m, y_n). From the structural analysis, the components (in the x, y, z direction of the angular deflection at each (m, n) structural junction are $\phi_{xm,n}$, $\phi_{zm,n}$, and

$$\Delta\phi_p = \left[\phi_{xm,n} + \phi_{zm,n}(x_m/2f)\right]\left[1 + (x_m/2f)^2\right]^{-1/2},$$

$$\Delta\phi_q = \left[\phi_{ym,n} + \phi_{zm,n}(y_n/2f)\right]\left[1 + (y_n/2f)^2\right]^{-1/2}.$$

b. Weight Functions.

1. For each value of $x_\ell = x_m$ determine and store $K(\ell)$, as defined for (69). $K(\ell)$ are the number of structural junctions at each $x_\ell = x_m$. There are 2N values of x_ℓ.

2. For $b = -a$ in (49), $\xi_{yi} = y_i/b$ and $b = y_{K(\ell)}$ where $y_{K(\ell)}$ are the maximum values for y for each x_ℓ. Compute and store $\xi_{yi}(\ell) = y_i(\ell)/y_{K(\ell)}$ for each value of $i = -K, -(K-1), -(K-2), -(K-3) \ldots +(K-2) +(K-1) +K$ and each corresponding value of $\ell = -N, -(N-1), -(n-2) \ldots +(N-2), +(N-1), +N$. (Note $K = K(\ell)$ from item 1 in Section 8b.)

3. Using values of $\xi_{yi}(\ell)$ from above compute and store $A_{1y}, A_{2y} \ldots A_{Ny}$ from (58) to (61).

4. Compute and store $\xi_{xi} = x_\ell/x_{\ell\ \max.}$, and $A_{1x}, A_{2x}, \ldots A_{Nx}$ from (58) to (61) for each $\ell = -N, -(N-1) \ldots +(N-1), +N$.

5. Compute and store p_{iy}, p_{ix}, and $W_{i\ell}$ from (66) and (72) using the results of item 3 and 4. (Note $p_i(x_\ell) = p_{iy}$, and $p_\ell = p_{ix}$.)

c. Radiation Function

1. Using the results of items 1 to 3 in Section 8a, compute and store values for $M(x_m, y_n)$ from (23). θ and ϕ are variables.

2. Using the $\Delta\phi_p$ and $\Delta\phi_q$ from item 3 in Section 8a compute and store p_1^*, p_2^*, p_3^*, q_1^*, q_2^*, q_3^* from (31) to (36).

3. From (24), (30) and (22),

$$\bar{n} \cdot (\bar{R}_1 + \bar{s}) = [\cos\theta \cos\phi - (k/\ell)(x_m + \Delta x - \Delta x_f)]$$

$$(p_2^* q_3^* - p_3^* q_2^*)/A + [\cos\theta \sin\phi - (k/\ell)(y_n + \Delta y - \Delta y_f)]$$

$$(p_3^* q_1^* - p_1^* q_3^*)/A + [\sin\theta - (k/\ell)(x_m^2/4f + y_n^2/4f + \Delta y - \Delta y_f)]$$

$$(p_1^* q_3^* - p_2^* q_1^*)/A,$$

where,

$$A = [(p_1^{*2} + p_2^{*2} + p_3^{*2})\,(q_1^{*2} + q_2^{*2} + q_3^{*2})$$

$$- (p_1^* q_1^* + p_2^* q_2^* + p_3^* q_3^*)^2]^{1/2} .$$

Compute and store $\bar{\pi} \cdot (\bar{R}_1 + \bar{s})$ from above and $M(x_m, y_m)$ from (23), for $(k/\ell) = 1$ and $\Delta x_f = \Delta y_f = \Delta y_f = 0$.

4. Take $A(x,y,x^2/4f + y^2/4f) = 1$ and using results of item 3 in Section 8c, compute and store $4(x_m, y_n)$ from (68).

5. Evaluate, tabulate and plot (71), using results of items 4 and 1 in Section 8c. The equations are to be evaluated at, $\theta = -\pi$, $-(\pi - 0.05\pi)$, $-(\pi - 0.10\pi)$, ... $+ (\pi - 0.10\pi)$, $+ (\pi - 0.05\pi)$, π and $\phi = -\pi$, $-(\pi - 0.05\pi)$, $-(\pi - 0.10\pi)$, ... $+ (\pi - 0.05\pi)$, π. The SC 4020 is used for the plotting.

APPENDIX A - STRUCTURAL ANALYSIS

(By J. R. Lloyd and K. C. Valanis)

1.0 GENERAL.

In Sections III and IV of this study, use is made of a structural analysis program, currently available in the General Dynamics computer library. The following is a brief outline of the theory underlying this program as it has been updated for application to RATIO structures.

1.1 GENERAL APPROACH

The analysis method is based on an extension of the well known matrix displacement method for the analysis of complex frames. It has the following features:

1. The truss analysis applies to an arbitrary three-dimensional structure having pinned, elastic, or rigid joints.
2. The six degrees of freedom at the two ends of the truss members are used to describe structural deformations. Shear panels may be accomodated in the analysis.
3. Loads in any of the six degrees of freedom may be introduced at any point on the structure.
4. Curved truss members with non-uniform cross sections can be handled, and there is no theoretical limit on the number of members meeting at a joint. (Straight members with constant cross sections will be assumed.)
5. Account may be taken of thermal loads and moments, due to temperature fields.

6. The stresses in the structure are well below the elastic limit of the structural material.

1.1.1 NOMENCLATURE

A	Cross sectional area of an element for tension and compression.
A^1	Cross sectional area of an element for shear.
(a)	A matrix which places a structural element in a specific relationship to the aggregate of such elements constituting the structure.
(C)	A transformation matrix relating the fixed and local coordinate systems.
E	Modulus of elasticity.
G	Shear modulus of elasticity.
I_x, I_z	Moment of inertia of an element about its x, z- axes.
J	Polar moment of inertia.
K	Cross section form factor.
(k)	The stiffness matrix of a generic element in its local coordinate system.
(K)	A stiffness matrix in the fixed coordinate system.
ℓ	Length of an element
M_x, M_y, M_z	Bending moment, applied about the X, Y, Z- axes.
M_{Tx}, M_{Tz}	Moments about the X, Z- axes induced by thermal loading.
(p)	A generalized force vector in a local coordinate system.
(P)	A generalized force vector in a fixed coordinate system.
P_x, P_y, P_z	A force acting in the direction of the X, Y, Z- axes.

The matrix displacement method is particularly applicable to RATIO antenna structures in which displacements are the important unknowns. It is also of great value in computing quasistatic aperture deformation patters from time-varying loads and for parameteric studies of loads created by the attitude control system.

The analysis has been programed for the 7090 computer, and is a catalogued program at General Dynamics/Astronautics.

Theoretically, the complexity of a structure that can be analyzed on the computer is limited by the computer memory and structural symmetry. The greater the symmetry the greater are the number of structural joints that can be analyzed. At present, a structure with as many as 200 non-symmetrical joints is being handled. This is adequate for the highly redundant structural arrangement in the full aperture RATIO antennas.

The following assumptions apply to the analysis,

1. The component elements of the structure are straight beams.
2. The beam cross-section and length of the beam centroidal axis before and after bending are the same.
3. Shear deformation is small and negligible.
4. Structural equilibrium is not altered by deformation in the structure.
5. The reaction forces and torques are applied at the structural junctions. The mass of the structure is subdivided into lumped masses located at the structural junctions.

(r)	A generalized deflection vector in the fixed coordinate system.
(R)	A generalized force vector in the fixed coordinate system.
u,v,w	A deflection in the x, y, z- directions.
x,y,z	A right handed Cartesian coordinate system called the "local coordinate system."
U,V,W	A deflection in the X, Y, Z- directions.
X,Y,Z	A right handed Cartesian coordinate system called the "fixed coordinate system."
ϕ, ψ, θ	A rotation about the x, y, z- axes.
(L)	The stiffness matrix of the generic element, referred to the fixed coordinate system.

2.0 STIFFNESS DETERMINATION*

2.1 STIFFNESS MATRIX OF A SINGLE ELEMENT -- Consider an aggregate structure consisting of straight uniform elements that are capable of withstanding direct load, shear, bending, and torsion. An element or truss member in this structure is arbitrarily orientated with respect to fixed reference system of axis, X, Y, Z.

Let the axis of the element and the two principal axes of its cross-section define a "local" system of axes denoted by x, y, z. (i.e., one of the local axes is coincident with the longitudinal axis of an element.) Three displacements and three rotations with respect to these axes at each end of the element, indicated in Figure 2 (a), completely define the state of deformation of the element. When the structure consisting of many elements is considered, the numerical designations in Figure 2 (b) will be used. In Figure 1 the vectors may represent either displacements or forces, and the right hand screw rule is adopted for the rotation or moments.

For a single member the following expression may be written with respect to the local system:

$$(p) = (k)\ (u) \tag{1}$$

where (p) is a vector or a 12 column matrix of the force, (u) is a 12 column matrix of the displacements, and (k) is a 12-by-12 stiffness matrix.

---

*Reference "Energy Theorems and Structural Analysis," J. H. Argyris Aircraft Engineering, Oct., Nov., Dec., 1954, Feb., Mar., Apr., May, 1955.

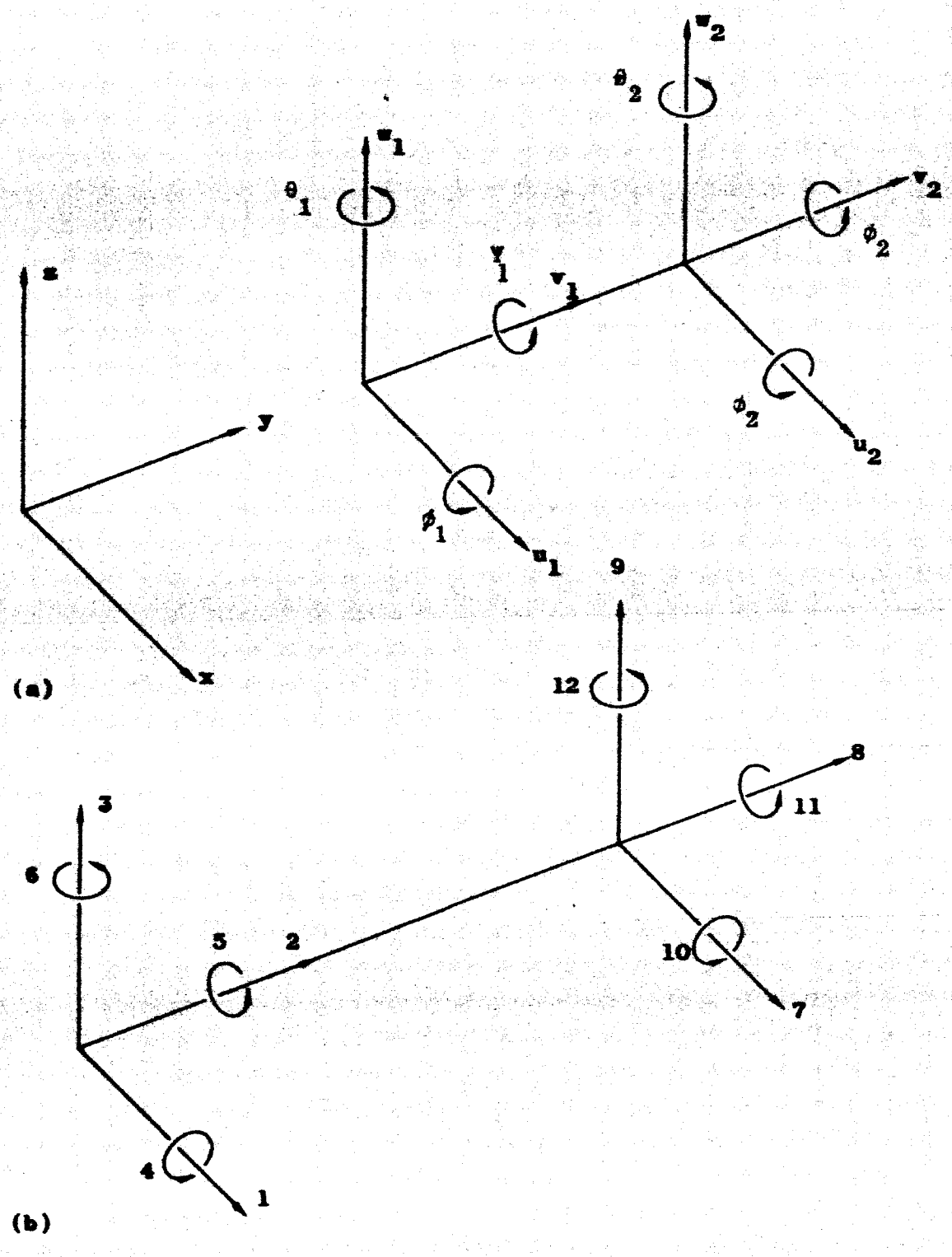


Fig. A-1. Designations for displacements at two ends of an element.

A vector in the reference or fixed system can be transformed to the local system by

$$\begin{bmatrix} x \\ y \\ z \end{bmatrix} = \begin{bmatrix} l_1 & m_1 & n_1 \\ l_2 & m_2 & n_2 \\ l_3 & m_3 & n_3 \end{bmatrix} \begin{bmatrix} X \\ Y \\ Z \end{bmatrix}$$

where l, m, and n are the direction cosines. From this we obtain,

	1	2	3	4	5	6	7	8	9	10	11	12
1	$12EI_z/l^3$ $+GA'_x/l$					$-6EI_z/l^2$	$-12EI_z/l^3$ $-GA'_x/l$					$-6EI_z/l^2$
2		EA/l						$-EA/l$				
3			$12EI_x/l^3$ $+GA'_z/l$	$6EI_x/l^3$					$-12EI_x/l^3$ $+GA'_z/l$	$6EI_x/l^2$		
4			$6EI_x/l^2$	$4EI_x/l$					$-6EI_z/l^2$	$2EI_x/l$		
5					GJ/l						$-GJ/l$	
6	$+6EI_z/l^2$					$4EI_z/l$	$+6EI_z/l^2$					$2EI_z/l$
7	$-12EI_z/l^3$ $-GA'_x/l$					$+6EI_z/l^2$	$12EI_z/l^3$ $+GA'_x/l$					$+6EI_z/l^2$
8		$-EA/l$						EA/l				
9			$-12EI_x/l^3$ $-GA'_z/l$	$-6EI_x/l^2$					$12EI_x/l^3$ $+GA'_z/l$	$-6EI_x/l^2$		
10			$6EI_x/l^2$	$2EI_x/l$					$-6EI_x/l^2$	$4EI_x/l$		
11					$-GJ/l$						GJ/l	
12	$6EI_z/l^2$					$2EI_z/l$	$-6EI_z/l^2$					$4EI_z/l$

Fig. A-2. Stiffness matrix of a generic element.

$$
\begin{bmatrix} u_1 \\ v_1 \\ w_1 \\ \varphi_1 \\ \psi_1 \\ \theta_1 \\ u_2 \\ v_2 \\ w_2 \\ \varphi_2 \\ \psi_2 \\ \theta_2 \end{bmatrix} = \begin{bmatrix}
l_1 & m_1 & n_1 & & & & & & & & & & \\
l_2 & m_2 & n_2 & & & 0 & & & 0 & & & 0 & \\
l_3 & m_3 & n_3 & & & & & & & & & & \\
 & & & l_1 & m_1 & n_1 & & & & & & & \\
 & 0 & & l_2 & m_2 & n_2 & & 0 & & & 0 & & \\
 & & & l_3 & m_3 & n_3 & & & & & & & \\
 & & & & & & l_1 & m_1 & n_1 & & & & \\
 & 0 & & & 0 & & l_2 & m_2 & n_2 & & 0 & & \\
 & & & & & & l_3 & m_3 & n_3 & & & & \\
 & & & & & & & & & l_1 & m_1 & n_1 & \\
 & 0 & & & 0 & & & 0 & & l_2 & m_2 & n_2 & \\
 & & & & & & & & & l_3 & m_3 & n_3 &
\end{bmatrix} \begin{bmatrix} U_1 \\ V_1 \\ W_1 \\ \Phi_1 \\ \Psi_1 \\ \Theta_1 \\ U_2 \\ V_2 \\ W_2 \\ \Phi_2 \\ \Psi_2 \\ \Theta_2 \end{bmatrix} \qquad (3)
$$

Or, in matrix form:

$$(u) = (C)(U), \qquad (4)$$

where (C) is a transformation matrix between the "fixed" and "local" axes.

Let (P) be the forces defined with respect to the fixed systems, then

$$(P) = (C)'(p), \qquad (5)$$

where the prime denotes transposition.

From the principle of invariance of the work,

$$(p)'(u) = (P)'(U). \tag{6}$$

On substituting Eqs. (4) and (5) in (1) or (6) we get

$$(P) = (C)'(k)(C)(U), \tag{7}$$

or

$$(P) = (L)\ (U). \tag{8}$$

(L) is the stiffness matrix of the element with respect to the fixed coordinate system and is found from the expression

$$(L) = (C)'(k)(C). \tag{9}$$

2.2 STIFFNESS MATRIX OF A BAY -- The structure is divided into bays. The aggregate stiffness of a bay is identified with the stiffness of the elements.

Consider a bay in Fig. 3 that consists of six elements, forming a pyramid with 3 joints. The deformation of this bay is defined by 24 displacements and therefore a 24-by-24 stiffness matrix. The numerical scheme in Fig. 4 uses circled numbers to identify elements and ordinary numbers to identify displacements.

Let the displacement matrix of the bay be denoted by (U_b) and the displacement matrix of element j by (U_j), then for one element,

$$(U_j) = (a_j)(U_b), \tag{10}$$

where (a_j) is a 24-by-12 transformation matrix.

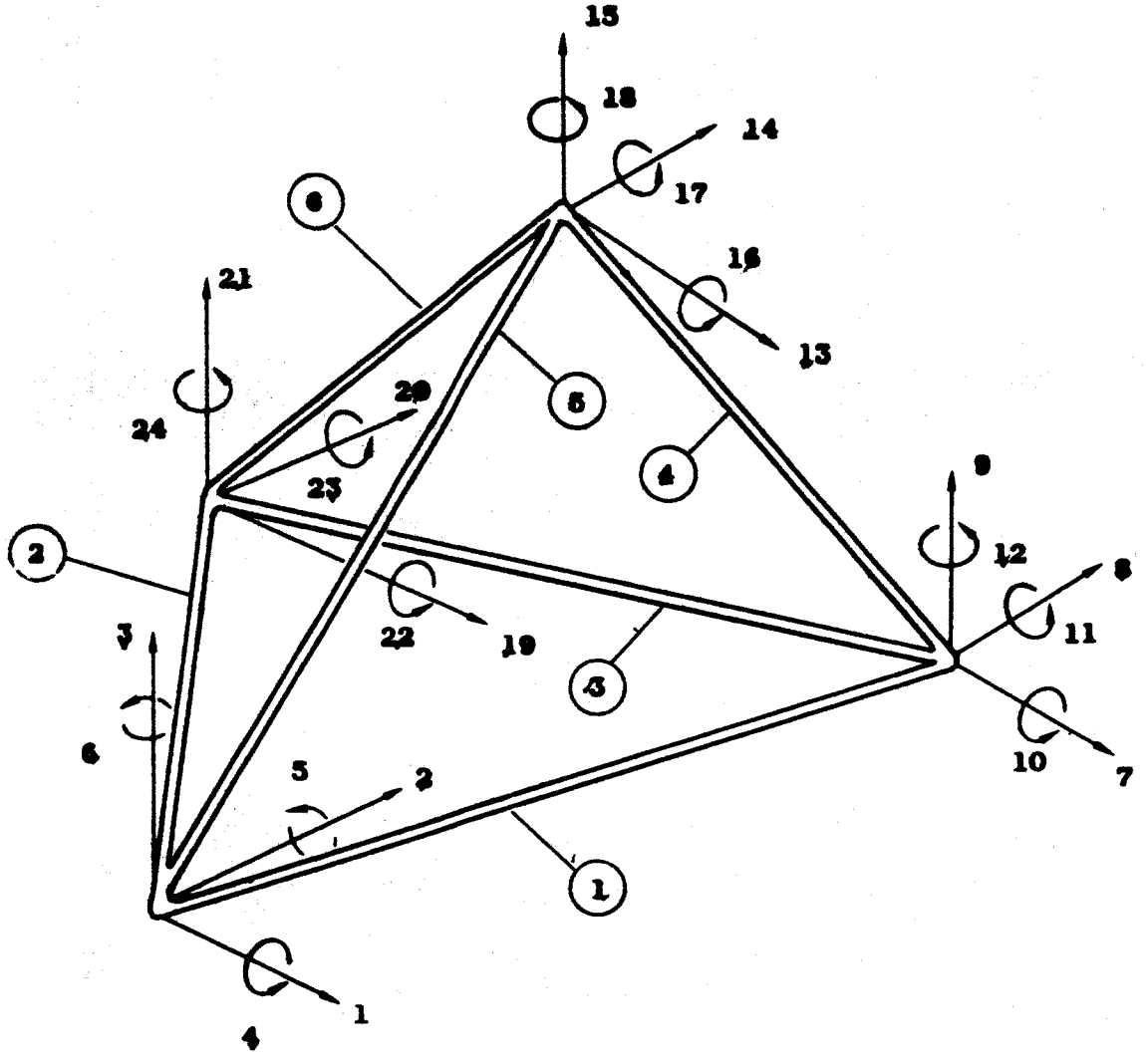


Fig. A-3. An elementary bay.

The load relation takes the form:

$$(P_b) = (a_j)'(P_j), \tag{11}$$

hence the stiffness of the element referred to the bay

$$(L_{jb}) = (a_j)'(L_j)(a_j). \tag{12}$$

Therefore, the total stiffness matrix (K) of the bay is given by

$$(K) = \sum_{j=1}^{m} (L_{jb}), \tag{13}$$

where m is the number of elements in the bay.

By the above procedure the stiffness matrix of all the bays can be computed.

3.0 METHOD OF ANALYSIS

The approach to the analysis is to divide the structure into simple bays. Once the stiffness matrices of all the bays have been obtained, the structure can be analyzed by taking each bay separately, geometrically eliminating the bay from the structure, and incorporating its elastic effect in the adjacent bay. This procedure is repeated until only one bay is left. The last bay is then analyzed by equating the displacements and forces at its joints with the displacements and forces of the adjacent bays.

3.1 MATHEMATICAL FORMULATION OF THE ANALYSIS -- Let the bays be designated by the numerals (1), (2), --- (n-1), (n). Consecutively, numbered bays have common boundaries.

Let $r^{(j)}$, $R^{(j)}$ and $K^{(j)}$ denote the displacement, force and stiffness matrices respectively of the j^{th} bay. Then,

$$R^{(j)} = K^{(j)} r^{(j)} \quad . \tag{14}$$

Partitioning R, r, and K into components, b, on the interconnecting boundary, and components, r, on the rest of the bay,

$$R = \begin{bmatrix} R_b \\ R_r \end{bmatrix} , \tag{15}$$

$$r = \begin{bmatrix} r_b \\ r_r \end{bmatrix} , \tag{16}$$

and

$$K = \begin{bmatrix} K_{bb} & K_{br} \\ K_{rb} & K_{rr} \end{bmatrix} \quad . \tag{17}$$

Substituting Eqs. (15), (16), and (17) in Eq. (14),

$$\begin{bmatrix} r_b^{(j)} \\ r_r^{(j)} \end{bmatrix} = \begin{bmatrix} K_{bb}^{(j)} & K_{br}^{(j)} \\ K_{rb}^{(j)} & K_{rr}^{(j)} \end{bmatrix}^{-1} \begin{bmatrix} R_b^{(j)} \\ R_b^{(j)} \end{bmatrix} . \tag{18}$$

At the boundary of adjacent bays, equilibrium between externally applied and internal forces must be satisfied; therefore,

$$R_b^{(j)} + R_b^{(j-1)} = R_b^{(j,\ j-1)} \tag{19}$$

where $R_b^{(j,\ j-1)}$ are the external forces applied at the boundary joints.

Since compatibility of displacements must also be satisfied at the boundary,

$$r_b^{(j)} = r_b^{(j-1)}. \tag{20}$$

From Eq. (18), (19), and (20), the following relations may be derived,

$$R_b^{(j)} = R_b^{(j,\, j-1)} - K_{br}^{(j-1)}\left[K_{rr}^{(j-1)}\right]^{-1} R_r^{(j-1)} \tag{21}$$

$$K_{bb}^{(j)} = K_{bb}^{(j)} + K_{bb}^{(j-1)} - K_{br}^{(j-1)}\left[K_{rr}^{(j-1)}\right]^{-1} K_{rb}^{(j-1)} \tag{22}$$

$$r_r^{(j-1)} = \left[K_{rr}^{(j-1)}\right]^{-1}\left[R_r^{(j-1)} - K_{rb}^{(j-1)}\, r_b^{(j)}\right] \tag{23}$$

Eqs. (21), (22), and (23) are used iteratively to solve for all loads and displacements in the structure.

In addition to the above, expressions have been developed for evaluating the effects of thermal loads and loads that are not applied at the joints. Computer programs are being written for various structural configurations that are applicable to the RATIO antenna. These programs account for conventional joint loads and thermal loads.

4.0 THERMAL LOADING

Consider a typical member under thermal loading where the temperature is a function of the local coordinates x, y, z. Assume that the member is simply supported. The stress in the member is given by the expression,*

$$\sigma_y = - E\alpha T + (P_T/A) + (M_{Tz}/I_z)\, x + (M_{Tz}/I_x)\, z \tag{24}$$

where,

$$P_T = \int_A E\alpha T(x, y, z)\, dA \quad , \tag{25}$$

$$M_{Tz} = \int_A E\alpha T(x, y, z)\, x\, dA, \tag{26}$$

$$M_{Tx} = \int_A E\alpha T(x, y, z)\, z\, dA \quad . \tag{27}$$

The displacements of the member can be calculated from,

$$v = (1/E) \int_0^{\ell} (P_T/A)\, dy \quad , \tag{28}$$

$$(d^2u/dy^2) = -M_{Tz}/EI_z \quad , \tag{29}$$

$$(d^2w/dy^2) = -M_{Tx}/EI_x \quad . \tag{30}$$

*Levy, R. S., Switzky, H., Torray, M., Newman, M., and Meissner, C. J., "A Survey of Structural Design Problems in a Combined Thermal and Load Environment," Aeronautical Systems Division, Air Force Systems Command, U. S. Air Force, Wright-Patterson Air Force Base, Ohio, Report 61-645, pp. 777 et. seq.

If axial expansion and rotation of the ends of the member are prevented forces are introduced. The axial end force is found from the expression,

$$P = (A/\ell)\int_0^{\ell} (P_T/A)\,dy \tag{31}$$

In the yz plane the moments M_{1x} and M_{2x} are such that the slopes at the ends of the element are zero. The additional moment distribution due to the end moments is

$$M_x = M_{1x} + (M_{2x} - M_{1x})y/\ell \tag{32}$$

Hence:

$$d^2w/dy^2 = -\left[M_{Tx} + M_{1x} + (M_{2x} - M_{1x})y/\ell\right]/EI_x \tag{33}$$

or

$$w = \int_0^y \int_0^y M_{Tx}\,dy\,dy + (M_{1x}\,y^2/2) + (M_{2x} - M_{1x})y^3/\ell(3)$$

Where M_{1x} and M_{2x} can be found from the boundary conditions,

$$w = o\,,\ y = \ell$$

$$dw/dy = o\,,\ y = \ell \tag{34}$$

M_{1z} and M_{2z} may be found by a similar argument.

For a uniform temperature variations along the length of a member,

$$P = P_T\ ,$$

$$M_{1x} = - M_{Tx} \quad , \tag{36}$$

$$M_{2x} = - M_{Tx} \quad , \tag{37}$$

$$M_{1z} = - M_{Tz} \quad , \tag{38}$$

$$M_{2z} = - M_{Tz} \quad , \tag{39}$$

The forces and torques exerted by the element on the joints is shown in Figure 4,

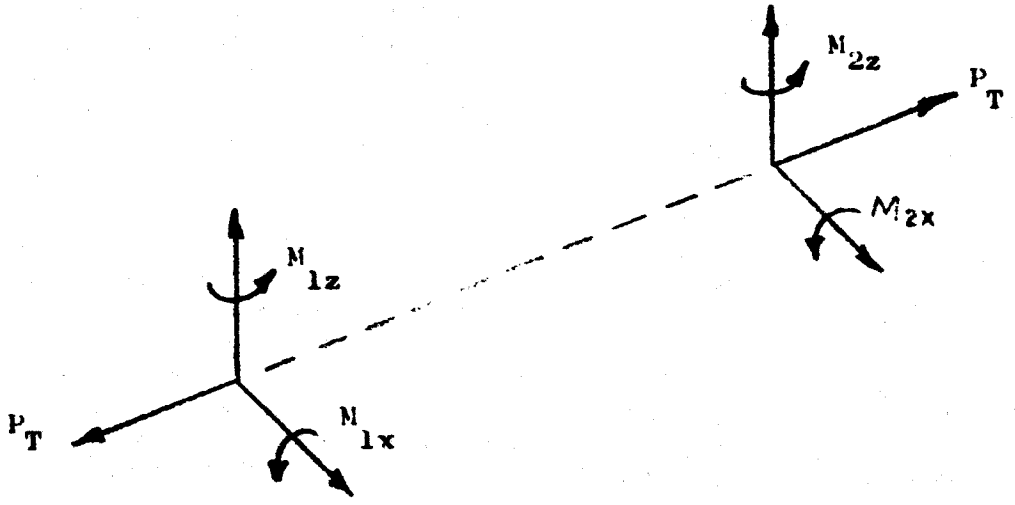


FIGURE A-4

Forces of thermal loading

and give rise to the matrix

$$(F) = (0 \quad -P_T \quad 0 \quad M_{1x} \quad 0 \quad -M_{1z} \quad 0 \quad P_T \quad 0 \quad -M_{2x} \quad 0 \quad M_{2z}) \tag{40}$$

The matrix (P_j) of the forces in the direction of the fixed axes is given by the relation,

$$(P_j) = (c_j)^T (F_j) \tag{41}$$

also,

$$(P_{jB}) = (a_j)^T (P_j) \tag{42}$$

Finally the matrix (R) of the external forces applied at the joints of the bay is given by the relation,

$$(R) = \sum_{j=1}^{m} P_{jB} \, . \tag{43}$$

5.0 LOADS NOT APPLIED AT THE JOINTS

Loads that are not applied at the structural joints can be treated in a manner similar to the thermal loads. Whatever the loading, it can always be resolved into components along the local axes of the element. The joints of the element are, then, frozen and the forces exerted by the loading on the joints are calculated. These forces define the matrix (F_j). The total loads on the joints of a bay are given by (30), (31) and (32).

To find the stresses in a member so loaded, two types of loading must be considered and their effects superposed:

(a) The forces in the member arising due to the forces (R) formed from (F).

(b) The self-equilibrating forces on the element itself consisting of the initial loading and the reactions of the frozen joints.

6.0 MEMBERS WITH NON-UNIFORM PROPERTIES

Divide the member into parts having approximately uniform cross-section and elastic properties. The stiffness matrix (K) of the member is then found by the assembly of the smaller parts, in the way already outlined.

The ends of the member now form its boundary with the rest of the structure. With the previous notation, we partition K, p, and u so that,

$$\begin{bmatrix} p_b \\ p_r \end{bmatrix} = \begin{bmatrix} K_{bb} & K_{br} \\ K_{rb} & K_{rr} \end{bmatrix} \begin{bmatrix} u_b \\ u_r \end{bmatrix} \tag{14}$$

Take the case where $(p_r) = 0$. That is, the member is loaded at its end points. Then,

$$p_b = K_{bb}\, u_b + K_{br}\, u_r \tag{45}$$

$$0 = K_{rb}\, u_b + K_{rr}\, u_r \tag{46}$$

Now eliminate u_r,

$$p_b = \left[K_{bb} - K_{br}\, K_{rr}^{-1}\, K_{rb} \right] u_b \tag{47}$$

or

$$u_b\, \bar{K}_{bb} = p_b \,. \tag{48}$$

Comparing (48) with (1) we see that for such an element $(\bar{K}_{bb})$ should be used instead of (K).

If the member is loaded at intermediate points, we follow the previous procedure by freezing the joints, i.e.,

$$u_b = 0 \quad . \tag{49}$$

Equation (41) becomes,

$$p_b = K_{br} u_r \quad . \tag{50}$$

$$p_r = K_{rr} u_r \quad . \tag{51}$$

or,

$$u_r = K_{rr}^{-1} p_r \quad , \tag{52}$$

$$p_b = K_{br} K_{rr}^{-1} p_r \quad . \tag{53}$$

p_b are now the reactions that the joints exert on the member; consequently the loads on the joints due to the loading on the member are $-p_b$.

If we make the reference system of the whole member coincide with the "local" system at one of the ends of the member, we reduce the arbitrary element to a straight element with a system of axes coinciding with the local system, a stiffness matrix (K_{bb}), and induced loads on the joints given by $(-p_b)$. Hence we again have a standard case.

APPENDIX B - THERMAL DISTORTIONS

(By P. Slysh)

1.0 GENERAL

Thermal distortions in RATIO structures, as a result of thermal gradients, are influenced by the following factors:

(1) The structural configuration, i.e. whether the structure is of a truss or panel type, length-to-radius-of gyration ratios for the truss members, wall thicknesses of the panels, member cross-sections, number and sizes of panel or truss members, conditions at the structural junctions, volume of the structural material in the total structural volume, shape of the structural volume, etc.

(2) Surface coating and construction material properties, i.e., surface emissivity and absorptivity, material modulus of elasticity, coefficient of thermal conductivity, etc.

(3) Angle of incidence of the solar radiation, i.e., the attitude of the structure relative to the sun, and the attitude of the structural members relative to each other.

(4) Intra-structural reradiation paths, i.e., the number of paths through which radiant energy can be transferred within the structural volume.

(5) Radiation environment, i.e., the solar constant, as well as the albedo background and earth's shadowing as effected by orbital altitude and inclination.

(6) On-board heat sources, which can either minimize (through a regulation system) or increase the thermal gradients.

(7) The turning rate of the structure relative to the sun.

In the following analysis a rectangular structural volume is assumed which is illuminated by the sun on one side. A hypothetical, aggregate-macroscopic structure is taken to occupy this volume and to have the following properties:

(a) The structural volume is occupied by an approximately rectangular-lattice, truss framework with each of the truss members having the same length-to-radius-of-gyration ratio.

(b) The framework is oriented at an arbitrary, average angle with respect to the incident solar radiation. The structure is not rotating.

(c) Pin joints connect all structural members.

(d) The extinction of the radiant energy through the structure is proportional to e exp. x, where x is the depth of penetration of the solar radiation in the structural volume. To some extent, by this means, the intra-structural reradiation effects are taken into account.

(e) Low-earth-orbit solar constant is used, the albedo radiation is neglected, there are no on-board heat sources, and there is no shadowing by the earth.

(f) Thermal gradients are generated only in the direction of the sun's rays. All the incident radiant energy is reradiated from the side of the structural volume opposite the side receiving the radiation. The surface thermal properties and material properties of the structure are constant throughout the structural volume.

For the above conditions, assuming no external constraints, parametric expressions are developed for deflections along the length of the structure.

These expressions indicate the dependence of the deflections on the thermal, material, and structural parameters, and serve as a guide to first order estimates or steady state thermal deflections in RATIO structures.

2.0 THERMAL GRADIENT

The temperature change, ΔT, across the length of structural volume, Δx, in Fig. 2 can be approximated by,

$$\Delta T = I\, A_c a_1\, (\Delta x)/k\, A_o \qquad (1)$$

where,

A_c, ft^2, is the average structural projected area (i.e. illuminated by the sun) in the volume, $2L\, d_1(\Delta x)$

A_o, ft^2, the conductive cross-section through the construction material in the direction of the heat flow,

a_1, aggregate solar absorptivity,

I, Btu/ft^2, incident solar radiation,

k, $Btu\text{-}ft/ft^2 \cdot F$, coefficient of thermal conductivity.

Assuming (from Lambert's law) that the effective radiation received by a surface is proportional to the square of cosine of the angle between the incident radiation and the surface, the average projected length of a truss member is,

$$L_{oav} = (2L_o/\pi) \int_o^{\pi/2} \cos^2 \Theta d\Theta = Lo/2 \qquad (2)$$

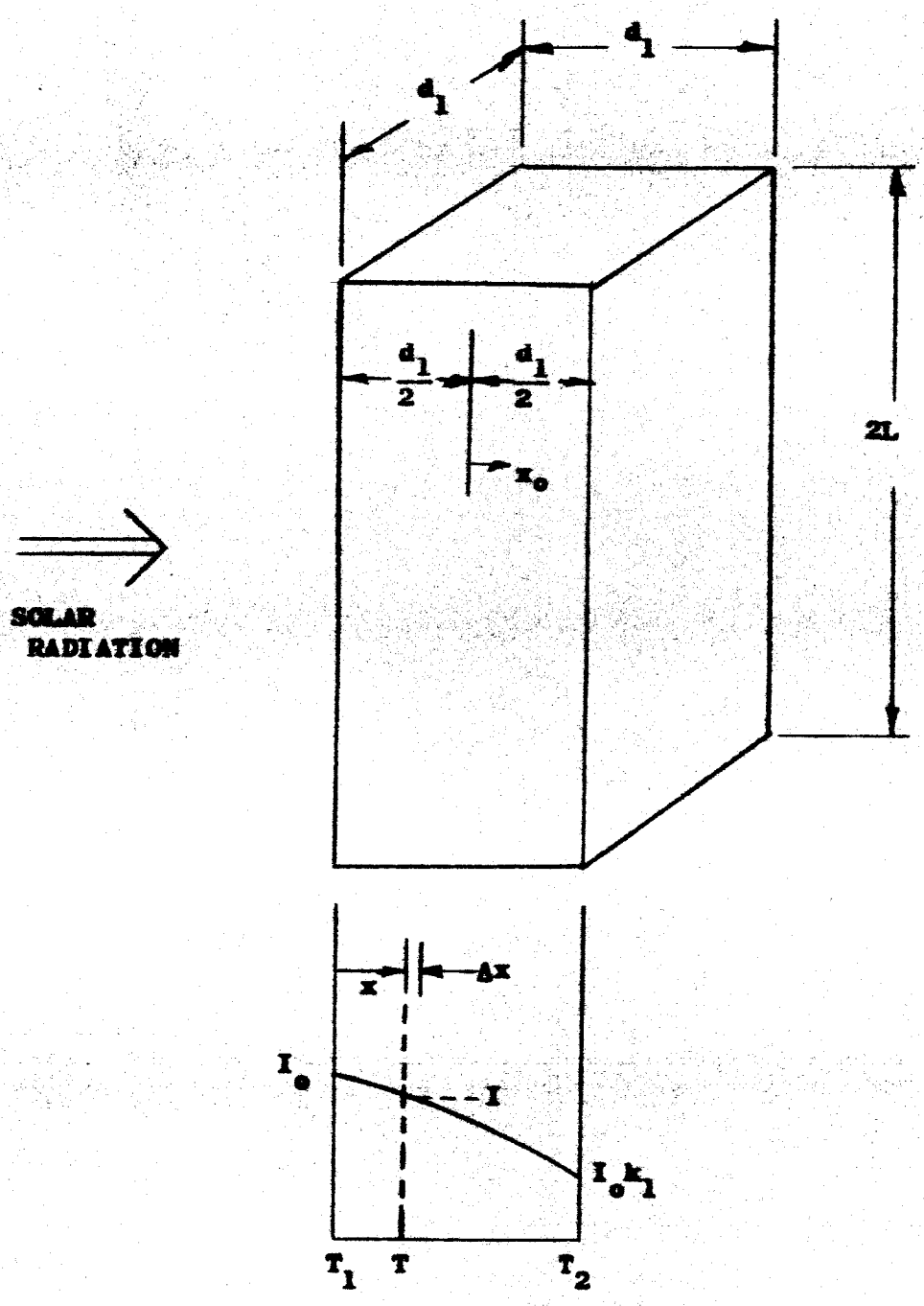


Fig. B-1 Assumed structural model

where,

L_o is the length of a truss member.

The ratio of the volume to average projected area of the construction material for a tubular truss structure is, using Eq. 2,

$$V_c/A_c = (\pi/4)\, L_o\, [d_o^2 - (d_o - 2k_2 d_o)^2]/(L_o d_o/2) = 2\pi k_2\, (1 - k_2)\, d_o, \qquad (3)$$

where,

d_o is the outside diameter of the tubular truss member,

k_2 is the ratio of tube wall thickness to tube outside diameter,

V_c is the volume of the construction material.

From Fig. 2, assuming an exponential extinction of solar radiation through the structure,

$$I = I_o \exp.\, [(x/d_1) \log k_1]. \qquad (4)$$

Also, since the conductive path is in the direction of d_1, and there are three orthogonal directions for heat flow, assume,

$$A_o \cong V_{cT}/3d_1, \qquad (5)$$

and from Eq. (3) take,

$$A_c = xV_{cT}/d_1 d_o 2\pi\, k_2\, (1 - k_2), \qquad (6)$$

where,

V_{cT} is the total volume of the construction material.

Substituting Eq. 4, 5 and 6 in Eq. 1 and performing the integration, the temperature drop between x = o and x is,

$$T_1 - T_2 = [3I_o a_1 d_1^2/2\pi k\, k_2\, (1-k_2)\, d_o \log^2 k_1] \left\{ e \exp.\, [x/d_1) \log k_1] \right.$$
$$\left. [(x/d_1) \log k_1 - 1] + 1 \right\}, \qquad (7)$$

and between $x = 0$ and $x = d_1$,

$$T_1 - T_2 = [3 I_e a_1 d_1^2 / 2\pi k k_2 (1 - k_2) d_o \log^2 k_1] \left\{ k_1 (\log k_1 - 1) + 1 \right\}. \quad (8)$$

It is evident from Eqs. 7 and 8 that the thermal gradient will increase with decreasing values of d_o and increasing values of d_1.

In the above it was assumed that k_1 is independent of d_1 or the ratio of the volume of the construction material, V_{cT}, to the volume occupied by structure, V_{sT}. If this assumption is not to be made, and if the overlaps in elements of the area A_c are taken to be proportional to x then,

$$1 - k_1 = [A_{cT} / 2Ld_1] k_3 (d_1/L), \quad (9)$$

where,

k_3 is a proportionality constant indicating the degree of overlap in elements of A_c,

A_{cT} is the total A_c.

Substituting Eq. 6 in Eq. 9, for $x = d_1$,

$$k_1 = 1 - (V_{cT}/V_{ST}) k_3 k_4 / 2\pi k_2 (1 - k_2), \quad (10)$$

where,

$k_4 = d_1/L$.

From Eqs. 10, 7 and 8 it is seen that the ratio V_{cT}/V_{sT} has a complex effect on the thermal gradients.

3.0 INDUCED DISTORTIONS

The flexural distortion of a beam can be described by,

$$(EI_1)\ d^2y/dL^2 = \int_{-d_1/2}^{+d_1/2} d_1 EBT(x)\ x\,dx, \qquad (11)$$

where,

y is the beam deflection,

E is the modulus of elasticity of the construction material,

I_1 is the section moment of inertia of the truss members,

B is the linear coefficient of thermal expansion,

L and x are defined in Fig. 2.

From Eq. 7 take,

$$T(x) = [3\ I_o a_1 d_1^2/2\pi k\ k_2(1 - k_2)d_o\ \log^2 k_1]\ \{ e\ \exp.$$
$$[\log k_1(x+d_1/2)/d_1]\ [\log k\ (x + d_1/2)/d_1 - 1] + 1\} . \qquad (12)$$

The moment of inertia I_1 can be approximated by,

$$I_1 = (1/12)\ (A_o/d_1)\ d_1^3 = (1/12)A_o d_1^2 . \qquad (13)$$

Substituting Eqs. 5, 12, and 13 in Eq. 11, performing the integration and simplifying,

$$yd_o/L^3 = [V_{sT}/V_{cT}]\ [27\ Ia_1 B\ k_4^2/2\pi k\ k_2\ (1 - k_2)\ ]\ [k_1(0.5\ \log^2 k_1$$
$$-2\ \log^2 k_1 + 3)/\log^4 k_1 - (\log^4 k_1 + 3)/\log^4 k_1\ ], \qquad (14)$$

where,

k_1 is defined by Eq. 10.

In Eq. 14 V_{sT}/V_{cT} may be considered the independent variable. The quantity in the second bracket is based on the solar, structural, and material constants. The quantity in the third bracket is a function of V_{sT}/V_{cT} and the constants.

The increase in structural deflection, y, with V_{sT}/V_{cT} is due primarily to the reduction in the section moment of inertia, I_1, with increasing V_{sT}/V_{cT} (when L and d_o are held constant). The quantity in the third bracket of Eq. 14 which decreases with V_{sT}/V_{cT} diminishes this effect on y. However, it is estimated that this diminishing effect may not be sufficient. Eq. 14 is therefore tentative.

For the conditions that,

$$0 < [V_{cT} k_4 k_3 / V_{sT}\, 2\tau k_2(1 - k_2)] < 0.3, \tag{15}$$

and,

$$\frac{V_{sT}}{V_{cT}} > 10, \tag{16}$$

Eq. 14 with k_1 (from Eq. 10) substituted into it, can be approximated by,

$$y\, d_o/L^3 = [V_{sT}/V_{cT}]\, [27\, I_o a_1 B\, k_4^2/2\tau k\, k_2(1 - k_2)]$$

$$\{0.042 - 0.059\, [V_{cT} k_4 k_3 / V_{sT} 2\, k_2(1 - k_2)]\}\ . \tag{17}$$

The deflection parameter, $y d_o/L^3$, from Eq. 17 is plotted as a function of V_c/V_s in Fig. 3 for the following assumed structural and material constants:

$I_o = 0.82 \times 10^{-3}$ BTU/in.^{2}-sec.,

$k = 0.002$ BTU-in./in.^{2}-$^\circ$F-sec. (for aluminum),

$B = 12.3 \times 10^{-6}$ in./in.^{2}-$^\circ$F (for aluminum),

$k_3 = 0.7$,

$k_4 = 0.1$,

$a_1 = 0.02$.

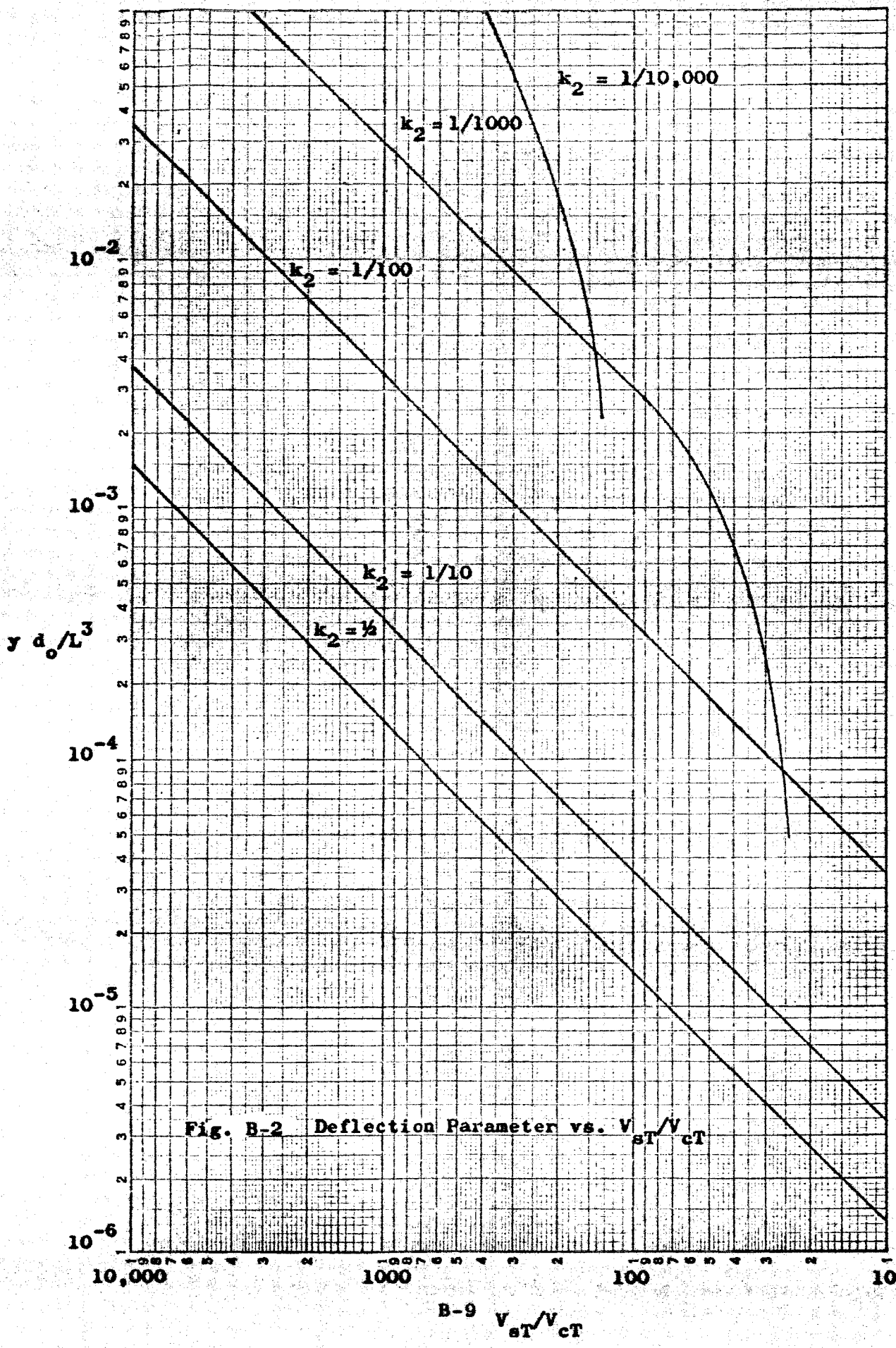


Fig. B-2 Deflection Parameter vs. V_{sT}/V_{cT}

It is evident from Fig. 2 that for a given L and d_o the deflections increase with V_{sT}/V_{cT} and k_2.

3.1 EFFECTS OF (V_{sT}/V_{cT}) ON ELASTIC RIGIDITY

To obtain a first order estimate of the effects of (V_{sT}/V_{cT}) on the elastic rigidity of the structure in Fig. 1, assume that attitude control actuators, having a mass M_A, are attached at both ends. Assume for this example that the mass of the structure is included in the mass of the actuators, then the maximum deflection, Y_m, in the structure due to a total applied moment M_o is,

$$Y_m = (0.021)\, L^2 M_o/EI_1$$

where (as previously defined)

2L is the structure length

E is the modulus of elasticity

I_1 is the section moment of inertia.

Since $M_o = 2M_A L^2 \dot{W}$ (where $\dot{W}$ is the angular acceleration about the center of mass of the structure and actuators), and taking $I_1 = (1/12)\, d_1^4 (V_{cT}/V_{sT})$,

$$Y_m = 0.5\, M_A \dot{W}\, (V_{sT}/V_{cT})/k_4^4 E$$

$$k_4 = d_1/L\ .$$

It is evident that the deflection, Y_m, increases at least linearly with V_{sT}/V_{cT}.

The tendency for Y_m to increase with V_{sT}/V_{cT} is also estimated for configuration in which four or six actuators are distributed along the length of the structure.

The structural properties for minimizing thermal distortions will, therefore, also serve to minimize load deflections.

In the example of Fig. 2, for $k_2 = 1/2$, $M_A = 1$ lb.-sec.^{2}/in., $E = 10^7$ psi, and $d_o/L^3 = 10^{-6}$ in., the thermal and load deflections are equal when $\dot{W} = 280$ rad/sec.^{2} Such large angular accelerations are not likely, ($\dot{W} = 1$ or 0.1 rad./sec.^{2} is more likely) therefore, the thermal distortions will tend to swamp the load deflections.

4.0 DEPENDENCE OF V_{cT}/V_{sT} ON THE SUBDIVISION OF A STRUCTURAL VOLUME

In Eqs. 14 and 17 V_{cT}/V_{sT} and k_2 can be chosen independently. However, the number of subdivisions in the structural volume as well as the length-to-radius-of-gyration ratios of the truss members are affected by these choices.

If it is assumed that the structural volume in Fig. 1 is subidvided into a square lattice truss network such that the ratio of the lengths of the vertical to the lengths of the horizontal truss members if proportional to $2\ L/d_1$ then the total number of vertical truss members in the structural volume is,

$$n_1 = (n' + 1)^2\ n', \tag{18}$$

and the number of horizontal truss members is,

$$n_2 = 2(n' + 1)^2\ n', \tag{19}$$

where,

n' is the number of times each side of the structural volume is subdivided.

If the length-to-radius-of-gyration ratios k_5 for the vertical and horizontal truss (tubular) members are the same,

$$k_5 = 4\, L_o/d_o\, (2 - 4k_2 + 4k_2^2) = 4L_{ol}/d_{ol}\, (2 - 4k_2^2), \tag{20}$$

where,

d_o and L_o, are the outside diameter and length of the vertical truss members,

d_{ol} and L_{ol}, are the outside diameter and length of the horizontal truss members.

Using,

$$V_{cT} = (\pi/4)\, L_o[d_o^2 - (do - 2\, d_o k_2)^2]\, n_1 + (\pi/4)\, L_{ol}[d_{ol}^2 - (d_{ol} - 2d_{ol}\, k_2)^2]\, n_2 \tag{21}$$

and Eqs. 18, and 19,

$$(V_{cT}/V_{sT}) = [4\pi/k_5^2]\, [k_2\, (1 - k_2)/(1 - 2k_2 + 2k_2^2)^2]\, [(n' + 1)^2/(n')^2]\, [(8L^3 + 2d_1^3)/2\, Ld_1], \tag{22}$$

or,

$$(V_{cT}/V_{sT}) = (\pi/4)\, k_2\, (1 - k_2)(n' + 1)^2\, d_o^2\, [(4L^3 + d_1^3)/L^3 d_1^2], \tag{23}$$

where,

k_5 is the length-ro-radius-of-gyration ratio for the truss members and L and d_1 are defined in Fig. 1.

Eq. 23 indicates that for a given k_2, L, d_1, and d_o, V_{sT}/V_{cT} decreases with increasing n'. From Eq. 14 or Fig. 2 it follows, that increasing n' results in smaller thermal deflections. The structural complexity of a large number of small truss members can, therefore, be traded for reduced

thermal distortions and increased structural weight (i.e. decreased V_{sT}/V_{cT}). Ultimately, the finer the mesh of a wire (non-tubular) structure, the smaller the thermal distortions, and the greater the structural weight.

5.0 INTERPRETATION OF RESULTS

Based on the above it appears that the thermal distortions of a structure, whose volume is occupied by an approximately uniform square lattice (aggregate-macroscopic) tubular truss system, are reduced by:

(1) Increasing the tube wall-thickness-to-outside-diameter ratio k_2,

(2) Increasing the ratio of the volume of structural material to structure volume, V_{cT}/V_{sT},

(3) Decreasing the length-to-radius-of-gyration ratio for the truss members,

(4) Reducing the length of the structure or increasing its thickness in the direction of the incident solar energy,

(5) Decreasing the aggregate solar absorptivity, a_1, of the coating material,

(6) Decreasing the ratio of the linear coefficient of thermal expansion to the coefficient of thermal conductivity, B/k, for the structural material. ($B/k = 20.0 \times 10^{-3}$ for hard steel, 10.0×10^{-3} for soft steel, 6.1×10^{-3} for aluminum, 2.2×10^{-3} for copper),

(7) Increase the number and decrease the size of the truss members occupying the structural volume.

The above deductions based on the following assumptions.

Future efforts will be directed toward:

(1) The reradiation within the structure has been neglected.

(2) Only tubular sections have been considered.

(3) The bowing of individual truss members due to thermal gradients in the members has been neglected.

(4) The same structural material and surface coating was assumed for all members in the structural volume.

APPENDIX C - SIMPLE BEAM APPROACH

(By P. Slysh)

In Section III a planar model of a RATIO antenna is analyzed. This model includes a non-uniform contour, that approximates a circular aperture, and locations for actuator and feed masses at distributed points on the antenna structure. It is assumed now that the contour is made square and the number of actuators is increased such that for O-A axis rotation the actuator at each structural junction (depending on the actuator distribution case) is accompanied by actuators at each of the other junctions that lie in a line parallel to the O-A axis. If only O-A axis rotation is considered, and the structure is tapered only in the plane perpendicular to the O-A axis, it is possible, because of the structural and loading symmetry, to limit the deflection analysis to one characteristic beam lying perpendicular to the rotation axis. The results of this analysis are characteristic of the entire structure.

The investigation of this model leads to an essentially closed form solution for the rms surface deviations (d). If model and loading-condition simplifications are justifiable and the discrepancies in the performance results are tolerable it is possible to use this closed form solution for various optimizations. These may include the determination of optimum structural taper for a given actuator distribution case, or the optimum structural mass fraction (k_S) for a given taper. Comperable optimizations on the planar model requires an iterative computational procedure.

The notations in Section III 3.1 are used in the following analysis.

1.0 STRUCTUAL, MASS AND INERTIAL PROPERTIES.

In the planar model the ratio of the lengths of all the structural members to the area of the reflecting surface is $448\ L/\ 208\ L^2 = 2.15/L$. For the O-A axis rotation half of the total beam lengths are taken as the load carrying members. The width of the reflector surface area, L_1, on the simple beam model which results in the same structural mass per unit of load-carrying beam length in the planar model is, therefore, computed from

$$2\ n'\ L/2\ n'\ L\ L_1 = (\tfrac{1}{2})(2.15/L), \tag{1}$$

or

$$L_1 = L/1.07.$$

n' is the maximum number of beam lengths sections in a half beam length. (n' = 8 in this case.)

Therefore, the mass of the simple beam,

$$M_S = 2\ n\ L\ L_1\ K/144\ g = 1.86\ K\ n'\ L^2/144\ g. \tag{2}$$

The mass of the simple beam is also given by

$$M_S = (2/k'_{S2}) \int_o^{n'L} m_x\ d_x, \tag{3}$$

where the load carrying mass per unit of beam length $m_x = p_s A$, and x is the distance from the neutral axis.

From Eq. (11) in Section III

$$A = (1/k_o)(W/B)\ 12\ I_o\ (t/W)^{1/2}\ (1 - j\ x)^{1/2}, \tag{4}$$

where

$$j = (1 - I_1/I_o)/n'\ L$$

and

$$I = I_o\ (1 - j\ x). \tag{5}$$

Using Eq. (4) in Eq. (3) and performing the integration,

$$M_S = -(4/3\ k'_{S2})\ p_S\ (1/k_o)(W/B)\left[12\ I_o\ (t/W)\right]^{1/2}\left[(1 - j\ n'\ L)^{3/2} - 1\right]. \tag{6}$$

Eliminating M_S and solving for I_o from Eqs. (6) and (2),

$$I_o = (1.86\ j\ n'\ L^2\ k'_{S2}\ K\ k_o)^2/12\ (t/W)$$

$$(1.33\ p_S\ 144\ g)^2\ (W/B)^2\ ((1 - j\ n'\ L)^{3/2} - 1)^2, \tag{7}$$

and using Eq. (7) in Eq. (4),

$$m_x = p_S A = 1.86\, j\, n' L^2\, K\, k'_{S2}\, (1 - j x)^{1/2}/1.33$$

$$(144\, g)\left[(1 - j n' L)^{3/2} - 1\right]. \qquad (8)$$

The mass moment of inertia of the antenna, including the structure and on-board masses, is given by,

$$\tfrac{1}{2} I_A = \int_o^{n' L} (x^2 m_x / k'_{S2})\, d x + (M_S/n_o)\, k'_{AF}\, L^2$$

$$(q_1 + 4 q_2 + 9 q_3 + \ldots n_{oo}^2\, q_{n_{oo}}), \qquad (9)$$

where

n_o is the total number of actuators

n_{oo} is the coordinate designation for the location of the actuator or actuators (note the max. $n_{oo} \leq n'$)

$q_1, q_2 \cdots q_{n_{oo}}$ are 1 or 0 and depend on the actuator distribution case.

By analogy with the case definitions in Section III:

Case	q_1	q_2	q_3	q_4	q_5	q_6	q_7	q_8	n_o	n_{oo}
1	0	0	0	0	0	0	0	0	1	0
2	0	1	0	0	0	0	0	0	2	2
3	0	0	0	1	0	0	0	0	2	4
4	0	1	0	1	0	0	0	0	4	2,4

Note that,

$$n_o = q_o + 2\,(q_1 + q_2 + \ldots q_{n_{oo}}).$$

The integral term in Eq. (9) is the inertia of the antenna structure, the other term is the inertia of the actuator-feed system.

2.0 BEAM DEFLECTIONS.

The rate of change in slope of the beam deflection y is given by,

$$I\,E\,d^2\,y/d\,x^2 = \text{the sum of the torques due to:} \qquad (10)$$

(1) the structural reaction forces

(2) the torques generated by the actuators

(3) the reaction forces due to the actuator masses

Using the I from Eq. (5), and the mass moment of inertia from Eq. (9), in Eq. (10),

$$I_o (1 - j x) E d^2 y/d x^2 = (1/k'_{S2}) a_A \int_x^{n'L} m_x x^2 d x$$

$$-(T/n_o)\left[q_o u (0) + q_1 u (0-1) + q_2 u (0-2) + \ldots q_{n_{oo}} \right.$$

$$\left. u (0-n_{oo}) \right] + a_A (L M_S k'_{AF}/n_o) \left[(L-x) q_1 u (0-1) + (2L - x) \right.$$

$$\left. 2 q_2 u (0-2) + \ldots + (n_{oo} L - x) n_{oo} q_{n_{oo}} u (0-n_{oo}) \right], \qquad (11)$$

where u () is a unit step function.

Performing the integrations indicated in Eq. (11), making use of the boundry conditions $(dy/dx) = 0$ and $y = 0$ at $x = 0$, and factoring out the terms used to normalize d in Section III,

$$(E\,K/a_A\,p_S^2\,g^2)\,y = \left[0.061\,(t/W)(W/B)^2\,((1 - j\,n'\,L)^{3/2} - 1)/\right.$$

$$\left.n'\,L^2\,(k'_{S2})^2\,k_o^2\,j^4\right]\left[-8.37\,(1/j^2)\,((1 - j\,x)^{5/2} - 1) + 1.9\right.$$

$$\left.(1/j^2)\,((1 - j\,x)^{7/2} - 1) - 11.9\,(x/j)\right] + \left\{\left[(5.05)\,10^5\,(t/W)\right.\right.$$

$$\left.(W/B)^2\,((1 - j\,n'\,L)^{3/2} - 1)^2/(k'_{S2})^2\,(k_o)^2\,n_o\,(n')^2\,j^3\right]$$

$$\left[(4.72)\,10^{-7}\,(8 + 2\,j\,n'\,L + 15\,j^2\,(n')^2\,L^2)(1 - j\,n'\,L)^{3/2}\right.$$

$$\left.-8)/j^2\,((1 - j\,n'\,L)^{3/2} - 1) + (3.35)\,10^{-5}\,(k'_{AF}/n_o)(q_1 + 4\right.$$

$$\left.q_2 + 9\,q_3 + \ldots\,n_{oo}^2\,q_{n_{oo}})\right]\left[q_o\,u\,(0) + q_1\,u\,(0\text{-}1) + q_2\,u\right.$$

$$\left.(0\text{-}2) + \ldots + q_{n_{oo}}\,u\,(0\text{-}n_{oo})\right] - 0.061\,(1 - j\,n'\,L)^{3/2}\,(8 + 12$$

$$\left.j\,n'\,L + 15\,j^2\,(n')^2\,L^2)\,(t/W)\,(W/B)^2/j^5\,n'\right\}\left[x\,\log\,(1 - j\,x)\right.$$

$$\left. - x - (1/j)\,\log\,(1 - j\,x)\right] - \left[4.23\,(t/W)(W/B)^2\,k'_{AF}\,((1 - j\,n'\right.$$

$$\left.L)^{3/2} - 1)^2/k_o^2\,k_{S2}^2\,n_o\,n'\,j^2\right]\left[\left[q_1\,u\,(0\text{-}1)\left[(L/j) - (1/j^2)\right]\right\{\right.$$

$$\left[(x \log (1 - j\,x) - x - (1/j) \log (1 - j\,x))\right] + x^2/2\,j\Big\}$$

$$+ 2\,q_2\,u\,(0\text{-}2)\left[(2\,L/j)\text{-}(1/j^2)\right]\Big\{\Big[(x \log (1 - j\,x) - x -$$

$$(1/j) \log (1 - j\,x))\Big] + x^2/2\,j\Big\} + \ldots + n_{oo}\,q_{n_{oo}})\,u\,(0\text{-}n_{oo})$$

$$(n_{oo}\,L/j)\text{-}(1/j^2) \quad (x \log (1 - j\,x) - x - (1/j) \log$$

$$(1 - j\,x)) \quad + x^2/2\,j \tag{12}$$

Eq. (12) may be simplified to,

$$y = C_1\,((1 - j\,x)^{5/2} - 1) + C_2\,((1 - j\,x)^{7/2} - 1) + C_3$$

$$x + C_4\left[x \log (1 - j\,x) - x - (1/j) \log (1 - j\,x)\right] + C_5\Big[1$$

$$\sum_{n_{oo}} n_{oo}\,q_{n_{oo}}\,u\,(0\text{-}n_{oo})\Big\{\Big[(n_{oo}\,L/j) - (1/j^2)\Big]$$

$$\left[x \log (1 - j\,x) - x - (1/j) \log (1 - j\,x)\right] + x^2/2\,j\Big\}\Big] \tag{13}$$

In Eq. (13) the constants C_1 to C_5 are a function of the structural and loading condition parameters E, K, a_A, p_S^2, g^2, (t/W), (W/B), j, n', L, k_o, k'_{S2} k'_{AF}, n_o, n_{oo}, q, and u().

Eq. (12) or (13) is the closed form solution for the beam deflection y at any position x. This solution, unlike that for the planar model in Section III, is based on a distributed spring-mass system for the structure. Lumped constants are only used for the actuator-feed masses.

3.0 WEIGHTED RMS DEFLECTIONS.

The weighted rms deflection is determined from

$$d = \left(\int_{o}^{n'' L} y^2 \, d\, x \right)^{1/2} / (n'' L)^{1/2}. \qquad (14)$$

Where n" is the number of beam length sections in a half beam length that correspond to the n_{oo} in the unit step functions u (). When no step function multiplies an integrand term n" = n'. Therefore, the limits of integration for each integrand term in Eq. (14) depends on U () and the presence or non-presence of u () in the integrand terms.

To reduce the complexity of the integration of Eq. (14) the following simplifications are made for some of the terms in the expression for y from Eqs. (12) or (13).

$$((1 - j\, x)^{5/2} - 1) \triangleq j\, x \qquad (15A)$$

$$((1 - j\, x)^{7/2} - 1) \triangleq j\, x \qquad (15B)$$

$$x \log x - x - (1/j) \log (1 - j x) \stackrel{\Delta}{=} - \tfrac{1}{2} j x^2. \qquad (15C)$$

Using the above simplifications and the following numerical parameter values, which correspond to loading conditions 1, 2, 5, and 8 in Section III 4.1, the normalized y in Eq. (15), is computed from Eq. (12).

$(t/W) = 0.01$ Uniform illumination

$(W/B) = 0.14$ Actuator distribution case 1,2,3,4

$p_S = (2.59)\ 10^{-4}$ $((1 - j n' L)^{3/2} - 1) = -0.9100$

$k'_{S2} = 0.75$ $((1 - j n' L)^{5/2} - 1) = -0.9820$

$k_o = 0.9$ $((1 - j n' L)^{7/2} - 1) = -0.9964$

$n' = 8$

$L = 300$

$(I_1/I_o) = 0.2$

$k'_{AF} = 0.25$

$k_S = 0.80$

$$(K\,E/a_A\,p_S^2\,g^2)\,y = (3.5)\,10^7\,x + (0.23)\,10^4\,x^2$$

$$-\begin{bmatrix} 1.51\,u\,(0) \\ 0.85\,u\,(0\text{-}2) \\ 0.93\,u\,(0\text{-}4) \\ 0.43\;\;u\,(0\text{-}2) + u\,(0\text{-}4) \end{bmatrix} 10^4\,x^2 \qquad (16)$$

The terms in the large brackets of Eq. (15) correspond to actuator distribution cases 1,2,3,4.

Using Eq. (16) in Eq. (14) and performing the integration,

$$(K\,E/a_A\,p_S^2\,g^2)^2\,d^2 = (2.63)\,10^{16}\,L^2 + (2.07)\,10^{13}\,L^3$$

$$+ (4.31)\,10^9\,L^4$$

$$-\begin{bmatrix} 0 \\ 1.72 \\ 18.80 \\ 9.36 \end{bmatrix} 10^{12}\,L^3 \qquad + \begin{bmatrix} 0 \\ -13.30 \\ 105.00 \\ 13.64 \end{bmatrix} 10^8\,L^4 \qquad (17)$$

$$(K\,E/a_A\,p_S^2\,g^2)\,d = \begin{bmatrix} 54.5 \\ 54.0 \\ 50.4 \\ 52.1 \end{bmatrix} 10^9 \qquad (18)$$

For the same numerical parameter values the corresponding values of the normalized d from Section III Fig. 32 are

$$(K E/a_A p_S^2 g^2)\, d = \begin{bmatrix} 150 \\ 42 \\ 15 \\ 29 \end{bmatrix} 10^9 \qquad (19)$$

The trends in d values in going from case 1 to case 4 are the same for (18) and (19) however there is as much as a $\pm$ 300% discrepancy in the values. This discrepancy is accounted for by (1) the non equivalence of the simple beam end planar models, (2) the simplifications in Eqs. (15A), (15B), (15C), (3) the use of lumped constant parameters for the planar model vs. distributed constant parameters for the simple beam model, (4) when drawing an equivalency between the simple and planar models the assumption that half of the total beam lengths in the planar model are responsible for carrying the load, (5) the assumption that the actuators in the planar model are distributed along lines parallel to the OA axis, and (6) the use of a square contour reflector for the planar model in drawing the comparison with the simple beam model.

4.0 CONCLUSIONS.

It appears that a simple beam model does not yield results that are compatible with the planar model. A discrepancy of $\pm$ 300% has showed up for one case. The discrepancy may be still greater for other cases.

Except for the use of distributed constant parameters all other assumptions made in arriving at the simple beam model tend to make the simple beam model a less accurate and less versatile representation than the planar model of the actual configuration.

APPENDIX D - SIMPLE STRUCTURAL-BEAM APERTURE

(By P. Slysh, checked by G. A. Burns)

The structural and radiation properties of a simple, planar-beam aperture is analyzed in this appendix.

Consider the aperture, shown in Fig. D-1, to be driven at a constant angular acceleration a_1 about an axis perpendicular to the paper at point O. Two configurations of inertial actuators (i.e., reaction-flywheels) are assumed:

Configuration 1: A single actuator with a mass M_o located at point O.

Configuration 2: Two actuators each with a mass $M_{o1}/2$ located at points 1 and 2.

The deflection, y, when $x \geq 0$, for Configuration 1 is,

$$y = (a_1 m/EI)\,(x_o^3 x^2/6 - x_o^2 x^3/12 + x^5/120); \tag{1}$$

and for Configuration 2:

$$(EI/a_1)\, y = x^2(m x_o^3/6 + M_{o1} x_o^2/4) - x^3(m x_o^2/12 - M_{o1}/12) + m x^5/120, \tag{2}$$

where m is the mass per unit length of the beam, E the modulus of elasticity, I the beam section modulus, and M_{o1} the mass of the two actuators in Configuration 2.

Neglecting the x^5 terms, Eqs. (1) and (2) are, for $x \geq 0$,

$$y = B_1 x^2 + B_2 x^3, \tag{1a}$$

$$y = B_{10} x^2 + B_{20} \tag{2a}$$

and for $x \leq 0$,

$$y = -B_1 x^2 + B_2 x^3, \tag{1b}$$

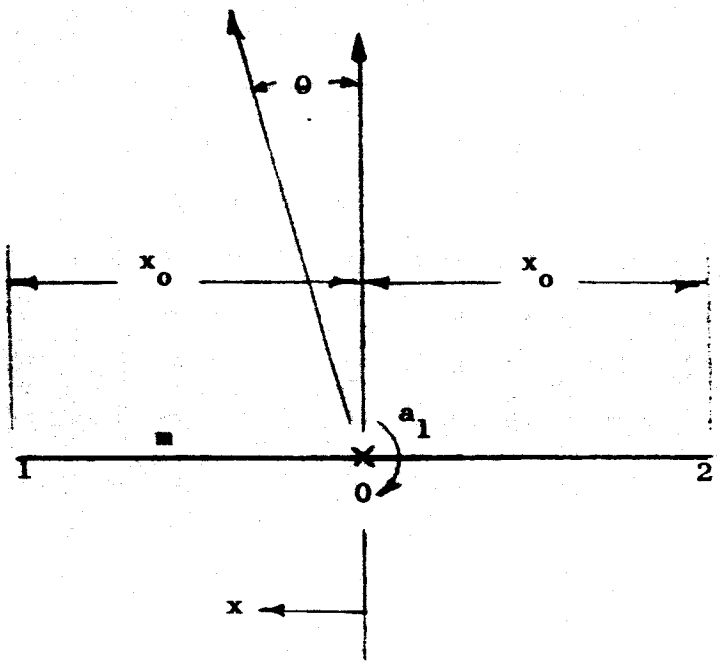


Fig. D-1 Structural beam-aperture model

$$y = -B_{10}x^2 + B_{20}x^3, \tag{2b}$$

where,

$$B_1 = a_1 m x_o^3/6EI,$$

$$B_2 = -B_1/2,$$

$$B_{10} = B_1(1 + 1.5\ M_{o1}/x_o m),$$

$$B_{20} = -(1 + M_o/x_o m)/(2 + 3\ M_{o1}/x_o m)\ x_o.$$

The radiation pattern in the plane of the paper may be expressed (approximately) as,

$$g(u) + (x_o/2) \int_{-1}^{1} f(x) \exp (jux - jy)\, dx, \tag{3}$$

where,

$$u = (\pi x_o/\lambda) \sin \theta,$$

λ is the wavelength, θ is the direction to a point in the field at which $g(u)$ is the radiation intensity, and $f(x)$ is an aperture illumination function, that is, $f(x)$ describes the amplitude of the illumination in the aperture as a function of x.

Substituting Eqs. (1a) and (1b) into Eq. (3),

$$g(u) = (x_o/2) \int_{o}^{1} f(x) \exp j(ux - B_1x^2 - B_2x^3)\, dx$$

$$+ (x_o/2) \int_{-1}^{o} f(x) \exp j(ux + B_1x^2 - B_2x^3)\, dx. \tag{4}$$

Expanding the exp(-jy) term,

$$g(u) = (x_o/2) \sum_{m=o}^{n} ((-j)^m/m!) \int_o^1 (B_1x^2 + B_2x^3)^m f(x)(\exp jux)\, dx$$

$$+ (x_o/2) \sum_{m=o}^{n} ((-j)^m/m!) \int_{-1}^{o} (-B_1x^2 + B_2x^3)^m f(x)(\exp jux)\, dx, \quad (5)$$

where m = 0, 1, 2, . . . n. Integrating, expanding and rearranging the first three terms (i.e., m = 0, 1, 2) of Eq. (5) for f(x) = 1, that is, for constant illumination across the aperture, an approximate expression for g(u) is obtained as

$$g(u)/x_o = j(B_1/u + 2B_1/u^2 - 2B_1/u^3) \cos u + j(B_1/u - 2B_1/u^2 - 2B_1/u^3)$$

$$+ j(2B_1/u^3) + \left[(-B_1 - 2B_2)/u - (8B_1^2 + 20B_1B_2 + 12B_2^2 + 2B_1)/u^2\right.$$

$$+ (2B_1 + 12B_2)/u^3 + (48B_1^2 + 240B_1B_2 + 240B_2^2)/u^4 - (480B_1B_2$$

$$\left. + 1440B_2^2)/u^6)\right] \cos u - \left[(-2 + B_1 + 2B_1^2 + 4B_1B_2 + 2B_2^2)/u\right.$$

$$- (6B_2 + 2B_1)/u^2 - (2B_1 + 24B_1^2 + 80B_1B_2 + 60B_2^2)/u^3 + 12B_2/u^4$$

$$\left. + (48B_1^2 + 480B_1B_2 + 720B_2^2)/u^5 - 1440B_2^2/u^7\right] \sin u - B_1/u^3$$

$$+ 480B_1B_2/u^6. \quad (6)$$

Using Eq. (6), typical power patterns, $p(u) = (g(u))^2$, are estimated in Fig. D-2. It is seen that the structural deformations (i.e., for $B_1 = 1$ and $B_2 = -1/2$) result in a shift in the position of the main lobe of the radiation

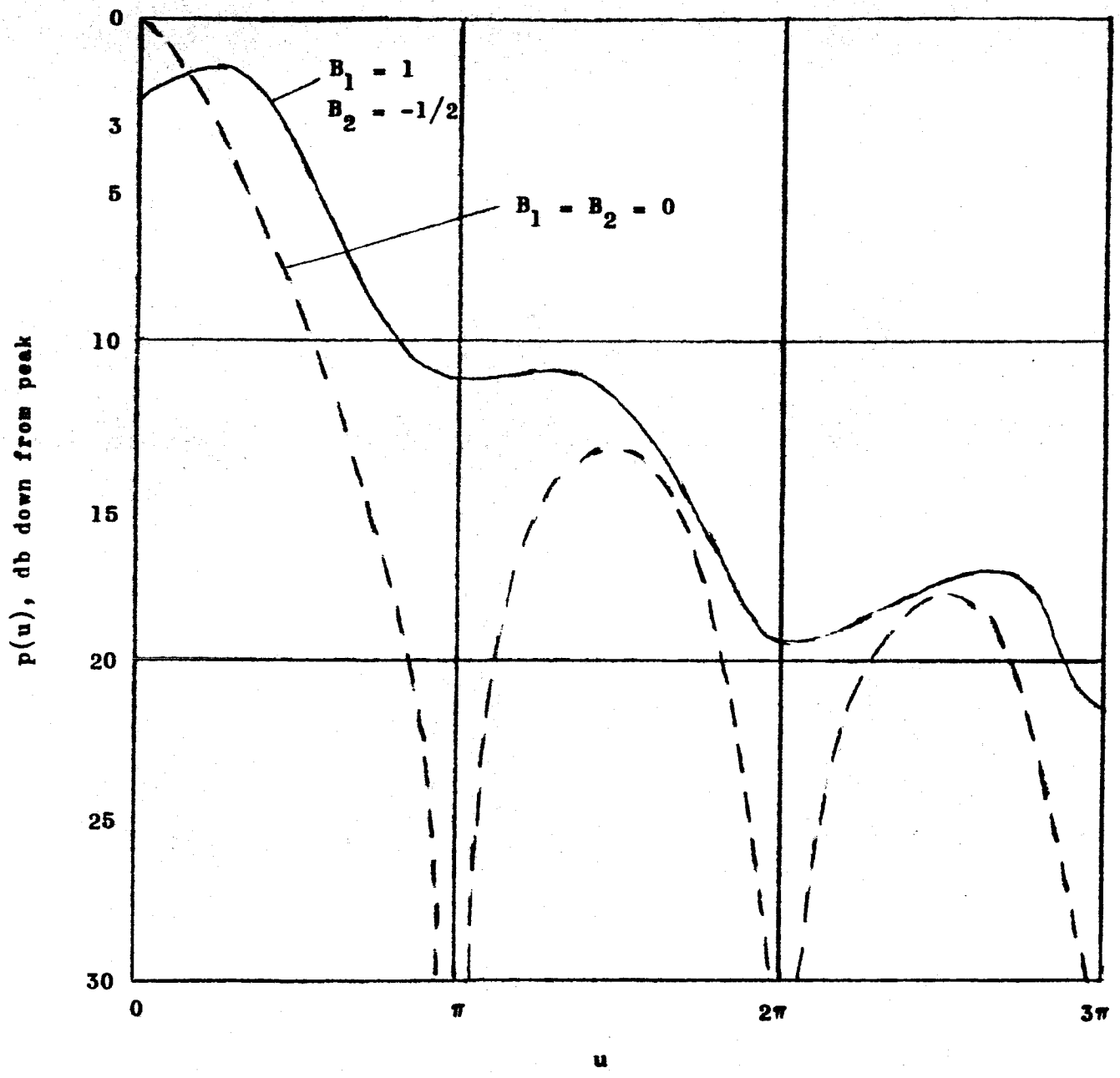


Fig. D-2 Normalized power pattern

pattern when compared with the static, non-loaded case ($B_1 = B_2 = 0$). Also, as expected, the side lobes increase and the nulls are minimized.

The radiation pattern for Configuration 2 can be drawn for comparable operating conditions, such as for the same a_1, or the same total beam and actuator mass. In the latter case, the torque/mass constant, k_1, of the actuator would enter into the problem formulation such that,

$$(M_{o1}/M_o) = (1 - 2a_1 x_o^2/k_1)^{-1} > 1, \tag{7}$$

where M_o is the mass of the actuator in Configuration 1.

The influences of B_1, B_2, k_1, a_1, λ, etc. on the shifting of the main lobe, degradation of the side lobes etc. should be studied. These influences are extremely complex and it appears that even for the chosen example, they can only be studied through numerical (parametric) examples.

It is evident that, in spite of the simple two dimensional model of Fig. D-1, the simplifications in Eqs. (1), (2), and (3), the idealization $f(x) = 1$, and the approximations that $m = 0, 1, 2$, the expression for $p(u)$ is nevertheless unwieldy. In the computer simulations partly developed in this study, none of these idealizations and simplifications are made and the numerical solutions for the structural deflection and radiation patterns are a great deal less approximate.

APPENDIX E - MEASUREMENT OF "RATIO" APERTURE DISTORTIONS

(By P. Slysh)

In an operational RATIO antenna it may be desirable to implement a system for measuring the coordinate, linear and angular distortions, u, at discrete points on the reflector with respect to a reference coordinate system. Such measurements were, in part, planned for the 600 foot radio telescope that was being built at Sugar Grove, West Virginia. For RATIO antennas, in which structural compliances are likely to be large, such measurements would be useful for much smaller dish sizes. This appendix considers the problems of and suggests one approach to implementing these measurements on RATIO antennas.

Reflector distortions may be determined by direct measurements between given points on the reflector surface and a mechanical reference axis. Alternately, sequential measurements may be made between successive points on the reflector surface, the first of which measurements would be with respect to the reference.

Since the measurement errors, as well as the gaging equipment complexity and weight, are estimated to increase with the distance over which the measurements are made, it follows that for a given accuracy the sequential measurement approach results in less equipment complexity and weight. However, it is believed that the sequential measurements will require on-board data processing (or the equivalent) to convert the equipment readouts into the u distortions.

Possible gaging equipment or transducer techniques for implementing the sequential gaging system include: (1) autocollimators and reflecting mirrors located at distributed structural junctions; the linear displacements normal to the line of sight between the autocollimators and mirrors,

as well as the angular displacements about these normals, may be determined automatically and used to compute the distortions, u; (2) strain gage deployed to sample structural strains from which the distortions may be computed; and (3) optical or infra-red ranging methods.

An autocollimator approach is probably the simplest, and most reliable. A description of one such approach is started by considering a straight line, in Figure E-1, along which the linear deflections u_1, u_2, . . ., and the angular deflections u_{11}, u_{21}, . . ., are to be determined.

The collimators, located at points 1, 2, 3, . . ., generate in-line, tandem IR beams that illuminate detectors on either side of each collimator. (The detectors are also located at points 1, 2, 3, . . .) The response from a detector at a typical point "b" due to collimator at an adjacent point "a" is proportional to the displacement m_{ab}.

If u_{01}, u_{11}, u_{21}, . . ., the angular deflections in the plane of the paper at points 0, 1, 2, 3, . . ., are taken as positive for counter clockwise rotations, then,

$$hu_{01} = m_{01} + u_1,$$

$$hu_{11} = -m_{10} + u_1 = m_{12} + u_2 - u_1,$$

$$hu_{21} = -m_{21} - u_1 + u_2 = m_{23} + u_3 - u_2,$$

$$hu_{31} = -m_{32} - u_2 + u_3 = m_{34} + u_4 - u_3,$$

$$hu_{41} = -m_{43} - u_3 + u_4 = m_{45} + u_5 - u_4.$$

If $u_{01} = u_0 = 0$ it is evident that a solution for u_{11}, u_{21}, u_{31}, . . ., and u_1, u_2, u_3, . . ., can be obtained from these equations.

Now consider the application of the above method to the measurement of displacements at the grid junctions shown in Figure E-2. The displacement

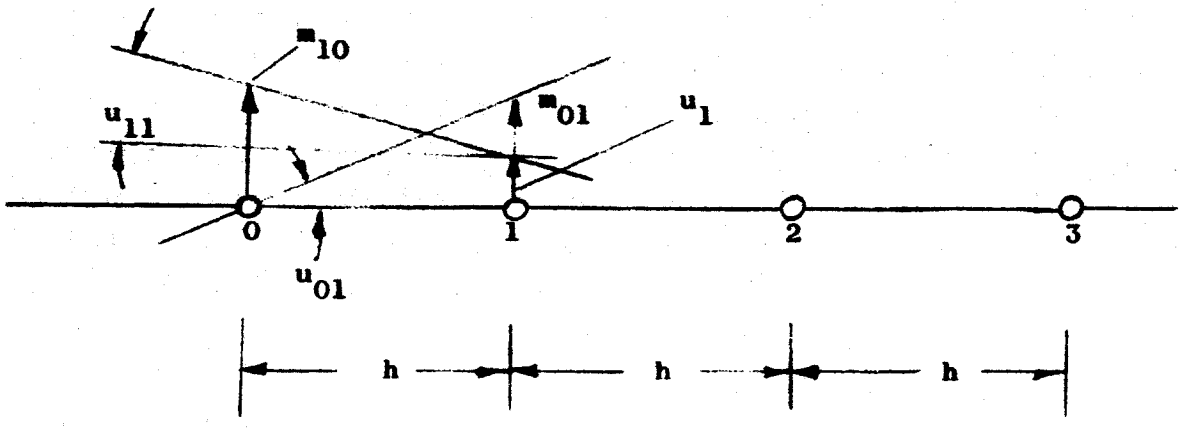


FIGURE E-1 Instrumentation of nodal deflections along a straight line

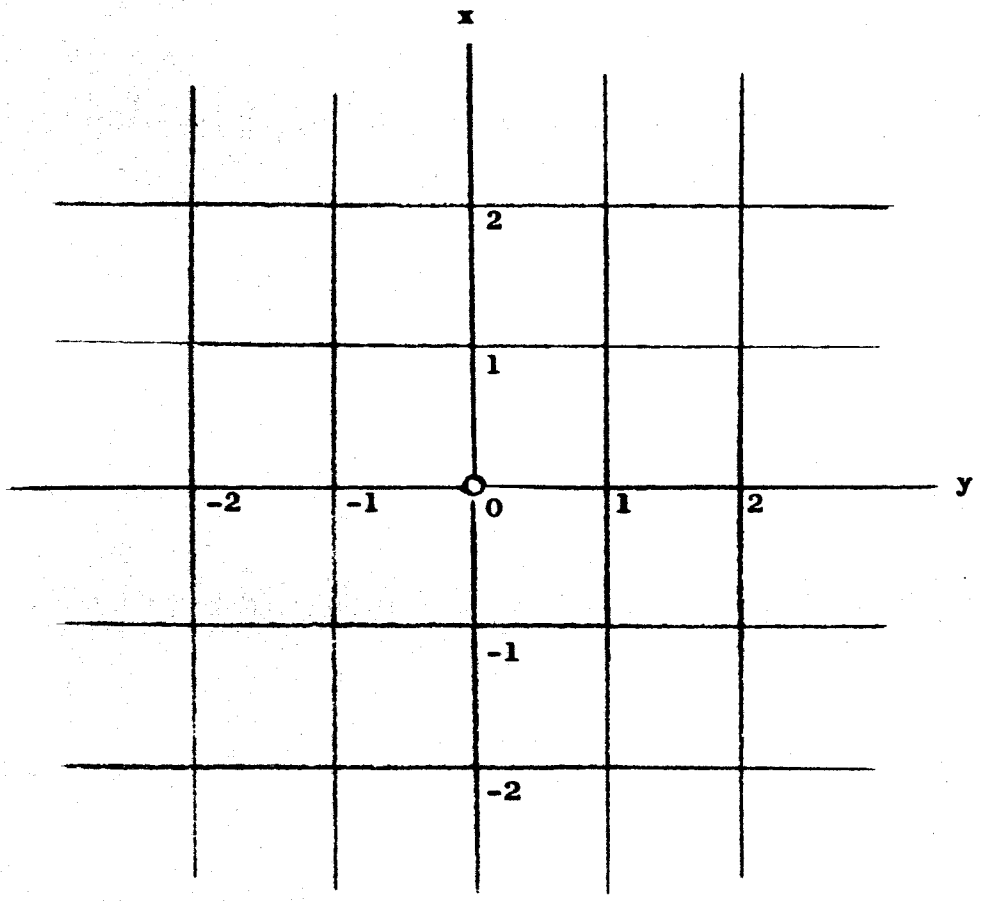


FIGURE E-2 Structural grid.

measurements are to be made normal to the plane of the grid.

Taking the $u_0 = u_{01} = 0$ at $x = y = 0$ as a reference, it follows that the displacements along $x = 0$ can be determined. If $x = 0$, $y = 1$ is now taken as a new reference the displacements along $y = 1$ may be determined, etc.

The above method can be extended to measuring displacements normal to a paraboloidal surface. With these measurements it is possible to develop an aperture calibration function that describes the orientation of the main lobe of the radiation pattern as a function of the aperture distortions.

It is noted that the measurement accuracy is best at the center of the aperture if the main reference is taken at the apex. This is consistent with the performance features of typical antennas in which the errors at the center of the aperture have the greatest effect on aperture performance.

An adaptive multiple-feed system may be competitive with the described gaging method as a means for obtaining a continuous aperture calibration. The adaptive system may typically divide the received r-f radiation into separate channels. The phases and amplitudes at the channel outputs can then be compared (with sum and difference networks) to determine the location of the peak in the main lobe. Preliminary considerations indicate that aperture gaging methods are likely to yield greater main-lobe pointing accuracies than adaptive feed systems.

APPENDIX F - CONTROL SYSTEM CONSIDERATIONS

(By P. Slysh)

1.0 INTRODUCTION

The following is an outline of an approach to the study of RATIO control systems. This approach is considered in this appendix to clarify aspects of RATIO control system problems.

It is to be assumed in this appendix that the control system only induces a single, fundamental flexural mode in the structure. This assumption makes it possible to develop manageable relationships between the applied torque and the separation between r-f and mechanical axes. The following is an outline of some of the salient control system features that can result from this assumption.

2.0 CONTROL AXES

The r-f axis is typically defined by the orientation of the main lobe of the radiation pattern, and the reference axis may be established by an astronertial platform. If the mechanical axis of the antenna is taken as a line passing through the apex and focal point, then the displacement between the r-f and mechanical axes may be defined by the matrix-vector relationship (see Figure F-1),

$$(\theta_o) - (\theta_1) = (f_1 [u]), \tag{1}$$

where, u is the generalized displacement, with respect to the mechanical axis, at the structural junctions. This displacment consists of three linear and three angular orthogonal displacements that in effect describe the departure of the reflector surface from that of a true paraboloid.

It follows from Eq. (1) that the structural compliances that give rise

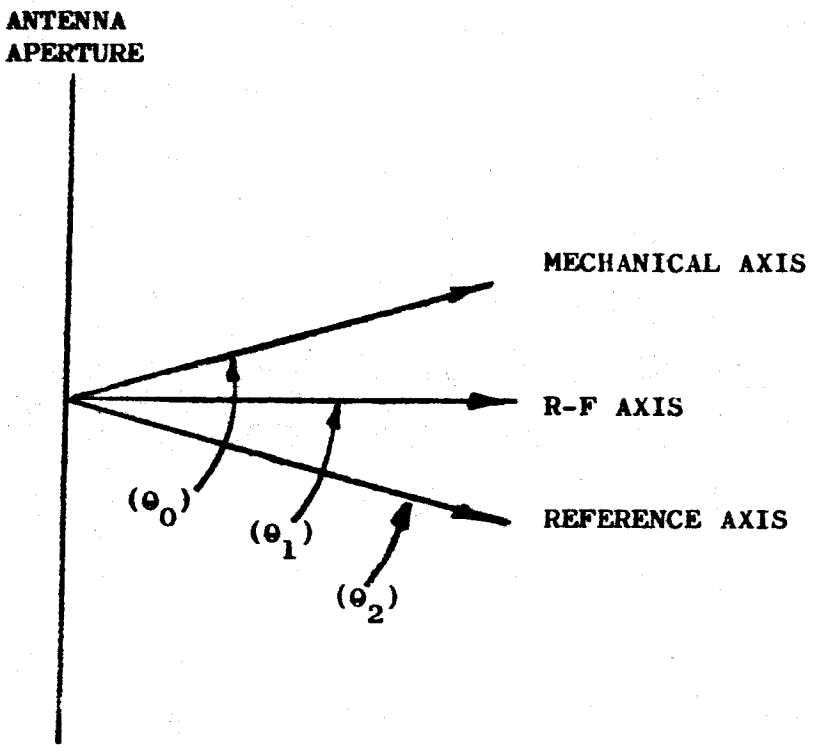


FIGURE F-1 Control axes

to (u) are in effect responsible for a compliance between the r-f and mechanical axis. When the expected displacements between the r-f and mechanical axes are large compared to the required pointing accuracy, as will be assumed here, then the compliances are critical factors in the performance of the control system.

The displacements (u) may be caused by manufacturing and assembly tolerances, thermal stresses, structural deflections due to actuator reactions, and creep in the structural material. Only structural deflections due to actuator reactions are considered here.

An extension of the work under the current study contract NAS7-228, is applicable to the evaluation of $(f_1 [u])$. This work is also directly applicable to the evaluation of (u) if the displacements are caused by steady state actuator torques and structural reactions. Account is taken only of the dynamics of the structural deflections due to the actuator reactions.

If the astronertial platform is mounted at or near the apex or focus, such that the compliances between the platform mount and the mechanical axis are negligible, then the instrumentation of the data take-off (θ_o) - (θ_2), (in Figure F-1), may include automatic boresighting between the apex and focus, and a resolver train to generate the coordinate angles between the boresight and reference axes. It is also possible to determine

$$(\theta_o) - (\theta_2) = (f_2 [u']), \tag{2}$$

where u' is the generalized coordinate displacement or motion at the structural junctions with respect to the reference axis (i.e. inertial space).

A possible method for instrumenting the measurement of (u) is described in Appendix E.

Because of the availability of the $(\theta_o) - (\theta_2)$ data takeoff, a transformation,

$$(u') = (T)\,(u), \tag{3}$$

may be generated. (T) is a matrix for transforming the displacements u to u′ (i.e. from a body fixed reference to an inertially fixed reference.)

From Eqs. (1) to ((3),

$$((\theta_1) - (\theta_2)) = (f_1\,[u]) + (f_2\,[(T)(u)]), \tag{4}$$

or

$$((\theta_1) - (\theta_2)) = f_1\,[(T)^{-1}(u')] + (f_2\,[u']). \tag{5}$$

It is evident that the instrumentation of $((\theta_1) - (\theta_2))$ is possible through the instrumentation of $((\theta_o) - (\theta_2))$ and $((\theta_o) - (\theta_1))$. The vector $((\theta_1) - (\theta_2))$ is the variable to be controlled. By analogy with the above, if the displacement rates in $(\dot{u})$ and $(\dot{u}')$ are obtained by differentiating the outputs of displacement sensors,

$$((\dot{\theta}_1) - (\dot{\theta}_2)) = (f_3\,[\dot{u}]) + (f_4\,[(T_1)(\dot{u}')]), \tag{6}$$

and, if inertial rate sensors are used, in which case $\dot{u}$ and the displacement rates in (T) are sensed directly, then,

$$((\dot{\theta}_1) - (\dot{\theta}_2)) = (f_3\,[(T_1)^{-1}(\dot{u}')]\,) + (f_4[[\dot{u}']). \tag{7}$$

Eqs. (5) and (6) indicate that the displacement rates between the r-f and references axes can be obtained by instrumenting a transformation between the mechanical-axis and reference-axis coordinate system and by sensing the relative (with respect to the mechanical axis) or absolute (with respect to the reference axis) displacement rates at the structural junctions.

3.0 CONTROL SYSTEM DESCRIPTION

Neglecting structural damping, the coordinate forces and torques, P, at the structural junctions (in Figure F-1) can be expressed in matrix forms

$$(P) = (K)(u) + (M)\,(\ddot{u}'), \tag{8}$$

where (K) and (M) are the displacement and mass matrices for the antenna structure.

If position and velocity feedback loops are used between the r-f and reference axes then (P) is also given by,

$$\begin{aligned}(P) = {} & [((\theta_1) - (\theta_2))_i - ((\theta_1) - (\theta_2))_o](G_1) \\ & + [((\dot{\theta}_1) - (\dot{\theta}_2))_i - ((\dot{\theta}_1) - (\dot{\theta}_2))_o](G_2),\end{aligned} \tag{9}$$

where the subscripts i and o refer to the input and output respectively, and (G_1) and (G_2) are the feedback and controller gain (matrix) functions.

Thus the collection of forces and torques, (P), as caused by structural spring and inertial forces, are nominally equal to the amplified, actuating (velocity and position) error functions.

Equating Eqs. (8) and (9), and using Eqs. (3), (5), and (6),

$$\begin{aligned}& \{((\theta_1) - (\theta_2))_i - (f_1\,[(T)^{-1}(u')])\}\,(G_1) \\ & + \{((\dot{\theta}_1) - (\dot{\theta}_2))_i - (f_3\,[(T)^{-1}(\ddot{u}')]) - (f_4[\ddot{u}'])\}\,(G_2) \\ & = (M)\,(\ddot{u}') + (K)\,((T)^{-1}(u')).\end{aligned} \tag{10}$$

A block diagram of the system described by Eq. (1)) is shown in Figure F-2. In addition to the feedback of $((\theta_1) - (\theta_2))$ and $((\dot{\theta}_1) - (\dot{\theta}_2))$ subsidiary feedback loops for $((\theta_o) - (\theta_2))$, and $((\theta_o) - (\theta_1)$ may be

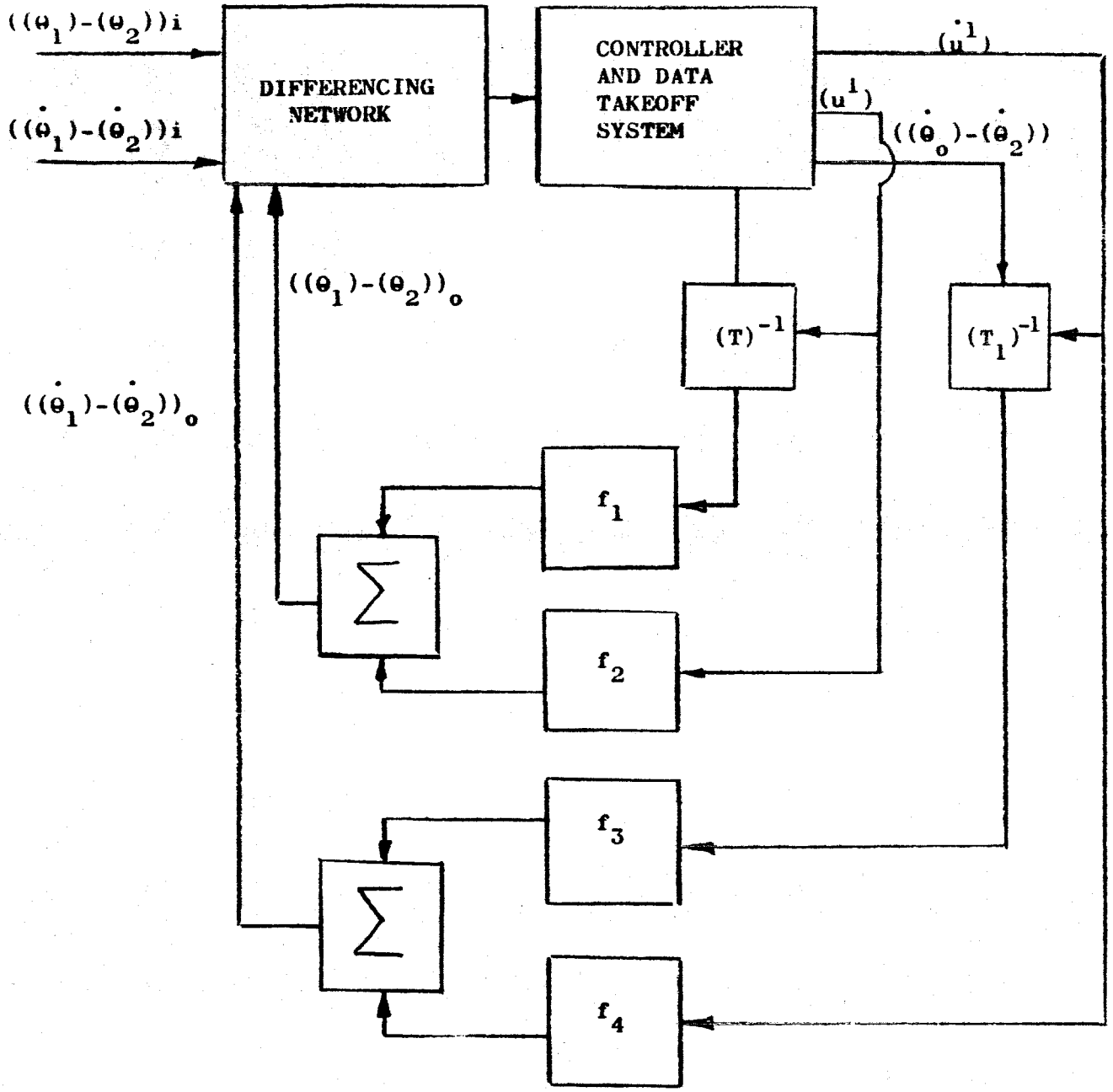


FIGURE F-2 Diagram of attitude control system

considered.

The control system is to primarily function in a position control mode. However, the performance of the control system in slewing, tracking and slave modes of operation may also be investigated per the above.

4.0 METHOD OF ANALYSIS

For given inputs, $((\theta_1) - ((\theta_2))_i$, and $((\dot{\theta}_1) - (\dot{\theta}_2))_i$, Eq. (10) nominally represents a set of simultaneous (linear) differential equations describing u' and $\dot{u}'$, the three linear and three angular displacements and displacement rates at each structural junction.

Since the structure to be considered may have on the order of a hundred structural junctions (and each junction has six degrees of freedom) it is evident that generalized and rigorous solutions for u' (or $\dot{u}'$) represent a formidable undertaking. However, if only the first primary modes of oscillation are considered then the complexity of the problem is reduced by at least an order of magnitude.

The computational time constants, as for f_1 to f_4 and the transformations (T), in Figure F-2, may be considered neglegible compared to expected system response rates.

With solutions for u' and $\dot{u}'$ it is possible through the procedure indicated by Eqs. (5) and (7) to determine the controlled variable at the output, $((\theta_1) - (\theta_2))_o$ and $((\dot{\theta}_1) - (\dot{\theta}_2))_o$. Thus the input-output characteristics can be examined in both the time and frequency domains.

Externally induced force and thermal fields will act to perturb the input-output relationship in the control system.

NON-TAPERED CONFIGURATIONS				TAPERED CONFIGURATIONS			
PARAMETER	I	II	III	PARAMETER	I T	II T	III T
L	300	200	100	L	300	200	100
D	5400	2933	1467	D	5400	2930	1467
r_{FW}	100	67	33		100	67	33
M_S, Eq.(4)	32.5	14.5	3.6	M_S, Eq.(4)	32.5	14.5	3.6
M, Eq.(5)	0.036	0.016	0.004	M, Eq.(5)	0.036	0.016	0.004
M_2	0.027	0.012	0.003	M_2	0.027	0.012	0.003
A, Eq.(1)	0.68	0.45	0.23	A_o Eq.(11)	1.1	0.73	0.37
B, Eq.(2)	34.0	27.5	19.6	B_o Eq.(12)	61.0	49.4	35.1
I, Eq.(3)	160	71	18	I_o Eq.(16)	420	186	67
				A	Fig. 7	Fig. 7	Fig. 7
				I	Fig. 8	Fig. 8	Fig. 8
M_A, M_T, M_p	(1)	(0.4450)	(0.1110)	M_A, M_T, M_p	(1)	(0.4450)	(0.1110)
I_A	(1)	(0.1970)	(0.0123)	I_A	(1)	(0.1970)	(0.123)
$w_A a_A$	(1)	(1.59)	(3.46)	$w_A a_A$	(1)	(1.59)	(3.46)
$w_{A\ MAX}$	(1)	(1.5)	(3.0)	$w_{A\ MAX}$	(1)	(1.5)	(3.0)
F, Fig.4, 4a	(1)	(0.2960)	0.0370	F, Fig.11,12	(1)	(0.2960)	(0.0370)
T, Fig.5	(1)	(0.1970)	0.0124	T, Fig. 5	(1)	(0.1970)	(0.0124)

QUANTITIES IN ( ) ARE SCALING FACTORS FOR QUANTITIES IN FIG. 15 AND LOADING CONDITIONS AS INDICATED

Fig. III-16. Parameter values for configurations I, II and III, non-tapered and tapered, K = 0.1.